

University of Alberta

Ozone Mass Transfer Modeling in an Impinging-Jet Bubble Column

By

Katherine A. Clarke



A thesis submitted to the Faculty of Graduate Studies and Research

in partial fulfillment of the requirements of the degree of

Master of Science

In

Environmental Engineering

Department of Civil and Environmental Engineering

Edmonton, Alberta

Fall 2004



Library and
Archives Canada

Bibliothèque et
Archives Canada

Published Heritage
Branch

Direction du
Patrimoine de l'édition

395 Wellington Street
Ottawa ON K1A 0N4
Canada

395, rue Wellington
Ottawa ON K1A 0N4
Canada

Your file *Votre référence*

ISBN: 0-612-95724-1

Our file *Notre référence*

ISBN: 0-612-95724-1

The author has granted a non-exclusive license allowing the Library and Archives Canada to reproduce, loan, distribute or sell copies of this thesis in microform, paper or electronic formats.

L'auteur a accordé une licence non exclusive permettant à la Bibliothèque et Archives Canada de reproduire, prêter, distribuer ou vendre des copies de cette thèse sous la forme de microfiche/film, de reproduction sur papier ou sur format électronique.

The author retains ownership of the copyright in this thesis. Neither the thesis nor substantial extracts from it may be printed or otherwise reproduced without the author's permission.

L'auteur conserve la propriété du droit d'auteur qui protège cette thèse. Ni la thèse ni des extraits substantiels de celle-ci ne doivent être imprimés ou autrement reproduits sans son autorisation.

In compliance with the Canadian Privacy Act some supporting forms may have been removed from this thesis.

Conformément à la loi canadienne sur la protection de la vie privée, quelques formulaires secondaires ont été enlevés de cette thèse.

While these forms may be included in the document page count, their removal does not represent any loss of content from the thesis.

Bien que ces formulaires aient inclus dans la pagination, il n'y aura aucun contenu manquant.

Canada

“Dance like nobody’s watching;
Love like you’ve never been hurt.
Sing like nobody’s listening;
Live like it’s heaven on earth.”

~ Mark Twain~

This manuscript is dedicated to my family who have helped me along this journey. To my mum and dad, Bob and Denise Clarke, for always believing in me and supporting all of my endeavours. To my brothers Robert, Ian and Michael: Reach for your dreams no matter how impossible they seem; it's amazing what you can achieve. To my Grandad: Thank you for the time that we spent together and the conversations that we shared. To my Granny: For always being with me in spirit, and giving me that extra push when I needed it most.

Acknowledgements

I would like to thank Dr. Mohamed Gamal El-Din for his continual guidance and support throughout this project. I am appreciative of the commitment and patience that he has shown during the completion of this thesis. Thank you to Dr. Daniel Smith for his input into this project.

Many thanks to the staff in the Environmental Engineering Building, part of the Department of Civil and Environmental Engineering at the University of Alberta. Thank you to the professors of this department, whose love and pursuit of knowledge is inspiring. To the technical and support staff for helping me in all other facets of this journey.

I would like to recognize all of the friends that I have made while on this journey, studying with me in this program. Thank you for your support. A special thank you to Diane Su for your uplifting spirit, and the laughs we shared during the most trying times.

A special thank you to my friends and family for their continuous encouragement and understanding.

Table of Contents

Chapter 1 Introduction.....	1
Problem Statement.....	1
Research Objectives.....	1
Chapter 2 Literature Review	4
Ozone Reactivity.....	5
Ozone Contactors.....	8
Hydrodynamics.....	9
Bubble Flow Regimes.....	17
Bubble Columns	20
Modifications With Jet Distributors.....	22
Modeling of Hydrodynamics	26
Gas Hold-up.....	38
Bubble Properties.....	50
Gas-Liquid Interfacial Area	55
Mass Transfer.....	59
Gas Solubility.....	64
Influences on Mass Transfer.....	66
Volumetric Liquid Mass Transfer Coefficient.....	67
Chapter 3 Materials and Methods.....	78
Transient Back Flow Cell Model.....	78
Steady-State Back Flow Cell Model.....	82
Impinging-Jet Bubble Column.....	88
Mixing Study	91
Experimental.....	91
Analysis.....	92
Gas Holdup Study.....	94
Experimental.....	94
Analysis.....	95
Bubble Properties.....	96
Experimental.....	96
Analysis.....	98
Ozone Mass Transfer Study.....	102
Experimental.....	102
Analysis.....	104

Chapter 4 Results and Discussion	105
Mixing in the Bubble Column	105
Gas Hold-up	123
Bubble Properties.....	141
Mass Transfer	157
Chapter 5 Conclusions and Recommendations.....	179
Chapter 6 References.....	182
Chapter 7 Appendices.....	202

List of Tables

Table 2-1:	Correlations of axial dispersion coefficients proposed by previous researchers.....	35
Table 2-2:	Correlations of gas holdup proposed by previous researchers.....	44
Table 2-3:	Correlations of bubble size and interfacial area proposed by previous researchers.....	57
Table 2-4:	Correlations of overall mass transfer coefficients proposed by previous researchers.....	76
Table 4-1:	Operating conditions corresponding to Figure 4-6	110
Table 4-2:	Operating conditions corresponding to Figure 4-7	110
Table 4-3:	Coefficients used in Equation 4-7.....	120
Table 4-4:	Relationships being compared in Figure 4-24.	138
Table 4-5:	Relationships being compared in.....	156
Table 4-6:	Measurable operating parameters for the mass transfer study.....	158
Table 4-7:	Numerically determined operating parameters for the mass transfer study.....	158
Table 4-8:	Operating conditions and resulting overall mass transfer coefficients ...	161
Table 4-9:	Volumetric mass transfer rate, based on two approaches of determining the interfacial area.....	176
Table 4-10:	Relationships being compared in Figure 4-49	177

List of Figures

Figure 2-1:	Definition of measurement lengths and angles of bubbles	53
Figure 3-1:	Schematic diagram representing the BFCM for co-current flow conditions of bubble column reactors, indicating the presence of two mixing zones	78
Figure 3-2:	Bubble column pilot-scale set-up.....	89
Figure 3-3:	Impinging-jet bubble column and representation of two mixing zones ...	93
Figure 3-4:	Digital photography set-up	98
Figure 3-5:	Bubble dimensions.....	99
Figure 3-6:	Digital photograph of gas bubble at $u_G = 0.019$ m/s and $u_L = 0.003$ m/s	101
Figure 4-1:	Effects of the number of cells on the BFCM	106
Figure 4-2:	Residence time distribution curve for tracer #28, at probe #1	107
Figure 4-3:	Residence time distribution curve for tracer #28, at probe #2.....	108
Figure 4-4:	Residence time distribution curve for tracer #28, at probe #3	108
Figure 4-5:	Residence time distribution curve for tracer #28, at probe #4.....	109
Figure 4-6:	Influence of liquid flow rate on the residence times of the tracers, port #4	110
Figure 4-7:	Influence of gas flow rate on the residence time of the tracers, port #4.	111
Figure 4-8:	Dependency of the backmixing coefficient on the superficial gas velocity	113
Figure 4-9:	Dependency of the backmixing coefficient on the superficial liquid velocity.....	114
Figure 4-10:	Comparison between the experimentally determined and regression fitted backmixing ratios for zone one	117
Figure 4-11:	Comparison between the experimentally determined and regression fitted backmixing ratios for zone two	117
Figure 4-12:	Comparison of the use of one mixing zone and two mixing zones to characterize the impinging-jet bubble column.....	119
Figure 4-13:	Comparison between the experimentally determined and regression fitted backmixing ratios for the entire bubble column.....	121
Figure 4-14:	Relationship between the mixing ratio and the superficial gas velocity at specific superficial liquid velocities.....	122
Figure 4-15:	Pressure at three pressure sensors as a function of time, corresponding to tracer 13, run 5	124
Figure 4-16:	Calibration curves for three pressure sensors, corresponding to tracer 13, run 5	125
Figure 4-17:	Representation of the difference between the gas holdup in the upper and lower sections of the bubble column reactor	127
Figure 4-18:	Relationship between the gas hold-up and the superficial gas velocity under the injection mode of operation ($n = 153$)	129
Figure 4-19:	Relationship between the gas hold-up and the superficial gas velocity under the ejection mode of operation ($n = 29$).....	130
Figure 4-20:	Relationship between the gas hold-up and the superficial liquid velocity under different modes of operation.....	131

Figure 4-21:	Relationship between the gas hold-up and the superficial gas velocity under different modes of operation.....	132
Figure 4-22:	Relationship between the gas hold-up and the superficial gas velocity at varying superficial liquid velocities.....	133
Figure 4-23:	Relationship between the gas hold-up and the superficial liquid velocity	136
Figure 4-24:	Comparison between the experimentally measured gas hold-up and the regression fitted gas hold-up.....	137
Figure 4-25:	Comparison between published correlations at $u_L = 0.02$ m/s.....	139
Figure 4-26:	Comparison between published correlations at $u_G = 0.015$ m/s	140
Figure 4-27:	A digital image of the gas bubbles at $u_G = 0.001$ m/s and $u_L = 0.008$ m/s	142
Figure 4-28:	A digital image of the gas bubbles at $u_G = 0.011$ m/s and $u_L = 0.028$ m/s	142
Figure 4-29:	Relationship between bubble diameter and superficial liquid velocity ..	144
Figure 4-30:	Relationship between bubble diameter and superficial gas velocity	145
Figure 4-31:	Comparison between measured and predicted bubble diameters (d_B), approach one	147
Figure 4-32:	Comparison between measured and predicted bubble diameters (d_B), approach two	147
Figure 4-33:	Comparison between measured and predicted Sauter mean bubble diameters (d_S), approach one	149
Figure 4-34:	Comparison between measured and predicted Sauter mean bubble diameters (d_S), approach two	149
Figure 4-35:	Relationship between bubble diameter (d_S) and u_G at varying u_L , approach one	151
Figure 4-36:	Relationship between bubble diameter (d_S) and u_G at varying u_L	151
Figure 4-37:	Comparison between correlations predicting the bubble diameter at $u_L = 0.019$ m/s.....	154
Figure 4-38:	Comparison between correlations predicting the interfacial area at $u_L = 0.019$ m/s.....	157
Figure 4-39:	Sum of the squares of the residuals plot for trial #6	162
Figure 4-40:	Sum of the squares of the residuals plot for trial #13	163
Figure 4-41:	Sum of the squares of the residuals plot for trial #21	164
Figure 4-42:	Dissolved ozone concentration profile for trial #6	165
Figure 4-43:	Dissolved ozone concentration profile for trial #13	166
Figure 4-44:	Dissolved ozone concentration profile for trial #21	167
Figure 4-45:	Relationship between the superficial gas velocity and the overall mass transfer coefficient	169
Figure 4-46:	Relationship between the superficial liquid velocity and the volumetric mass transfer coefficient	170
Figure 4-47:	Relationship between the superficial gas velocity and the overall mass transfer coefficient at specific superficial liquid velocities	172

Figure 4-48:	Relationship between the gas hold-up and the volumetric mass transfer coefficient at $u_L = 0.014$ m/s.....	174
Figure 4-49:	Relationship between the interfacial area and the volumetric mass transfer coefficient at $u_L = 0.014$ m/s.....	175
Figure 4-50:	Comparison between correlations predicting the mass transfer coefficient, $k_L a$	178

Chapter 1 Introduction

Problem Statement

More stringent water quality regulations have been implemented, resulting in the use of ozone to meet requirements for water and wastewater treatment. Ozone is a highly effective means of treating both drinking water and wastewater. An important component of the optimization of this treatment process lies in the reactor's ability to efficiently transfer the ozone gas into the liquid, with minimal off-gassing. Recently, an impinging-jet bubble column reactor (IJBCR) which employs venturi injectors as gas distributors has been proposed. The purpose of this work was to investigate the applicability of the transient and steady-state backflow cell models for modeling the hydrodynamic and mass transfer characteristics of the impinging-jet bubble column.

Research Objectives

The objectives of this research are to model:

- 1) the backflow ratio (i.e. backmixing) of the reactor;
- 2) the gas hold-up of the reactor;
- 3) the properties of the bubbles in the reactor; and
- 4) the ozone mass transfer characteristics of the reactor.

The data used for this research was taken from the work of Gamal El-Din (2001d), who carried out experiments on an impinging-jet bubble column. The bubble column was operated under co-current upward flow conditions, with the venturi injectors operating in

both injection (positive pressure) and ejection (negative pressure) modes. Collected data includes: 1) tracer data; 2) gas hold-up data; 3) bubble size data; and 4) dissolved ozone concentration profile data. The collected tracer and dissolved ozone concentration data were subject to analysis using the transient and steady-state back flow cell models respectively. These models were originally proposed by Gamal El-Din and Smith (2001a, 2001c), who also proposed a hydrodynamic model.

The operational conditions of the impinging jet bubble column were summarized based on two operations:

1) Tracer studies

- a. steady state operation in terms of gas and liquid flow rates;
- b. impulse tracer input;
- c. venturi operation modes: injection and ejection;
- d. theoretical hydraulic retention time: 48 to 190 seconds;
- e. superficial liquid velocity: 7.71×10^{-3} to 2.82×10^{-2} m/s; and
- f. superficial gas velocity: 8.90×10^{-4} to 1.54×10^{-2} m/s.

2) Ozone dissolution

- a. steady state operation in terms of gas and liquid flow rates;
- b. bubble column operation modes: co-current and counter-current;
- c. gas introduction modes: injection and ejection;
- d. superficial liquid velocity: 7.50×10^{-3} to 2.80×10^{-2} m/s; and
- e. superficial gas velocity: 1.80×10^{-3} to 1.40×10^{-2}

With the application of the transient and steady-state back flow cell modes, backmixing and overall mass transfer coefficient models were to be developed. These parameters were then correlated with the superficial gas velocity (u_G), and the superficial liquid velocity (u_L) of the reactor.

Chapter 2 Literature Review

With increasing concern surrounding waterborne pathogens in drinking water, as well as increasingly stringent regulations for contaminants present in wastewater, ozone has emerged as a promising alternative. Unlike chlorine, ozone reactions with organics do not produce trihalomethanes, an important public health concern (Mariñas et al. 1993). However, reactions with natural organic matter (NOM) that contains bromide result in brominated by-products, of which the bromate ion is particularly worrisome. Ozone displays superior disinfecting abilities when compared with chlorine, chlorine dioxide, and chloramines because of its high oxidizing potential. It is, up until now, one of the best disinfectants for inactivating the waterborne pathogen *Cryptosporidium parvum* (Long et al. 1999).

Apart from its most common use as a disinfectant, ozone is also a popular agent used for controlling tastes, odours and colour, and as a coagulant aid, as a method of controlling algae growth, and as an oxidizing agent. Ozone is readily able to oxidize inorganic materials (iron and manganese), organic micropollutants (taste and odour causing compounds, pesticides), and organic macropollutants (colour imparting compounds) (Long et al. 1999, Beltrán et al. 2001). Ozone is also used to treat industry effluents and domestic wastewater (Beltrán et al. 2001).

In addition to being used on its own, ozone can be used in conjunction with ultraviolet (UV) irradiation and hydrogen peroxide (H_2O_2). Combinations of these technologies, known as advanced oxidation technologies, allow for the generation of the hydroxyl

radical ($\cdot\text{OH}$) that has very powerful oxidizing abilities. This type of process is known as advanced oxidation technologies (Beltrán et al. 1997).

Brominated by-products are often created from reactions between ozone and bromine containing NOM. These are of primary concern as the bromate ion is currently classified as a possible human carcinogen, and as such, its presence in water is regulated (10 $\mu\text{g/L}$) (Singer and Reckhow 1999). The two most effective means of controlling the formation of bromate are lowering the pH of the solution and minimizing the concentration of residual ozone (Reckhow 1999). If bromate ions are formed, there are methods available for their removal. Chemical reduction using reduced sulfur compounds is common, as well as absorption with granular activated carbon (GAC), and decomposition by means of UV irradiation (Snoeyink and Summers, 1999).

Ozone Reactivity

Once it dissolves in water, ozone is a highly reactive molecule, and as such, there are many reactions occurring at the same time (Singer and Reckhow 1999). The two primary methods in which ozone will react in a system include: 1) direct reaction with molecular ozone; and 2) indirect reaction with radical species formed when ozone decomposes in water.

Direct reactions with molecular ozone are limited and selective; some reactions are rapid while others are slow. Alternatively, indirect reactions with $\cdot\text{OH}$ are fast and are not selective. Research has shown that reaction rates initiated by the $\cdot\text{OH}$ tend to be much

quicker, and range between 10^7 to 10^{10} 1/m·s (Singer and Reckhow 1999). Generally, the rate determining step for the oxidation of compounds by means of $\cdot\text{OH}$ is the rate at which the hydroxyl radicals are generated (Singer and Reckhow 1999).

Research on ozone reaction kinetics has been extensive, however, there are some discrepancies. Some studies report a second order reaction ($m = 2$) occurring in ozone demand free water, others report first order reactions ($m = 1$), while still others have determined the reactions to be pseudo-first order reactions (Gurol and Singer 1982, Sotelo et al. 1989). The variation in the reaction rates is attributed to the constituents in the water (Martin et al. 1992).

A simple kinetic model is as follows:

$$r = -\frac{d[\text{O}_3]}{dt} = k[\text{O}_3]^m \quad \text{Equation 2-1}$$

Where r = rate of decomposition of ozone [1/s]

k = reaction rate constant [1/s]

$[\text{O}_3]$ = concentration of ozone [mg/L]

m = order of reaction [dimensionless]

The kinetic rate constant (k) is a function of the pH of the system and the concentration of hydroxyl radical scavengers (Sotelo et al. 1989).

Oke et al. (1998) discussed the constantly decreasing decay kinetics of ozone. A model that takes into consideration the changing water characteristics is proposed as follows:

$$k = a + b \exp^{-c\Delta[O_3]} \quad \text{Equation 2-2}$$

Where k = specific ozone utilization rate [1/s]

a, b, c = kinetic parameters based on concentration – time data

ΔO_3 = change in ozone concentration

This formula uses the same basis as Equation 2-1, where k is replaced with the term k_w .

Ozone decomposition reactions are very fast, ranging from seconds to minutes. This characteristic of ozone implies minimal ozone residue will be found in treated water. As such, ozone is generally applied directly into microorganism reduction contactors as the primary disinfectant, with the addition of another disinfectant (i.e. chloramines) to supply a residual disinfectant concentration.

The auto-decomposition of ozone is affected by several factors: 1) temperature; 2) pH; 3) ultraviolet (UV) light; 4) concentration of ozone; 5) concentration of radical scavengers (carbonate and bicarbonate species); 6) hydrogen peroxide concentration; 7) ferrous ion concentration; and 8) natural organic matter concentration (Bablon et al. 1991, Singer and Reckhow 1999). Oke et al. (1998) also noted the influence of alkalinity and hardness on the decomposition of ozone.

At lower pH levels (≤ 7), the decay of ozone is dominated by direct reactions, and influenced only minimally by the initiation reaction caused by hydroxyl radicals (Sotelo et al. 1987, Masschelein 2000). As the pH level increases, the decomposition of ozone occurs due to the initiation reactions of the hydroxyl radicals and the presence of hydroxide ions. The hydroxide ions will subsequently generate hydroxyl radicals and peroxy radicals. At pH values greater than 9, the role of the hydroxide ion increases (Masschelein 2000).

Radical scavengers (bicarbonate and carbonate species) react with hydroxyl radicals, slowing down the chain of decomposition reactions (Singer and Reckhow 1999, Mariñas et al. 1993). This decrease in decomposition rate will result in one of two possibilities: 1) availability of ozone for direct and selective reactions increases; or 2) fewer hydroxyl radical oxidation reactions will occur (Bablon et al. 1991).

Ozone Contactors

The main objective of contacting units is to allow for contact time between ozone and constituents present in the liquid to be treated. These contactors must also effectively promote the mass transfer of ozone gas into the liquid phase. Finch et al. (2001) recommend that ozone contactors be designed in such a fashion as to ensure that a “maximum mass of ozone is introduced with complete, instantaneous mixing to further the chemical reaction”. Primarily, efficient ozone contactors are designed with consideration to the hydrodynamics of the contactor, the development of residual ozone, as well as the distribution of ozone in contacting units. However, the following

parameters must also be taken into account: 1) concentration-time (Ct) concept; 2) ozone transfer efficiency; 3) detention time; 4) ozone dose; 5) ozone residual; and 6) efficiency for oxidation or disinfection (Bellamy 1995).

Factors that may influence the efficiency of reactors include: 1) method of contacting the ozone gas and the liquid; 2) configuration of the contacting unit; 3) use of baffles and their placement in the contacting unit; 4) placement of the diffusing apparatus; 5) water flow rates that must be accommodated for; 6) the gas to liquid flow ratios with respect to the flow rates; and 7) the minimum rate (most efficient) of gas flow to achieve the ideal mixing and residual time (Bellamy 1995).

Hydrodynamics

To ensure the most efficient operating system, the hydrodynamics of ozone contactors must be accurately modeled. It is most useful to accurately model full-scale operations, under realistically more complex conditions. Some of the more important parameters that should be considered when modeling reactors include: 1) geometry of the reactor; 2) retention time; 3) dissolved ozone concentration throughout the reactor; 4) operational conditions of the system; and 5) mixing characteristics of all phases (Bellamy 1995).

Perhaps the most difficult parameter to model within a reactor is the mixing characteristics of the individual phases (gas phase and the liquid phase). The difficulty in modeling various phases lies simply in the fact that mixing is rarely ideal. The actual phases are not represented by the ideal mixing cases, but more as a combination of these.

Ideal cases that are easily modeled include: 1) batch reactors; 2) plug flow reactors; and 3) completely mixed flow reactors. However, in most cases, the approximation to ideal flow is not realistic. Particular to bubble columns, a portion of the liquid phase is backmixed, thus demonstrating less than ideal flow conditions (Deckwer et al. 1983). Consequently, models have been developed in an attempt to model the flow of gases and liquids in realistic situations. The developed models generally fall into two categories: 1) continuous models; and 2) discrete models. In both cases, the complexity of the model depends on the number of parameters used as input variables (Kaštánek et al. 1993).

Continuous (Differential) Models

At the time of their development, these models consisted of differential equations used to characterize the hydrodynamic behaviour of the ozone contactor. These models are derived for mixing conditions that deviate slightly from an ideal plug flow regime (Kaštánek et al. 1993). Generally, continuous models are used when describing turbulent flows in pipes, very long tubes with laminar flow, and others (Levenspiel 1999).

The most common differential model is the Axial Dispersion Model (ADM). The ADM assumes: 1) dispersion is represented by diffusion laws; 2) concentration profile is uniform in the radial direction; and 3) axial dispersion is uniform throughout the water column (Mariñas et al. 1993). The ADM resembles the plug flow regime, with some degree of backmixing superimposed on top (Zhou et al. 1994). Zhou et al. (1994) further described the backmixing process as being the redistribution of material by slippage or

eddies, repeated during the course of the flow of the fluid through the reactor. This model should be applied to systems that deviate only slightly from the ideal plug flow regime, such as cases where the ratio between the height and the diameter of a column is high (Kaštanek et al. 1993).

The ADM is based on the similarities between the axial mixing of a fluid and the diffusion of a fluid. As such, Fick's law of diffusion governs (Kaštanek et al. 1993):

$$\frac{dc}{dt} = D_L \cdot \frac{d^2c}{dx^2} \quad \text{Equation 2-3}$$

Where D_L = liquid axial dispersion coefficient = molecular diffusion + turbulent

diffusion [m²/s]

c = tracer concentration [mg/L]

x = axial coordinate [m]

If a convective flow (turbulent diffusion) is assumed, the dimensionless equation that describes the hydrodynamics of a bubble column becomes:

$$\frac{dC}{d\theta} = \left(\frac{1}{Pe_L} \right) \cdot \frac{d^2C}{dz^2} + \frac{dC}{dz} \quad \text{Equation 2-4}$$

Where $C = \frac{c}{c_0}$ Equation 2-5

$z = \frac{x}{L}$ Equation 2-6

$\theta = \frac{t \cdot u_L}{L}$ Equation 2-7

$Pe_L = \frac{u_L \cdot L}{D_L}$ Equation 2-8

C = dimensionless tracer concentration

c = tracer concentration [mg/L]

c₀ = mean tracer concentration in the reactor corresponding to a given
volume of pulse feed [mg/L]

z = dimensionless axial coordinate

x = axial coordinate [m]

L = characteristic length of the reactor [m]

θ = dimensionless time

t = time [s]

Pe_L = liquid phase Peclet number [dimensionless]

u_L = superficial velocity of convective liquid flow [m/s]

D_L = liquid phase diffusion coefficient [m²/s]

Mixing is generally caused by three mechanisms: 1) convection; 2) turbulent eddies; and 3) molecular diffusion (Yang et al. 1992). The degree of mixing is characterized by the dimensionless Peclet number (Pe_L). Intuitively, from the equation describing Pe_L, it is

obvious that as the superficial liquid velocity increases, the Pe_L will increase. In cases where the flow regime approaches that of plug flow (increasing u_L), Pe_L is equal to infinity. In situations when the flow regime differs significantly from the plug flow regime, $Pe_L = 0$ (i.e. completely mixed systems) (Kaštánek et al. 1993). Moustiri et al. (2001) also determined that the degree of liquid phase mixing depended on the superficial velocities of both the liquid and the gas: 1) at a specific u_L and as u_G increased, backmixing in the liquid phase decreased; and 2) at a specific u_G , backmixing in the liquid phase increased with an increase in u_L .

Other models included under the category of differential equations include (Kaštánek et al. 1993):

a) Multistage dispersion model

- i. The number of stages in the reactor, as well as the Pe_L number can define the backmixing of the fluid. Two parameters increase the model's flexibility and applicability; and
- ii. A combination of plug flow and axial dispersion flow.

b) Cross-flow model

- i. Existence of two liquid phase regions: plug flow and stagnant flow; and
- ii. Mixing occurs between these two regions.

c) Time-delay model

- i. Assumes plug flow of the liquid superimposed with fluid elements that rejoin the main fluid stream after a certain time delay.

Discrete (Combined) Models

When modeled under steady state conditions, discrete models generally result in sets of algebraic equations. The discrete models can be further divided based on the extent of fluid backmixing: a) single-stage combined models; and b) multistage (cascade) models. With these models, there are approximately four types of flows that are simultaneously occurring. These flows include zones of plug flow regime, axial dispersion flow regime, zones of perfect mixing, as well as dead zones. All these types of flow are interconnected by flow through the main flow stream, cross-flow stream, circulation flow stream, or bypass flow stream of the fluid (Kaštánek et al. 1993).

Discrete flow models are generally applied to situations where the flow of the fluid deviates only slightly from an ideal completely mixed regime. Some of the discrete models that have been developed were used to model mixing in areas in the reactor where it was assumed that no mixing occurred. In reality, however, there is some degree of mixing occurring in these zones. In other developed models, a slow exchange of mass between the perfectly mixed zone and the dead zones is assumed (Kaštánek et al. 1993).

Stagewise models that have been developed represent the axial mixing occurring in different stages of a reactor of constant volume. These stages are generally

interconnected by the main and backflow streams of the fluid. In these situations, the extent of the mixing is usually characterized using the number of stages in the reactor, the backflow ratio (backflow rate from the proceeding cell divided by the liquid flow rate through the reactor), and the parameters associated with the stagewise model that is being used (Kaštanek, 1993).

The simplest of the stagewise models, termed the cell model, is also referred to as the continuous flow stirred tanks in series (CFSTR in series). This model assumes that there is a series of perfectly mixed stages in the reactor and no backflow between stages. The mathematical equation describing the cell model is as follows (Kaštanek et al. 1993):

$$\frac{1}{N_{CFSTR}} = 2 \cdot \left(\frac{D_L}{u_L \cdot L} \right) - 2 \cdot \left(\frac{D_L}{u_L \cdot L} \right)^2 \cdot \left(1 - e^{-\frac{u_L \cdot L}{D_L}} \right) \quad \text{Equation 2-9}$$

Where N_{CFSTR} = number of cells in the modeled reactor

As the flow becomes less ideal, the backmixing of the liquid in the reactor stages can be modeled. A proposed relationship between the backflow of cells and the axial dispersion model is as follows (Kaštanek et al. 1993):

$$\frac{D_L}{u_L \cdot L} = \frac{f_e + \frac{1}{2}}{N_{CFSTR}} \quad \text{Equation 2-10}$$

Where f_e = backflow coefficient = ratio of backflow between adjacent stages to the net flow of a phase through the reactor

Variations on Equations 3 and 4 are extensive, each being based on the interconnectivity of the different reactor stages.

As was the case with continuous models, there is a term to describe the occurrence of backmixing. With respect to the cell models, this term is the backflow ratio (r). The relationship between the Peclet number and the backflow ratio is as follows (Smith and Gamal El-Din, 2002):

$$r = \frac{Q_B}{Q_L} = \frac{N_{BFCM}}{Pe_L} - 0.5 = \frac{D_L \cdot \varepsilon_L \cdot N_{BFCM}}{u_L \cdot L} - 0.5 \quad \text{Equation 2-11}$$

Where Q_B = back flow rate

Q_L = liquid flow rate

N_{BFCM} = number of cells in series

Pe_L = Peclet number of the liquid phase (dimensionless)

D_L = liquid-phase axial dispersion coefficient (m^2/s)

ε_L = liquid-phase holdup (dimensionless)

u_L = superficial liquid-phase velocity (m/s)

0.5 = refers to the perfect mixing level within each cell

Bubble Flow Regimes

In reactors, the prevailing hydrodynamic characteristics of the gas phase will depend on the bubbling regime. There are four primary regimes: 1) bubbly-flow; 2) turbulent; 3) slugging; and 4) homogeneous (Kaštánek et al. 1993).

The bubbly flow regime is characteristic of systems that display a nearly uniform distribution of bubble sizes throughout the reactor, as well as a uniform radial distribution of these bubbles. Generally, individual bubbles do not interfere with each other while rising, and have rise velocities equal to the rise velocity of free bubbles in an infinite liquid range. Bubble rise velocities range from 0.2 to 0.3 m/s in air water systems. Bubbly flow regimes are a characteristic of systems with low superficial gas velocities (≤ 0.05 m/s) (Kaštánek et al. 1993).

A mixture of large and small bubble sizes characterizes a turbulent flow regime, also termed heterogeneous flow regime. The bubbles in this system undergo simultaneous coalescence and break-up. In this system, bubble rise velocities can range up to 1 m/s (Kaštánek et al. 1993).

The slugging regime is also known as the plug-flow regime. This type of flow is generally found in bubble columns with diameters smaller than 0.15 m. The large bubbles tend to be comparable in size to the diameter of the column (Kaštánek et al. 1993).

The fully developed homogeneous bubbling regime can exist in turbulent flow situations. In these conditions, there is a demonstrated uniform bubble distribution, with the bubbles in close proximity to one another. As such, there is a nearly constant bubble rise velocity, and negligible interference (Kaštánek et al. 1993). Kulkarni et al. (1983), illustrated that the prevailing hydrodynamic condition occurring in a downflow bubble column is homogeneous flow. The authors noted that attaining homogeneous conditions in an upflow bubble column will occur only at $u_G < 0.05$ m/s. It has been reported that during the homogeneous bubbling regime, the gas hold-up is a linear function of the superficial gas velocity (Krishna et al. 1991, Moustiri et al. 2001). However, as the flow regime transitions to a heterogeneous flow, this linear dependence is no longer displayed (Krishna et al. 1991).

Gamal El-Din and Smith (2003b) studied the properties of bubbles produced in an impinging-jet bubble column using both digital photographic techniques and particle dynamics analyzer methods. They noted that the gas phase turbulence in the axial direction would increase at a near linear rate as u_G increased, and that when the superficial gas velocity was held constant, an increase in u_L resulted in an increase in gas phase turbulence. They further confirmed that, at low u_G values ($u_G \leq 4.5 \times 10^{-3}$ m/s), an increase in turbulence as u_L increased could be a result of the bubbly flow regime. This is discussed as being a result of decreasing Sauter mean bubble diameter causing an increase in the entrainment of gas bubbles in the reactor. Gamal El-Din and Smith (2003b) also noted that, at high u_G values ($u_G \geq 4.5 \times 10^{-3}$ m/s), the gas phase turbulence

in the axial direction decreased as u_L increased, most likely because the gas-liquid flow regime approached that of homogeneous bubbly flow regime.

The transition between the homogeneous bubbling regime and the turbulent flow regime must be considered, as the interfacial mass transfer rate can be significantly affected. It has been shown that in the homogeneous flow regime, higher gas hold-up values have occurred, resulting in higher specific interfacial areas and higher volumetric mass transfer rates (Kaštanek et al. 1993). Reilly et al. (1994) suggested that the transition from homogeneous to heterogeneous flow is highly dependent on the density of the gas phase; as the density of the gas increases, the superficial gas velocity at which the transition occurs increases. The critical superficial gas velocity at which the transition occurs will decrease with an increase in liquid viscosity (Deckwer and Schumpe 1993).

The transition between homogeneous and heterogeneous flow regimes was studied by Zahradník and Fialová (1996). The links between the bubbling regime and the mixing of individual phases were investigated. In their co-current bubble column, the extent of the mixing of both phases was characterized by their respective Peclet numbers. Prior to the transition from homogeneous flow to heterogeneous flow, the axial mixing of the gas was low, and increased linearly to the point of transition. In the heterogeneous flow regime, the extent of axial mixing varied slightly with the gas flow rate. At values of $u_G \geq 0.12$ m/s, the Peclet number remained constant, indicating that mixing was determined primarily by the extent of liquid circulation with a minimal effect from gas dispersion.

Bubble Columns

Bubble columns are perhaps the most common type of contactors, operated in many forms (single stage to six stages contacting units). These reactors can be operated in both co-current and counter-current flow, as well as in semi-batch modes (Charpentier 1981). Bubble columns are simple and inexpensive reactors capable of operating successfully when efficient and fast ozone dissolution is required, or when ozonation is required in situations where chemical reactions control the rate of the ozonation reactions. These reactors are highly efficient, displaying high mass transfer abilities, and lower energy requirements than other reactors (Bollyky 1981). The mass transfer efficiency in these reactors is influenced by the concentration of ozone in the gas phase, the gas and liquid flow rates, as well as the water depth and the size of bubbles created (Kuo and Yocum 1982).

According to Deckwer and Schumpe (1993) bubble column reactors offer the following advantages: 1) minimal maintenance; 2) high liquid phase content for reactions to occur; 3) superior heat transfer properties and temperature control; 4) good interphase mass transfer; 5) handles input of solids in the system; 6) minimal space requirements; and 7) cheap construction costs.

The main disadvantage of bubble columns is the large degree of liquid phase back-mixing that occurs. Proper modeling is therefore essential to make accurate estimates of its capabilities (Charpentier 1981, Deckwer and Schumpe 1993). Other disadvantages include: 1) high gas pressure drop due to the high static head of the liquid; 2) decrease in

the specific interfacial area for length/diameter ratios greater than 12 to 15 because of coalescence (coalescence may be minimized by inserting fixed or fluidized packings, grids, or perforated plates, or by pulsation); and 3) channelling of gas bubbles, as well as inadequate contact between the ozone and the liquid, can occur under low gas flow rates. Deckwer and Schumpe (1993) noted that the coalescence of bubbles is also a problem.

Zhou et al. (1994) determined that in the counter-current and co-current flows, the dissolved ozone profiles are affected by the extent of the backmixing process, the mass transfer process, and the decay of ozone. Zhou et al. (1994) stated that under identical operational conditions, the counter-current flow is much better than the co-current flow in terms of ozone absorption efficiency.

According to Briens et al. (1992), bubble columns operated in a liquid downflow regime resulted in larger gas hold-ups, when compared with bubble columns operating in a liquid upflow regime. In downflow bubble columns, the gas bubbles are forced to move opposite to their natural direction of buoyancy (Bando et al. 1988). As such, the residence time of the gas bubbles is longer, enhancing the efficiency of the reactor (Bando et al. 1988). The longer the bubbles are entrained in the liquid, the more time is available for the transfer of ozone gas into the liquid, making it available for disinfection. To ensure high reactor efficiency, the liquid velocity must be greater than the bubble rise velocity (Bando et al. 1988). If the liquid flow velocity is too low (smaller than the bubble rise velocity), gas will accumulate at the top of the reactor, thereby minimizing the amount of gas actually transferring into the reactor. It is therefore desirable that smaller bubbles are

produced, resulting in slower bubble rise velocities, and allowing for an increased rate of mass transfer. Also, the bubble size was found to vary with the liquid flow direction; bubbles were much larger in the liquid downflow operation (Briens et al. 1992). Finally, bubble columns operating in a liquid downflow regime demonstrated a volumetric liquid mass transfer rate nearly double that of bubble columns operating in a liquid upflow regime (Briens et al. 1992).

A counter-current bubble column was investigated by Hidaka et al. (1998). Based on their experiments, they determined that the gas hold-up increased with increasing liquid and gas velocities. With the increase in both gas and liquid flow velocities, the degree of liquid phase axial dispersion also increased.

Modifications With Jet Distributors

Bubble column reactors can be altered to modify the flow of liquid in the system, for example, with the addition of baffles. Other devices of interest included venturi injectors, jet reactors, ejectors, and tubular loop reactors. Charpentier (1981) illustrated that these alternative systems achieved higher gas phase dispersion, as well as intense mixing between the liquid and gas phases. These new designs have been shown to enhance the rate of mass transfer. The most notable advantage to using injectors is the high volumetric flow rate. This leads to higher shear rates, which result in smaller bubbles being formed, and thus the creation of higher interfacial areas (Charpentier 1981).

Higher shear rates caused by turbulence will create larger interfacial areas, thus enhancing the mass transfer of ozone. It was this general idea that led Gamal El-Din and Smith (2003a) to study the use of venturi injectors intersecting at a 125° angle in their impinging-jet bubble column. Pilot-scale tests were carried out and the results indicated that the intersecting venturi injectors significantly increased the mass transfer capabilities of the reactor.

Zhou and Smith (2000) also studied a venturi type injector, and determined that the gas bubbles formed by the venturi were smaller, due to the higher mixing intensity of the injector, than those formed in an alumina diffusing stone. Large interfacial areas were formed, enhancing the mass transfer rate.

Similar investigations regarding the performance of jet-pump application were observed by Wright et al. (1997). Experiments showed that this type of contactor displayed very high gas hold-up, as well as superior mass transfer capabilities. The mass transfer rate for this contactor was independent of the gas to liquid flow ratio.

The performance of venturi injectors was studied by Thalasso et al. (1995) in three different positions in the reactor: 1) completely emerged; 2) partially emerged with the outlet submersed; or 3) completely immersed. The highest rates of mass transfer were obtained when the venturi injectors were completely immersed.

Work carried out by Havelka et al. (2000) involved two ejectors operating in a co-current bubble column. The liquid-phase mixing in the column occurred primarily from the gas flow. The extent of liquid phase mixing increased (Pe_L for the liquid decreased) when the gas flow rate increased. For this reactor, it was shown that the volumetric liquid-side mass transfer coefficient is related solely to the gas hold-up of the system (Havelka et al. 2000).

Huynh et al. (1991) studied a bubble column reactor employing the use of a venturi injector positioned upward with a downstream bubble column. It was determined that this injector was capable of inducing high shear rates, thus preventing bubbles from coalescing, shearing bubbles into smaller bubbles, and creating a larger gas hold-up. When porous plates were introduced at the inlet of the bubble column, coalescence was visible. This led to larger bubbles with higher bubble rise velocities, and hence, smaller rates of mass transfer. Again, in comparing the porous plate distributor and the venturi “distributor”, it was determined that the gas hold-up in the bubble column was much larger with the venturi distributor, and higher volumetric mass transfer coefficients were obtained (Huynh et al. 1991).

A co-current downflow bubble column using an injection nozzle as a diffuser was studied by Bando et al. (1988). Since the rise velocity of the bubbles will increase as their diameter increases, the diffuser in the reactor must ensure the generation of bubbles with small diameters (Bando et al. 1988). For this reason, Bando et al. (1988) chose to use a gas-liquid injection nozzle as a sparger. Initially violent mixing and turbulent flow were

observed near the nozzle. Following this, as the distance from the nozzle increased, the flow became stable and approached the bubbly flow. Bando et al. (1988) noted that in the visually turbulent section of flow, gas hold-up was higher, and then decreased until it reached a constant in the section of bubbly flow. It was also noted that the diameter of the bubbles in the section of turbulent flow were smaller than those in the section of bubbly flow. The increase in bubble diameter is attributed to the coalescence of bubbles. In the turbulent section of flow, gas hold-up was larger than in the calm section. This observation is again attributed to the coalescence of bubbles.

Schulz and Prendiville (1993) investigated the use of a venturi sidestream injection system. They showed that turbulent mixing conditions prevailed, resulting in limited problems associated with bubble channelling. However, because the contact time in this injection system is minimal, proper design is required to ensure that the concentration-time criteria is sufficient to ensure adequate microbial reduction.

Schulz et al. (1995) further investigated the use of a sidestream injection contactor. Advantages to this type of contactor include: 1) mixing regime closely resembles plug flow regime; 2) injectors are less susceptible to plugging; 3) turbulent gas-liquid mixing leads to effective dissolution of ozone into water; and 4) improved mass transfer, and subsequently, disinfection efficiencies. However, drawbacks to this type of injection contactor include: 1) potential for gas-liquid segregation; 2) higher head losses introduced; 3) small contact time; and 4) additional booster pumping is required. Schulz et al. (1995) proposed a new configuration to the typical sidestream injection system.

This contactor uses the sidestream venturi injector in combination with a down flow tube (SVI-DT). A pilot study involving the use of this contactor was carried out to determine the SVI-DT hydrodynamic characteristics and ozone mass transfer and utilization rates. The SVI-DT contactor displayed a dispersed gas-bubble flow pattern. However, at variable superficial liquid velocities, the dispersed gas bubble flow patterns varied. Consequently, the gas hold-up was also altered. High rates of mass transfer were demonstrated (~ 95%). Ozone residuals and colour removal were greater than those found in conventional fine-bubble diffusion contactors (Schulz et al. 1995).

Modeling of Hydrodynamics

When considering the hydrodynamics of bubble columns, the flow pattern in the liquid is considered to be either: 1) Completely mixed flow; 2) Plug flow; or 3) Dispersed plug flow (Deckwer et al. 1983). The applicability of the completely mixed flow reactor is limited to columns with diameters > 0.3 m, or to columns with a small length to diameter ratio (Deckwer et al. 1983). It is further suggested that the actual flow pattern in a bubble column is close to the mixed regime, however, a considerable amount of backmixing occurs and must be taken into account (Deckwer et al. 1983).

The intensity of the backmixing at the reactor inlet creates a concentration jump within this vicinity. This jump in concentration is often interpreted as an area of enhanced mass transfer (Deckwer et al. 1983, Salazar et al. 1993).

In the experiments conducted by Zahradník and Fialová (1996), both homogeneous and heterogeneous flow regimes were studied in a bubble column under co-current flow conditions. Under homogeneous flow regimes ($u_G < 0.04$ m/s), the gas flow was approximated by the plug flow model. However, as the limiting superficial gas velocity increased past the point of transition ($u_G = 0.04$ m/s), a certain of gas and liquid backmixing occurred. The degree of gas phase backmixing was relatively small (backflow coefficient = 0.1) compared with the liquid phase backmixing (backflow coefficient ≤ 5). The mixing regime of both phases under heterogeneous flow conditions were modelled according to the back flow cell model (Zahradník and Fialová 1996). The work of Zahradník and Fialová clearly showed the variability of flow in bubble column reactors.

A study conducted by Borole et al. (1993) attempted to characterize the hydrodynamics of a bubble column using a 2-dimensional transient dispersion model. At the point of gas entry, there was a region of strong recirculation that was not accurately modeled using the dispersion model; it was suggested that the use of a variable dispersion coefficient might solve this problem.

Deckwer et al. (1983) evaluated the use of the axial dispersion model under various operating conditions. From their experiments, several conclusions were drawn: 1) the ADM should only be applied to regions in the bubble column reactors where completely developed dispersion flow patterns exist. Thus, the ADM should not be employed in regions close to the gas distributor, as a fully established dispersive flow occurs only after

the gas has travelled a certain distance; 2) the use of an incorrect model will lead to inaccurate dependencies, i.e. if the plug flow model (PFM) was employed, there was a resultant dependency on u_L (responsible for enhancing Pe_L), whereas if the ADM was employed, this dependency on u_L was rather insensitive to liquid mixing (Pe_L); and 3) when determining the $k_L a$ values, $k_L a$ is only slightly influenced by Pe_L . However, if this dependency was eliminated and the plug flow model (PFM) was employed, the concentration jump at the inlet of the reactor was misinterpreted as a zone of enhanced mass transfer, rather than a result of the partial backmixing of the liquid phase.

Zhou and Smith (1995) employed the back flow cell model (BFCM) to characterize the axial dispersion occurring in a bubble column. They noted that the mixing of this model was based on the exchange flow (i.e. flow from the cell closest to the inlet to the next cell) and on the back flow (i.e. from that 'next cell' back to the cell closest to the inlet of the reactor) between equally spaced cells. The backflow in the cells was assumed to represent what was occurring in the liquid phase, while the backflow was assumed to be negligible in the gas phase. Plug flow conditions in the gas phase (the number of cells is greater than 10) were presumed to prevail in their pilot scale bubble column. Further assumptions included: 1) the bubble column was operated under steady-state conditions; 2) the resistance to mass transfer was due to the liquid side interface; 3) the rate of ozone decay was negligible in the gas phase, but well represented by a pseudo first-order rate in the liquid phase; 4) the gas hold-up and the specific interfacial area were constant along the height of the bubble column reactor; and 5) Henry's law was applicable when modelling the ozone gas.

Zhou and Smith (1995) tested the applicability of the BFCM for modeling the mass transfer of ozone and derived algebraic mass balance equations between the cells in the bubble column reactor. The bubble column that was tested operated in both co-current and counter-current flow regimes. Ozone concentration profiles were fitted to the BFCM and used to determine estimates of $k_L a$. It was determined that the BFCM was able to describe the backmixing and dissolved ozone concentration profiles in the bubble column reactor. Zhou and Smith (1995) concluded that backmixing was affected by both gas and liquid flow rates.

Gamal El-Din and Smith (2001b) further deviated from the axial dispersion model and develop the alternative Transient Back Flow Cell Model (TBFCM). This model hypothesizes a series of cells resembling continuous flow stirred tank reactors (CFSTRs). These cells were interconnected by the back and exchange flows of the liquid. The gas was assumed to flow in plug flow manner throughout the height of the column. Five main assumptions govern this model: 1) backflow occurs only in the liquid phase; 2) because of the buoyancy of bubbles, backmixing in the gas phase was negligible; 3) the bubble column operates at constant gas and liquid flow rates; 4) no mass transfer or chemical decay was considered for the inert tracer; and 5) the gas hold-up and interfacial area of bubbles was constant along the height of the column. The uniqueness of this model lies in the fact that each cell in the TBFCM can be characterized by variable degrees of backmixing, as well as variable volumes due to changes in cross sectional area. The

resulting set of ordinary first-order differential equations are easily solved using simple numerical techniques.

Numerical RTD curves and experimental RTD curves (sampling in both co-current and counter-current modes of operation) indicated that this model can accurately predict backmixing in the liquid phase over a range of operating conditions. It was noted that as the gas flow rate increased, the backflow ratios increased in both modes of operation. Also, as the liquid flow rate increased, the backflow ratios decreased. This last effect was more pronounced in the co-current mode of operation (Gamal El-Din and Smith 2001a).

All of the above models were used in a variety of circumstances to predict the mixing that occurs in bubble column reactors. With the axial dispersion model and its variations, the degree of mixing can be described by the axial dispersion coefficient, or the Peclet number. In other cases, such as the TBFCM developed by Gamal El-Din and Smith (2001a), the backflow ratio serves as a representation of the degree of mixing that occurs in bubble columns.

Deckwer et al. (1974) performed experiments on two bubble columns, fitted with either a porous plate diffuser or a cross holding 56 nozzles. The bubble columns were operated in the co-current flow regime, with gas velocities no greater than 50 mm/s. To determine the dispersion coefficient in the bubble columns, both stationary and transient methods were employed, with analysis carried out using the axial dispersed plug flow model. This

resulted in an equation that could be used to determine the dispersion (i.e. backmixing) occurring in these two bubble columns. This equation is as follows:

$$D_L = 2.7 \cdot d^{1.4} \cdot u_G^{0.3} \quad \text{Equation 2-12}$$

Where D_L = axial dispersion coefficient [cm²/s]

d = diameter of the column [cm]

u_G = superficial gas velocity [cm/s]

The dispersion number is related to the backflow ratio by the formula:

$$r = \frac{N_{BFCM}}{Pe_L} - 0.5 = \frac{D_L \cdot \varepsilon_L \cdot N_{BFCM}}{u_L \cdot L} - 0.5 \quad \text{Equation 2-13}$$

Where ε_L = liquid hold-up [dimensionless]

The model proposed by Houzelot et al. (1985), who investigated the pre-mixing of gas and liquid in a tube, prior to its introduction into a bubble column, is very similar to the equation proposed by Deckwer et al. (1974). Houzelot et al. (1985) determined that the type of distributor did not change the axial dispersion in the bubble column. Superficial gas velocities ranged from 2.5×10^{-3} to 6×10^{-3} m/s, and the superficial liquid velocities ranged from 2.5×10^{-4} to 10^{-3} m/s. The equation that Houzelot et al. (1985) proposed to describe the axial dispersion in bubble columns is:

$$D_L = 0.04 \cdot u_G^{0.47} \quad \text{Equation 2-14}$$

Where D_L = axial dispersion coefficient [m²/s]

u_G = superficial gas velocity [m/s]

Kantak et al. (1994) used previously collected data from a large number of bubble columns operated in both two (gas – liquid) and three (gas – liquid – solid) phases, with varying superficial gas and liquid velocities. The outcome of their modeling efforts was:

$$D_L = 0.2 \cdot d^{1.25} \cdot \frac{u_G}{\varepsilon_G} \quad \text{Equation 2-15}$$

Where D_L = axial dispersion coefficient [cm²/s]

d = diameter of the bubble column [cm]

u_G = superficial gas velocity [cm/s]

ε_G = gas hold-up [dimensionless]

The study conducted by Marifñas et al. (1993) focused on investigating the hydrodynamics of packed and unpacked bubble columns, operated in both co-current and counter-current flow modes, using fine and coarse bubble diffusers. The data were analyzed using the transient dispersion model, assuming: 1) that the dispersion could be represented by diffusion laws; 2) the concentration profile was uniform in the radial direction; and 3) the axial or longitudinal dispersion was uniform throughout the bubble

column. A model was proposed to predict the dispersion occurring in their unpacked counter-current fine diffusing bubble column. It is as follows:

$$D_L = 0.00185 + 9.7 \cdot \frac{\text{Re}_G^{1/2}}{\text{Re}_L^{5/3}} \quad \text{Equation 2-16}$$

$$\text{Where } \text{Re}_G = \frac{u_G d_B}{\nu_L} \quad \text{Equation 2-17}$$

$$\text{Re}_L = \frac{u_L d_B}{\nu_L} \quad \text{Equation 2-18}$$

D_L = dispersion number

Re_G = gas phase Reynolds number [dimensionless]

Re_L = liquid phase Reynolds number [dimensionless]

u_G = superficial gas velocity [cm/min]

u_L = superficial liquid velocity [cm/min]

d_B = average bubble diameter [cm]

ν_L = kinematic viscosity of liquid [cm²/min]

Roustan et al. (1996) conducted experiments on a pilot-scale bubble column operating with a porous distributor in both co-current and counter-current flow regimes. Unlike the models discussed above, this bubble column was modeled based on mass balance equations describing stirred tanks in series. Tracer experiments revealed that the number of cells in the CFSTR model ranged from two to nine, indicating that the bubble column

could be characterized as either a well mixed reactor, or a plug flow reactor. Caution should be exercised here, as the modeling of a bubble column as a well-mixed reactor, or as a plug flow reactor, depends on the operating conditions (gas and liquid flow rates). A general trend observed under both flow regimes was an increase in the number of cells with increasing liquid flow rate. It was also observed that an increase in the gas flow rate resulted in a decrease in the number of cells predicted.

The following table illustrates other correlations that have been developed by researchers, relating the degree of mixing to the properties of the system.

Table 2-1: Correlations of axial dispersion coefficients proposed by previous researchers

Author	Reactor Details	Operating Conditions	Proposed Relationship
Deckwer et al. (1974)	2 bubble columns a- diameter = 20 cm height = 723 cm cross with 56 nozzles b- diameter = 15 cm height = 440 cm glass sintered porous plate	Co-current	$D = 2.7 \cdot d^{1.4} \cdot u_G^{0.3}$ $u_G = \text{cm/s}, d = \text{cm}, D = \text{cm}^2/\text{s}$
Houzelot et al. (1985)	Height = 4 m Diameter = 0.05 m	$u_G = 2.5 \times 10^{-3}$ to 6×10^{-3} m/s $u_L = 2.5 \times 10^{-4}$ to 1×10^{-3} m/s Various gas and liquids: Gas properties Viscosity Pressure Surface tension With and without perforated plate	$D = 0.04 \cdot u_G^{0.47}$ $u_G = \text{m/s}, D = \text{m}^2/\text{s}$
Kawagoe et al. (1989)	2 bubble columns Diameters: 0.159, 0.290 m Perforated plates 2 regions of flow: - inner annulus (center)- D_{G1} - outer annulus by wall- D_{G2} - inner and outer annulus- D_{G0}	$u_G = 10^{-2}$ to 10^{-1} m/s	$D_{G1} = 26.2 \cdot \left(\frac{u_G}{\varepsilon_G}\right)^{3.03} \cdot d^{1.79}$ $D_{G2} = 19.4 \cdot \left(\frac{u_G}{\varepsilon_G}\right)^{3.4} \cdot d^{2.1}$ $D_{G0} = 0.66 \cdot D_{G1} + 0.39 \cdot D_{G2} + 0.0078 \cdot \left(\frac{u_G \cdot h}{\varepsilon_G}\right)$ $u_G = \text{m/s}, d = \text{m}, h = \text{m}, D = \text{m}^2/\text{s}$
Mariñas et al. (1993)	height: 16 feet diameter: 6.375 inches crystalline alumina stone	Counter-current $u_G = 0.0226$ scfm $u_L = 440$ gpm	$D_N = 0.00185 + 9.7 \cdot \frac{\text{Re}_G^{\frac{1}{2}}}{\text{Re}_L^{\frac{3}{5}}}, D_N = \frac{D}{u \cdot L}$

			$D_N = \text{dispersion number, } u_G = \text{cm/min, } u_L = \text{cm/min,}$ $v_L = \text{cm}^2/\text{min, } d_p = \text{cm, } L = \text{cm}$
Kantak et al. (1994)	Various bubble columns from previously published research Diameters: 4.2 to 320 cm	Churn-turbulent flow regime With and without solids $u_G = 0$ to 85 cm/s	$D = 0.2 \cdot d^{1.25} \cdot \frac{u_G}{\varepsilon_G}$ $u_G = \text{cm/s, } d = \text{cm, } D = \text{cm}^2/\text{s}$
Chen et al. (2002)	Diameter: 15.8 cm Height: 1.33 m Perforated ceramic plate	$u_G = 1.33$ to 9.48 mm/s $u_L = 1.42$ to 4.25 mm/s	$D = 1.696 \cdot u_G^{0.803}$ $u_G = \text{mm/s, } D = \text{m}^2/\text{s}$
Shawaqfeh (2002)	Diameter: 7.4 cm Height: 63 cm 2 nozzles injecting into a perforated plate	$Q_G = 22$ to 105 L/min $Q_L = 0.61$ to 0.32 L/min	$D = a \cdot u_G^b \cdot \exp(c \cdot u_L)$ <p>Flow: $a = 0.014 \pm 0.0015$ $b = 0.45 \pm 0.059$ $c = -48.85 \pm 7.492$</p> <p>Pseudo-Batch: $a = 0.014 \pm 0.0016$ $b = 0.43 \pm 0.064$ $c = -27.86 \pm 8.176$</p> $u_G = \text{m/s, } u_L = \text{m/s, } D = \text{m}^2/\text{s}$

To predict the backmixing of the gas phase in bubble column reactors, Shetty et al. (1992) proposed a two-bubble-class hydrodynamic model to measure the residence time distribution of the gas phase. This model is applicable to conditions with high superficial gas velocities, where the gas flow regime changes from homogeneous flow to turbulent flow. At this point, the large bubbles flow through the column in a plug flow manner. The smaller bubbles, however, have lower rise velocities, and were circulated with the liquid, following its backflow through the reactor. As a result, the smaller backmixing bubbles could be modeled using the ADM. Shetty et al. (1992) concluded that the gas phase backmixing of a bubble column was heavily dependent on the superficial gas velocity, and somewhat dependent on the diameter of the column. The hydrodynamic model proposed by Shetty et al. (1992) was verified through a comparison of the predicted residence time distribution (RTD) curves with the RTD curves from literature experimental data, as well as their own experimental data. However, the authors acknowledged the need to incorporate the effects of bubble coalescence and break-up.

In a similar manner, Kawagoe et al. (1989) assumed two bubble groups were present in a bubble column reactor employing perforated plates. Larger bubbles were present in the centre of the column, and smaller bubbles occurred along the column walls. Within the central core, the larger bubbles had increased bubble rise velocity, resulting in more intense gas phase mixing, but shorter residence times than the smaller bubbles situated in the annulus beside the bubble column wall. Nonetheless, Kawagoe et al. (1989) applied the ADM to characterize the gas phase hydrodynamics in both the central core of larger bubbles, and the peripheral annulus of smaller bubbles. Two separate models were

developed. The application of this model is based on: 1) gas velocity; 2) column diameter; and 3) liquid system properties.

Gas Hold-up

Gas hold-up (ε_G) can be simply described as the ratio of the volumetric fraction of gas to the total volume (volumetric gas fraction and volumetric liquid fraction) of the reactor. Gas hold-up is not a constant quantity, as it varies in both the axial and radial directions (Deckwer and Schumpe 1993). The gas hold-up can be estimated as follows:

$$\varepsilon_G = \frac{V_G}{V_G + V_L} \quad \text{Equation 2-19}$$

Where ε_G = gas hold-up [dimensionless]

V_G = Volume of gas [m³]

V_L = Volume of liquid [m³]

The gas hold-up of a system gives insight into other key parameters, such as mass transfer, and is essential to achieving efficient reactor designs (Deckwer 1992, Kaštánek et al. 1993). Knowing the gas hold-up of a system, it is possible to determine the interfacial area of the gas bubbles in the system, and therefore, to determine the mass transfer rate of the reactor (Deckwer 1992, Kaštánek et al. 1993).

Gas hold-up is easily measured using pressure profiles. The difference in pressure measured at various points along the column, in addition to the known properties of the gas, will give an estimation of the gas hold-up in the system:

$$\varepsilon_G = 1 - \frac{\Delta P}{\rho_L \cdot g \cdot \Delta x} \quad \text{Equation 2-20}$$

Where ΔP = pressure difference

ρ_L = density of the liquid [g/cm³]

g = acceleration due to gravity [cm/s²]

Δx = difference in two measuring points [cm]

The gas hold-up of a system is dependent on the superficial gas velocity (u_G) and superficial liquid velocity (u_L) of the system (Deckwer, 1992). If u_L is low, it could be assumed that gas hold-up is not significantly affected by this parameter; in this case, gas hold-up becomes a function of the gas velocity only (Deckwer, 1992). A near linear dependence of gas hold-up on superficial gas velocity is often observed when on a log scale (Biñ et al. 2001).

$$\varepsilon_G = a \cdot u_G^b \quad \text{Equation 2-21}$$

Where a = coefficient of correlation

b = a function of the flow regime in the reactor, the gas distributor, and the properties of the individual phases.

Deckwer (1992) indicated that the type of distributor had a major influence on the gas hold-up of bubble columns. He indicated that gas hold-up would be increased by distributors used in the following order: 1) perforated plates; 2) sintered plates; 3) injector nozzles; 4) ejector nozzles. It was also observed that gas hold-up would increase with the presence of small bubbles in the reactor. This was attributed to the smaller rise velocities in comparison to those of larger bubbles. With the slower rise velocity, the bubbles were retained in the reactor for longer periods of time, thus increasing the gas hold-up. Again, the type of distributor affected bubble coalescence. It was worth noting that the gas hold-up of a system was independent of the scale of the reactor (i.e. diameter of tubular reactors) (Forret et al. 2003).

The mode of operation of a bubble column will also affect the gas hold-up of the system. Roustan et al. (1996) showed that, in a pilot-scale bubble column where the gas was distributed with a ceramic porous diffuser, co-current flow operations had the lowest gas hold-up, followed by batch flow, and finally counter-current flow (largest gas hold-up).

As was previously discussed, there was an increased degree of mixing near the inlet of the reactor, which increases the transfer of gas into the liquid. As a result, a higher

amount of gas hold-up was measured near the bottom of the bubble column reactor (Biň et al. 2001).

Zahradník et al. (1997) performed experiments with two different types of plate distributors, creating either the homogeneous flow regime or the turbulent flow regime. With respect to the distributor creating the homogeneous flow regime, the authors determined that there was a significant increase in gas hold-up as the aspect ratio (height of column/diameter of column) decreased. A relationship of this type was not demonstrated in the heterogeneous flow regime.

Deckwer and Scumpe (1993) illustrated that an increase in gas-density caused an increase in the gas hold-up of the system, due to a reduction in the size of bubbles formed. The bubbles with a smaller rise velocity are retained for a longer period of time in the reactor.

There are many correlations that attempt to predict the gas hold-up of a bubble column reactor under varied operating conditions. These include: sparger type, bubble column diameter and height, packed or unpacked columns, physical properties of the gas and the liquid, presence of a third phase (solids), or flow regime. However, the two main consistencies when modeling for gas hold-up is the dependency on superficial gas and/or liquid velocities.

Other influences on the gas hold-up include gas density and liquid viscosity (Friedel et al 1980), as well as the design of the sparger. Huynh et al (1991) determined that a

venturi/bubble column combination yielded significantly larger gas hold-up values than the porous plate distributor that was also tested. Although it was determined by Patil et al. (1984) that sparger design did not significantly influence gas hold-up in their sectionalised bubble column, they suggested that in a bubble column operating as one section, the sparger design might have a predominant effect.

The influence of flow regime on the gas hold-up of a system has also been discussed. Although not studied, this phenomena is worthy of discussion. Many authors have studied the transition between flow regimes and the resulting gas hold-up in these flow regimes (Gavrilescu and Tudose 1996, Kago et al. 1989, Krishna et al. 1991, Krishna and Ellenberger 1996, Sarrafi et al. 1999, Shetty et al. 1992). Each of the authors noted above describes the transition between the homogeneous bubbly regime and the churn-turbulent regime. It has been noted that in the homogeneous flow regime, the gas hold-up increased linearly as the superficial gas velocity increased. As the flow approached the transition flow regime, there was a slight decrease in the gas hold-up. As the flow approached the churn-turbulent regime, there was an increase in the gas hold-up of the system. In some instances, this increase was either linear or nearly linear. In the heterogeneous (churn-turbulent) flow regime, the increase in gas hold-up was less pronounced than in the homogeneous flow regime. These observations occurred in bubble columns operating with many types of gas distributors: glass filters, stainless filters, perforated plates, spider spargers, and single orifice spargers.

In the case of Zahradník et al. (1997), the ejection system was operated in a batch flow regime under two conditions: 1) free suction (ejection) 2) forced gas supply (injection). In the case of free suction, it was concluded that the gas hold-up was well described by their exponential model. With respect to the forced gas supply mode of operation, the dispersion efficiency decreased as the gas feed rate increased, and with this increase in gas feed rate there was an increase in the non-uniformity of the gas hold-up distribution.

Huynh et al. (1991) studied the use of a bubble column employing venturi distributors, and a bubble column using a porous plate distributor at the outlet of the venturi. Superficial liquid velocities ranged between 0.175 and 0.350 m/s and superficial gas velocities ranged between 0.03 and 0.25 m/s. Using a venturi distributor, the authors observed less coalescence of bubbles, resulting in larger gas hold-up values. It was also postulated that the higher shear stresses created by the venturi injectors led to a larger amount of smaller bubbles, further enhancing gas hold-up. However, when the air passed through the porous plate, the authors noted a significant amount of coalescence only 0.10 m downstream from the point of gas injection. The authors clearly demonstrated that, at any superficial gas velocity, the venturi distributor resulted in larger gas hold-up.

The following table serves only as a brief summary of some of the previous gas hold-up correlations that have been proposed in the literature, along with their operating conditions.

Table 2-2: Correlations of gas holdup proposed by previous researchers

Author	System Characteristics	Range of Parameters	Correlation Proposed
Kato and Nishiwaki (1972)	3 bubble columns a- diameter = 6.6 cm height = 201 cm b- diameter = 12.2 cm height = 200 cm c- diameter = 21.4 cm height = 405 cm Perforated plates with holes of varying diameters	Co-current $u_G = 0.5$ to 25 cm/s	$\varepsilon_G = \frac{u_G}{31 + 4.5 \cdot u_G^{0.8} \cdot (1 - e^{-0.040 \cdot u_G^{1.8}})}$ $u_G = \text{cm/s}$
Akita and Yoshida (1973)	Diameter: 15.2 cm Height: 400 cm Gas sparger: Single hole drilled into centre of plate	Continuous gas flow Batch liquid flow $V_G = 19.1$ to 1510 m/h	$\frac{\varepsilon_G}{(1 - \varepsilon_G)^4} = 0.2 \cdot \left(\frac{g \cdot d^2 \cdot \rho_L}{\gamma} \right)^{\frac{1}{8}} \left(\frac{g \cdot d^3}{v_L^2} \right)^{\frac{1}{12}} \left(\frac{u_G}{\sqrt{g \cdot d}} \right)$ $g = \text{cm/s}^2, d = \text{cm}, u_G = \text{m/h}, \rho = \text{g/cm}^3, v = \text{g/cm} \cdot \text{s}, \gamma = \text{g/s}^2$
Kumar et al. (1976)	3 bubble columns diameter: 5, 7.5, 10 cm Conical entrance to bubble column Orifice plates at conical entrance with varying dimensions	$u_G = 0.14$ to 14.01 cm/s	$\varepsilon_G = 0.728 \cdot u_G^* - 0.485 \cdot (u_G^*)^2 + 0.975 \cdot (u_G^*)^3$ $u_G^* = u_G \cdot \left\{ \frac{\rho_L^2}{\gamma \cdot (\rho_L - \rho_G) \cdot g} \right\}^{\frac{1}{4}}$ $g = \text{cm/s}^2, u_G = \text{cm/s}, \rho = \text{g/cm}^3, \gamma = \text{dyne/cm}$
Zahradnik and Kaštánek (1979)	2 bubble columns diameter: 0.152, 0.292 m brass sieve plate	turbulent bubble regime batch liquid flow continuous gas flow $u_G = 0.031$ to 0.276 m/s	$\varepsilon_G = \frac{u_G}{0.3 + 2.0 \cdot u_G}$ $u_G = \text{m/s}$

Friedel et al. (1980)	Diameter: 0.15 m Height: 2.3 m Four radially mounted gas sintered plates	Downflow	$\varepsilon_G = \left(\frac{1 + 0.685 \cdot \frac{(1 - \varepsilon^*)^{3.112}}{\varepsilon^{*0.395}} \cdot \left(\frac{\rho_L}{\rho_G} \right)^{0.0346}}{\left(\frac{\mu_L}{\mu_G} \right)^{0.254} \cdot Fr^{0.36} \cdot We^{0.543}} \right)^{-1}$ $\varepsilon^* = \frac{Q_G}{Q_G + Q_L}, Fr = \frac{I^2}{g \cdot d}, We = \frac{I^2 \cdot d}{\rho_L \cdot \sigma}$ <p>I = total mass flow density (kg/m²s) Q = cm³/s, ρ = g/cm³, μ = mPa·s, g = cm/s², d = cm, σ = mN/m</p>
Otake et al. (1981)	Diameter: 0.05 m Height: 1.5 m 2 types of multi-nozzles 2 types of single nozzles	Co-current Counter-current Upflow u _G = 7x10 ⁻³ to 8.24x10 ⁻² m/s u _L = Counter-current: up to 1.4x10 ⁻¹ m/s Co-current: up to 1.5x10 ⁻¹ m/s	$\varepsilon_G = 0.38 \cdot u_G^{0.86} \cdot \exp\left(\frac{-2.49 \cdot u_L}{\sqrt{g \cdot d}}\right)$ <p>For uniform bubbly flow u_G = m/s, u_L = m/s, g = m/s², d = m</p>
Ohkawa et al. (1985)	Diameters: 5, 6, 7 cm Height: 2.0 m Nozzle injectors	Downflow u _L = 13.0 to 20.0 m/s	$\varepsilon_G = 3.96 \times 10^{-1} \cdot u_L^{0.78} \cdot \left(\frac{d_n}{d}\right)^{-1.56} \cdot L_j^{0.38}$ <p>d_N diameter of nozzle (m), L_j – liquid jet length (m), u_L – m/s</p>
Sada et al. (1986)	Diameter: 7.8 cm Height: 150 cm Perforated plate gas distributor	Liquid: batch flow Gas: continuous flow	$\frac{\varepsilon_G}{(1 - \varepsilon_G)^4} = 0.046 \cdot u_G$ <p>For the churn-turbulent regime u_G = m/s</p>
Idogawa et al. (1987)	Diameter: 0.05 m Height: 0.83 m Perforated plate	Liquid: batch flow Gas: continuous flow	$\frac{\varepsilon_G}{(1 - \varepsilon_G)} = 0.059 \cdot u_G^{0.8} \cdot \rho_G^{0.17} \cdot \left(\frac{\sigma_L}{72}\right)^{-0.22 \exp(-P)}$

			$u_G = \text{cm/s}, \rho = \text{kg/m}^3, \sigma = \text{mN/m}, P_i = \text{MPa}$
Uchida et al. (1989)	Diameter: 4.6×10^{-2} m Height: 1 m Porous glass ball filter with a nozzle		$\frac{u_G}{\varepsilon_G} = 0.175 \cdot \left(\frac{g \cdot d^2 \cdot \rho_L}{\sigma} \right)^{-\frac{1}{8}} \cdot \left(\frac{g \cdot d^3}{\nu^2} \right)^{-\frac{1}{12}} \cdot \left(\frac{d \cdot u_s}{\nu} \right)^{\frac{1}{2}} (g \cdot d)^{\frac{1}{2}}$ $+ 3.5 \times 10^{-3} \cdot \left(\frac{g \cdot d^2 \cdot \rho_L}{\sigma} \right)^{\frac{3}{4}} \cdot \left(\frac{d_B \cdot u_s}{\nu} \right)^{\frac{2}{7}}$ $\times (1 + 0.85 \cdot \varepsilon_G) \cdot (u_L + u_G)$ $d = \text{m}, g = \text{m/s}^2, \sigma = \text{N/m}, \rho = \text{kg/m}^3, \nu = \text{m}^2/\text{s}, d_B = \text{m}, u_s = \text{m/s}, u_G = \text{m/s}, u_L = \text{m/s}$
Yamagiwa et al. (1990)	4 bubble columns Diameter: 0.034, 0.005, 0.060, 0.070 m Height: 1.20, 1.50, 1.80, 2.00 m Cylindrical nozzle	Downflow $Q_L = 3.17 \times 10^{-4}$ to 2.00×10^{-3} m ³ /s	$\varepsilon_G = 9.96 \times 10^{-3} \cdot Fr^{0.06} \cdot Re^{0.17} \cdot \left(\frac{d_N}{d} \right)^{-0.60} \cdot \left(\frac{L_j}{d_N} \right)^{0.35}$ $d_N = \text{m}, d = \text{m}, L_j = \text{m}$
Huynh et al (1991)	Diameter: 0.095 m Height: 0.79 m Venturi injector Porous plate	$u_L = 0.175$ to 0.350 m/s	$\varepsilon_G = 0.2087 \cdot u_G^{0.700} \cdot u_L^{-0.5147}$ Porous Plate Distributor $\varepsilon_G = 1.106 \cdot u_G^{0.70} \cdot u_L^{0.1540}$ Venturi/Bubble column combination $u_G = \text{m/s}, u_L = \text{m/s}$
Krishna et al. (1991)	Diameter: 0.16 m Height: 1.2 m	Churn-turbulent flow Homogeneous bubble flow	For homogeneous bubble flow regime: $\varepsilon_G = 4 \cdot u_G$ $u_G = \text{m/s}$
Borole et al. (1993)	Diameter: 61 cm Conical bottom	Co-current $u_G = 3, 6, 8, 9$ cm/s $u_L = 0, 0.45, 0.6$ cm/s	$\varepsilon_G = 0.25 \cdot u_G^{0.3} \cdot \left[3.0 - 3.3 \cdot \left(1 + \frac{d_{\text{cone}}}{d_{\text{cyl}}} \right) + \left(1 + \frac{d_{\text{cone}}}{d_{\text{cyl}}} \right)^2 \right]$

			$d_{\text{cone}} = m, d_{\text{cyl}} = m, u_G = m/s$
Reilly et al. (1994)	Diameter: 0.15 m Height: 2.7 m Gas sparger: 4 tubes with holes	Liquid: batch flow Gas: continuous flow	Bubbly Flow Regime: $\epsilon_G (1 - \epsilon_G) = 2.84 \cdot \rho_G^{0.04} \cdot u_G \cdot \sigma^{-0.12}$ $\rho = \text{kg/m}^3, u_G = \text{m/s}, \sigma = \text{N/m}$
Kundu et al. (1995)	Diameter: 51.6 mm Height: 2030.0 mm Nozzle ejector system 6 nozzles with varying diameters	Co-current Downflow $Q_L (\text{m}^3/\text{s}) = (0.07-0.34) \cdot 10^{-3}$ $Q_G (\text{m}^3/\text{s}) = (0.16-360.0) \cdot 10^{-6}$	$\epsilon_G = 1 - \exp(-6.87 \times 10^{-3} \text{Re}_L^{0.16} A_r^{0.17} H_r^{-0.22} Su^{1.15} Mo^{0.58})$ 88 <math>\langle \text{Re}_L \rangle < 10481</math> Reynolds number of the liquid based on the contactor diameter, $(\rho_L V_L d_c) / \mu_L$ 29.03 <math>\langle A_r \rangle < 169.78</math> area ratio of contactor to nozzle $(d_c/d_n)^2$ 1 <math>\langle H_r \rangle < 31</math> height ratio of the liquid column inside the contactor to the diameter of the contactor (h_c/d_c) $0.375 \times 10^5 < Su < 0.574 \times 10^7$ Suratmann number, $(\sigma_L \rho_L d_c) / \mu_L^2$ $0.111 \times 10^{-10} < Mo < 0.517 \times 10^{-6}$ Morton number, $(\rho_L \sigma_L^3) / (g \mu_L^4)$ $\rho = \text{kg/m}^3, V = \text{m/s}, \mu = \text{kg/ms}, d_c = m, d_n = m, h_c = m, \sigma = \text{N/m}, g = \text{m/s}^2$
Laari et al. (1997)	2 bubble columns a- diameter: 0.19 m height: 0.67, 1.26, 1.765 m T-junction nozzle b- diameter: 0.97 m height: 4.64 m 3 T-junction nozzles	Bubble column a: $u_G = 1$ to 3 cm/s Bubble column b: Max $u_G = 550 \text{ dm}^3/\text{min}$ Max $u_L = 50 \text{ dm}^3/\text{min}$	$\epsilon_G = 1.801 \cdot u_G^{0.923} \cdot \frac{P_{KIN}}{V_{MIX}} \left(\frac{P_{KIN}}{V_{MIX}} \right)_{CR} = 2173 \frac{W}{m^3}$ $\epsilon_G = 1.801 \cdot u_G^{0.923} \left(\frac{\frac{P_{KIN}}{V_{MIX}}}{\left(\frac{P_{KIN}}{V_{MIX}} \right)_{CR}} \right)^{0.0751}$

			$\frac{P_{KIN}}{V_{MIX}} \left(\frac{P_{KIN}}{V_{MIX}} \right)_{CR} = 2173 \frac{W}{m^3}$
			$u_G = \text{m/s}$
Zahradnik et al. (1997)	Diameter: 0.29 m Height: 3 m Ejector distributor	Semi-batch flow $Q_L = 2.0 - 7.2 \text{ m}^3/\text{h}$ $Q_G = 1 - 18.3 \text{ m}^3/\text{h}$	$\varepsilon_G = 2.81 \cdot u_G^{0.9}$ $u_G = \text{m/s}$
Yamashita (1998)	Diameter: 0.16 m Height: 3 m Sparger: pipe with two holes	Gas: continuous feed Takes into account the three zones in a bubble column: 1- entrance region 2- bulk region 3- foam layer	$\varepsilon_M = 1 - (1 - \varepsilon_b) \left[\frac{(H_L - H_N)}{H_L - H_N + (4.8 \times 10^{-2} \cdot u_G^{0.36})} \right]$ $H_L = \text{clear liquid height (m)}$ $H_N = \text{gas inlet height (m)}$ $u_G = \text{m/s}$
Chen et al. (2002)	Diameter: 15.8 cm Height: 1.33 m Perforated ceramic plate	$u_G = 1.33 \text{ to } 9.48 \text{ mm/s}$ $u_L = 1.42 \text{ to } 4.25 \text{ mm/s}$	$\varepsilon_G = 5.168 \cdot u_G^{1.063}$ $u_G = \text{mm/s}$
Shawaqfeh (2002)	Diameter: 7.4 cm Height: 63 cm Nozzle with perforated plate	$Q_G = 22 \text{ to } 105 \text{ L/min}$ $Q_L = 0.61 \text{ to } 3.2 \text{ L/min}$	$\varepsilon_G = 0.775 \cdot u_G^{0.657}$ $u_G = \text{m/s}$
Anabtawi et al. (2003)	2 bubble columns: a- rectangular 0.0195 x 0.22 x 1.0 m b- cylindrical diameter: 0.074m height: 1.0 m gas nozzle	Co-current Upflow	Column a: $\varepsilon_G = 0.549 \cdot u_G^{0.81} \cdot \mu^{-0.15} \cdot H^{-0.22}$ Column b: $\varepsilon_G = 0.362 \cdot u_G^{0.60} \cdot \mu^{-0.24} \cdot H^{-0.38}$ $H = \text{clear liquid height (m)}, u_G = \text{m/s}, \mu = \text{Pa}\cdot\text{s}$
Mandal et al. (2003)	Conical entrance Ejector assembly High velocity liquid jet	Downflow $Q_L = 1.68 \times 10^{-4}$ $3.02 \times 10^{-4} \text{ m}^3/\text{s}$ $Q_G = 0.083 \times 10^{-4}$	$\varepsilon_G = 0.365 \cdot \text{Re}_L^{-0.164} \cdot \text{Mo}^{-0.029} \cdot A_r^{0.032} \cdot H_r^{0.207}$

Akosman et al. (2004)	Diameter: 0.05 m Height: 0.8 m Orifice ejector	1.22x10 ⁻⁴ m ³ /s Co-current Downflow u _G = 2x10 ⁴ to 6x10 ⁴ m/s	$\varepsilon_G = 1.73 \cdot \left(\frac{P}{V}\right)^{0.52} \cdot u_G^{0.82} \cdot \left(\frac{\sigma}{\sigma_w}\right)^{13.3}$ $\frac{P}{V} = \frac{\frac{1}{2} \cdot \rho_L \cdot F_L \cdot u_0^2}{V \cdot (1 - \varepsilon_G)} = \text{power input per liquid volume in column}$ <p>F_L = fluid number, u₀ = superficial liquid velocity in nozzle, V = volume u_G = m/s, u₀ = m/s, σ = mN/s, ρ = kg/m³, F_L = m³/s, V = m³</p>
-----------------------	--	--	--

Bubble Properties

As previously mentioned, the efficient design of a bubble column reactor depends largely on the gas hold-up of the system, which in turn depends on the properties of the bubbles. One of the most important properties of the bubbles is their size; the larger the exposed bubble surface area, the larger the mass transfer rate of the system. The diameter of bubbles in the reactor is dependent on: 1) the diameter of the primary bubbles formed exiting the diffuser; 2) the diameter of the bubbles in equilibrium in the reactor; and 3) the rate of coalescence and/or shearing of bubbles (Voigt and Schügerl 1979).

There are several methods currently in use to measure bubble diameter. The first method involves the measurement of the mass transfer of a gas into the liquid phase, also described as gas phase conversion. This chemical method is essentially based on the chemical rate of absorption, and has been successfully applied by many investigators (Kulkarni et al. 1983, Kumar et al. 1976, Meikap et al. 2001, Radhakrishnan and Mitra 1987).

A second method employs the use of an electric probe, and has been used by several researchers (Yamashita et al (1979), Idogawa et al. (1987), Roustan et al. 1996). This technique is an intrusive method that involves the placement of probes inside the bubble column. Signals are sent from one probe to another, placed a set distance away. The time it takes the signal to go from one probe to another is affected by the presence of bubbles. In a study conducted by Yamashita et al. (1979), the probes were set vertically into the bubble column and the rising velocity of a bubble was calculated. The vertical length of

the bubble was determined based on the contact time of the bubble with the probe and the time required for passage between the two probes (Yamashita et al. 1979).

A very common non-invasive technique is the use of photographs. Cameras are set at a certain distance the bubble column, and photographs of the bubbles are taken. From these photographs, bubble diameters can be easily determined. However, the photographic technique is only capable of giving accurate results for bubbles near the walls of the bubble column. Other methods of bubble measurement include gas disengagement techniques, or the use of lasers.

There is also some discrepancy as to what occurs throughout the length of the bubble column. Akita and Yoshida (1974) and Lage and Espõsito (1998) propose that bubble sizes are dependent on the balance between the rates of coalescence and break-up of individual bubbles. It has been further suggested by Winterton (1994) that the system must be in equilibrium with respect to the rate of coalescence and break-up (steady-state conditions) before an accurate representation of bubble diameters can be provided.

Furthermore, Akita and Yoshida (1974) noted that the initial bubble size is independent of surface tension, liquid viscosity, liquid density and gas density. However, these results do introduce conflicting information, as it is known that the properties of the water (i.e. surface tension, temperature) can influence the size of bubbles, i.e. larger gas bubbles can be created in soapy water than in clean water. Idogawa et al. (1987) proposed that the diameter of a bubble is independent of the gas velocity of the system, and that the

pressure exerted on the system has no effect on bubble size. However, Idogawa et al. (1987) proposed that as the gas density increases, bubble diameter will decrease, and that as the surface tension increases, the diameter of the bubbles increases. The authors noted that the bubble characteristics were independent of viscosities up to 3MPa, and were dependent on the surface tension below 5 MPa. Because of discrepancies of this nature, Meikap et al. (2001) suggested that, because bubble column mixing and flow patterns are complex to model, correlations should be based primarily on the dynamic and geometric properties of the bubble column reactor being used i.e. phase flow rates, diameter of bubble column.

The count mean bubble diameter of the bubbles in bubble columns is defined as:

$$d_B = \frac{\sum_{i=1}^{i=N} d_i}{N} \quad \text{Equation 2-22}$$

Where N = total number of bubbles

d_i = diameter of the i^{th} bubble

The Sauter bubble diameter (d_s) is required to calculate the interfacial area of the system, and is calculated as follows:

$$d_s = \frac{\sum n_i d_i^3}{\sum n_i d_i^2} \quad \text{Equation 2-23}$$

Where n_i = number of bubbles with diameter d_i

Where d_i is determined through two methods:

Method 1: $d_i = \sqrt[3]{a^2 b}$ Equation 2-24

Method 2: $d_i = \frac{a + b}{2}$ Equation 2-25

Where a = length of the bubble

b = height of the bubble

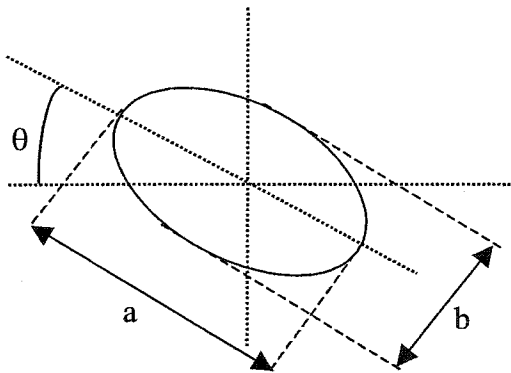


Figure 2-1: Definition of measurement lengths and angles of bubbles, adapted from Yamashita et al. (1979)

Akita and Yoshida (1974) determined that, because of the coalescence and break-up rates inside bubble columns, bubbles sizes should always be measured in the middle of the column. The coalescence and break-up rates are functions of superficial gas velocity, superficial liquid velocity, as well as properties of the liquid. Moustiri et al. (2001)

showed that the Sauter mean diameter of the bubbles increased with an increase in the superficial gas velocity.

Tools that employ lasers, such as particle dynamics analyzers, are not invasive and are more accurate than conventional photographic methods. Laser Doppler anemometry (LDA), as well as phase Doppler anemometry (PDA), can be used to simultaneously determine: 1) bubble size, 2) bubble size distribution; 3) gas phase axial and radial velocity distributions; and 4) gas-phase and liquid-phase turbulence intensities in both axial and radial directions (Gamal El-Din and Smith 2003b). Gamal El-Din and Smith (2003b) used LDA and PDA to analyze the bubbles formed in their previously presented impinging-jet bubble column. Through these advanced techniques, it was confirmed that, as the superficial liquid velocity increased, d_s decreased. Alternatively, as the superficial gas velocity increased, d_s increased. However, it was also determined that increasing the superficial gas velocity resulted in a decrease in the count mean bubble diameter. The researchers also determined that, as the superficial gas velocity increased, the specific interfacial area of the bubbles subsequently increased. It was further noted that, as the superficial liquid and gas velocities increased, there was a resultant increase in gas hold-up.

Zhou and Smith (2000) evaluated the applicability of a particle dynamics analyzer that employed phase Doppler anemometry (PDA) techniques in their studies on bubble properties, and the mass transfer of ozone in diffuser bubble columns. The particle dynamics analyzer tested was capable of measuring gas bubbles to an accuracy of 3% in

the middle of the column. The authors determined that the mean diameter of the gas bubbles varied only slightly with the gas flow rate. They further demonstrated that larger surface areas were being formed at higher gas flow rates, indicating that the gas flow rate is the most important factor affecting the mass transfer of ozone. It was also determined that the gas hold-up was significantly affected by the gas flow rate; as the superficial gas velocity increased, the gas hold-up increased. This is likely a result of smaller bubbles being formed, and therefore possessing a longer retention time in the bubble column.

Gas-Liquid Interfacial Area

The rate of mass transfer is a direct function of the specific interfacial area (a), and as such, the interfacial area is the most influential parameter when attempting to model reactor mass transfer efficiency (Deckwer 1992, Cockx et al. 1999). The specific interfacial area (a) of the bubbles in the reactor can be determined through the following formula:

$$a = \frac{6\varepsilon_G}{d_s} \quad \text{Equation 2-26}$$

Where a = specific interfacial area [1/length]

ε_G = gas hold-up [dimensionless]

d_s = Sauter mean bubble diameter [length]

As is the case with gas hold-up, many correlations have been proposed in an attempt to predict the diameter and interfacial areas of bubbles under the operating conditions of the investigated bubble columns. The following table serves as a means to summarize some of these correlations.

Table 2-3: Correlations of bubble size and interfacial area proposed by previous researchers

Author	Bubble column details	Operating conditions	Proposed relationship
Akita and Yoshida (1974)	3 Columns -h: 250 cm -size: 7.7 x 7.7 cm 15 x 15 cm 30 x 30 cm perforated plates: - single orifice - multiple orifice	Photographic method	$d_{vs} = 26 \cdot d \cdot \left(\frac{g \cdot d^2 \cdot \rho_L}{\gamma} \right)^{-0.50} \cdot \left(\frac{g \cdot d^3}{v_L^2} \right)^{-0.12} \cdot \left(\frac{u_G}{\sqrt{g \cdot d}} \right)^{-0.12}$ <p>$d_{vs} = \text{mm}, d = \text{cm}, g = \text{cm}^2/\text{s}, \rho = \text{g}/\text{cm}^3, \gamma = \text{g}/\text{s}^2, v = \text{g}/\text{cm} \cdot \text{s}, u_G = \text{m}/\text{h}$</p>
Kumar et al. (1976)	3 Columns -5, 7.5, 10 cm Conical head Replaceable orifice plates	Chemical method $u_G = 0.21 - 14.01$ cm/s	$1 < \text{Re} < 10 \quad d_{vs} = 1.56 \cdot \text{Re}_N^{0.58} \cdot \left(\frac{\gamma \cdot d_N^2}{\Delta \rho \cdot g} \right)^{\frac{1}{4}}$ $10 < \text{Re} < 2100 \quad d_{vs} = 0.32 \cdot \text{Re}_N^{0.425} \cdot \left(\frac{\gamma \cdot d_N^2}{\Delta \rho \cdot g} \right)^{\frac{1}{4}}$ $1000 < \text{Re} < 70,000 \quad d_{vs} = 100 \cdot \text{Re}_N^{0.4} \cdot \left(\frac{\gamma \cdot d_N^2}{\Delta \rho \cdot g} \right)^{\frac{1}{4}}$ <p>$d_{vs} = \text{cm}, \gamma = \text{dyne}/\text{cm}, d = \text{cm}, \rho = \text{g}/\text{cm}^3, g = \text{cm}/\text{s}^2$</p>
Kulkarni et al. (1983)	1 Column -d: 0.075 m -h: 2.65 m Ring type distributor	Chemical method Downflow $u_G = 0.022$ to 0.025 m/s $u_L = 0.195$ to 0.36 m/s	$a = 225 \cdot V_G^{0.635} \cdot V_L^{-2.05} \cdot \sigma_L^{-0.11}$ <p>$a = 1/\text{m}, V_G = \text{m}/\text{s}, V_L = \text{m}/\text{s}, \sigma = \text{N}/\text{m}$</p>
Radhakrishnan and Mitra (1984)	1 Column -d: 32 mm -h: 1080 mm Multi orifice nozzle	Chemical method $Q_L = 18 - 208$ ml/s $Q_G = 20 - 850$ ml/s	$a = 225 \cdot \varepsilon_L^{-2.65}$ <p>$a = 1/\text{m}$</p>

Idogawa et al. (1987)	1 Column -d: 0.05 m -h: 0.83 m perforated plate	Electric Probe Semi-batch flow $u_G = 0.5 - 5$ cm/s $p_i = 0.1 - 5$ MPa	$d = 3.91 \cdot \rho_G^{-0.07} \cdot \left(\frac{\sigma}{72} \right)^{0.22 \cdot \exp(-p_i)}$ $d = m, \rho = \text{kg/m}^3, \sigma = \text{mN/m}$
Bando et al. (1988)	2 Columns a- diameter: 0.70 m height: 1.80m b- diameter: 0.164 m height: 3.50 m nozzle injector perforated sparger	Chemical method Co-current Downflow $V_L = 0.01$ to 0.20 m/s $V_G =$ up to critical velocity	$a = 5400 \cdot \exp(0.10 \cdot u_{LN}) \cdot \varepsilon_G$ $u_{LN} = \left(\frac{d}{d_N} \right)^2$, superficial liquid velocity in the nozzle $a = 1/\text{m}, u_L = \text{m/s}, u_{LN} = \text{m/s}, d = \text{m}, d_N = \text{m}$
Roustan et al. (1996)	1 Column -d: 0.15 m -h: 2.5 m Porous distributor	Photographic Method Electric Probe $Q_L = 0.30 - 1.32$ m^3/h $Q_G = 0.12 - 1.32$ m^3/h	$d = 2.935 \cdot u_G^{0.751}$ $d = \text{mm}, u_G = \text{m/h}$
Sarrafi et al. (1999)	1 Column -rectangular: 0.10 x 0.15 x 1.50 m orifice plate	Photographic method $u_G = 0 - 0.08$ m/s	$d = \left(\frac{6 \cdot d_0 \cdot \sigma}{g \cdot (\rho_L - \rho_G)} \right)^{\frac{1}{3}}$ $d_{vs} = m, d_0 = \text{orifice diameter (m)}, \sigma = \text{N/m}, g = \text{m/s}^2, \rho = \text{kg/m}^3$

Mass Transfer

As was previously discussed, one of the primary goals of an ozone reactor is to create a homogeneous solution of dissolved ozone, ensuring maximum amounts of ozone are made available for pollutant degradation or microorganism reduction. Thus, the transfer of ozone gas into the liquid phase is of prime importance. At any given time, three main activities are being carried out simultaneously: diffusion, convection, and chemical reactions (Charpentier 1981).

The absorption of the gas by the liquid via diffusion at the interface is a major activity that is continuously occurring (Danckwerts 1970). Kuo (1982) discussed the mass transfer process in a gas-liquid system and stated that this process consists of several steps: 1) diffusion of ozone through the gas phase, and into the gas-liquid interface; 2) transport across this interface to the liquid layer boundary; and 3) transfer across the liquid boundary layer (i.e., liquid film) into the bulk of the liquid.

Developed models attempt to characterize what occurs during the gas absorption process and serve two purposes: 1) to provide a basis for predicting rates of physical gas-absorption in various situations from first principles; and 2) to predict, not the rate of physical absorption, but the effect of a chemical reaction on the rate of absorption (Danckwerts 1970). Equations representing these models are often derived assuming that: 1) the resistance from the liquid phase controls the rate of mass transfer; 2) both the gas and liquid flow at steady state conditions; 3) the mass transfer through the free liquid surface is negligible; and 4) Henry's law holds (Nakao et al. 1983).

Charpentier (1981) postulated that gas absorption could be influenced by the resistance of both the gas-phase and the liquid-phase films. It is often assumed that the resistance at the interface between the two phases is negligible. As such, the rate of absorption is characterized by the following mathematical formula:

$$\Phi = \phi a = k_G a (p - p_i) = k_L a (C^*_A - C_{AO}) \quad \text{Equation 2-27}$$

Where Φ	= rate of absorption per unit volume of reactor	[gm·mol/cm ³ ·s]
a	= effective interfacial area per unit packed volume	[1/cm]
ϕ	= average rate of transfer of gas per unit area	[gm·mol/cm ² ·s]
p	= partial pressure in the bulk gas	[atm]
p_i	= partial pressure at the interface	[atm]
C^*_A	= saturated concentration of gas	[mol/L]
C_{AO}	= bulk concentration of dissolved gas	[mol/L]
k_G	= local gas side mass transfer coefficient	[cm/s]
k_L	= local liquid side mass transfer coefficient	[cm/s]

Three models that have been adequately developed for the purpose of describing the rate of gas mass transfer include: 1) two-film model; 2) Higbie surface-renewal model; and 3) Danckwerts surface-renewal model (Danckwerts 1970).

Two-Film Model

This model assumes that there is a uniform gas-phase film thickness (δ_G) and a uniform liquid-phase film thickness (δ_L) around the interface between the gas and liquid phases. It is assumed that the liquid found below this film has a homogeneous composition maintained by regular agitation of the liquid. This model also assumes that any convective transport of gas into the bulk liquid is absent; the transport of gas into the bulk liquid is accomplished through molecular diffusion alone (Charpentier 1981).

Danckwerts (1970) comments that this model is not realistic for the simple reason that the proposed discontinuities of the liquid surface cannot be entertained, nor can the idea that the film thickness is uniform. However, he does say that the main idea being proposed, that the gas must diffuse into the liquid before it can be transported throughout the bulk of the liquid, is valid and is an “essential feature”.

Surface Renewal Models

These models assume that liquid elements at the interface are replaced by other liquid elements from the bulk liquid. While any given element of liquid is at the interface, it absorbs gas rapidly at first, then slows down based on the amount of time that it has been exposed to the gas. In other words, the element of liquid will continue to absorb gas as if it were a layer of infinite depth, but the rate of absorption will decrease over time as the concentration of gas increases. This type of replacement of liquid elements is brought about by the circulation of liquid (Charpentier 1981).

The replacement of all the liquid, or elements at the surface of the liquid, does not occur at the same time. Rather, these elements are replaced in random order. As such, the elements at the surface of the liquid absorb gas at varying rates, because of their varying surface ages. It is because of this age variation that there are several different mathematical models. Generally, each model assumes a different average age of liquid elements at the interface (Danckwerts 1970).

The model proposed by Higbie is one of many proposed surface renewal models. This particular surface renewal model assumes that every element at the surface of the interface is exposed to the absorbing gas for an equal amount of time (θ) before it is replaced by a liquid element from the bulk liquid. During its time at the interface, each element of liquid will absorb an equal amount of gas (V_G) per unit area (Charpentier 1981).

The system of equations is as follows:

$$V_G = 2(C^*_A - C_{AO})(D_A\theta/\pi)^{1/2} \quad \text{Equation 2-28}$$

$$\phi = V_G/\theta = 2(C^*_A - C_{AO})(D_A/\pi\theta)^{1/2} \quad \text{Equation 2-29}$$

$$k_L = 2(D_A/\pi\theta)^{1/2} \quad \text{Equation 2-30}$$

Where C^*_A = saturated concentration of gas [mol/L]

C_{AO} = bulk concentration of dissolved gas [mol/L]

D_A = molecular diffusivity in a very dilute solution [cm²/s]

- θ = time of exposure of liquid to gas [s]
- k_L = local liquid side mass transfer coefficient [cm/s]
- V_G = amount of gas absorbed by unit area during time of contact
[g mol/cm²]

As in the film model, the hydrodynamic properties of the system are accounted for through θ .

Charpentier (1981) noted that Higbie's primary assumption (equal exposure time) is not applicable for many vessels (packed columns, plate columns, mechanically agitated vessels) that are currently used in the industry. This model may be more suited for situations that use gas bubbles, liquid droplets, liquid jets, and liquids flow under laminar conditions.

A second surface-renewal model has been proposed by Danckwerts (1970). The underlying concept of the replacement of particles is similar, however, Danckwerts assumes that the probability of an element of liquid being replaced is not a function of the exposure time. The exposure time, θ , from Higbie's model has been replaced with a term accounting for the rate of surface renewal. This surface renewal rate (s) also takes into account the hydrodynamic properties of the system as follows (Danckwerts, 1970):

$$r = (A^* - A^0)(D_{As})^{1/2} \quad \text{Equation 2-31}$$

- Where r = rate of reaction of gas per unit volume [gm·mol/cm³·s]
- A^* = concentration of dissolved gas at the interface, in equilibrium with gas at the interface [gm·mol/cm³]
- A^0 = concentration of gas in the bulk of the liquid [gm·mol/cm³]
- D_A = diffusivity of dissolved gas [cm²/s]
- s = fractional rate of surface-renewal [1/s]

Gas Solubility

The dissolution of a gas into a liquid depends largely on the solubility of the gas, which is described as the ability of a gas to dissolve into a liquid. Solubility is often described by Henry's Law, and is based on the partial pressure of the gas (i.e. ozone) in the system. Sawyer et al. (1994) defined Henry's Law by stating: "the weight of any gas that will dissolve in a given volume of a liquid, at constant temperature, is directly proportional to the pressure that the gas exerts above the liquid".

Henry's law is as follows:

$$C_{O_3}^* = \frac{P_{O_3}}{H} \quad \text{Equation 2-32}$$

Where H = Henry's coefficient [atm·cm³/g·mol]

P_{O_3} = Partial pressure of ozone gas [atm]

$C_{O_3}^*$ = Equilibrium concentration of ozone gas [g·mol/cm³]

When dealing with gas solubility, Henry's law serves only to indicate the extent of a system's equilibrium, in essence, how far the system is away from equilibrium.

Three main influences on gas solubility are temperature, pressure, and the presence of other compounds, such as organics and inorganics. The temperature will influence the solubility of a gas in a liquid. As the temperature increases, there is a decrease in the solubility of the gas. However, when gases are dissolved into organic solvents, the situation is often reversed (Petrucci and Harwood 1997).

Pressure affects the solubility of a gas to an even greater extent than the temperature of the solution. As the pressure increases, there is a resultant increase in solubility. It should be noted that for gases at high pressures, Henry's law fails. At these high pressures, gases will often ionize in water, or will actually react with the constituents in the water (Petrucci and Harwood 1997). Finally, the solubility of a gas (such as ozone) can also be affected by the presence of any inorganic or organic matter present in the solution (Beltrán et al. 1997).

Once in water, the diffusion of ozone follows Fick's Law with a rate constant of

$D_{O_3} = 1.74 \cdot 10^{-9} \text{ m}^2/\text{s}$. This value should be corrected for physical properties that may vary, and this should be done using the Nernst-Einstein relationship. This relationship is as follows:

$$\frac{D_L \cdot \mu}{T} = \text{Constant}$$

Equation 2-33

Where D_L = diffusivity in water [cm²/s]

μ = viscosity of the liquid [g/cm·s]

T = absolute temperature [K]

However, in order to apply a diffusivity equation, it is necessary to assume that the concentration of the diffusant (i.e. gas) is homogeneous throughout the bulk liquid.

Influences on Mass Transfer

Sotelo et al. (1989) discussed that the overall rate of ozone absorption by water depends on many factors. These are: ozone's ability to diffuse into the liquid solution, the auto decomposition of ozone, and the occurrence of any chemical reactions between ozone and other dissolved constituents.

With a decrease in temperature, there was a subsequent decrease in the amount of ozone dissolved into the water, thereby lowering the volumetric mass transfer rate (Hsu et al. 2002, Sotelo et al. 1989). With respect to the pH of the solution, if the pH increased, the concentration of dissolved ozone decreased. It was postulated that high pH values will induce the decomposition of ozone, limiting its availability for diffusion (Sotelo et al. 1989).

It can be generalized that, as ionic strength increases, the absorption rate of ozone will decrease. In some situations, this relationship is obvious. However, in the presence of other compounds the above-stated relationship is insignificant (Sotelo et al. 1989).

Further to their study, the effects of gas flow rate, ozone partial pressure, and mixing speed were studied. It was concluded that both the gas flow rate and the mixing speed influenced the mass transfer coefficient (k_L), as well as the interfacial area (a). It was found that the partial pressure of ozone will not only affect the liquid driving force, but the gas driving force as well (Sotelo et al. 1989). Similarly, Hsu et al. (2002), concluded that, as the agitation speed increased, the volumetric mass transfer rate increased.

Volumetric Liquid Mass Transfer Coefficient

After its generation, ozone must be dissolved into solution, where it can be used as an effective disinfectant. In general, this process involves the bubbling of ozone gas into a liquid whereby ozone is transferred from the gas phase into the liquid phase. The rate of mass transfer is generalized by the following equation (Deckwer, 1992):

Absorption Rate:

$$\frac{dC}{dt} = k_L a \cdot (C_L^* - C_L) \quad \text{Equation 2-34}$$

Where k_L = local liquid mass transfer coefficient [m/s]

- a = specific interfacial area of gas bubbles [1/m]
 C_L^* = concentration of dissolved ozone in equilibrium with the bulk ozone gas [mg/L]
 C_L = concentration of dissolved ozone in the bulk liquid [mg/L]

The dynamic axial dispersion model (DADM) proposed by Chen et al. (2002) takes into account the hydrodynamics of the bubble column reactor, the gas-liquid mass transfer, and the pseudo-first-order decomposition rate of ozone. This model allows for the prediction of dynamic variations in ozone concentration, pollutant concentration, and oxygen concentration. Chen et al. (2002) showed that as u_G increased, the concentrations increased and reached steady-state conditions faster. Validation of this model was carried out in a counter-current bubble column. The DADM model assumes: 1) homogeneous bubbling regime is present; 2) the end effect of the column is neglected; 3) pressure varies linearly with column height; 4) Henry's law is applicable; and 5) reactions occurring in the gas phase are neglected (Chen et al. 2003). Chen et al. (2003) applied the DADM and evaluated the ozone transfer efficiency of a counter-current bubble column, using a mixture of oxygen and ozone in the gas phase, with pollutants present in the test water. The DADM effectively predicted variations in oxygen concentration throughout the experiment (from beginning to steady state).

Zhou et al. (1994) discussed the modeling of ozone bubble column reactors. It is clear that the actual flow pattern inside bubble columns is closer to mixed flow than plug flow,

however, with backmixing in the liquid phase. The ADM was formulated, and applied. Assumptions surrounding the ADM were: 1) the liquid phase is in axial dispersion; 2) the gas phase is in plug flow regime; 3) both fluids flow under steady state conditions; 4) pressure depends on column height; 5) gas hold-up and interfacial area remain constant along the height of the bubble column; 6) resistance to mass transfer is mainly from the liquid side; 7) the decay rate of ozone is pseudo-first-order in the liquid phase (negligible in the gas phase); and 8) Henry's law is applicable. The model incorporated the mass transfer of ozone, the decay of ozone, and contactor mixing characteristics. The developed equations can be easily used through numerical methods to predict the concentration of dissolved ozone in a bubble column. Validation of this model was carried out in both counter-current and co-current flow regimes. The model was able to accurately predict the concentration of ozone throughout the length of the column, even at boundaries where there can be a large amount of mixing (inlet).

Contrary to the majority of studies carried out on bubble column reactors, Kim et al. (2002a) investigated the applicability of the axial dispersion reactor model (ADM) in a pilot-scale contactor. The advantages of using pilot-scale studies include the ability to simulate actual contactor configurations and operating conditions. Kim et al. (2002a) were able to determine the mass transfer capabilities of a full scale reactor, and thus, its inactivation efficiency. The experiments were conducted using treated river water, using *Cryptosporidium muris* and *Cryptosporidium parvum* oocysts. Inactivation was determined using biological surrogate indicators. Bubble-diffuser column mass balances were used to obtain the expressions corresponding to the steady-state dissolved and gas-

phase concentrations. The developed model takes into account the variations in ozone decomposition demands (first-order and second-order kinetic rates), disinfection kinetics (pseudo first-order rate), and temperature effects. Validation of this model proved that the ADM accurately represented ozone concentration profiles and inactivation data of the targeted *Cryptosporidium* oocysts (Kim et al. 2002b).

In a study by Salazar et al. (1993), mass transfer experiments were conducted in a jet bubble column operating in a co-current mode. The inlet was conical in shape, and gas was injected into this inlet with a jet. The energy provided by this set up allowed for dispersion and breakage of gas bubbles, resulting in a larger interfacial area. The superficial gas and liquid velocities ranged from 0.03 to 0.09 m/s and from 0 to 0.006 m/s, respectively. Salazar et al. (1993) found that this jet system increased the mass transfer rate of a normal (perforated plate) bubble column by about 1.5. It was also determined that there was a negligible relationship between the superficial liquid velocity and the overall $k_L a$ for this reactor.

The study conducted by Zhou and Smith (2000) examined venturi injectors as well as plate diffusers. As the gas flow rate increased, the interfacial area of the gas bubbles increased accordingly. The authors further revealed that the ozone mass transfer coefficient was strongly affected by the gas flow rate. The authors stated that the increase in mass transfer rate could be attributed to the larger interfacial areas formed at these increased gas flow rates.

Gamal El-Din and Smith (2001a) discussed the applicability of the 2P-ADM proposed by Zhou et al. (1994) and noted that the non-linear partial differential equations were difficult to solve and time consuming. As a result, Gamal El-Din and Smith (2001a) proposed a variation to the ADM and the 2P-ADM, the one phase ADM (1P-ADM). The 1P-ADM describes only the liquid phase, with the variation of gas phase concentration being described by an exponential function. Through mass balance equations of the liquid phase, a linear second-order differential equation was developed which can be easily solved analytically. When tested under real water conditions for both co-current and counter-current operations, it was shown that the 1P-ADM provided excellent predictions with respect to the concentration of dissolved ozone.

Furthermore, Gamal El-Din and Smith (2003a) conducted experiments on an impinging-jet bubble column operated under co-current flow conditions. Based on the 1P-ADM model, the mass transfer of the bubble column was analyzed in clean deionized water where first-order equations adequately described the ozone auto-decomposition process. The use of the 1P-ADM proved to be in excellent agreement with the dissolved ozone concentration profiles. Dissolved ozone concentration profiles were determined to be more sensitive to changes in the overall mass transfer rate ($k_{L}a$) than to changes in the axial dispersion coefficient of the liquid phase (D_L). Although $k_{L}a$ was minimally affected by D_L (and thus u_L), Gamal El-Din and Smith (2003a) developed an equation to predict $k_{L}a$ based on u_G and u_L :

$$k_L a = 20.54 \cdot u_G^{1.13} \cdot u_L^{0.07}$$

Equation 2-35

Where $k_L a$ = overall mass transfer coefficient [1/s]

u_G = superficial gas velocity [m/s]

u_L = superficial liquid velocity [ms/]

When compared with previously published correlations, the work of Gamal El-Din and Smith (2003a) displayed an enhanced rate of mass transfer. The improved rate of mass transfer was attributed to the novel design of the gas injectors used. These injectors were placed at an intersecting angle of 125° , resulting in a high degree of turbulence, thus increasing the shearing of large bubbles into smaller bubbles and producing a larger interfacial area available for mass transfer.

Injectors have also been employed as means of ozone dissolution in full and pilot scale operations. Bellamy et al. (1991) studied the use of a side-stream gas eductor, injected in-line with the main process stream. This study revealed higher ozone transfer efficiencies (from a higher degree of mixing), an increase in colour removal, and a decrease in the contact time required to achieve the desired results. Holder and Leow (1994) used a venturi side-stream oxygen dissolver system as a method of controlling odours in a full scale operation.

Mariñas et al. (1993) developed a dispersion model, based on their tracer studies. This model, the transient dispersion model (TDP), is based on the following assumptions:

1) the ozone contactor operates under steady-state conditions; 2) dispersion occurs in the liquid phase only; 3) the two-film model is a valid representation of ozone transfer; 4) ozone is stable when in the gas phase; and 5) The rate of ozone decomposition is represented by:

$$\frac{dC}{dt} = -k_d C^n \quad \text{Equation 2-36}$$

Where k_d = apparent decomposition rate constant of ozone [L/mg·min]

C = residual ozone concentration at a specific time [mg/L]

n = reaction order coefficient

Based on mass balance equations, tracer tests and ozonation tests, the TDP was proven to accurately predict residual ozone in a pilot-scale ozone bubble-diffuser contactor. Experiments were conducted using both a coarse and a fine bubble diffuser, under actual water operating conditions (Mariñas et al. 1993).

A model used to predict the mass transfer of ozone in a bubble column has been developed by Huang et al. (1998). This model is a refined version of that proposed by Mariñas et al. (1993), and now includes an n^{th} order expression (Mariñas et al. (1993) for the decomposition rate of ozone. This model was used to perform ozonation tests, and determined that the 1st order reaction rate was a better representation than the 2nd order reaction rate. In using this model it is necessary to consider the enhancement factor, the

gas velocity, the concentration of ozone in the bulk of the liquid and the gas hold-up of the reactor. Equations for the bubble column system were derived based on: 1) mass balance; 2) absorption equilibrium; and 3) effects of hydrostatic pressure. Also, the film model describing mass transfer was employed to describe the absorption and decomposition of ozone. The derived system of equations was validated, and proved to accurately describe the mass transfer occurring in a bubble column reactor.

A model was developed by Wright et al. (1997) that accurately depicts the mass transfer in a co-current gas-liquid downflow contactor incorporating venturi suction. The developed model is based on the mass transfer of the system, with boundary conditions being the walls of the unit, the inlet streams, and the outlet streams. Assuming plug flow behaviour, the set of equations was solved using the Runge-Katta technique. The volumetric mass transfer rate was solved for after experimentally determined variables were input. The proposed model demonstrates a relationship with the gas to liquid flow ratio. The problem with the applicability of this model lies in its assumption of plug flow behaviour. In reality, the flow is not ideal, as is illustrated by the case that the authors tested (annular flow). This model predicts that this particular co-current gas-liquid downflow contactor exhibits high mass transfer rates.

Gamal El-Din and Smith (2001c) proposed a cell-based model termed the back flow cell model (BFCM). This model was based on the presence of two series of interconnected cells, representing the gas and liquid phases. The two phases are interconnected by an exchange flow, with backflow occurring in the liquid phase only. This is due to the

buoyancy of the bubbles, allowing insignificant amount of backmixing to occur in the gas phase. Unique to this model is its ability to make predictions based on a variable cell volume along the height of the reactor, a variable mixing coefficient along the height of the reactor, and the formulation and solving techniques of the BFCM can be carried out using a simple spreadsheet approach (Gamal El-Din and Smith 2001a).

Other models that have been developed are presented in the table below.

Table 2-4: Correlations of overall mass transfer coefficients proposed by previous researchers

Author	Reactor Details	Operating Conditions	Proposed Relationship
Akita and Yoshida (1973)	Diameter: 15.2 cm Height: 400 cm Gas sparger: Single hole drilled into centre of plate	Continuous gas flow Bath liquid flow $V_G = 19.1$ to 1510 m/h	$k_L a = 0.6 \cdot D_L^{0.5} \cdot \varepsilon_G^{1.1} \cdot v_L^{-0.12} \cdot \left(\frac{\gamma}{\rho_L} \right)^{-0.62} \cdot d^{2.17} \cdot g^{0.93}$ $g = \text{cm/s}^2, d = \text{cm}, u_G = \text{m/h}, \rho = \text{g/cm}^3, v = \text{g/cm}\cdot\text{s}, \gamma = \text{g/s}^2,$ $D_L = \text{liquid diffusivity}, k_L a = 1/\text{h}$
Akita and Yoshida (1974)	3 Columns -h: 250 cm -size: 7.7 x 7.7 cm 15 x 15 cm 30 x 30 cm perforated plates: - single orifice - multiple orifice		$k_L = 0.5 \cdot g^{\frac{5}{8}} \cdot D_L^{\frac{1}{2}} \cdot \rho_L^{\frac{3}{8}} \cdot \gamma^{\frac{-3}{8}} \cdot d_{vs}^{\frac{1}{2}}$ $k_L = \text{cm/s}, d_{vs} = \text{mm}, g = \text{cm}^2/\text{s}, \rho = \text{g/cm}^3, \gamma = \text{g/s}^2$
Hikita et al. (1981)	2 Columns -Column 1 d: 10 cm h: 150 cm 2 nozzles -Column 2 d: 19 cm h: 240 cm 3 nozzles	$u_G = 4.2 - 38$ cm/s Continuous gas flow Continuous and batch liquid flow	$k_L a = 14.9 \cdot g^{0.752} \cdot u_G^{0.76} \cdot \rho_L^{0.852} \cdot \mu_G^{0.243} \cdot \mu_L^{-0.079} \cdot \sigma^{-1.016} \cdot D_L^{0.604}$ $k_L a = 1/\text{s}, g = \text{cm/s}^2, u_G = \text{cm/s}, \rho = \text{g/cm}^3, \mu = \text{g/cm}\cdot\text{s}, \sigma = \text{g/s}^2,$ $D_L = \text{cm}^2/\text{s}$
Deckwer et al. (1983)	4 Bubble Columns 1- Cross of nozzles d: 0.2 m h: 7.2 m 2- Sintered Plate d: 0.15 m h: 4.4 m 3- Cross of nozzles d: 0.2 m h: 2.5 m	Bubble Columns 1,2 $u_L = 0.01 - 0.03$ cm/s Bubble Columns 3,4 $u_L = 0.01 - 0.12$ cm/s	$k_L a = 0.467 \cdot u_G^{0.82}$ $k_L a = 1/\text{s}, u_G = \text{m/s}$

	4- Sintered + perforated plates d: 0.14 m h: 2.7 m											
Kulkarni et al. (1983)	Bubble Column d: 0.075 m h: 2.65 m Ring type distributor	Downflow $u_G = 0.022 - 0.025$ m/s $u_L = 0.195 - 0.36$ m/s	$\frac{k_L a \cdot d^2}{D_L} = 9.7 \cdot \left(\frac{u_G \cdot \mu_L}{\sigma_L} \right)^{0.873} \cdot \left(\frac{\mu_L}{D_L \cdot \rho_L} \right)^{0.5}$ $\left(\frac{\sigma_L^3 \cdot \rho_L}{\mu_L^4 \cdot g} \right)^{0.695} \cdot \left(\frac{d \cdot V_L \cdot \rho_L}{\mu_L} \right)^{-0.245}$ <p>$k_L a = 1/s, d = m, D_L = m^2/s, u_G = m/s, \mu = Pa/s, \sigma = N/m, \rho = kg/m^3, g = m/s^2, V_L = m^3$</p>									
Cho and Wakao (1988)	Bubble Column D: 11 cm H: 40 cm Single nozzle Three porous tubes	Organic solutes	<p>Single nozzle: $k_L a = 6.5 \times 10^3 \cdot D_L^{0.5} \cdot u_G^{0.81}$</p> <p>3 porous tubes: $k_L a = 2.3 \times 10^4 \cdot D_L^{0.5} \cdot u_G^{0.81}$</p> <p>$k_L a = 1/s, D_L = m^2/s, u_G = m/s$</p>									
Roustan et al. (1996)	Bubble Column d: 0.15 m h: 2.5 m Porous distributor	Co-current and counter-current $u_L = 16.95 - 74.58$ m/h $u_G = 16.89 - 24.10$ m/h	<table border="1"> <thead> <tr> <th></th> <th>Co-current</th> <th>Counter-current</th> </tr> </thead> <tbody> <tr> <td>Re = 680</td> <td>$k_L a = 0.092 \cdot u_G^{0.516}$</td> <td>$k_L a = 0.105 \cdot u_G^{0.564}$</td> </tr> <tr> <td>Re = 1912 - 2986</td> <td>$k_L a = 0.110 \cdot u_G^{0.625}$</td> <td>$k_L a = 0.055 \cdot u_G^{-0.932}$</td> </tr> </tbody> </table> <p>$k_L a = 1/min, u_G = m/h$</p>		Co-current	Counter-current	Re = 680	$k_L a = 0.092 \cdot u_G^{0.516}$	$k_L a = 0.105 \cdot u_G^{0.564}$	Re = 1912 - 2986	$k_L a = 0.110 \cdot u_G^{0.625}$	$k_L a = 0.055 \cdot u_G^{-0.932}$
	Co-current	Counter-current										
Re = 680	$k_L a = 0.092 \cdot u_G^{0.516}$	$k_L a = 0.105 \cdot u_G^{0.564}$										
Re = 1912 - 2986	$k_L a = 0.110 \cdot u_G^{0.625}$	$k_L a = 0.055 \cdot u_G^{-0.932}$										
Chen et al. (2002)	Bubble Column d: 15.8 cm h: 1.33m Perforated plate	$u_G = 1.33 - 9.48$ mm/s $u_L = 1.42 - 4.25$ mm/s Counter-current flow	$k_L a = 0.2567 \cdot u_G^{0.560}$ <p>$k_L a = 1/s, u_G = mm/s$</p>									

Chapter 3 Materials and Methods

Transient Back Flow Cell Model

The main hypothesis of the transient back flow cell model (TBFCM) is that the axial dispersion occurring in the liquid phase is represented by the occurrence of a back flow and an exchange flow. A schematic representation of the TBFCM occurring in a bubble column operating in a co-current flow regime is shown in Figure 3-1 (Gamal El-Din and Smith, 2001c).

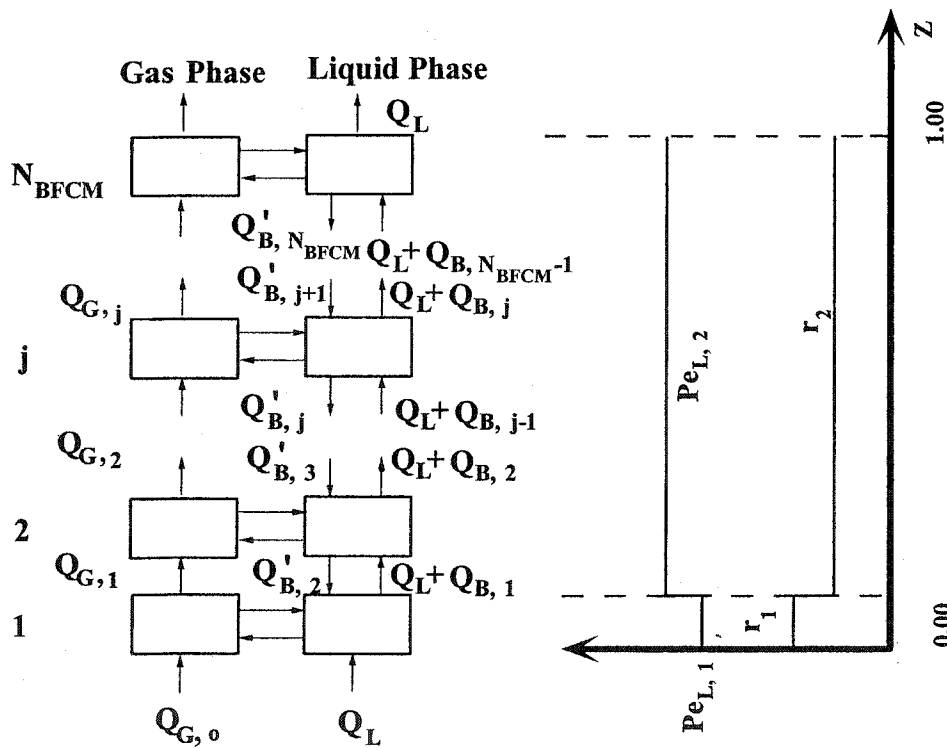


Figure 3-1: Schematic diagram representing the BFCM for co-current flow conditions of bubble column reactors, indicating the presence of two mixing zones, adapted from Gamal El-Din and Smith (2001c)

The TBFCM involves two series (liquid phase and gas phase) of completely mixed cells. Each series consists of a certain number of cells equal to N_{BFCM} . In order to assume plug flow operating conditions, the NBFCM should be equal to or greater than 10. However, reactors displaying small aspect ratios may still be modeled, with respect to the gas phase and according to the plug flow regime, with NBFCM less than 10, due to the large buoyancy of the gas bubbles. The TBFCM allows more freedom in modelling, in the sense that it incorporates the possibility of having variable cell volumes along the height of the bubble column reactor. The development of the TBFCM assumes that the mixing parameter characterized by the liquid phase Peclet number (Pe_L) varies along the height of the column. The existence of distinct regions of mixing can therefore be considered (Gamal El-Din and Smith 2001c).

Governing assumptions behind the development of the TBFCM used in the application of bubble columns are as follows (Gamal El-Din and Smith 2001c):

- 1) backflow will only occur in the liquid phase;
- 2) because of the buoyancy of gas bubbles and the large reactor aspect ratio, the backmixing in the gas phase is negligible;
- 3) the bubble column reactor is operating under steady state conditions (constant liquid and gas flow rates);
- 4) when conducting tracer tests with an inert tracer, no mass transfer and chemical decay processes take place; and
- 5) the gas hold-up and the interfacial area of the bubbles is constant along the height of the column.

The developed equations representing the TBFCM previously described by Gamal El-Din and Smith (2001a) are as follows:

For cell: $j = 1$

$$\frac{dY_1}{dt} = -\frac{1+r_1}{f_1\tau/N_{BFCM}}Y_1 + \frac{r_2}{f_1\tau/N_{BFCM}}Y_2 \quad \text{Equation 3-1}$$

For cells: $2 \leq j \leq N_{BFCM}-1$

$$\frac{dY_j}{dt} = \frac{1+r_{j-1}}{f_j\tau/N_{BFCM}}Y_{j-1} - \frac{1+r_j+r_j}{f_j\tau/N_{BFCM}}Y_j + \frac{r_{j+1}}{f_j\tau/N_{BFCM}}Y_{j+1} \quad \text{Equation 3-2}$$

For cell: $j = N_{BFCM}$

$$\frac{dY_{N_{BFCM}}}{dt} = \frac{1+r_{N_{BFCM}-1}}{f_{N_{BFCM}}\tau/N_{BFCM}}Y_{N_{BFCM}-1} - \frac{1+r_{N_{BFCM}}}{f_{N_{BFCM}}\tau/N_{BFCM}}Y_{N_{BFCM}} \quad \text{Equation 3-3}$$

Where $Y_j = \frac{C_j}{C_0^*}$ Equation 3-4

$$C_0^* = \frac{M}{V_c} = \frac{M}{V/N_{BFCM}}$$
 Equation 3-5

$$r_j = \frac{Q_{B,j}}{Q_L}$$
 Equation 3-6

$$r'_j = \frac{Q'_{B,j}}{Q_L}$$
 Equation 3-7

$$f_j = \frac{V_{C,j}}{V/N_{BFCM}}$$
 Equation 3-8

Where C_0^* = instantaneously-mixed tracer concentration at inlet of first cell [mg/L]

C_j = tracer concentration in cell number "j" [mg/L]

f_j = dimensionless correction factor for cell number "j"

j = cell number [dimensionless]

M = mass of injected tracer [kg]

N_{BFCM} = number of cells [dimensionless]

$Q_{B,j}$ = exchange flow rate for cell number "j" [m^3/s]

$Q'_{B,j}$ = back flow rate for cell number "j" [m^3/s]

Q_L = liquid flow rate [m^3/s]

r_j = dimensionless exchange-flow ratio for cell number "j"

r'_j = dimensionless back-flow ratio for cell number "j"

t = ozone contact time [s]

- V = total volume of the bubble column $[m^3]$
- V_C = average cell volume $[m^3]$
- V_{Cj} = volume of cell number “j” $[m^3]$
- Y = normalized tracer concentration for cell number “j” [dimensionless]
- τ = mean theoretical hydraulic retention time [s]

Steady-State Back Flow Cell Model

The same principles that the TBFCM is based on were used for the development of the steady-state back flow cell model. Assumptions 1 to 4 described above are also applicable to the steady-state BFCM. In addition to these assumptions, the following assumptions are also required (Gamal El-Din and Smith 2001c):

- 1) resistance to the mass transfer of ozone absorbance is restricted to the liquid side only;
- 2) an enhancement factor representing the mass transfer of ozone due to the occurrence of chemical reactions is 1.0, implying that the absorption of ozone into water follows the slow-chemical reaction regime;
- 3) the system is operating in a steady-state isothermal manner;
- 4) Henry’s law is applicable;
- 5) the other constituents of the feed gas, other than ozone, are considered to be inert;
- 6) the local mass transfer coefficient (k_L) is constant along the length of the reactor;

- 7) the hydrostatic pressure inside the reactor varies linearly with the reactor height;
- 8) the variability in the superficial gas velocity is due to the absorption of ozone, the depletion of dissolved ozone gas, the decrease in gaseous ozone concentration, and the decrease in hydrostatic pressure; and
- 9) the auto-decomposition of ozone occurring in the liquid phase can be described by a pseudo first-order rate, while the auto-decomposition of ozone occurring in the gas phase is considered to be negligible.

Applying mass balance equations to the co-current operation of the impinging-jet bubble column shown in Figure 3-1 will lead to sets of equations describing the dissolved ozone, the gaseous ozone, and the total gas within each cell. These equations are written as follows based on the model previously developed by Gamal El-Din and Smith (2001c).

It should be noted that these formulae differ slightly from those published in Gamal El-Din and Smith (2001c). The following formulae account for a variable mass transfer coefficient along the height of the reactor, as described by the varying liquid phase Stanton number (St_L). As a result, the assumption (noted above) of a constant rate of mass transfer is changed to an assumption of a variable rate of mass transfer. Also, the following formulae take into account the variable cell volume (f_j), the variable cross-sectional area ($f_{A,j}$), and the variable pressure ($f_{z,j}$) along the height of the bubble column.

Dissolved Ozone

For cell: $j = 1$

$$X_0 - (1 + r_1 + f_j \cdot f_{A,j} \cdot D_{A,j} + f_j \cdot f_{A,j} \cdot St_{L,j}) \cdot X_1 + r_1 \cdot X_2 + f_j \cdot f_{A,j} \cdot St_{L,j} \cdot (1 + \alpha \cdot f_{z,j} \cdot 0.5) \cdot Y_1 = 0 \quad \text{Equation 3-9}$$

For cells: $2 \leq j \leq N_{BFCM}-1$

$$(1 + r_{j-1}) \cdot X_{j-1} - (1 + r'_j + r_j + f_j \cdot f_{A,j} \cdot D_{A,j} + f_j \cdot f_{A,j} \cdot St_{L,j}) \cdot X_j + r'_{j+1} \cdot X_{j+1} + f_j \cdot f_{A,j} \cdot St_{L,j} \cdot (1 + \alpha \cdot f_{z,j} \cdot (j - 0.5)) \cdot Y_j = 0 \quad \text{Equation 3-10}$$

For cell: $j = N_{BFCM}$

$$(1 + r_{N_{BFCM}}) \cdot X_{N_{BFCM}} - (1 + r'_{N_{BFCM}} + f_j \cdot f_{A,j} \cdot D_{A,N_{BFCM}} + f_j \cdot f_{A,j} \cdot St_{L,N_{BFCM}}) \cdot X_{N_{BFCM}} + f_j \cdot f_{A,j} \cdot St_{L,N_{BFCM}} \cdot (1 + \alpha \cdot f_{z,j} \cdot (N_{BFCM} - 0.5)) \cdot Y_{N_{BFCM}} = 0 \quad \text{Equation 3-11}$$

Gaseous Ozone:

For cells: $1 \leq j \leq N_{BFCM}$

$$q_{G,j-1} \cdot Y_{j-1} \cdot (1 + \alpha \cdot f_{z,j} \cdot (j - 1.5)) - q_{G,j} \cdot Y_j \cdot (1 + \alpha \cdot f_{z,j} \cdot (j - 0.5)) - f_j \cdot f_{A,j} \cdot St_{G,j} \cdot ((1 + \alpha \cdot f_{z,j} \cdot (j - 0.5)) \cdot Y_j - X_j) \quad \text{Equation 3-12}$$

Total Gas:

For cells: $1 \leq j \leq N_{BFCM}$

$$q_{G,j-1} \cdot (1 + \alpha \cdot f_{z,j} \cdot (j - 1.5)) - q_{G,j} \cdot (1 + \alpha \cdot f_{z,j} \cdot (j - 0.5)) - f_j \cdot f_{A,j} \cdot St_{G,j} \cdot y_0 \cdot ((1 + \alpha \cdot f_{z,j} \cdot (j - 0.5)) \cdot Y_j - X_j) \quad \text{Equation 3-13}$$

Where $X_j = \frac{C_{L,j}}{C_{L,0}^*}$ Equation 3-14

$$C_{L,j}^* = \frac{P_j}{H} \cdot y_j$$
 Equation 3-15

$$r_j = \frac{Q_{B,j}}{Q_L}$$
 Equation 3-16

$$r_j' = \frac{Q_{B,j}'}{Q_L}$$
 Equation 3-17

$$D_{A,j} = \frac{k_w \cdot \varepsilon_L \cdot L}{N_{BFCM} \cdot u_L}$$
 Equation 3-18

$$u_L = \frac{Q_L}{A_{BC}}$$
 Equation 3-19

$$St_{L,j} = \frac{k_L a \cdot L}{N_{BFCM} \cdot u_L}$$
 Equation 3-20

$$\alpha = \frac{-\rho \cdot g \cdot \varepsilon_L \cdot L}{N_{BFCM} \cdot P_0}$$
 Equation 3-21

$$Y_j = \frac{y_j}{y_0}$$
 Equation 3-22

$$q_{G,j} = \frac{Q_{G,j}}{Q_{G,0}}$$
 Equation 3-23

$$St_{G,j} = \frac{k_L a \cdot L}{N_{BFCM} \cdot u_{G,0}} \cdot \frac{R \cdot T}{H}$$
 Equation 3-24

$$u_{G,0} = \frac{Q_G}{A_{BC}}$$
 Equation 3-25

$$f_j = \frac{V_{C,j}}{V / N_{BFCM}}$$
 Equation 3-26

$$f_{A,j} = \frac{V_{COMB}}{L \cdot A_{COMB}} \quad \text{Equation 3-27}$$

$$V_{COMB} = V_1 + V_2 \quad \text{Equation 3-28}$$

$$f_{z,j} = \frac{Z_{j,act}}{Z_{j,avg}} \quad \text{Equation 3-29}$$

$$Z_{j,avg} = \frac{j - 0.5}{N_{BFCM}} \quad \text{Equation 3-30}$$

Where A_{BC} = cross sectional area of the straight section of the impinging-jet bubble

column $[m^2]$

A_{COMB} = average cross-sectional area of the impinging jet bubble column

$[m^2]$

$C_{L,0}^*$ = equilibrium dissolved ozone concentration at inlet $[mg/L]$

$C_{L,j}$ = instantaneous dissolved ozone concentration in cell number "j"

$[mg/L]$

$D_{A,j}$ = dimensionless Damköhler number of cell number "j"

$f_{A,j}$ = dimensionless correction factor for the cross-sectional area of cell number

"j"

f_j = dimensionless correction factor for the volume of cell number "j"

$f_{Z,j}$ = dimensionless correction factor for the pressure for cell number "j"

g = gravitational acceleration $[m/s^2]$

H = Henry's law constant $[kPa \cdot L/mg]$

$k_L a$ = overall mass transfer coefficient $[1/s]$

k_w = specific ozone utilization rate constant $[1/s]$

L = total height of the bubble column [m]
 N_{BFCM} = number of cells in the BFCM
 P_0 = liquid hydrostatic pressure at inlet [kPa]
 P_j = liquid hydrostatic pressure in cell number "j" [kPa]
 $q_{G,j}$ = ratio of the gas flow rate flowing out of cell number "j" over the feed-gas flow rate flowing into the first cell [dimensionless]
 $Q_{B,1}$ = exchange flow rate for cell number "j" [m^3/s]
 $Q'_{B,2}$ = back flow rate for cell number "j" [m^3/s]
 Q_G = gas flow rate [m^3/s]
 $Q_{G,0}$ = gas flow rate flowing out of inlet [m^3/s]
 $Q_{G,j}$ = gas flow rate flowing out of cell number "j" [m^3/s]
 Q_L = liquid flow rate [m^3/s]
 Q_L = liquid flow rate [m^3/s]
 r_j = dimensionless exchange-flow ratio for cell number "j"
 r'_j = dimensionless back-flow ratio for cell number "j"
 $St_{G,j}$ = dimensionless Stanton number of the gas phase for cell number "j"
 $St_{L,j}$ = dimensionless Stanton number of the liquid phase for cell number "j"
 $u_{G,0}$ = superficial gas velocity at inlet [m/s]
 u_L = superficial liquid velocity [m/s]
 V_C = average cell volume [m^3]
 $V_{C,j}$ = volume of cell number "j" [m^3]
 V_{COMB} = total volume of the impinging-jet bubble column reactor [m^3]

V_1 = volume of the straight portion of the impinging-jet bubble column reactor
[m³]

V_2 = volume of the angular (base) portion of the impinging-jet bubble column reactor [m³]

X_j = dimensionless dissolved ozone concentration in the liquid phase for cell number “j”

y_0 = dimensionless ozone molar fraction in the gas phase at the inlet

y_j = dimensionless ozone molar fraction in the gas phase

Y_j = dimensionless ozone concentration in the gas phase for cell number “j”

$Z_{j,act}$ = actual dimensionless distance of cell number “j” based on the midpoint of cell number “j”

$Z_{j,avg}$ = average dimensionless distance of cell number “j” based on the midpoint of cell number “j”

α = dimensionless parameter

ε_L = dimensionless liquid phase hold-up

ρ = liquid density [kg/m³]

Impinging-Jet Bubble Column

The pilot-scale tests were conducted in an impinging-jet bubble column. A schematic diagram of the set up is shown below in Figure 3-2.

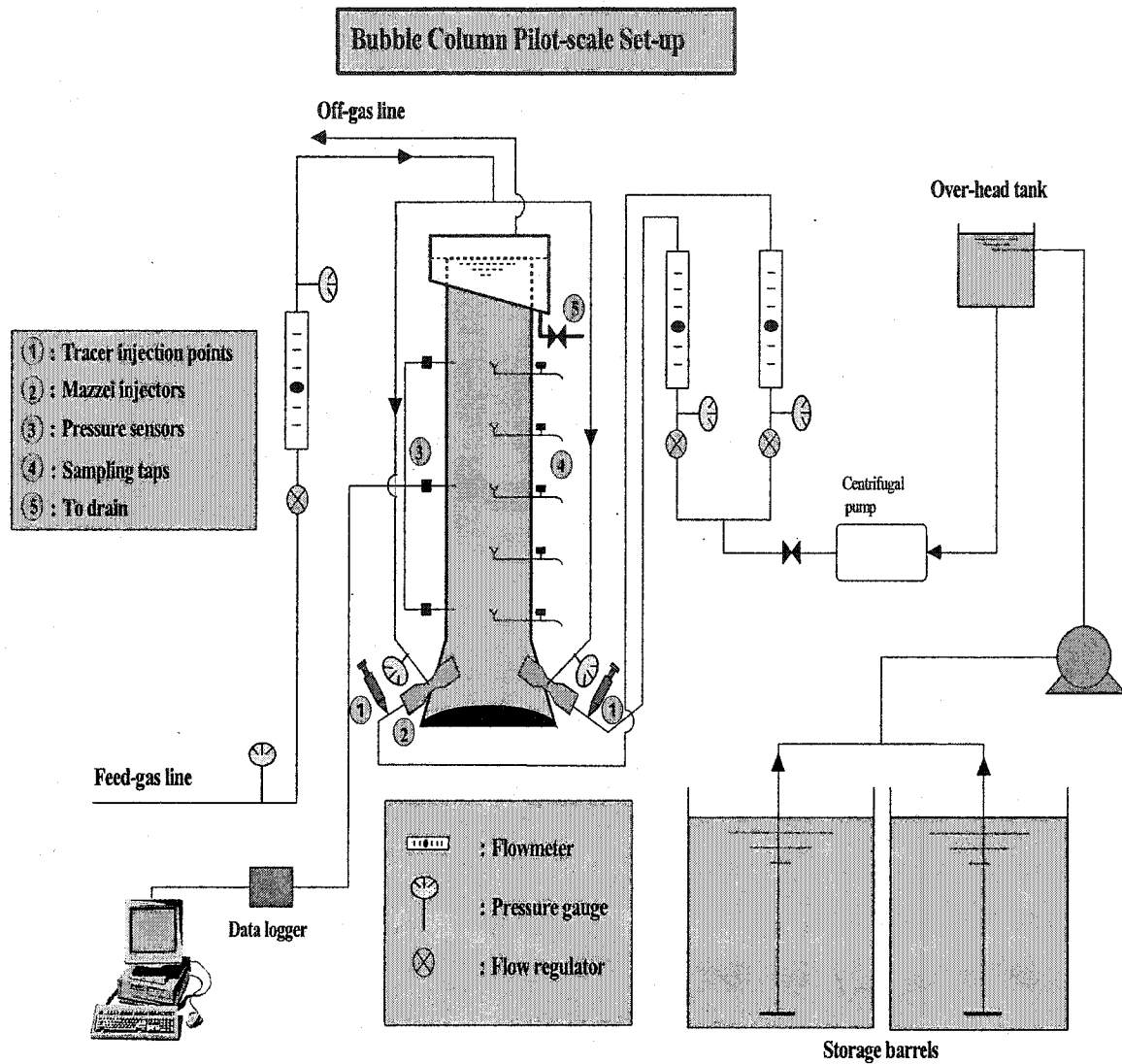


Figure 3-2: Bubble column pilot-scale set-up, adapted from Gamal El-Din and Smith (2001b)

The bubble column portion was made of PVC and had an inner diameter of 100 mm and a total height of 1,520 mm. The non-aerated water level inside the column was maintained at 1,315 mm, and held constant using an overflow weir at the top of the bubble column. A ring tube with a 20 mm diameter hole facing downwards was also placed at the top of the column (Gamal El-Din and Smith 2001b).

The base of the bubble column was elliptical in shape, and the sidewalls of the bottom of the bubble column had a conical shape. This geometry was used to reduce the effects of the backward fluid jet created as a result of the jet impingement, and to minimize any possible short-circuiting that might occur (Gamal El-Din and Smith 2001b).

Mazzei[®] venturi injectors, model type 384, were used as gas injectors. The venturi injectors were placed at an intersecting angle of 125°, 25 mm above the bottom of the bubble column. The distance between the centres of the nozzles was 60 mm (Gamal El-Din and Smith 2001b).

Five bell shaped sampling ports were inserted inside the bubble column at equal intervals along its height. These ports were situated inside the reactor at a distance equal to 1/3 of the column diameter. The bell shape of the sampling ports was chosen to minimize the entrainment of gas bubbles during sample withdrawal. Three Honeywell[®] pressure sensors (model 26PC) were also inserted inside the bubble column at a distance of 1/3 of the column diameter. The three probes were located at heights of 34.8 mm, 830 mm, and 1297 mm, measured from the bottom of the bubble column. The location of the sampling ports and pressure sensors is shown in Figure 3-2 (Gamal El-Din and Smith 2001b).

To minimize fluctuations in the liquid feed rate, peristaltic pumps were used to pump the water from storage tanks to an overhead tank. From there, the water was further pumped by a centrifugal pump into two lines leading to the injectors. The flow of the water was

measured in each of the lines using flowmeters. As the water passed through the venturi injectors, gas was introduced into the motive fluid (water) flow stream. The gas flow rate was monitored using gas rotameters. Pressure gauges were installed on the liquid flow lines, the gas rotameter exit, and at the throat of the injector (i.e. gas introduction point). These pressure gauges were calibrated prior to use (Gamal El-Din and Smith, 2001b). Throughout the entire set of experimental runs, the barometric pressure varied between 692.36 to 715.22 mm Hg.

The data that were used in the following analysis (mixing study, gas holdup study, bubble properties analysis, and overall mass transfer rate determination) were collected from experiments conducted by Gamal El-Din (2001).

Mixing Study

Experimental

Tracer tests were conducted on the impinging-jet bubble column, in an attempt to characterize the backmixing of non-ideal flow conditions. Pulse-input tracer tests were applied using an inert tracer, a potassium chloride (KCl) solution of known concentration, and a test liquid of clean deionized water (Gamal El-Din and Smith 2001a).

The impinging-jet bubble column was operated under co-current mode, with the venturi injectors operating in both ejection and injection modes. The tracer tests were conducted under a range of operating conditions; the liquid flow rate varied from 6.05×10^{-5} to 2.21

$\times 10^{-4} \text{ m}^3/\text{s}$, and the gas flow rate varied from 6.64×10^{-6} to $1.14 \times 10^{-4} \text{ m}^3/\text{s}$, resulting in a theoretical hydraulic residence time (τ) between 48 and 190 s. As was the case in the other experiments conducted on the impinging-jet bubble column, the system was allowed to reach steady state operation prior to the injection of the tracer. The background conductivity of the water was also taken into account (Gamal El-Din and Smith 2001a).

A potassium chloride solution of concentration 70 g/L was injected into the two venturi injectors simultaneously, upstream of the gas introduction point. Conductivity was continuously monitored every second at four locations along the height of the bubble column, until the total tracer mass was recovered. (Gamal El-Din and Smith, 2001a)

Analysis

The development of the TBFCM equations allows for the use of a variable mixing coefficient. Within the impinging-jet bubble column, two zones of mixing can be distinguished. The first zone is representative of the intense mixing caused in the first cell of the model where the impinging jets are located, and is represented by the backmixing ratio r_1 . The remainder of the column is represented by a second zone of mixing, with similar mixing conditions displayed along the height of the column. These conditions are represented by the backmixing ratio r_2 . The idea of having two mixing zones in a bubble column reactor is depicted in Figure 3-3, and is related to the BFCM.

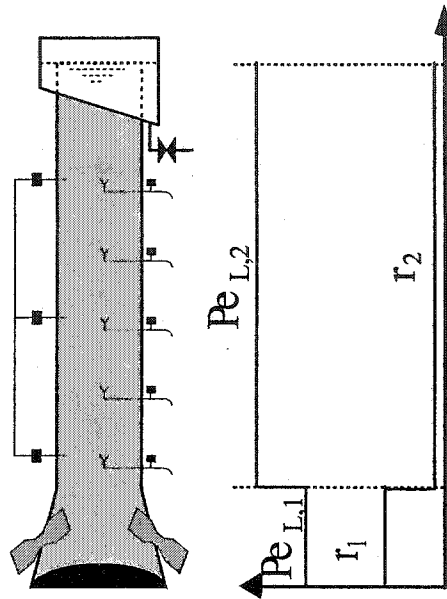


Figure 3-3: Impinging-jet bubble column and representation of two mixing zones, adapted from Gamal El-Din and Smith (2001b)

As a comparison, the presence of only one mixing zone (therefore, a constant r) in the bubble column was investigated. The most accurate and reliable method of characterizing the impinging-jet bubble column was determined.

The conductivity of the solution was measured every second by the probes. This enabled for accurate representation of the tracer concentrations in the residence time distribution (RTD) curves. Predictions of the tracer concentrations were plotted using the TBFCM. After many trials, it was determined that the data was most accurately predicted when the model used eight cells, instead of 10 (plug flow conditions).

Once it was determined that the prediction of tracer concentrations was more accurate using $N_{BFCM} = 8$, the predicted concentrations were compared with the experimentally measured concentrations. For each of the conductivity probes, the sum of squares of the residuals (SSR) between the model predictions and the experimental values was determined. The SSR values were added together (SSR_{Total}). The SSR_{Total} was minimized by changing the backmixing ratio between each cell. As previously described, this minimization technique was employed in two separate situations: 1) the presence of two zones of mixing (r_1 and r_2); and 2) the presence of one mixing zone (r).

After the backmixing ratios had been determined, linear regression was applied to determine a possible relationship with the operating conditions in the bubble column, namely the superficial gas velocity and the superficial liquid velocity. The developed relationship will be applicable to various operating conditions.

Gas Holdup Study

Experimental

The gas hold-up and tracer studies were carried out simultaneously. The impinging-jet bubble column was operated under co-current mode, with the venturi injectors operating in both ejection and injection modes. The superficial liquid velocity varied from 0.008 to 0.028 m/s, and the superficial gas velocity from 0.001 to 0.015 m/s. The system was allowed to reach steady state operation prior to the collection of pressure data (Gamal El-Din and Smith 2001a).

Once the bubble column was operating under steady state conditions, pressure was determined every 10 seconds at the static head levels of 348 mm, 830 mm, and 1,297 mm from the bottom of the bubble column reactor.

Analysis

Each day that a tracer study was carried out, the pressure sensors were calibrated. To do this, data from the three pressure sensors were taken every 10 seconds over a period of time, and immediately downloaded into the data logger. For each pressure sensor, the average reading was calculated, and then further used to determine the pressure along the height of the column. Linear regression techniques were used to produce a calibration curve for each of the pressure sensors, while at the same time producing an equation describing the actual hydrostatic pressure based on the pressure readings (recorded in volts) from the sensors.

The pressure data collected during the tracer experiments were standardized using the equations determined for pressure sensor calibration. The calibrated data was then used to determine the gas hold-up between the top and middle sensors (1,064 mm from bottom), and the middle and bottom sensors (589 mm from bottom). The gas hold-up between these regions was determined based on the following equation:

$$\varepsilon_G = 1 - \frac{\Delta P}{\Delta x} \quad \text{Equation 3-31}$$

Where ε_G = gas hold-up [dimensionless]

ΔP = change in measured pressure between two pressure sensor locations

[m]

Δx = height difference between two pressure sensor locations [m]

The gas hold-up values determined for both regions (top to middle and middle to bottom) were averaged, resulting in two average gas hold-up values, one for each of the two zones in the bubble column. The data were then subject to a residuals analysis, where influential data points were determined based on the standardized residuals. A linear regression technique was used to produce equations representing the gas hold-up of the impinging-jet bubble column as a function of the superficial liquid velocity and superficial gas velocity.

Bubble Properties

Experimental

A digital photographic technique was employed to determine the shapes and sizes of bubbles produced in the impinging-jet bubble column. Experiments were carried out in the impinging-jet bubble column using clean deionized water for the liquid phase and extra-dry air for the gas phase. Feed-gas flow rates varied from 8.2×10^{-6} to 1.0×10^{-4} m^3/s , and liquid flow rates varied from 6.0×10^{-5} to 2.2×10^{-4} m^3/s .

To minimize the distortion caused by the curved surface of the bubble column, a clear acrylic jacket (150 mm x 150 mm) with flat surfaces was placed surrounding the bubble column. Clean deionized water was placed in the gap between the bubble column reactor and the square jacket. As was the case in the other studies carried out on the impinging-jet bubble column, the system was allowed to operate for a period of time to assure that steady state conditions were met; a turnover period equal to at least eight times the theoretical reactor hydraulic retention time. For the purposes of scaling, a measuring tape displaying a known scale was placed in the vicinity where the photographic images were taken.

A Cannon Powershot G1[®] digital camera was levelled, mounted on a tripod and directed at the middle of the column height. Measurements were taken at a distance from the outside wall equal to 1/3 of the column diameter, minimizing any interference that the walls may have had on bubble properties. An adequate source of light was used.

A video photographic technique was also used to investigate the velocity of bubble swarms and to provide a rough estimate of the bubble rise velocity. The bubble swarms were followed over a certain distance along the height of the column, and the time required for them to travel over this distance was recorded. The video digital camera was operated at a capture speed of 15 frames per second and a resolution of 320/240 pixels. Following the recording, the video images were viewed using digital video software.

To capture the still images of the bubbles, the shutter speed was adjusted to 1/1000 s and the resolution to 2048/1536 pixels. Bubble sizes were measured by selecting several sharply focused bubbles, the size and shape of which could be determined. The size measurements of the bubbles were corrected using the proper scale factor.

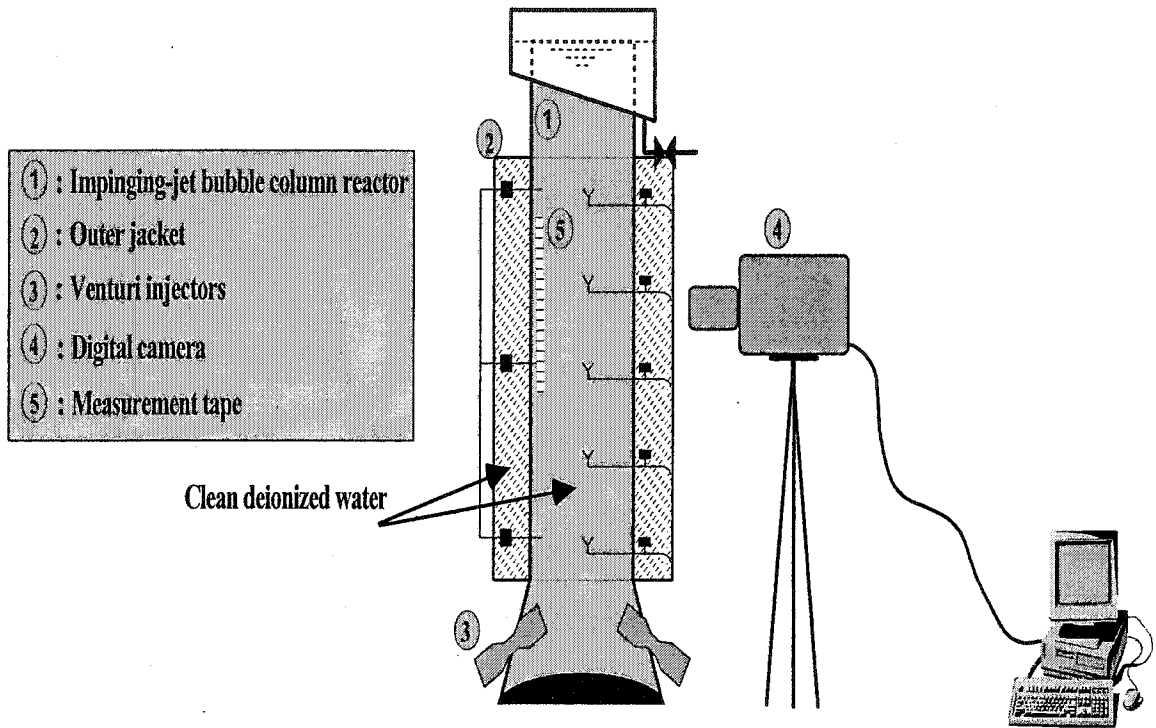


Figure 3-4: Digital photography set-up

Analysis

The diameters of the bubbles were measured according to the following methods. Figure 3-5 serves as an aid to comprehending the two methods.

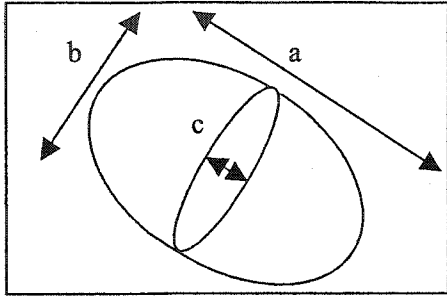


Figure 3-5: Bubble dimensions

The first method (arithmetic mean) assumes that the bubble is in the shape of an oblate sphere, and therefore, that the diameter of the bubble is the average of the lengths a and b. This is a two dimensional analysis of the bubbles. The formula used to solve for the arithmetic mean ($d_{B,1}$) of the bubbles is as follows:

$$d_{B,1} = \frac{a+b}{2} \quad \text{Equation 3-32}$$

Where a = longest side of bubble [mm]

b = shortest side of bubble [mm]

c = width of bubble [mm]

For an entire run, $d_{1,T}$, the bubble diameter, was determined as the average of the bubble diameters for the experimental run:

$$d_{1,T} = \frac{\sum_{i=1}^{i=N} \frac{a_i + b_i}{2}}{N} \quad \text{Equation 3-33}$$

Where N is the total number of bubbles considered.

The second method assumes that the bubble is an ellipsoid, and thus the diameter of the bubble considers all measurable lengths. This three dimensional technique is often simplified by assuming that b and c are of equal length, thus reducing this measurement to a two dimensional approach. Bubble diameter is determined as follows:

$$d_{B,2} = \sqrt[3]{abc} = \sqrt[3]{ab^2} \quad \text{Equation 3-34}$$

For an entire set of experimental runs, the average bubble diameter is calculated based on the following formula.

$$d_{B,2} = \frac{\sum_{i=1}^{i=N} \sqrt[3]{ab^2}}{N} \quad \text{Equation 3-35}$$

The bubble diameter values obtained using the above methods were further used to determine the Sauter mean bubble diameter. The Sauter mean bubble diameter is defined by the following equation:

$$d_s = \frac{\sum_{i=1}^{i=N} d_i^3}{\sum_{i=1}^{i=N} d_i^2}$$

Equation 3-36

Where N is the number of bubbles analyzed, and d_i is the diameter determined by either of the above methods ($d_{B,1}$ or $d_{B,2}$).

Preliminary investigations conducted by Gamal El-Din and Smith (2003b) revealed that the rise velocity of the bubble swarms ranged between 2.4×10^{-1} and 3.0×10^{-1} m/s. It was also revealed that the majority of the bubbles had an oblate ellipsoidal shape. An area on the photograph containing between 50 and 80 bubbles was sectioned off. An example of a picture that was taken and analysed is shown in Figure 3-6.

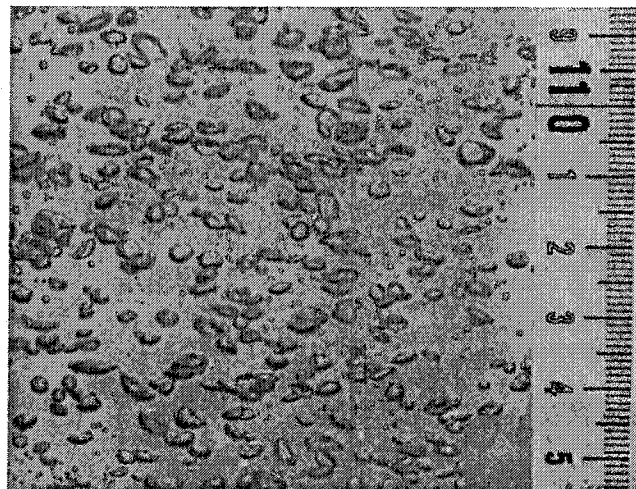


Figure 3-6: Digital photograph of gas bubble at $u_G = 0.019$ m/s and $u_L = 0.003$ m/s

Based on the operating conditions of the bubble column, a linear regression technique was employed to determine the relationship between the superficial liquid velocity, the superficial gas velocity, and the diameter of the bubbles ($d_{b,1}$, $d_{B,2}$, and d_s). This relationship was determined in the form of a linear equation. The linear equation was then applied to the gas hold-up data where the specific interfacial area (a) of the gas bubbles was determined by the well known equation:

$$a = \frac{6\varepsilon_G}{d_s} \quad \text{Equation 3-37}$$

Where a = specific interfacial area (1/m)

ε_G = gas hold-up (dimensionless)

d_s = Sauter mean bubble diameter (1/m)

Ozone Mass Transfer Study

Experimental

The pilot-scale tests were conducted in the impinging-jet bubble column described above. The test water used was clean, deionized water having similar characteristics to the water used in the ozone auto-decomposition study previously described. All materials used in the experiment were ozone-demand-free.

Ozone gas was generated by passing extra-dry pure oxygen through a corona discharge generator; model GLS-7, PCI-WEDECO[®]. Prior to its use, the ozone generator was allowed to stabilize for at least 30 minutes, ensuring stable ozone feed concentration. During the experiments, the concentration of ozone gas was monitored using four PCI-WEDECO[®] monitors. The feed gas line was monitored using model HC 400, and the off-gas line was monitored using model LC. The monitors were allowed to stabilize for at least 15 minutes prior to their use and were periodically calibrated by the KI method (APHA-AWWA-WEF 1995).

The impinging-jet bubble column was operated in the co-current flow mode, with the venturi injectors operating under injection (positive pressure) and ejection (negative pressure) modes. The bubble column was allowed to operate for approximately eight times the theoretical hydraulic retention time of the reactor, ensuring that it reached steady state operation. A constant off-gas concentration verified that the bubble column had reached steady state conditions. The impinging-jet bubble column was operated under a range of liquid flow rates (6.2×10^{-5} to 2.2×10^{-4} m³/s), feed-gas flow rates (1.4×10^{-5} to 1.1×10^{-4} m³/s), and feed-gas ozone concentrations (0.9 to 6.0 % w/w). The temperature of the liquid ranged from 19.5 to 24.5 °C.

Water samples were withdrawn directly into volumetric flasks from the five sampling taps along the height of the column. The flow of the liquid was such as to minimize any loss of ozone. The concentration of ozone was measured in the manner previously described in the kinetics study, using the Indigo method. Pressure data were taken

immediately using a Lakewood® data logger. The gas hold-up of the bubble column was determined using the pressure data collected continuously along the height of the column.

Analysis

The concentration data were analysed using the equations describing the steady-state BFCM. The three sets of equations were solved simultaneously for the predicted concentration using TK Solver® software. The runs were solved within the maximum iteration count of 20 iterations. The relative error in these cases was set to be no more than 1×10^{-6} . The output data was used in a simple spreadsheet, where one parameter minimization techniques were employed by changing the overall mass transfer coefficient $k_L a$. The sum of the squared residuals of the predicted and experimental concentrations was minimized.

$$SSR = \sum (C_{O_3, measured} - C_{O_3, calculated})^2 \quad \text{Equation 3-38}$$

Further to this, linear regression techniques were employed to determine the relationship between $k_L a$ and the superficial liquid and gas velocities. The obtained relationship was used in conjunction with knowledge of the gas hold-up and bubble properties of the impinging-jet bubble column to determine the local mass transfer coefficient k_L .

Chapter 4 Results and Discussion

Mixing in the Bubble Column

The hydrodynamics of bubble column reactors are often difficult to characterize. Many models, such as the axial dispersion model or the backflow cell model, have been developed in an attempt to predict the actual gas and liquid flow mixing patterns. In this research, the transient backflow cell model (TBFCM) was used to predict the mixing behaviour of the liquid media in the impinging-jet bubble column. The superficial liquid velocity ranged from approximately 0.008 to 0.028 m/s, while the superficial gas velocity varied between roughly 0.001 and 0.015 m/s.

The first step in the analysis of the mixing characteristics of the impinging-jet bubble column was to determine the most appropriate number of cells for modeling the transient back flow cell model (TBFCM). Residence time distribution (RTD) curves were used to fit the experimentally determined concentration data with the model predicted concentration profiles. The tracer concentration profile of the impinging-jet bubble column was predicted, with predictions made in the middle of each of the cells (six, eight, or ten). Based on the location of the probes, the corresponding experimentally measured tracer concentration was compared. Based on the sum of squares of the residuals, the number of cells, which produced the minimum, was determined to be the number of cells that most accurately represented the tracer concentration profile of the bubble column. A plot depicting the effect of the number of cells on the dimensionless tracer concentration (Y), as a function time (s), shown in Figure 4-1.

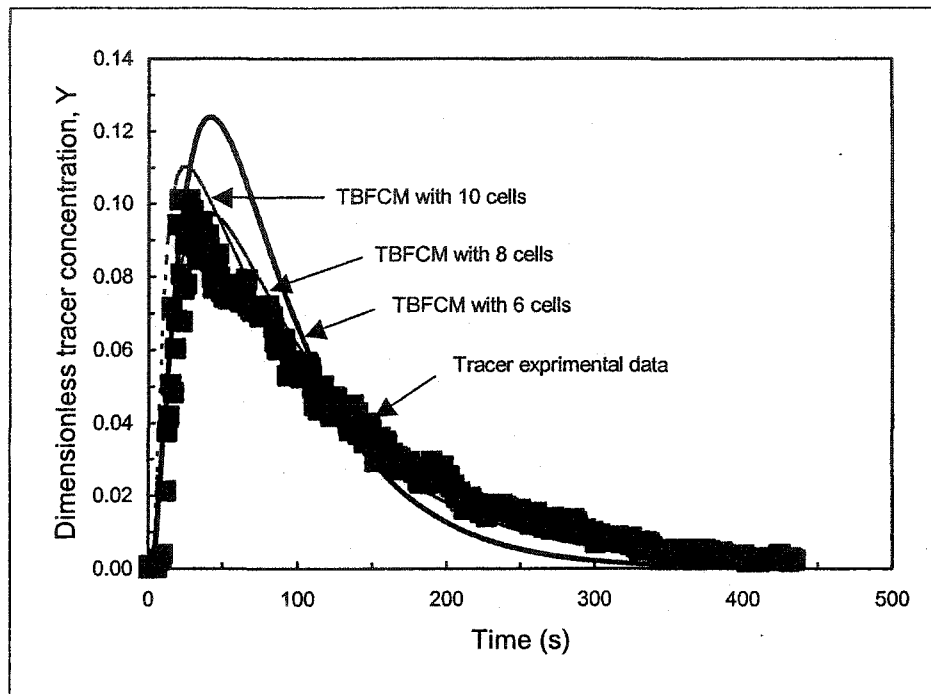


Figure 4-1: Effects of the number of cells on the BFCM

Analysis of the experimental residence distribution (RTD) led to the conclusion that the most appropriate number of cells required to accurately model the impinging-jet bubble column hydrodynamics was eight cells in series ($N_{\text{BFCM}} = 8$). The large buoyancy of the gas bubbles allows for the assumption that the gas phase flows through the reactor in plug flow manner (Gamal El-Din and Smith 2001a).

Based on the use of eight cells, the following four figures, (Figure 4-2, Figure 4-3, Figure 4-4, and Figure 4-5) depict the experimentally measured and model predicted tracer concentrations in each of the four probes.

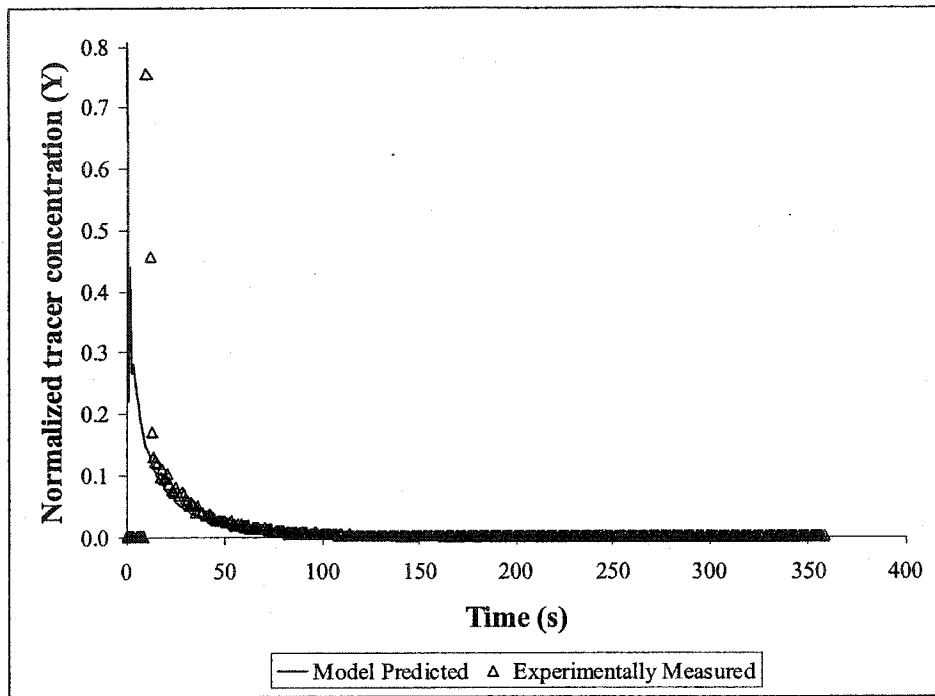


Figure 4-2: Residence time distribution curve for tracer #28, at probe #1

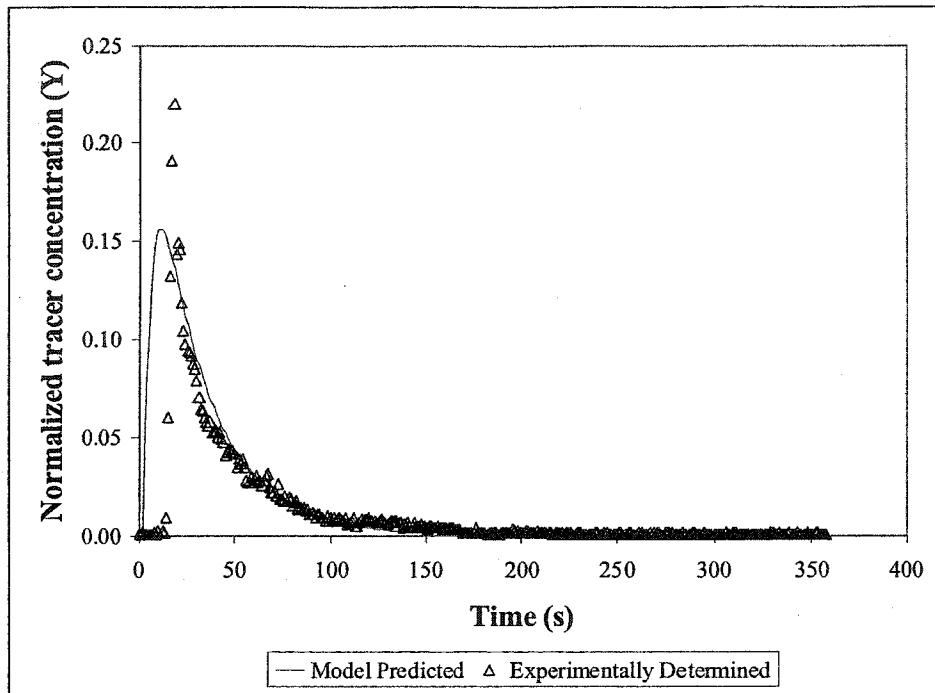


Figure 4-3: Residence time distribution curve for tracer #28, at probe #2

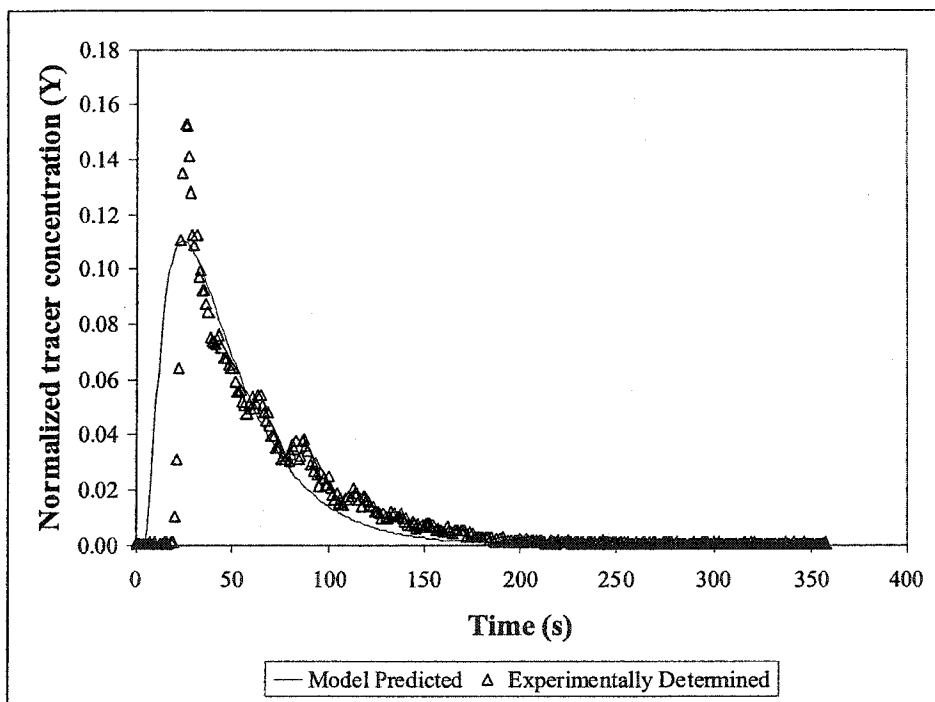


Figure 4-4: Residence time distribution curve for tracer #28, at probe #3

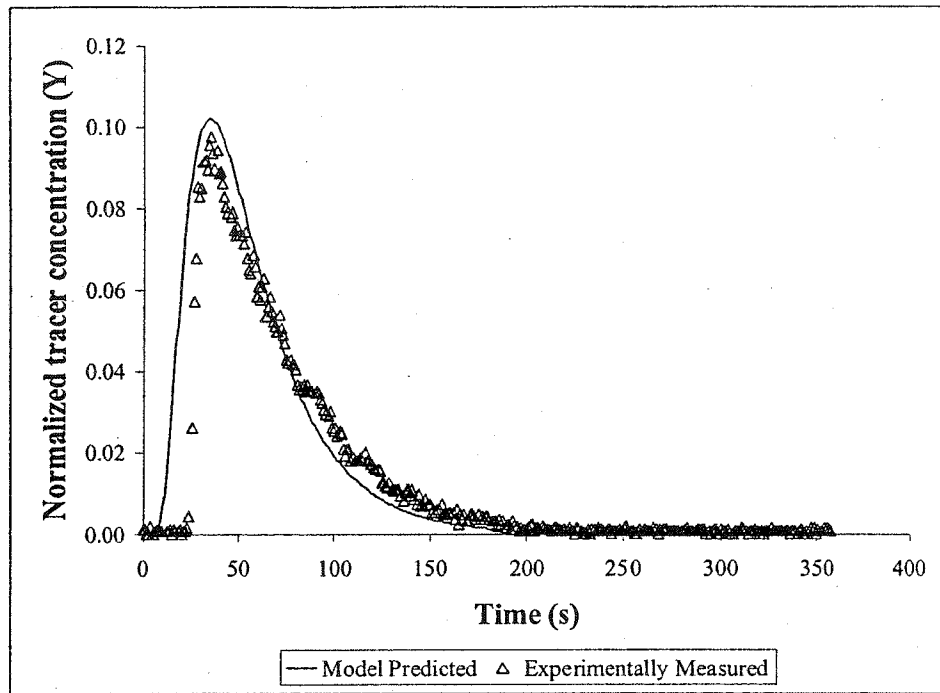


Figure 4-5: Residence time distribution curve for tracer #28, at probe #4

It is known that the residence time of a tracer in a bubble column reactor is influenced by the gas and liquid flow rates. Figure 4-6 depicts the relationship between the tracer residence time and the liquid flow rate, while Figure 4-7 shows the relationship between the residence time and the gas flow rate. Table 4-1 and table 4-2 summarize the tracer operating conditions, and correspond to Figure 4-6 and Figure 4-7 respectively. From Figure 4-6, it can be seen that, at a constant gas flow rate, an increase in the liquid flow rate results in a marked decrease in the residence time of the tracer. It appears, in Figure 4-7, that at a constant liquid flow rate, an increase in the gas flow rate does not influence the residence time in the impinging-jet bubble column.

Table 4-1: Operating conditions corresponding to Figure 4-6

	Tracer 15	Tracer 16	Tracer 17
Q_L (m ³ /s)	1.47×10^{-4}	1.84×10^{-4}	2.21×10^{-4}
Q_G (m ³ /s)	1.12×10^{-4}	1.12×10^{-4}	1.12×10^{-4}

Table 4-2: Operating conditions corresponding to Figure 4-7

	Tracer 20	Tracer 25	Tracer 12	Tracer 15
Q_G (m ³ /s)	1.34×10^{-5}	2.70×10^{-5}	9.45×10^{-5}	1.15×10^{-4}
Q_L (m ³ /s)	1.47×10^{-4}	1.47×10^{-4}	1.47×10^{-4}	1.47×10^{-4}

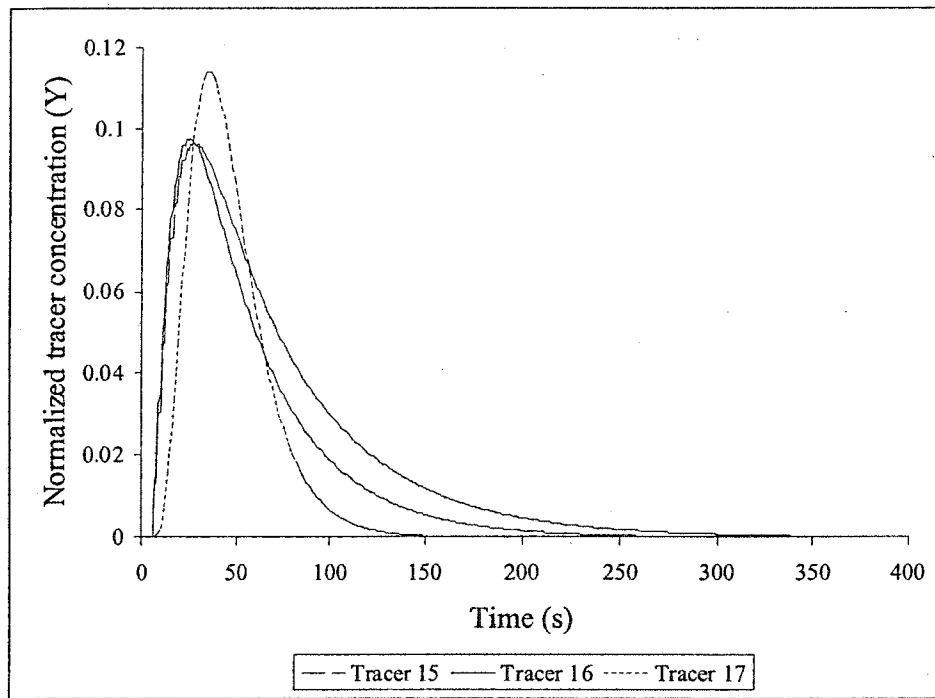


Figure 4-6: Influence of liquid flow rate on the residence times of the tracers, port #4

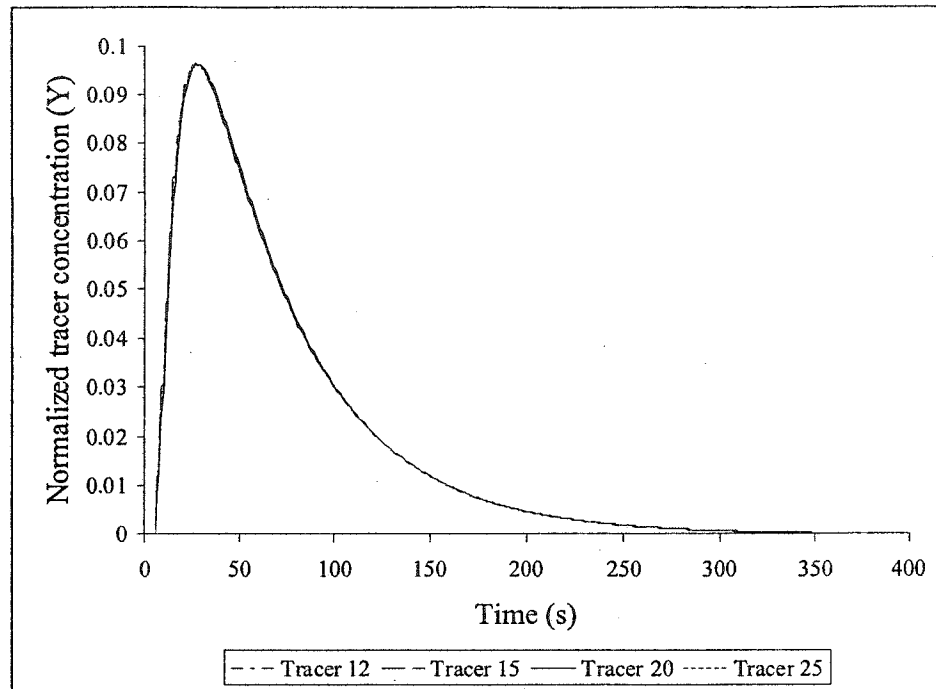


Figure 4-7: Influence of gas flow rate on the residence time of the tracers, port #4

A characteristic of the BFCM model is its ability to predict the hydrodynamics of the liquid phase in bubble columns based on multiple zones of mixing, each with its own backmixing coefficient. Bubble column hydrodynamics can be characterized in two ways: 1) the presence of two mixing zones; and 2) the presence of one mixing zone along the column height.

In the case of two mixing zones, the first of these two zones occurs in the region where the venturi injectors were situated. There was a large degree of mixing in this zone because of the intense turbulence generated by the gas-liquid jets impinging on one another. It is assumed that, along the rest of the bubble column, the turbulence decreases as a result of increasing distance from the venturi injectors. As such, it was prudent to

assume the occurrence of another zone of mixing, located past the first zone of intense mixing. In this second region of mixing, the turbulence and backmixing of the liquid was not as high as in the first mixing zone and can thus be characterized by a smaller mixing coefficient. Figure 3-3 illustrates this hypothesis and the respective extents of these two zones of mixing.

In the second situation, characterization of the bubble column hydrodynamics was achieved using only one mixing zone, and therefore, one mixing coefficient throughout the entire height of the bubble column. In both situations, linear regression analysis was applied, and equations predicting the back-mixing ratio along the height of the column were developed.

It was expected that there was a relationship between the degree of mixing in the liquid phase and the superficial velocities of the gas and liquid media. Figure 4-8 illustrates the relationship between the mixing coefficient for both zones of mixing and the superficial gas velocity. From this graph, there is no obvious relationship between the superficial gas velocity and the degree of backmixing occurring. This leads to the assumption that backmixing was most influenced by the turbulence generated in the liquid phase. It was noted however, that there was a larger degree of backmixing occurring in the first zone closer to the venturi jets. The turbulence generated from the gas-liquid jet impingement plays an important role in modeling the backmixing of the liquid phase in the reactor.

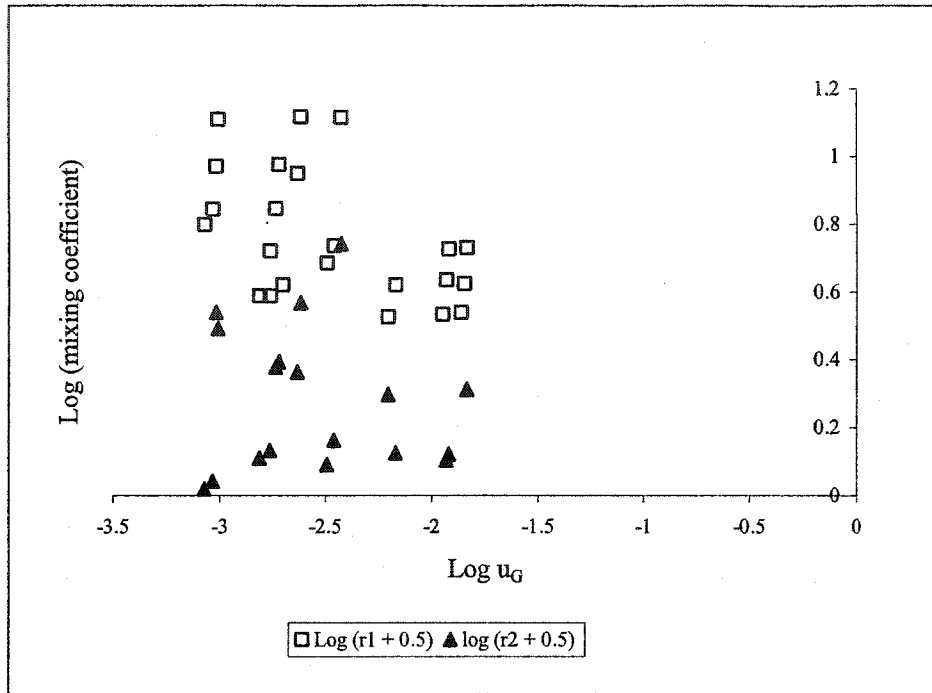


Figure 4-8: Dependency of the backmixing coefficient on the superficial gas velocity

A stronger relationship is displayed between the backmixing ratio and the superficial liquid velocity. As shown in Figure 4-9, it can be deduced that as the superficial liquid velocity increases, the backmixing coefficient decreases, which represents an increase in the axial dispersion coefficient. It is postulated that, as the superficial liquid velocity increases, the system's hydrodynamic behaviour becomes closer to the plug flow reactor regime.

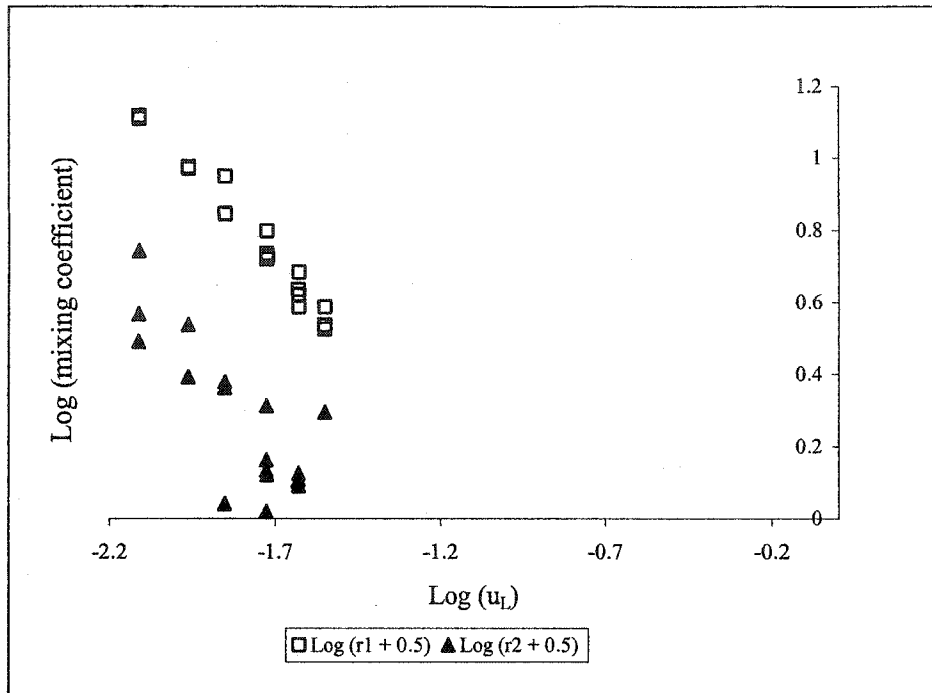


Figure 4-9: Dependency of the backmixing coefficient on the superficial liquid velocity

With respect to the occurrence of two mixing zones in the bubble column, linear regression analysis was applied. The resultant equations can serve as a means to predict the backmixing coefficient in the mixing zones. The generated equations and their respective coefficients of multiple determination (R^2) are as follows:

$$\text{Zone 1: } \log(r_1 + 0.5) = -1.04 - 0.02 \cdot \log(u_G) - 1.00 \cdot \log(u_L) \quad R^2 = 0.98$$

Equation 4-1

Equation 4-1 can be written as:

$$r_1 = 0.09 \cdot u_G^{-0.02} \cdot u_L^{-1.00} - 0.5 \quad \text{Equation 4-2}$$

$$\text{Zone 2: } \quad \text{Log}(r_2 + 0.5) = -1.69 + 0.12 \cdot \text{Log}(u_G) - 1.25 \cdot \text{Log}(u_L) \quad R^2 = 0.78$$

Equation 4-3

Equation 4-3 can be written as:

$$r_2 = 0.02 \cdot u_G^{0.12} \cdot u_L^{-1.25} - 0.5 \quad \text{Equation 4-4}$$

The developed equations indicate a strong relationship with the superficial liquid velocity and a weaker relationship with the superficial gas velocity. It was noted that the regression coefficient associated with the superficial liquid velocity was larger than that associated with the superficial gas velocity. This indicates that it was in fact the effect of the liquid flow rate that dominated the backmixing process, as previously presented in Figure 4-8 and Figure 4-9.

With respect to the equation generated to represent the first zone of mixing, it can be said that the experimental data were accurately modeled, as indicated by a high coefficient of multiple determination ($R^2 = 0.98$). However, the second zone presents a significantly lower coefficient of correlation, only 0.78. This is perhaps because the degree of mixing was influenced significantly by the turbulence generated by the gas injectors. It can be postulated that there was a relationship between the degree of mixing and the distance away from the venturi injectors. As the distance increases, the degree of mixing decreases. The representation of zones may be more accurate if more zones of mixing are included. It is possible that these smaller zones could more accurately represent the mixing occurring, as there would be more mixing coefficients to characterize the change in mixing intensity with increasing distance away from the jets.

Another method of determining the accuracy of the developed models is to plot the predicted values against the experimental values. The accuracy of the models was based on the proximity of the data points to a 45° line, a 1 to 1 representation. The following plots, Figure 4-10 and Figure 4-11, illustrate the accuracy with which the above equations predicted the backmixing ratios for zones 1 and 2, respectively. From these plots, it was noted that the data are relatively close to the 45° line, indicating good regression model prediction accuracy. The majority of the data lie within the 95% confidence intervals, with only a few data points lying outside these boundaries. This also indicates that the generated models are quite accurate.

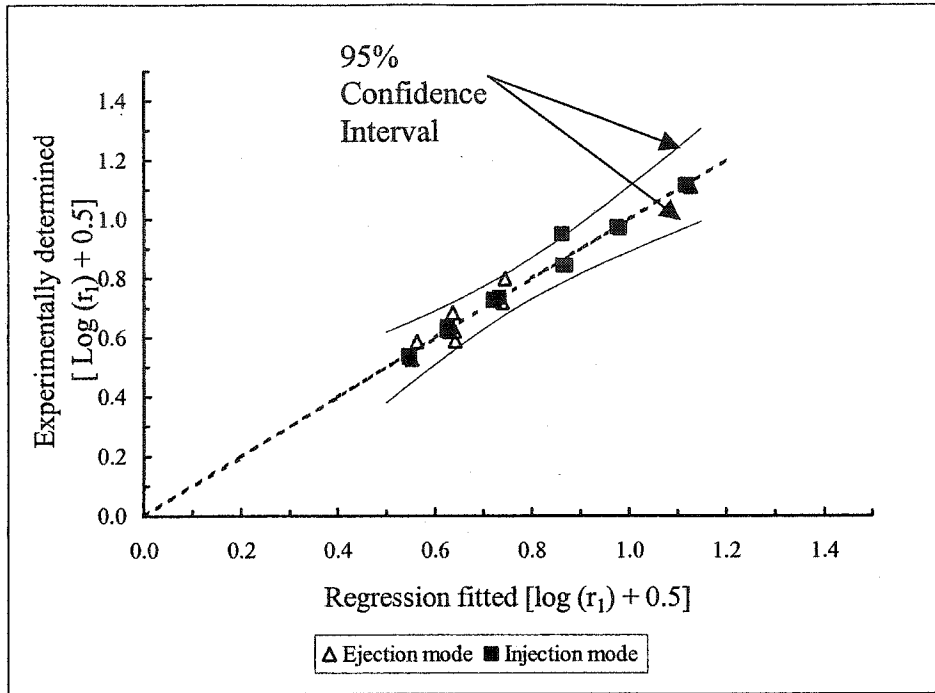


Figure 4-10: Comparison between the experimentally determined and regression fitted backmixing ratios for zone one

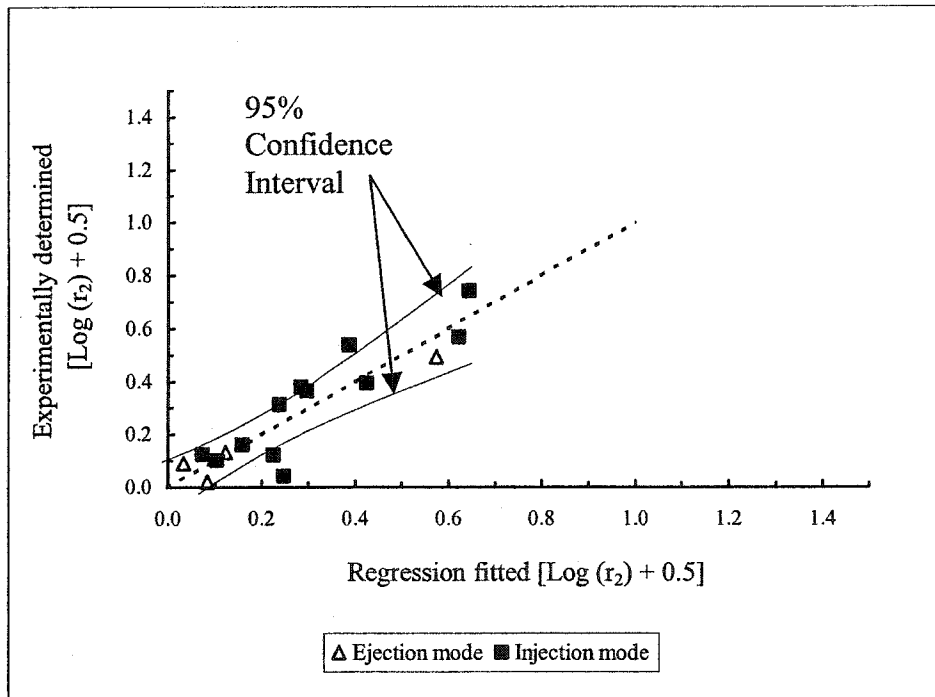


Figure 4-11: Comparison between the experimentally determined and regression fitted backmixing ratios for zone two

As with the previously proposed models representing the occurrence of two mixing zones, it was assumed that there was a similar dependence on gas and liquid velocities when modeling the reactor using only one mixing zone. There was thus a similarly weak relationship between the superficial gas velocity and the degree of backmixing. Kago et al. (1989) noted that axial mixing depends on the flow regime, and thus depends on the superficial gas velocity of the system.

When considering the presence of only one mixing zone in the bubble column, a similar analysis to the one previously described for the two mixing zones was undertaken. From linear regression analysis, a model predicting the back-mixing ratio, r , was developed.

$$\text{Log}(r + 0.5) = -0.88 + 0.08 \cdot \text{Log}(u_G) - 0.97 \cdot \text{Log}(u_L) \quad R^2 = 0.91 \quad \text{Equation 4-5}$$

Equation 4-5 can be written as:

$$r = 0.13 \cdot u_G^{0.08} \cdot u_L^{-0.97} - 0.5 \quad \text{Equation 4-6}$$

With equations developed to represent the two situations (one and two mixing zones) the prudence of modelling the reactor with only one mixing coefficient was investigated. To do this, the data predicted by the equations describing the two zones of mixing were averaged. These average values were then plotted against the predicted values as

determined by the formula representing the presence of one zone of mixing. The resultant graph is shown below in Figure 4-12.

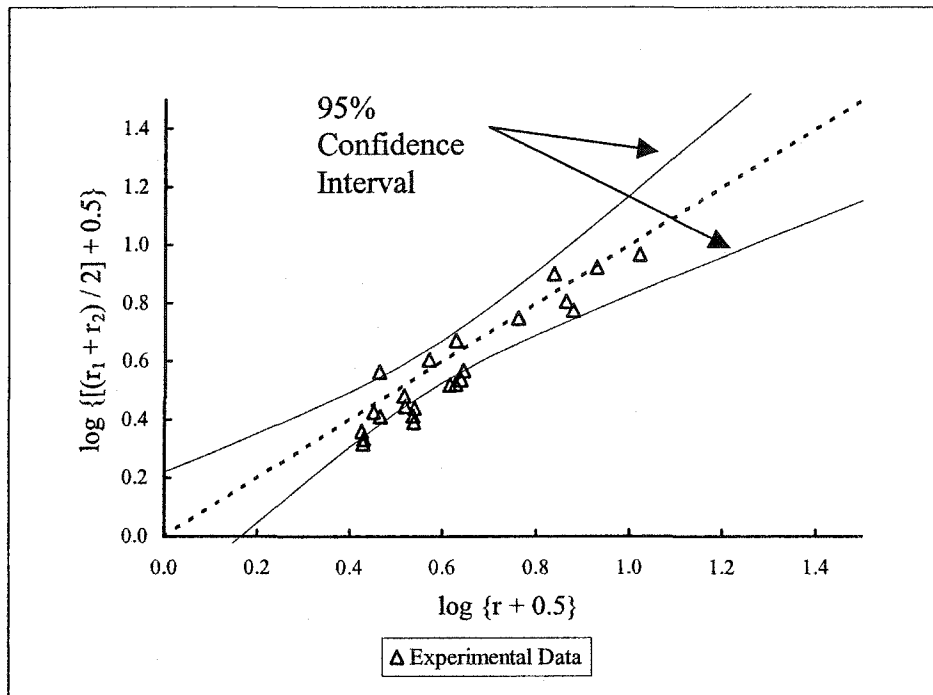


Figure 4-12: Comparison of the use of one mixing zone and two mixing zones to characterize the impinging-jet bubble column

It can be noted that the majority of the data points are captured within the 95 % confidence intervals, indicating that there is no significant difference in characterizing the bubble column with one mixing zone or two mixing zones. For simplicity, the impinging-jet bubble column will be modeled as having only one mixing zone from this point forward.

Zhou (1995) proposed a similar correlation to that described by Equation 4-3. This generalized form of the above model easily predicts the backmixing ratio in both co-current and counter-current flow regimes. The model proposed by Zhou (1995) is given below in its general form, along with the associated coefficients in Table 4-3.

$$\log(r + 0.5) = a + b \cdot \log(u_G) + c \cdot \log(u_L) \quad \text{Equation 4-7}$$

Table 4-3: Coefficients used in Equation 4-7

Flow regime	a	b	c
Counter-current + Co-current	2.45	0.40	-1.03
Counter-current	-1.06	0.34	-0.95
Co-current	-1.64	0.36	-1.21

Figure 4-13 indicates that the proposed model, employing a constant backmixing coefficient along the height of the impinging-jet bubble column, is justified as a prediction tool. This plot illustrates a comparison between the experimentally determined mixing ratio and the mixing ratio predicted by linear regression. The data points lie close to the 45° line, indicating good accuracy, and further confidence can be placed in the validity of the model, as the majority of the data points lie within the confines of the 95% confidence intervals.

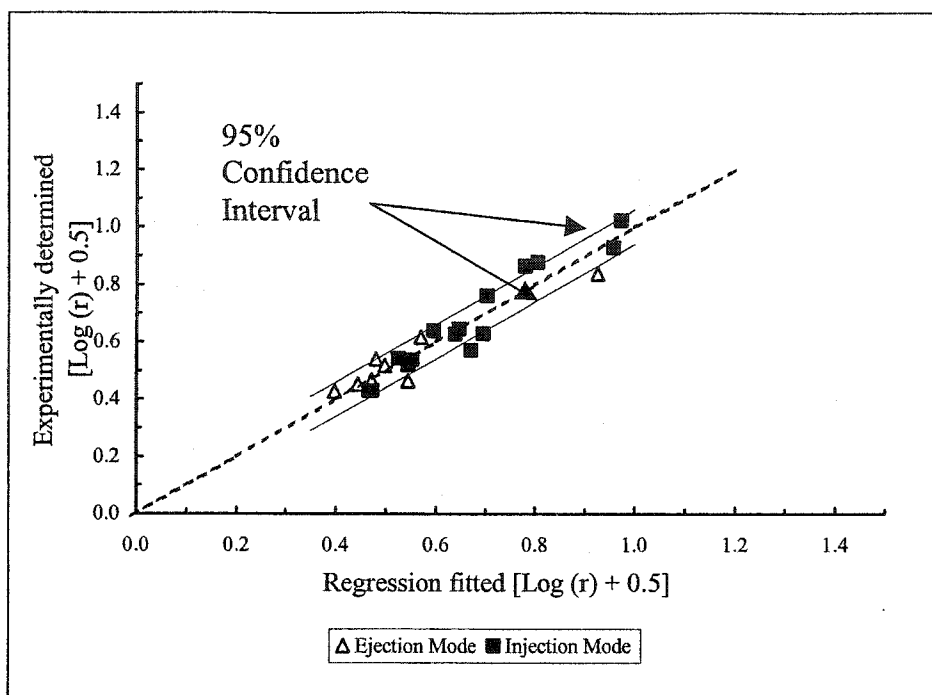


Figure 4-13: Comparison between the experimentally determined and regression fitted backmixing ratios for the entire bubble column

As previously discussed, when investigating the effect of the superficial liquid velocity only, the backmixing coefficient was seen to increase with an increase in u_L , which translates to an increase in the axial dispersion coefficient. Similar observations were made by Wachi et al. (1987) at high liquid up-flow rates. Their co-current bubble column operated with a gas supply nozzle which introduced gas horizontally into the bottom of the bubble column.

The relationships between the superficial liquid and gas velocities and the degree of backmixing are further displayed in Figure 4-14. This plot depicts the degree of backmixing against the superficial gas velocity, at varying superficial liquid velocities. It further illustrates that an increase in the superficial gas velocity combined with a decrease

in the superficial liquid velocity, results in an increase in the degree of backmixing. These observations are similar to those noted by Mariñas et al. (1993) in their experiments with bubble columns operating in both counter-current (packed, unpacked) and co-current (packed with plastic saddles) flow modes. This particular bubble column was 5.18 m high with an inside diameter of 0.15 m. The water was held constant at a depth of 4.88 m. Either fine or coarse ceramic diffusers were placed at the bottom of the bubble column reactor.

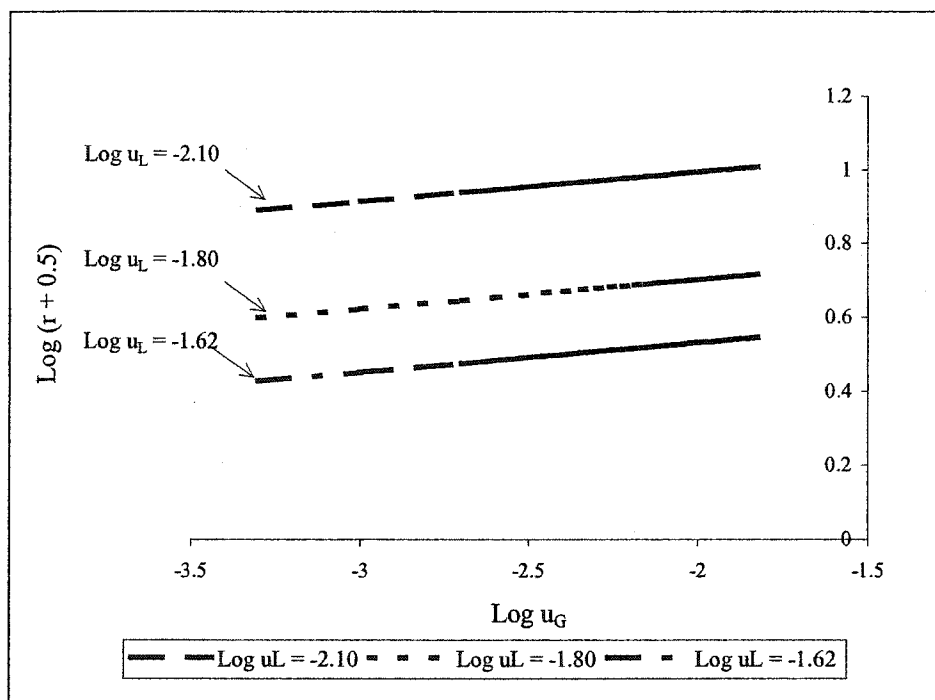


Figure 4-14: Relationship between the mixing ratio and the superficial gas velocity at specific superficial liquid velocities

Gas Hold-up

During the tracer and gas hold-up experiments, the gas flow rate (Q_G) varied from 6.5×10^{-6} to 1.15×10^{-4} m³/s and the liquid flow rate (Q_L) varied from 6.05×10^{-5} to 2.21×10^{-4} m³/s. This led to a superficial gas velocity (u_G) ranging between 8.00×10^{-4} and 1.46×10^{-2} m/s and superficial liquid velocity (u_L) ranging between 7.70×10^{-3} and 2.80×10^{-2} m/s.

The barometric pressure varied with each day, however it remained relatively constant throughout the testing period within the day. The temperature of the water varied during the experiments, with a maximum change in water temperature of 3°C within an experimental run. The variation of these two parameters was taken into account through the unique calibration curves determined for each day of operation.

Before any of the experiments began, the bubble column was allowed to operate until steady-state conditions prevailed. To assure this, the collected pressure data was graphed as a function of time. There were no significant fluctuations in the pressure identified by these graphs, indicating that the system had reached steady-state condition. An example is shown in Figure 4-15.

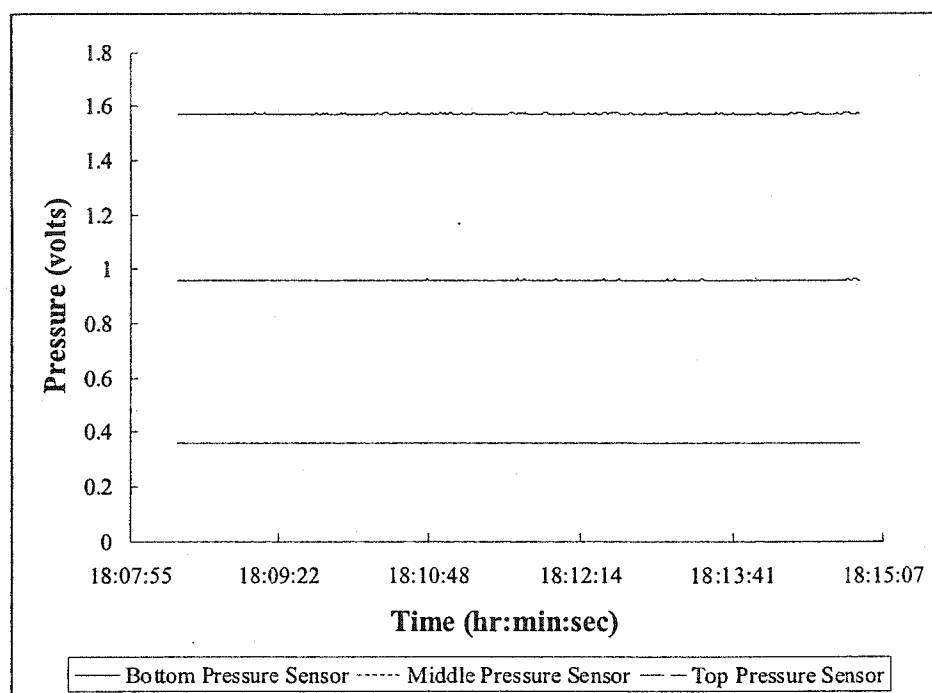


Figure 4-15: Pressure at three pressure sensors as a function of time, corresponding to tracer 13, run 5

Once it had been determined that the reactor was operating under steady-state conditions, the three pressure sensors in the bubble column were tested. The data were initially measured in volts, and then converted into the actual hydrostatic pressure. Calibration curves and their resultant linear equations were developed so that the collected data (reflecting the pressure at three points in the bubble column) could be adjusted accordingly, based on the hydrostatic pressure. These equations also allowed for the accurate prediction of the pressure along the height of the reactor. The linearity of the equations allowed for the successful and accurate representation of changes in pressure, as it is known that the hydrostatic pressure exerted by water increases linearly as depth increases. A set of calibration curves and the developed linear equations are shown in Figure 4-16.

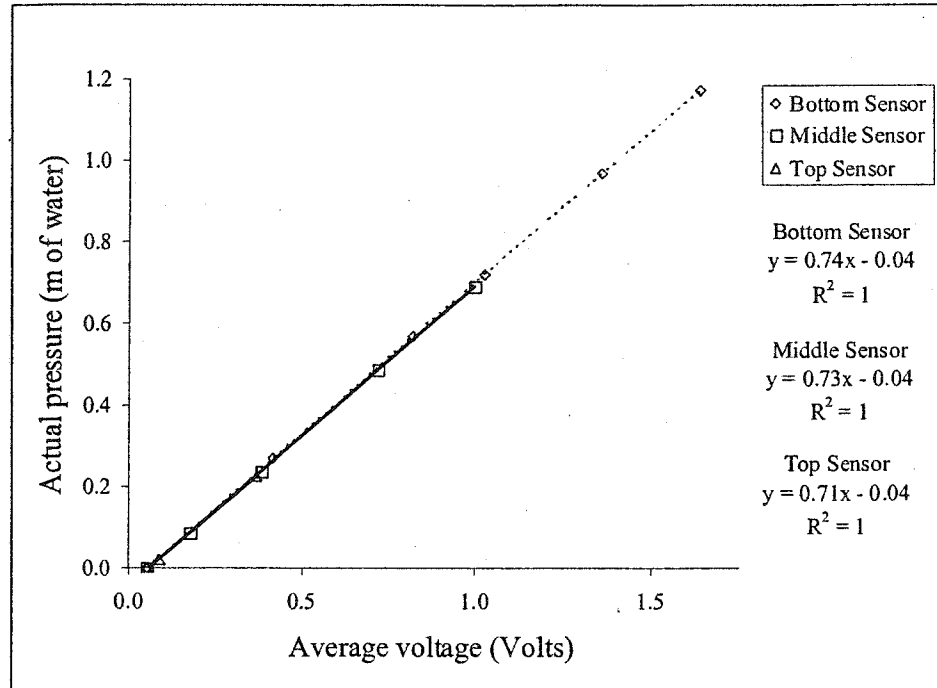


Figure 4-16: Calibration curves for three pressure sensors, corresponding to tracer 13, run 5

Using the calibration curves associated with a particular set of runs, the recorded pressures in volts were converted to pressure readings in meters of head. From these pressure data, the gas hold-up was calculated, using Equation 3-9. The gas hold-up in this equation was calculated based on the difference in pressure measured between the pressure sensors. To reiterate, there were three pressure sensors used to receive input regarding the pressure along the bubble column. As a result, there were two distinct zones in the bubble column. The upper measure gas hold-up occurs between the upper sensor and the middle sensor, and the lower measure gas hold-up occurs between the middle sensor and the lower sensor. Therefore, the upper measure gas hold-up was assumed to

remain the same in the upper half of the column, and the lower measure gas hold-up was assumed to remain the same in the lower half of the column.

Consequently, the calculation of gas hold-up leads to two values, one for the upper zone and one for the lower zone. According to the literature, superficial gas velocity has the strongest known relationship with gas hold-up, and as such, linear regression was performed on this relationship for both the upper and lower zones. The linear regression equations were compared following methods outlined by Zar (1999). It was found that, at the 95% confidence level, these two regression equations produced significantly different slopes, implying that the gas hold-up in the two sections of the bubble column were also significantly different. This differences is illustrated in Figure 4-17.

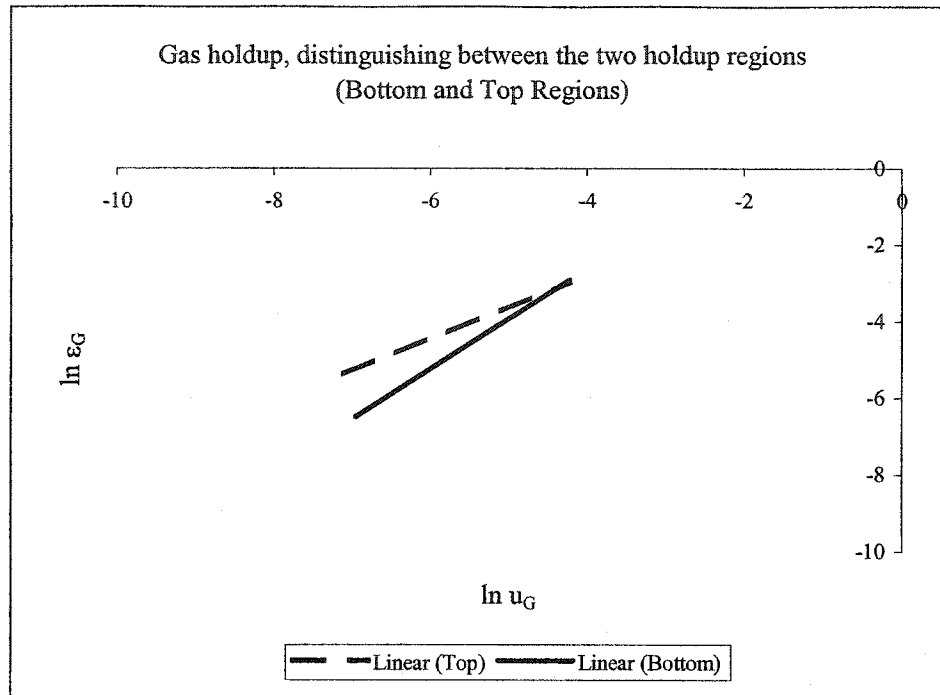


Figure 4-17: Representation of the difference between the gas holdup in the upper and lower sections of the bubble column reactor

Although it is an extremely important parameter, the gas hold-up of a reactor is very small, and as such, the added accuracy of having two distinct zones with different hold-up correlations will not significantly impact the mass transfer modeling. For reasons of simplicity, the gas hold-up calculated for the entire bubble column was considered to be the average of these two values.

Following a simple statistical procedure, standardized residuals were determined. As noted by Montgomery et al. (2001), outlying data points are considered to be data points with standard residuals that lie outside the limits of -2 and +2. Data were eliminated in this iteration. Only one iteration was performed, as approximately 95% of the standardized residuals lay within this range (Montgomery et al. 2001).

Pooling the pressure data considered to be valid, and taking into account the varying superficial liquid and gas velocities, regression analysis yielded a relationship between these two variables and the gas hold-up. This statistical technique was carried out for two situations: 1) ejection and injection modes analysed as two separate data sets; and 2) Ejection and injection modes analysed as one data set.

Considering the two modes of operation (injection mode and ejection mode) as being individual processes potentially leading to two different predictions of gas hold-up, linear regression allowed for the development of linear formulae predicting the gas hold-up in each case. The exponential forms of the linear equations are as follows:

$$\text{Injection: } \quad \varepsilon_G = 5.58 \cdot u_G^{1.104} \cdot u_L^{-0.002} \quad R^2 = 0.94 \quad \text{Equation 4-8}$$

$$\text{Ejection: } \quad \varepsilon_G = 0.007 \cdot u_G^{1.224} \cdot u_L^{-1.957} \quad R^2 = 0.86 \quad \text{Equation 4-9}$$

In each of the proposed relationships there is a clear dependency on the superficial gas velocity of the system. This is indicated by the large exponent of u_G . Figure 4-18 and Figure 4-19 illustrate this dependency, for the injection mode and ejection mode of operation respectively. As the superficial gas velocity increases, the gas hold-up increases as well, in a nearly linearly fashion. The 95% confidence intervals based on the predicted models do not capture the majority of the data set with respect to the injection mode of operation, even though the equation predicted a high coefficient of multiple

determination. This is possibly due to the large data set ($n = 153$), which narrows the confidence interval. The confidence interval with respect to the ejection mode of operation is slightly more reliable, including the majority of the data points with only a few outliers. This confidence interval is broader, as the data set is much smaller than that used for the injection mode of operation ($n = 29$).

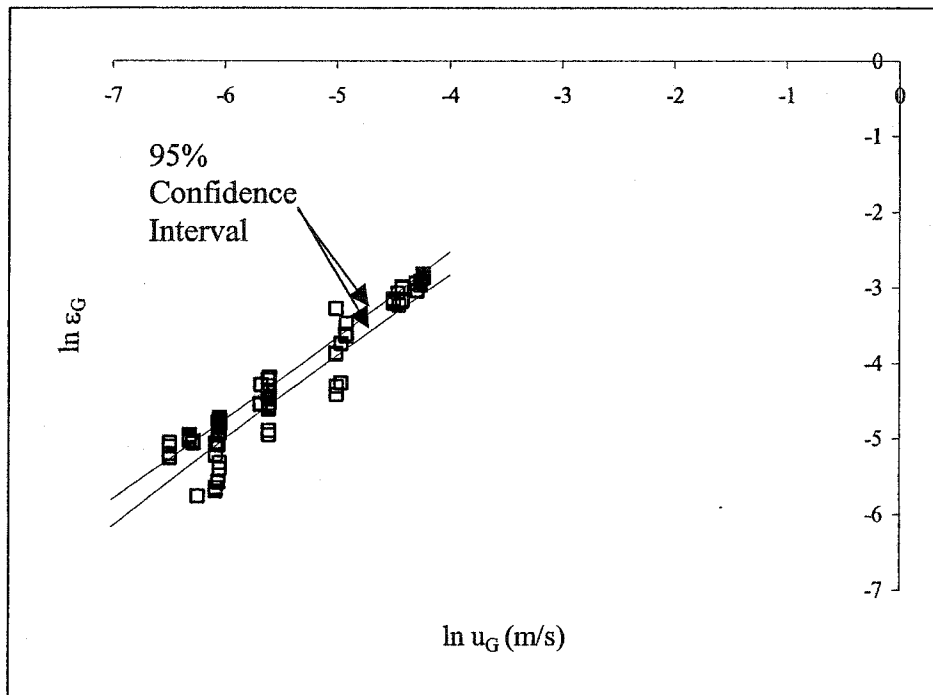


Figure 4-18: Relationship between the gas hold-up and the superficial gas velocity under the injection mode of operation ($n = 153$)

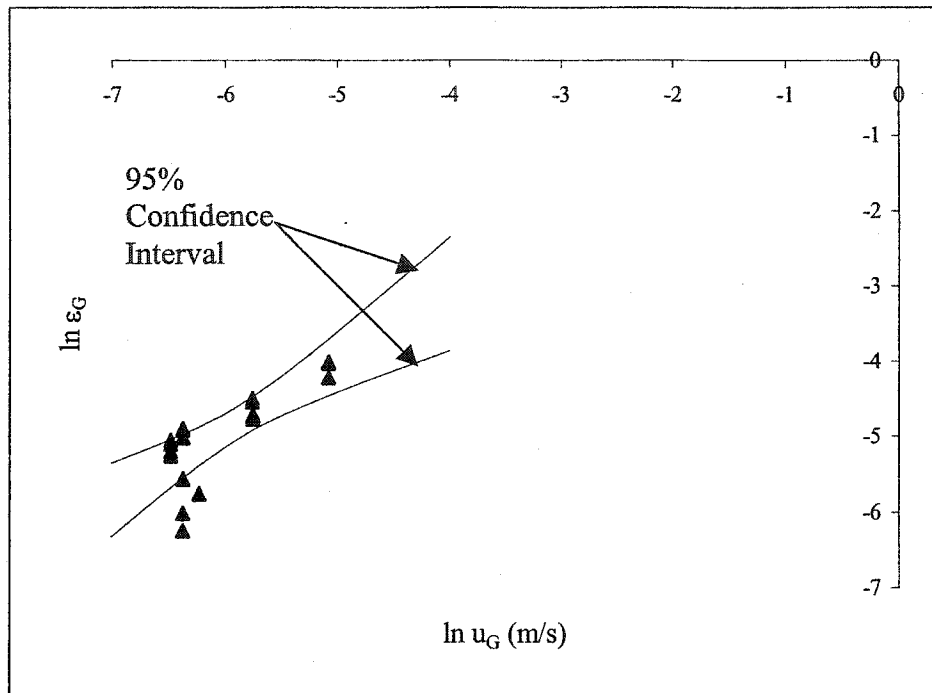


Figure 4-19: Relationship between the gas hold-up and the superficial gas velocity under the ejection mode of operation ($n = 29$)

The following figure, Figure 4-20, illustrates weak relationship existing between the superficial liquid velocity and the gas hold-up in the impinging-jet bubble column. From this figure, it can be seen that the data are scattered intermittently and without regularity; no clear trend is apparent. Further investigation is required, and will be discussed at a later point.

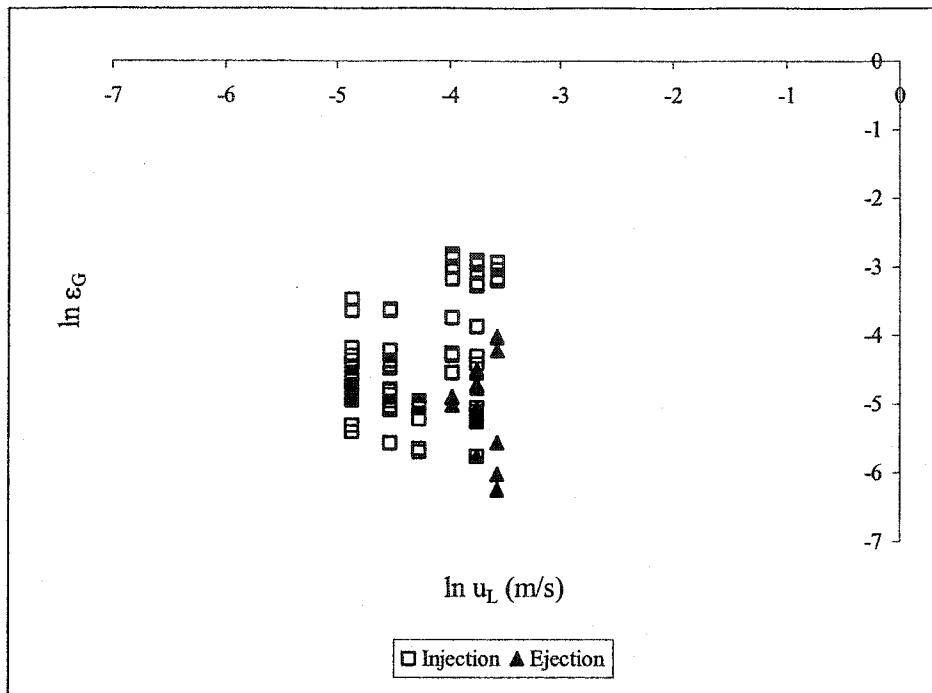


Figure 4-20: Relationship between the gas hold-up and the superficial liquid velocity under different modes of operation

It was determined, based on the two modes of operation, that the slopes of the lines are considered to be statistically different at the 95% confidence level. However, Figure 4-21 illustrates other findings. This plot depicts the relationship between the gas hold-up and the superficial gas velocity for both modes of operation. From this figure, it is clear that there is considerable overlap between the two data sets. As such, it is reasonable to conclude that, although the slopes are significantly different, the data sets themselves can be considered together as a whole.

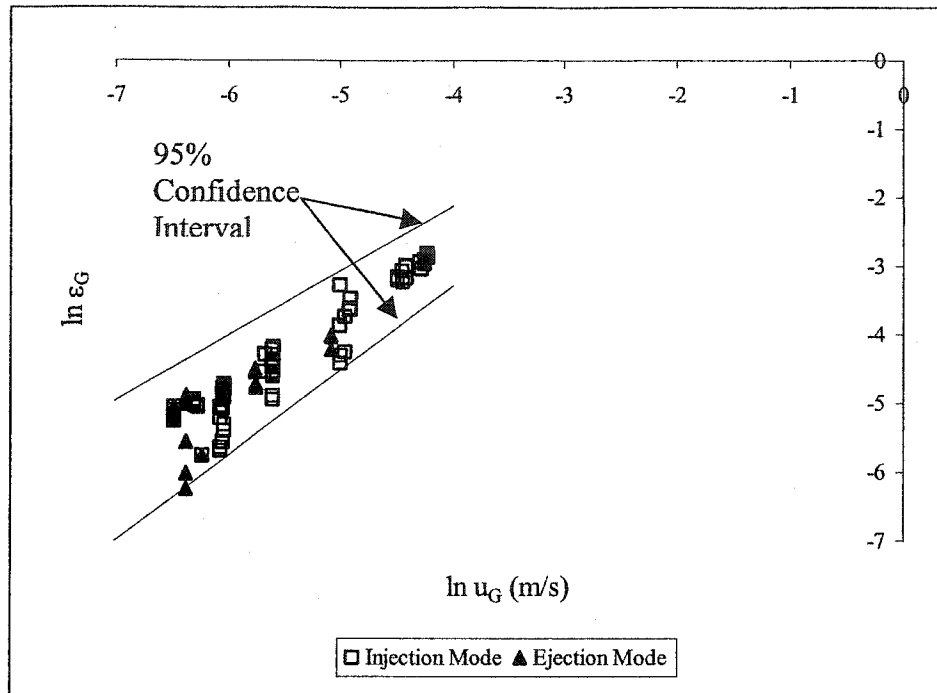


Figure 4-21: Relationship between the gas hold-up and the superficial gas velocity under different modes of operation

After combining the data from both modes of operation, linear regression was carried out again. Another equation was developed predicting the gas hold-up in the impinging-jet bubble column. The proposed equation is based on two conditions: 1) The gas hold-up of the bubble column is the average of the hold-ups determined in the lower half and the upper half of the reactor; and 2) The data sets for the operation of the venturis in both modes of operation can be considered as one data set. The relationship is as follows:

Average gas hold-up:

$$\varepsilon_G = 4.67 \cdot u_G^{1.109} \cdot u_L^{-0.046} \quad R^2 = 0.92 \quad \text{Equation 4-10}$$

Again, the developed relationship displays a clear and very strong dependence on the superficial gas velocity (u_G) of the system. This relationship is shown in **Figure 4-22**. It is obvious that as the superficial gas velocity increases, gas hold-up increases as well. As anticipated, more gas being injected into the system results in more gas becoming entrained in the liquid, causing a larger hold-up. This linear relationship was also observed by other authors (Akita and Yoshida 1973, Biń et al 2001, Patil et al. 1984, Roustan et al. 1996). The 95% confidence interval is relatively narrow, with data deviating from this interval.

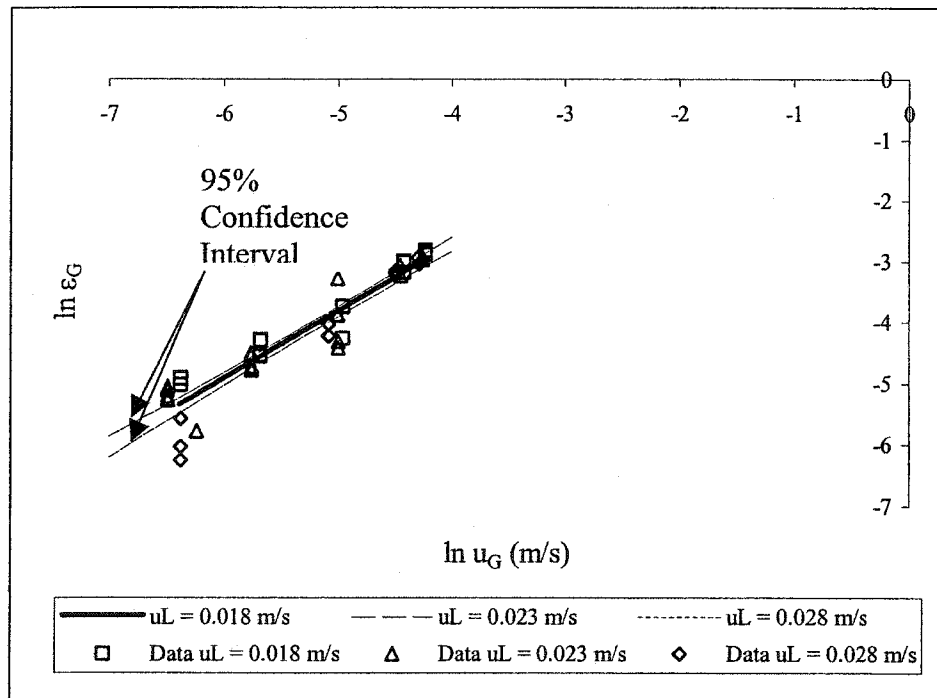


Figure 4-22: Relationship between the gas hold-up and the superficial gas velocity at varying superficial liquid velocities

Akita and Yoshida (1973) tested a bubble column operating with a gas sparger consisting of a single hole drilled into the centre of a resin plate. The system operated continuously

with respect to the gas flow rate (7.28×10^{-3} to 4.19×10^{-1} m/s), at varying temperatures. Akita and Yoshida concluded that the fractional gas hold-up increased with the superficial gas velocity. This relationship was found to be linear when the superficial gas velocity was plotted against $\epsilon_G / (1-\epsilon_G)^4$ on logarithmic scales. Similarly, Biń et al. (2001) tested the use of a porous gas distributor in tall bubble columns with gas flow rates between 8.33×10^{-5} and 3.33×10^{-4} m³/s, and liquid flow rates between 2.78×10^{-5} and 1.25×10^{-4} m³/hr. It was concluded there, as in this study, that the gas hold-up had a power law relationship ($\epsilon_G = 5.54 \cdot u_G^{1.03}$) with the superficial gas velocity in the column. When plotted on a logarithmic scale, a linear relationship was demonstrated. Patil et al. (1984) tested the use of a sieve plate sparger and a single point sparger in their sectionalized bubble column in semi-batch manner. The bubble column was sectionalized using four horizontal baffles, each with a central hole diameter of 0.274 m. A linear relationship between the fractional gas hold-up (log scale) and superficial gas velocity (arithmetic scale) existed for both types of spargers. It was also noted that the sectionalized bubble column produced larger gas hold-up values than a conventional bubble column with the same sparger design. This is possibly due to the fact that, as the gas passes through the baffle leading into the next section, gas bubbles are sheared into smaller bubbles and thus the coalescence of bubbles is limited. This would result in a lower bubble rise velocity and an increase in the amount of gas entrained in the bubble column. Roustan et al. (1996) investigated a pilot scale bubble column employing a porous distributor and operating in co-current, counter-current, and batch modes. It was determined that the gas hold-up depended strongly, and in a purely linear manner, on the superficial gas velocity of the operating system, no matter the operating mode.

Testing of the relationship between gas hold-up and superficial liquid velocity in the impinging-jet bubble column indicated that a strong relationship does not exist, indicated by the small exponential coefficient in the regression equation. These ideas are confirmed visually in Figure 4-23. Similar trends have been observed by Akita and Yoshida (1973), with their bubble column which operated with a single hole drilled into a partition between the gas chamber and the column, and Biń et al. (2001) whose bubble column employed porous gas distributors. In the confined plunging liquid jet contactor studied by Jakubowski et al. (2003), it was determined that the gas hold-up decreased slightly as the liquid flow rate increased, as was also observed in the current study. This is to be expected, as an increase in the liquid flow rate results in a smaller residence time of the bubbles in the bubble columns.

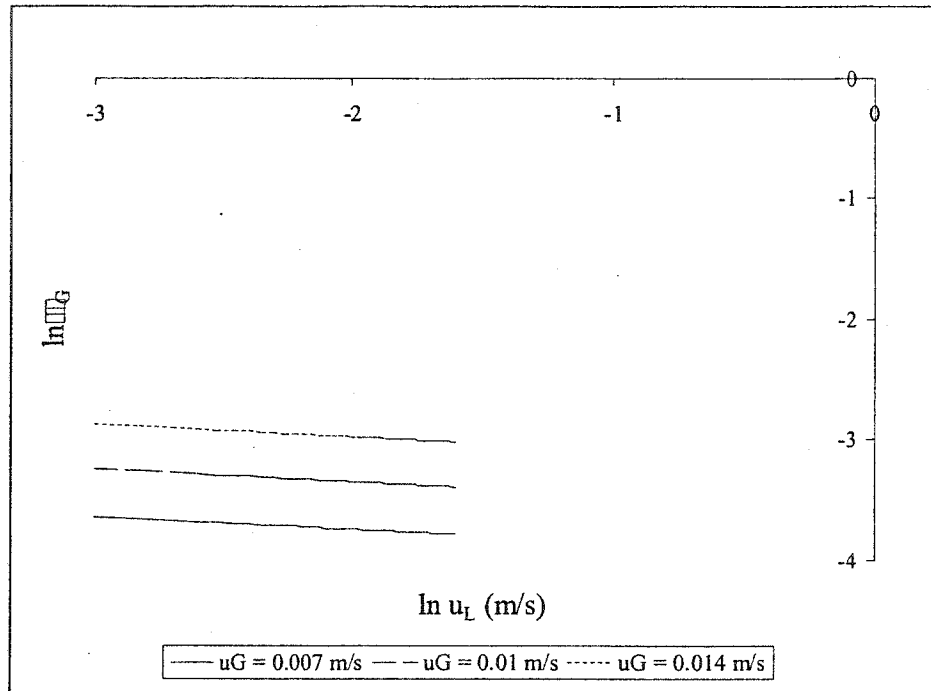


Figure 4-23: Relationship between the gas hold-up and the superficial liquid velocity

A model's ability to accurately predict gas hold-up can be proven by validating its applicability. Figure 4-24 illustrates the proposed model's ability to accurately predict the gas hold-up in the impinging-jet bubble column. A plot comparing the modeled gas hold-up values with the experimentally determined gas hold-up data is shown in Figure 4-24. A line of adequate fit was drawn through the data set, giving an R^2 coefficient equal to 0.92. In the ideal case, the predicted values would lie on a 45° angle with the experimental values. However, the 95% confidence intervals on the mean response capture the majority of the data.

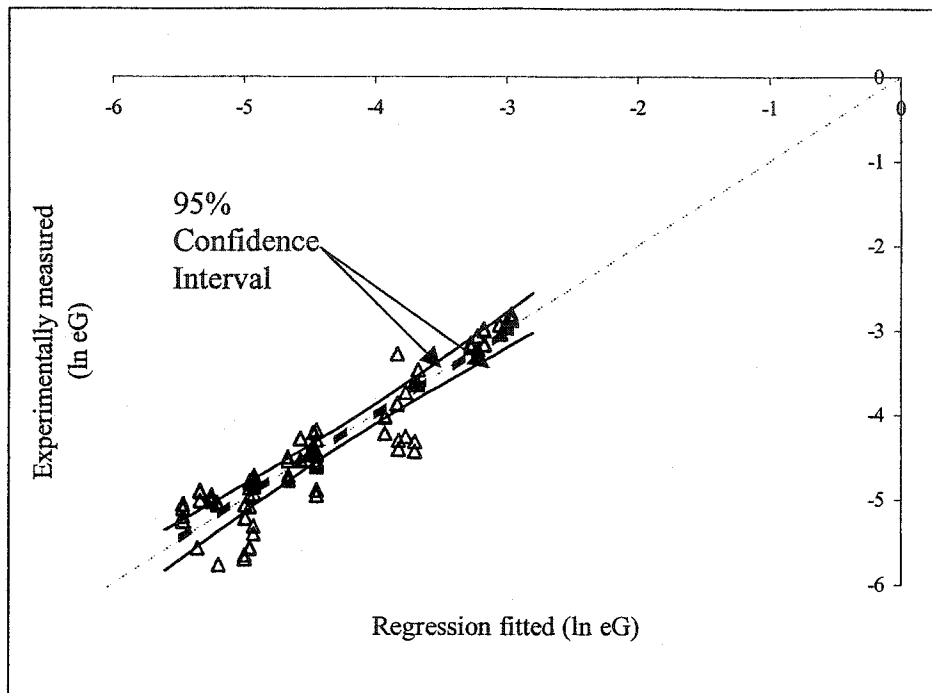


Figure 4-24: Comparison between the experimentally measured gas hold-up and the regression fitted gas hold-up

Relationships similar to the one proposed (Equation 4-10) have been developed by other authors, however, the apparatus vary and the operating conditions are not identical. Nonetheless, the relationships do provide insight into the operating hydrodynamics of bubble columns. The relationships being compared are summarized in Table 4-4. Specific operating conditions are illustrated in more detail in Table 2-2.

Table 4-4: Relationships being compared in Figure 4-25.

Author	Distributor Used	Proposed Correlation
Otake et al. (1981)	Multi nozzles Single nozzles	$\varepsilon_G = 0.38 \cdot u_G^{*0.86} \cdot \exp\left(\frac{-2.94 \cdot u_L}{\sqrt{g \cdot d}}\right)$
Huynh et al. (1991) a	Porous distributor	$\varepsilon_G = 0.2087 \cdot u_G^{0.700} \cdot u_L^{-0.5147}$
Huynh et al. (1991) b	Venturi / bubble column combination	$\varepsilon_G = 1.106 \cdot u_G^{0.70} \cdot u_L^{0.1540}$
Zahradník et al. (1997)	Ejector distributor	$\varepsilon_G = 2.81 \cdot u_G^{0.9}$
Chen et al. (2002)	Perforated ceramic plate	$\varepsilon_G = 5.168 \cdot u_G^{1.063}$
Shawaqfeh (2002)	Nozzle with perforated plate	$\varepsilon_G = 0.775 \cdot u_G^{0.674}$

Even with only a rough comparison of the relationships shown in Table 4-4, it is clear that the superficial gas velocity of the operating system is the most important variable, due to the strong relationship between the superficial gas velocity and the gas hold-up. Meanwhile the relationship between the gas hold-up of the system and the superficial liquid velocity is weak, as indicated by the small exponent. In the case of Zahradník et al. (1997), this variable was not included. Work conducted by Shetty et al. (1992) indicated that, in their bubble column, which operated with a perforated plate distributor, the gas hold-up did not depend on the superficial liquid velocity of the system, but varied significantly with the superficial gas velocity.

Comparing only a few of the published relationships with the proposed model (Equation 4-10) for the average gas hold-up leads to the conclusion that this new model results in gas hold-up predictions for the impinging-jet bubble column which lie within the range of previously published hold-up values. Figure 4-25 compares six relationships previously

proposed in the literature. Each of the models depicts a similar dependency on the superficial gas velocity. Figure 4-26 compares the same six relationships, and the influence that the superficial liquid velocity has on the system.

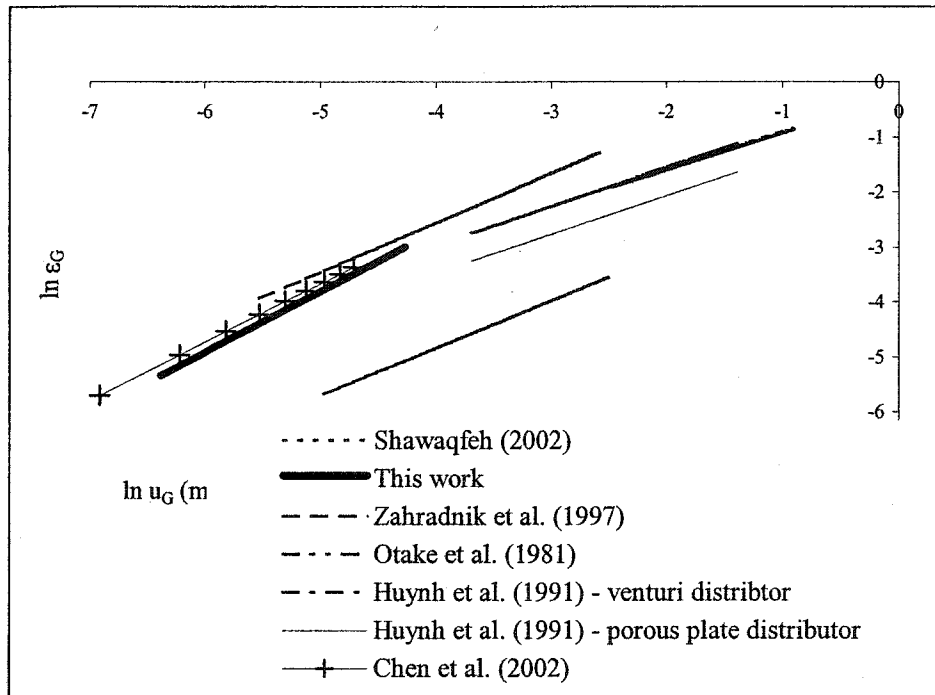


Figure 4-25: Comparison between published correlations at $u_L = 0.02$ m/s

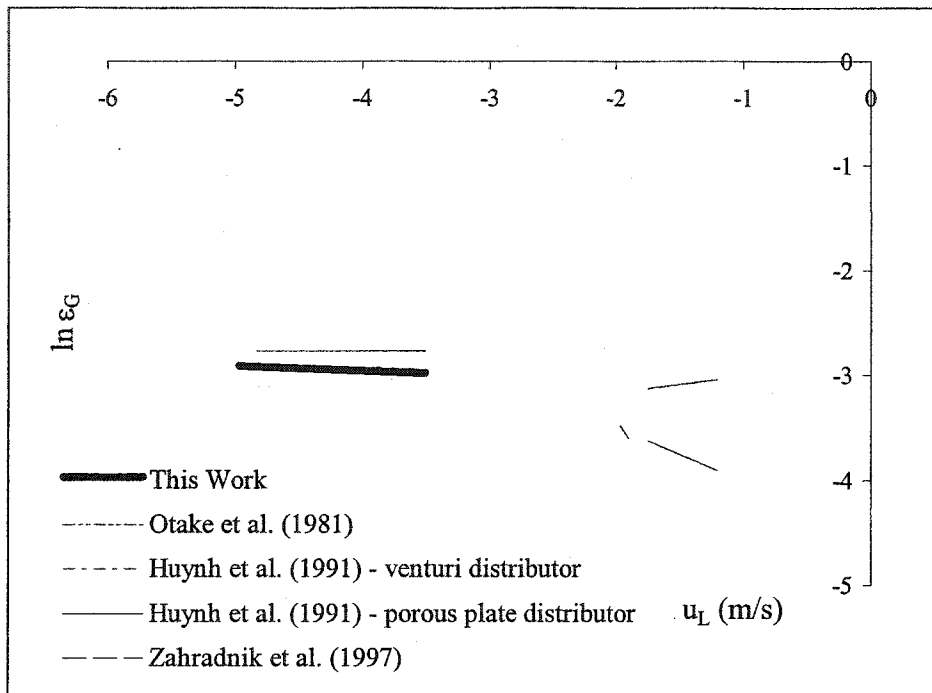


Figure 4-26: Comparison between published correlations at $u_G = 0.015 \text{ m/s}$

As shown in Figure 4-25, the impinging-jet bubble column has a lower gas hold-up than some of the reactors, however, gas hold-up increases more rapidly in the bubble column than in the reactors, as evidenced by the slope of the line. Figure 4-26 also illustrates that the impinging-jet bubble column predicts a gas hold-up comparable to that of the reactors it is compared with; the impinging-jet bubble column predicts neither the lowest nor the highest gas hold-up. This could be occurring for a number of reasons, such as the configuration and type of distributor affecting the size of bubbles produced. It is suspected that, in those cases described above, where smaller gas hold-up values are predicted, the shearing rates are less significant, resulting in larger bubbles being formed

with higher bubble rise velocities. Higher rise velocities decrease the residence time of bubbles in the reactor and thus minimize the gas hold-up.

Bubble Properties

Photographic techniques were employed in the studies conducted by Gamal El-Din (2001d) to determine the following bubble properties: 1) size of the bubbles; 2) interfacial area of the bubbles; and 3) the relationship between the phase velocities and the bubble properties. Experiments were carried out in the impinging-jet bubble column using clean deionized water for the liquid phase and extra-dry air for the gas phase. The feed-gas flow rate varied between 8.2×10^{-6} and 1.0×10^{-4} m³/s, and the liquid flow rate varied between 6.0×10^{-5} and 2.2×10^{-4} m³/s.

As was previously described, photos were taken of the bubbles produced in the bubble column. The photographs were taken at the middle of the height of the bubble column and focused on the midpoint of the diameter of the bubble column, assuming that at this point, the rate of coalescence and break-up was constant. It was also assumed that the bubble properties were uniform throughout the length of the contactor since the height of the bubble column was fairly short. From each picture, a frame containing between 50 to 80 bubbles was selected to be analyzed.

As shown in Figure 4-27 and Figure 4-28, the majority of the bubbles formed in the bubble column had the shape of an oblate sphere. This phenomenon is shown for low gas and liquid flow rates (Figure 4-27), as well as high gas and liquid flow rates (Figure 4-28). Similar observations with respect to the shape of the bubbles were made by

Yamashita et al. (1979), who used a 2-dimensional (rectangular) bubble column operating with a porous plate distributor.

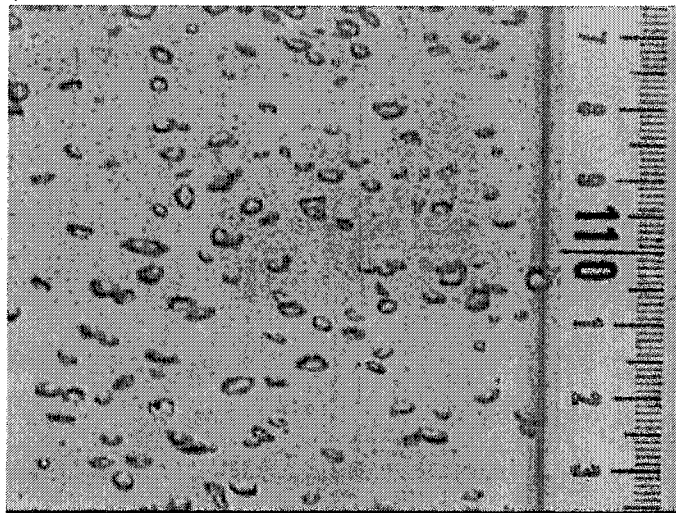


Figure 4-27: A digital image of the gas bubbles at $u_G = 0.001$ m/s and $u_L = 0.008$ m/s

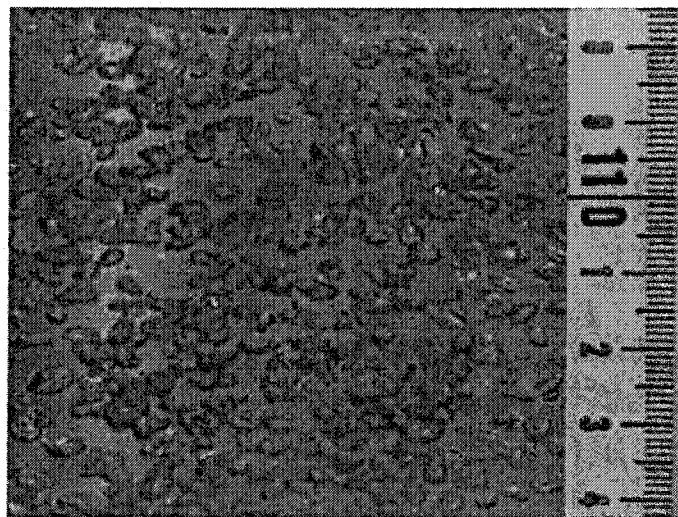


Figure 4-28: A digital image of the gas bubbles at $u_G = 0.011$ m/s and $u_L = 0.028$ m/s

Outlying data were eliminated by the same procedure used with data collected for the analysis of gas hold-up. Similar values were obtained from both approaches used to calculate the bubble diameter (d_B). The difference between the two methods of determining bubble diameters (d_B) ranged from 2.83% to 7.88 %, with respect to average measured bubble diameters. This resulted in a difference in Sauter mean bubble diameter of 3.55 to 5.29 %, with respect to the average measured bubble diameters. Both the count mean bubble diameter (d_B) and the Sauter mean bubble diameter (d_S) were calculated. d_B ranged from 1530 to 3100 μm , and d_S ranged from 1770 – 3400 μm . With respect to the maximum and minimum average bubble diameters (d_B), the minimum bubble diameters of 1.53 mm and 1.61 mm (approaches one and two respectively) occurred at $u_G = 0.009$ m/s and $u_L = 0.019$ m/s, while the maximum average bubble diameters of 3.10 mm and 3.24 mm (approaches one and two respectively) occurred at $u_G = 0.012$ m/s and $u_L = 0.024$ m/s. For the Sauter mean bubble diameters, the minimum determined bubble diameter for approach 1 and approach 2 were 1.77 mm and 1.86 mm, respectively ($u_G = 0.009$ m/s and $u_L = 0.019$ m/s), and the maximum bubble diameters for approach one and approach two were 3.40 mm and 3.59 mm, respectively ($u_G = 0.012$ m/s and $u_L = 0.024$ m/s).

It was thought that, similar to the gas hold-up and mixing coefficient, the bubble properties were influenced by the phase velocities of the system. The relationship between the superficial liquid and gas velocities and the diameter of the bubbles produced was investigated. Figure 4-29 and Figure 4-30 depict the relationship between the diameters of the bubbles produced as a function of u_L and u_G , respectively.

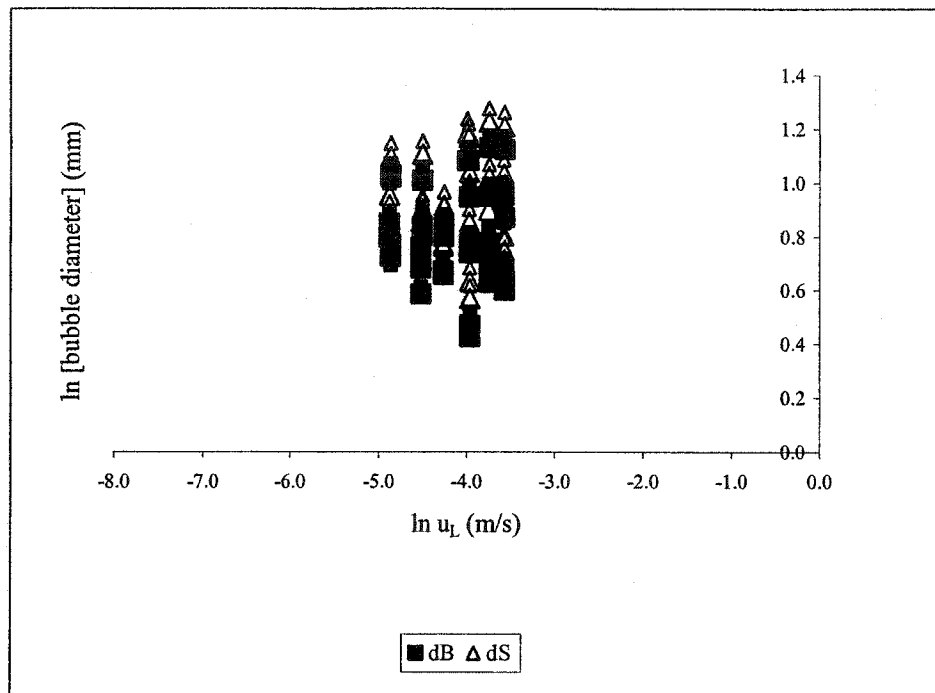


Figure 4-29: Relationship between bubble diameter and superficial liquid velocity

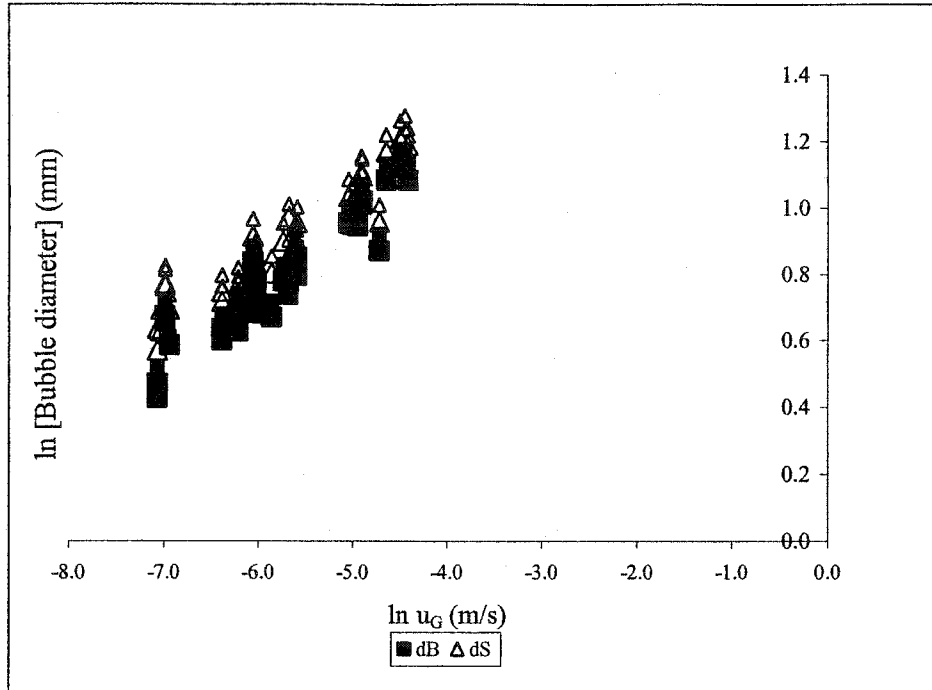


Figure 4-30: Relationship between bubble diameter and superficial gas velocity

Visual inspection of Figure 4-29 revealed no clear relationship between the superficial liquid velocity and the diameter of the bubbles formed, and therefore, further analysis was required. However, there was a clear relationship between the superficial gas velocity and the diameter of the bubbles formed, as shown in Figure 4-30. It is obvious that as the superficial gas velocity increases, the diameter of the bubbles subsequently increases.

To confirm the influences of the superficial phase velocities on the diameter of the bubbles produced, a linear regression technique was carried out. Since two approaches to estimating bubble diameters (d_B) were investigated, two regression analyses were also performed. The resultant relationships are as follows:

Approach 1: $d_{B,1} = 6.93 \cdot u_G^{0.223} \cdot u_L^{-0.034}$ [mm] $R^2 = 0.90$ Equation 4-11

Approach 2: $d_{B,2} = 7.72 \cdot u_G^{0.224} \cdot u_L^{-0.020}$ [mm] $R^2 = 0.89$ Equation 4-12

The above formulae indicate that the superficial gas and liquid velocities do influence d_B . As was the case with gas hold-up, there is more of a dependence on the superficial gas velocity than on the superficial liquid velocity. Although it is not evident from Figure 4-29, the above formulae indicate that there is a small relationship between d_B of the bubbles and the superficial liquid velocity.

The model's ability to accurately predict the diameter of the bubbles formed is demonstrated in Figures 4-32 and 4-33, for approaches one and two, respectively. The regression fitted values are plotted against the experimentally measured bubble diameters. The data are hugging a 45° line, indicating a good fit, and the majority of the data are captured within the 95% confidence intervals.

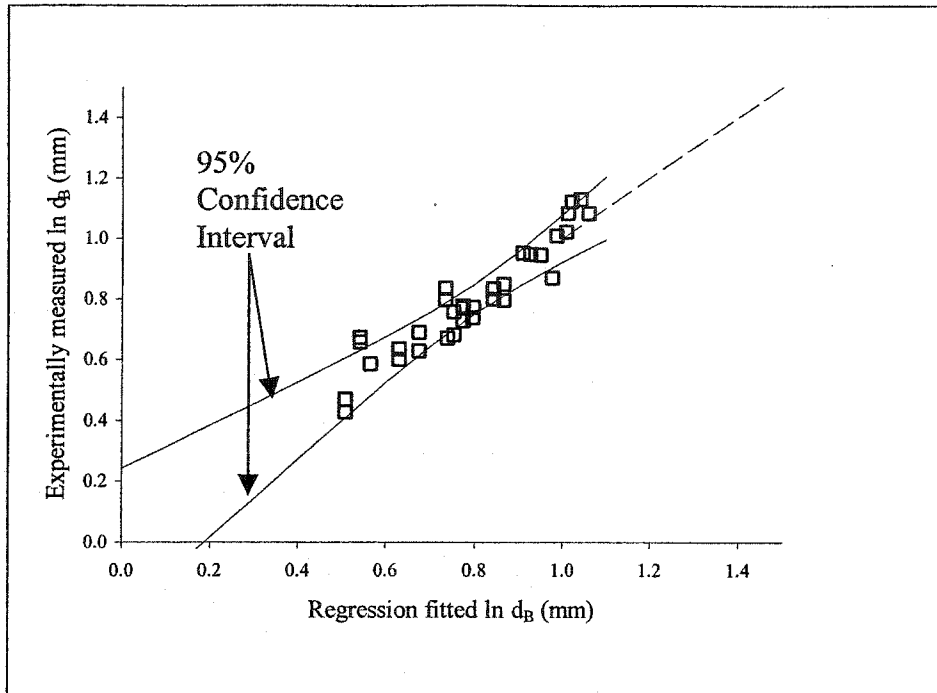


Figure 4-31: Comparison between measured and predicted bubble diameters (d_B), approach one

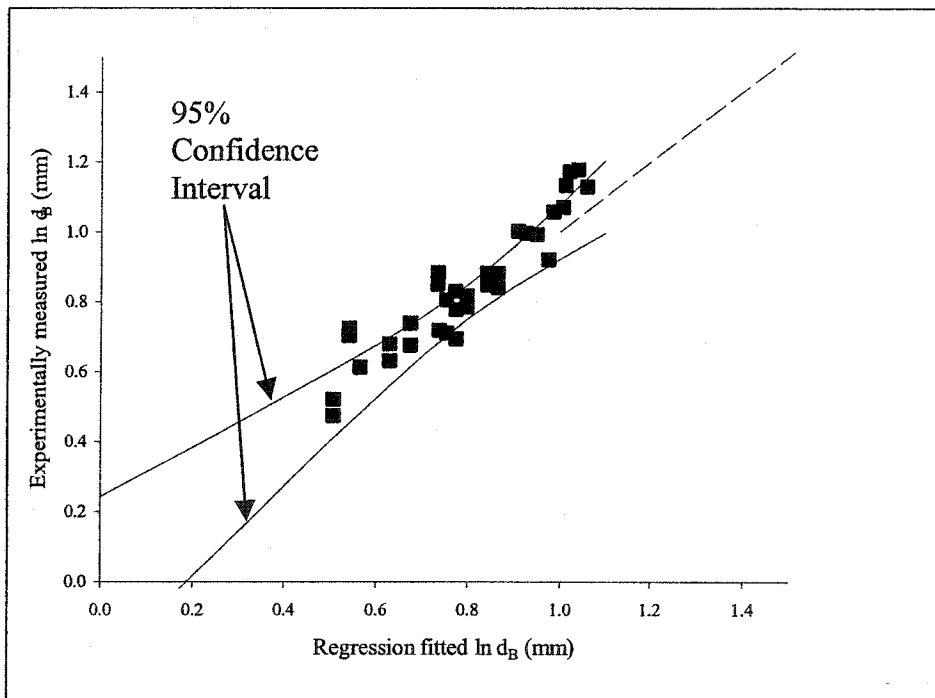


Figure 4-32: Comparison between measured and predicted bubble diameters (d_B), approach two

Furthermore, the Sauter mean bubble diameter was calculated. As this diameter is the most widely used in calculating additional parameters (interfacial area, mass transfer coefficient), a linear regression technique was again employed to determine a possible relationship between the Sauter mean bubble diameter and the phase velocities. The resulting regression equations, again for approaches one and two, are as follows:

$$\text{Approach 1: } d_{s,1} = 7.78 \cdot u_G^{0.207} \cdot u_L^{-0.008} \quad [\text{mm}] \quad R^2 = 0.89 \quad \text{Equation 4-13}$$

$$\text{Approach 2: } d_{s,2} = 8.22 \cdot u_G^{0.207} \cdot u_L^{-0.007} \quad [\text{mm}] \quad R^2 = 0.89 \quad \text{Equation 4-14}$$

It is again noted that there was a stronger dependency on the superficial gas velocity than on the superficial liquid velocity. The fit of these models was tested and is illustrated in Figure 4-33 and Figure 4-34, both of which display the adequacy of the models. The data lie close to the 45° line, and most of the data points fall within the 95% confidence limits. This indicates the model's ability to accurately predict Sauter mean bubble diameter, based on the superficial phase velocities of the system.

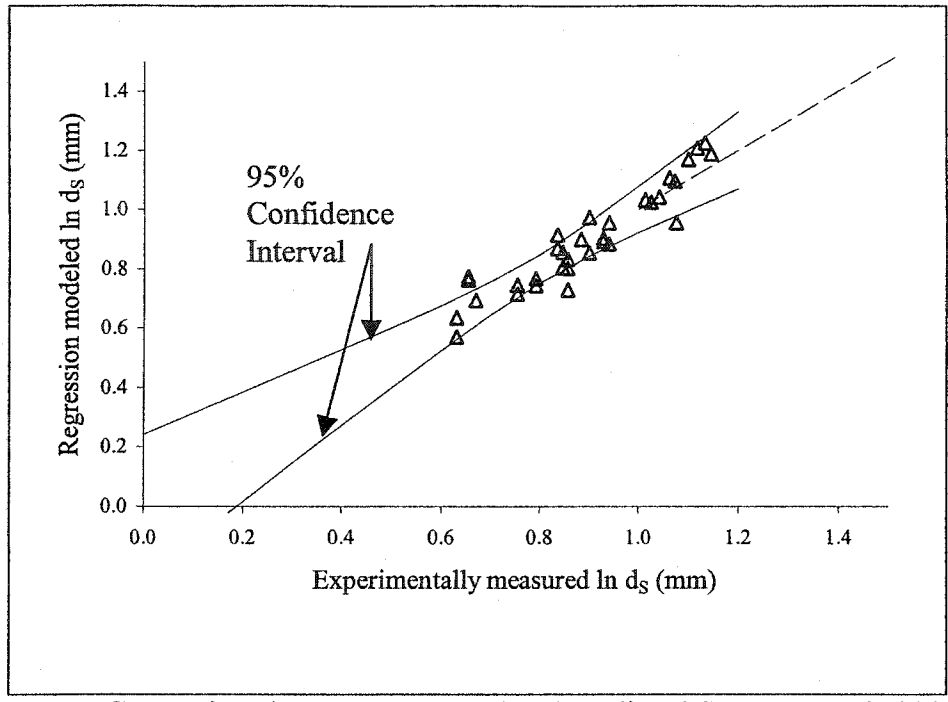


Figure 4-33: Comparison between measured and predicted Sauter mean bubble diameters (d_s), approach one

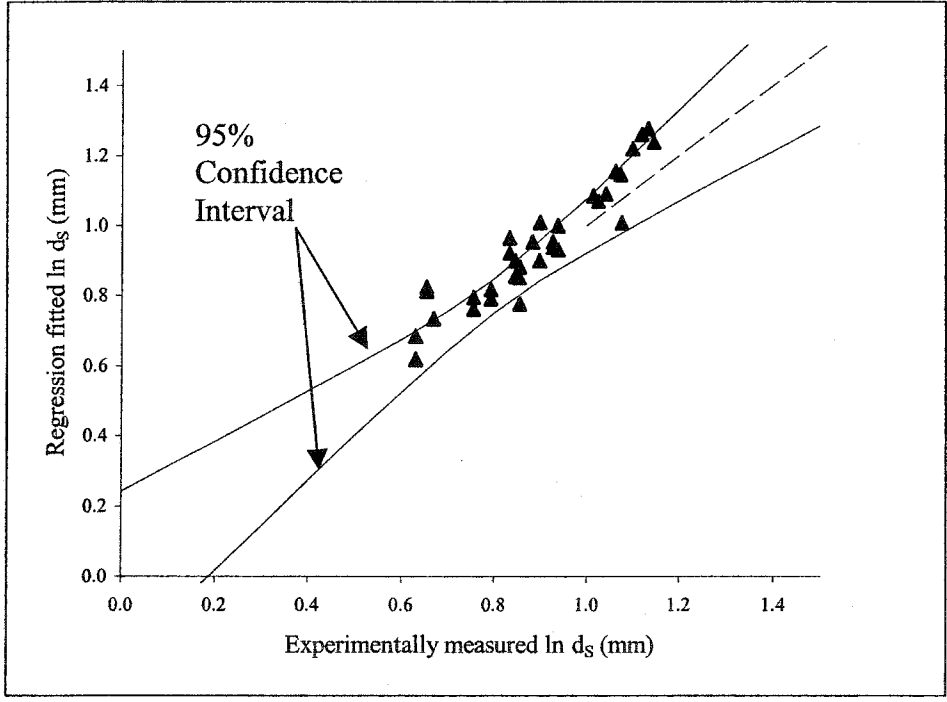


Figure 4-34: Comparison between measured and predicted Sauter mean bubble diameters (d_s), approach two

Many observations can be made from this plot. First, at the same gas hold-up values, approach two (ellipsoidal) predicts a larger bubble than approach one (oblate sphere). As the Sauter bubble diameter is based on the bubble diameter, the same observation for the Sauter bubble diameter is made between the two approaches. As the superficial gas velocity increases, the diameter of the bubbles increases. The proposed formulae indicate that there is a relationship between the superficial liquid velocity and the diameter of the bubbles.

To further illustrate the possibility of a relationship between the superficial liquid velocity and the diameter of the bubbles formed, more plots were generated. Figure 4-35 and Figure 4-36 depict the modeled bubble diameter as a function of superficial gas velocity, at varying superficial liquid velocities, for approaches one and two, respectively.

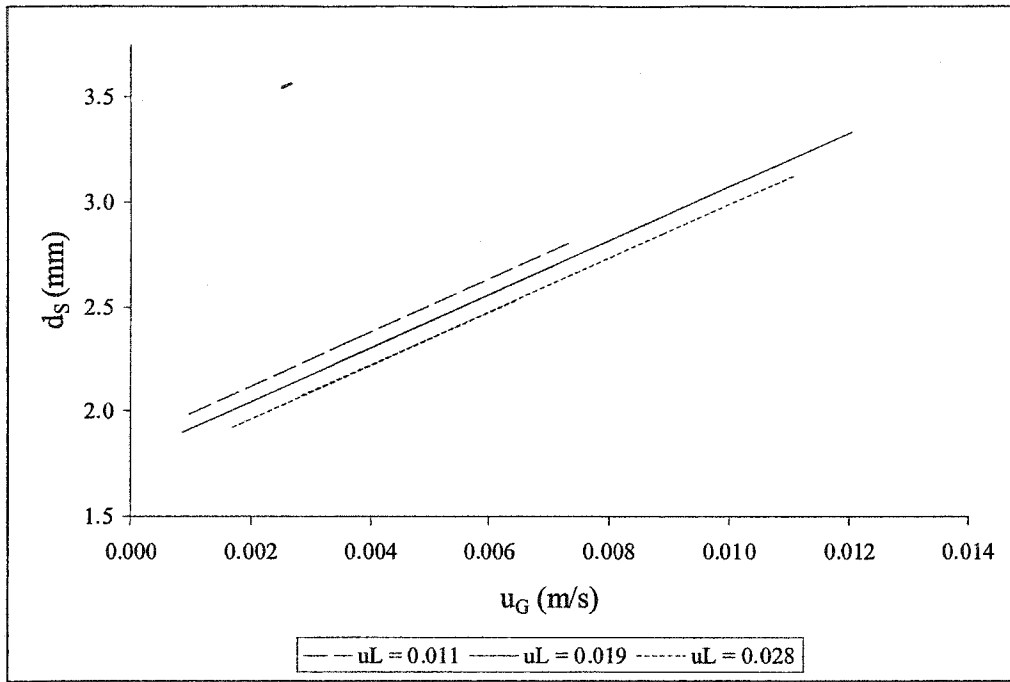


Figure 4-35: Relationship between bubble diameter (d_s) and u_G at varying u_L , approach one

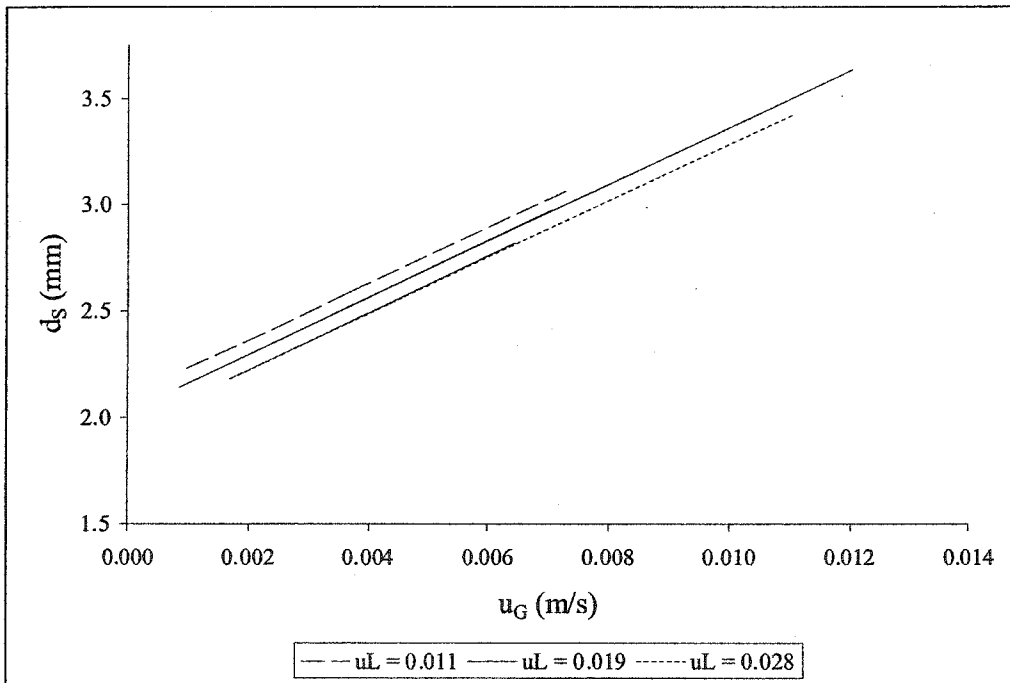


Figure 4-36: Relationship between bubble diameter (d_s) and u_G at varying u_L , approach 2

It is clear from these plots that, as the superficial liquid velocity of the system increases, the diameter of the bubbles decreases. Thus, as the liquid velocity increases, the shear rates increase as well, leading to the breakage of larger bubbles into smaller bubbles. The generation of smaller, more numerous bubbles is desirable. This allows for larger interfacial areas to be created, which results in an increased transfer rate of ozone into water. Although smaller gas bubbles can increase the gas hold-up, it was noted that at a larger u_L , this decreased ϵ_G (bubbles are pushed through the system at a much faster rate, thus minimizing the retention time and subsequent accumulation of bubbles in the reactor).

To compare our operating system with those of other authors, Figure 4-37 was developed. The bubble columns that were compared are described briefly in the following paragraphs.

Akita and Yoshida (1974) studied the bubble properties produced in three bubble columns (height = 250 cm) with square cross-sectional areas of 7.7 x 7.7 cm, 15 x 15 cm, and 30 x 30 cm, all of which were tested using a single orifice gas sparger. The 15 x 15 cm bubble column was also investigated using a perforated plate. The model which predicts the bubble size (d_B) produced in these bubble column reactors is as follows:

$$d_B = 26 \cdot d \cdot \left(\frac{g \cdot d^2 \cdot \rho_L}{\gamma} \right)^{-0.50} \cdot \left(\frac{g \cdot d^3}{v_L^2} \right)^{-0.12} \cdot \left(\frac{u_G}{\sqrt{g \cdot d}} \right)^{-0.12} \quad \text{Equation 4-15}$$

Where d_B = bubble diameter [mm]
 d = column diameter [cm]
 g = acceleration due to gravity [cm/s²]
 ρ_L = liquid density at 20°C [g/cm³]
 γ = surface tension at 20°C [g/s²]
 ν_L = kinematic viscosity of the liquid at 20°C [g/cm·s]
 u_G = superficial gas velocity [m/hr]

The study conducted by Roustan et al. (1996) used a pilot plant bubble column 2.5 m in height, with a diameter of 0.51 m. Both co-current and counter-current operations were studied, and the distributor used was a ceramic porous plate located at the bottom of the column. The relationship that was developed to characterize the bubble diameter (d_B) in this bubble column is as follows:

$$d_B = 2.935 \cdot u_G^{0.751} \quad \text{Equation 4-16}$$

Where d_B = bubble diameter [mm]
 u_G = superficial gas velocity [m/hr]

The impinging-jet bubble column, similar to the bubble column of Roustan et al. (1996), produces a larger bubble size as the superficial gas velocity increases. By contrast, in the bubble column of Akita and Yoshida (1974), the diameter of the bubbles produced decreases as u_G increases. This occurs because the formula predicting bubble size

formation relies at least as heavily, perhaps more, on properties of the liquid than on the superficial gas velocity. The bubble column of Roustan et al. (1996) and the impinging-jet bubble column rely solely on the superficial phase velocities, rather than on the properties of the fluid.

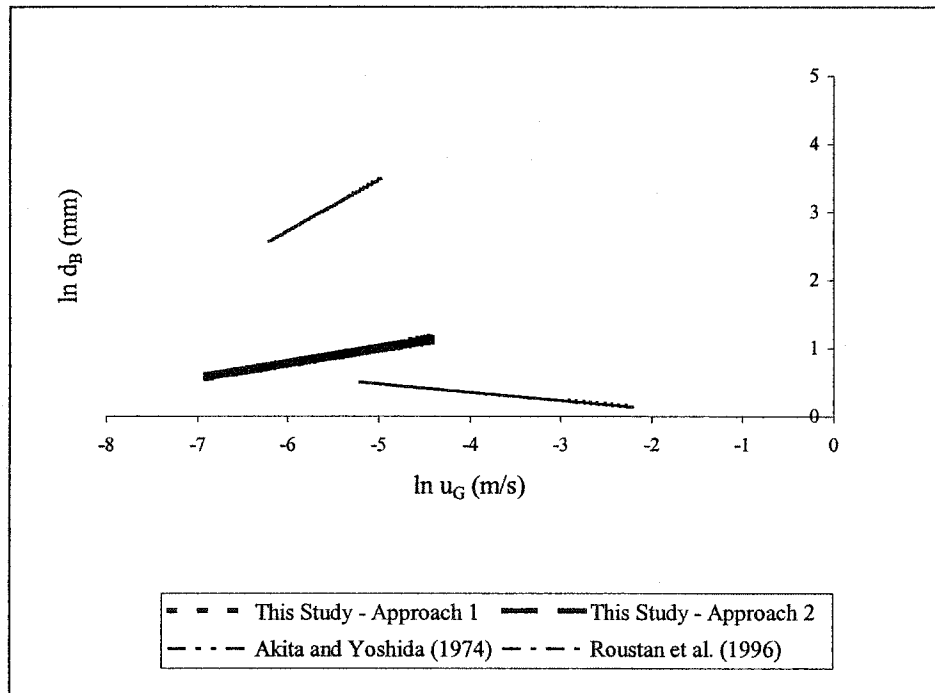


Figure 4-37: Comparison between correlations predicting the bubble diameter at $u_L = 0.019$ m/s

From the determination of the Sauter mean bubble diameter, the interfacial area of these bubbles was further calculated. This gives an indication of how much surface is available for the transfer of ozone gas into the liquid phase. The two approaches for determining the diameters will remain as individual approaches, and will be analysed as such.

It is anticipated that there is a relationship between the superficial gas and liquid velocities and the interfacial area of the bubbles. Linear regression techniques were applied and the resultant equations for both approaches are as follows:

Approach 1:

$$a_1 = 3.61 \cdot u_G^{0.902} \cdot u_L^{-0.038} \quad [1/\text{mm}] \quad R^2 = 1.00 \quad \text{Equation 4-17}$$

Approach 2:

$$a_2 = 3.40 \cdot u_G^{0.901} \cdot u_L^{-0.039} \quad [1/\text{mm}] \quad R^2 = 1.00 \quad \text{Equation 4-18}$$

It can be seen that, as the superficial gas velocity increases, there is also an increase in the interfacial area. This was seen with the bubble diameter as well. It can also be noted that, as the superficial liquid velocity increases, there is a slight decrease in the interfacial area produced. This is a result of the smaller diameters produced.

The above relationships are consistent with that observed between the bubble diameter and the superficial liquid velocity. Kulkarni et al. (1983) observed that an increase in superficial gas velocity resulted in an increase in interfacial area, while an increase in superficial liquid velocity resulted in a decrease in interfacial area.

A relationship between the superficial phase velocities of the system and the interfacial areas has been previously established, and as a result, there should be a relationship between the interfacial area and the gas hold-up of the system (both are significantly

influenced by u_G). This occurs because the gas hold-up of the system is also related to the superficial phase velocities of the system. Based on the formula

$$a = \frac{6 \cdot \varepsilon_G}{d_{vs}},$$

as the gas hold-up increases, the interfacial area will increase, generally as a

result of smaller bubble diameters.

The impinging-jet bubble column was compared with three other bubble columns for which authors provided correlations predicting the interfacial areas produced. The bubble columns and their authors are summarized in the following table. Further information is provided in the literature review section of this work.

Table 4-5: Relationships being compared in Figure 4-38

Author	Distributor Used	Proposed Correlation
Bando et al. (1988)	Co-current Downflow Conical entrance Gas-liquid injection nozzle	$a = 5400 \cdot \exp(0.10 \cdot u_{LN}) \cdot \varepsilon_G$ [1/m]
Kulkarni et al. (1983)	Downflow bubble column Ring type distributor with 18 holes	$a = 225 \cdot u_G^{0.635} \cdot u_L^{-2.05} \cdot v_L^{-0.11}$ [1/m]

Figure 4-38 illustrates the comparison of the three bubble columns described above and the impinging-jet bubble column. Varying degrees of interfacial area increase are predicted to accompany increases in the superficial gas velocity.

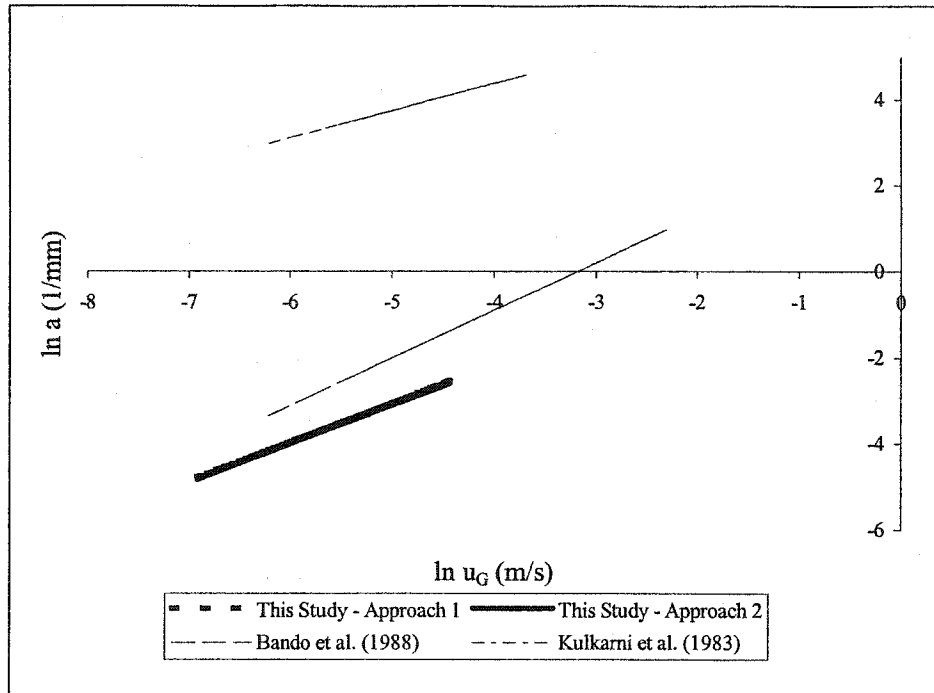


Figure 4-38: Comparison between correlations predicting the interfacial area at $u_L = 0.019$ m/s

Mass Transfer

The ozone mass transfer studies were carried out in the impinging-jet bubble column in both the injection and ejection modes of operation. The purpose of this section of analysis is to determine the mass transfer ability of the impinging-jet bubble column. It is anticipated that this bubble column, with its unique design, will exhibit an enhanced ability to transfer ozone into water. The steady-state BFCM was used for the analysis of mass transfer; operating parameters are summarized in the following two tables.

Table 4-6: Measurable operating parameters for the mass transfer study

Measured Parameters	Symbol	Units	Minimum	Maximum
Superficial gas velocity	u_G	m/s	0.0018	0.0138
Superficial liquid velocity	u_L	m/s	0.008	0.028
Temperature of the liquid	T_L	°C	19.5	24.5
Temperature of the air	T_{air}	°C	21.85	23.15
Equilibrium dissolved ozone concentration	$C_{L,0}$	mg/L	2.97	19.84
Density of water	ρ_w	kg/m ³	997.53	997.83
Liquid hydrostatic pressure	P_0	(kg/m ²)	21605	22339
Specific ozone utilization rate constant	k_w	1/s	0.015	0.025

Table 4-7: Numerically determined operating parameters for the mass transfer study

Determined Parameters	Symbol	Units	Minimum	Maximum
Gas holdup	ε_G	Dimensionless	0.005	0.048
Liquid holdup	ε_L	Dimensionless	0.952	0.995
Mixing coefficient	r	Dimensionless	2.33	9.47
Liquid Peclet number	Pe_L	Dimensionless	0.84	2.72

For each of the experimental runs, the concentration of ozone dissolved into the liquid was measured. Samples were taken from 5 sampling ports along the height of the column, as well as at the point of exit, for a total of 6 samples. The dissolved ozone concentration was measured according to the procedure outlined in the Materials and Methods section of this report. The measured ozone concentrations were used to give a prediction of the volumetric mass transfer rate.

To predict the concentration throughout the bubble column, a system of equations was developed. These equations are based on the equilibrium (mass balance) of ozone in the system, between the individual cells described by the back flow cell model. The mass balance equations were developed for dissolved ozone, gaseous ozone, and total gas, and are shown in the Methods and Materials section. The developed system of equations was set up within the TKSOLVER[®] software, and was solved using the iterative Newton-Raphson method. The output variables were the dissolved ozone concentration in the gas and liquid phases, and q_G . The specific ozone utilization rate (k_w) that was used (Gamal El-Din and Smith 2003a) was:

$$k_w|_{20^\circ C} = 2.61 \times 10^{-4} \quad [1/s]$$

Where k_w = specific ozone utilization rate constant

As previously mentioned, the measured ozone concentration data provided an estimate of the overall mass transfer coefficient. This estimated volumetric mass transfer coefficient was used in the formulation of the mass balance equations, and subsequently affected the liquid and gas phase Stanton numbers. As such, this initial guess for the mass transfer coefficient provided an estimate of the predicted ozone concentration. For our purposes, the concentration of ozone in the liquid phase is most important, as it serves as an indication of the model's accuracy when compared with the measured ozone concentrations in the liquid phase.

Once the concentration along the height of the bubble column was predicted, these concentrations were compared with the measured ozone concentrations. The sum of the squares of the residuals (SSR) between the concentrations was determined. A second iteration of the above process was performed, with a change being made to the overall liquid mass transfer coefficient. Again, the SSR was determined. This iterative approach continued until a minimum SSR value was obtained. This led to the determination of the most accurate volumetric mass transfer coefficient for the system.

The volumetric mass transfer coefficient was determined to three decimal points. The number of iterations needed to meet this requirement varied, as the rate of convergence varied for each experimental run. The number of iterations ranged from 41 to 382 within one trial. The following table, Table 4-8, serves as a summary of the operating conditions for each experiment, and shows the measured and calculated mass transfer coefficients for each experimental run.

Table 4-8: Operating conditions and resulting overall mass transfer coefficients

Trial #	u_L (m/s)	u_G (m/s)	r	ϵ_G	ϵ_L	T (°C)	Measured k_{La} (T=20) corrected (min ⁻¹)	Calculated k_{La} (T=20) corrected (min ⁻¹)
1	0.008	0.003	8.614	0.008	0.992	23.4	0.743	0.849
2	0.014	0.003	4.590	0.008	0.992	22.0	1.021	1.336
3	0.008	0.004	8.918	0.012	0.988	23.0	1.546	1.825
4	0.014	0.002	4.570	0.007	0.993	21.1	1.250	2.367
5	0.008	0.004	9.113	0.012	0.988	24.5	1.224	1.878
6	0.014	0.004	4.740	0.011	0.989	23.0	1.270	1.798
7	0.008	0.007	9.471	0.026	0.974	24.2	2.748	2.960
8	0.014	0.007	4.997	0.024	0.976	23.1	2.993	4.585
9	0.024	0.011	2.960	0.038	0.962	22.7	5.941	6.847
10	0.008	0.003	8.620	0.008	0.992	22.7	1.263	1.857
11	0.008	0.004	8.738	0.012	0.988	24.0	1.190	1.881
12	0.008	0.003	8.441	0.008	0.992	21.1	1.519	2.320
13	0.024	0.002	2.470	0.005	0.995	21.3	0.752	0.795
14	0.024	0.003	2.585	0.008	0.992	21.3	1.041	1.098
15	0.028	0.014	2.464	0.048	0.952	21.0	7.154	10.555
16	0.023	0.002	2.492	0.005	0.995	19.5	0.821	0.983
17	0.023	0.003	2.609	0.008	0.992	22.6	0.997	1.138
18	0.023	0.006	2.825	0.021	0.979	22.2	2.945	5.999
19	0.028	0.010	2.381	0.035	0.965	22.4	5.481	7.889
20	0.023	0.002	2.494	0.005	0.995	22.0	0.647	0.753
21	0.023	0.003	2.613	0.009	0.991	22.4	0.925	1.105
22	0.023	0.009	2.914	0.029	0.971	19.9	5.652	10.434
23	0.028	0.008	2.334	0.026	0.974	19.9	4.550	9.202

Discussion will focus around three trials: 6, 13, and 21. These trials were chosen at random, and once picked, were determined to give an accurate representation of the entire set of trial experiments.

Examples of SSR curves are shown in Figure 4-39, Figure 4-40, and Figure 4-41 for trials 6, 13, and 21 respectively. From these figures, the progression of minimization to a minimum SSR can be seen. At this minimum point, the volumetric mass transfer rate representing the system was determined.

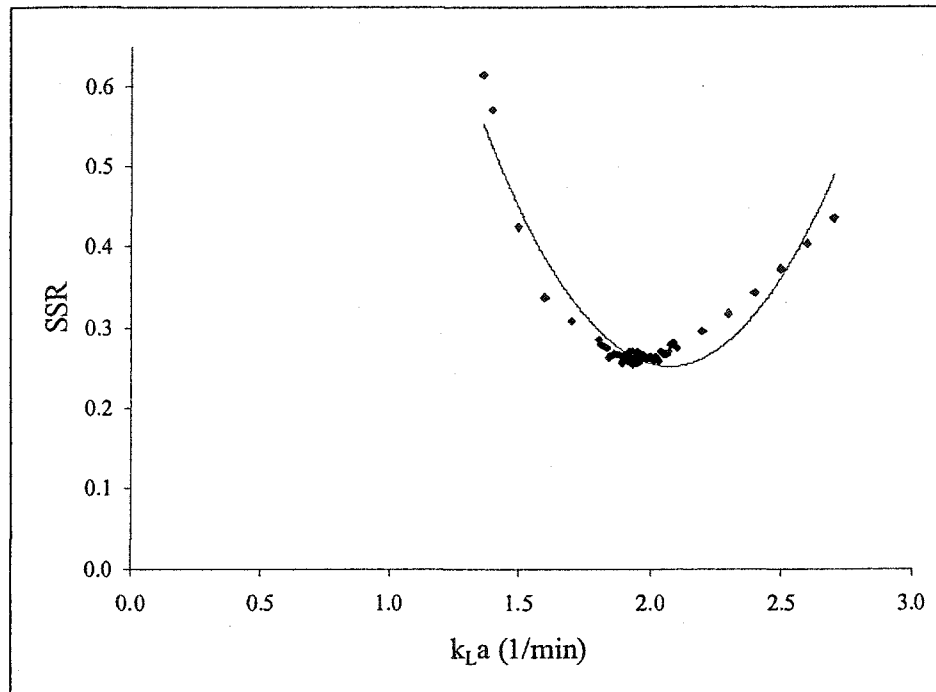


Figure 4-39: Sum of the squares of the residuals plot for trial #6

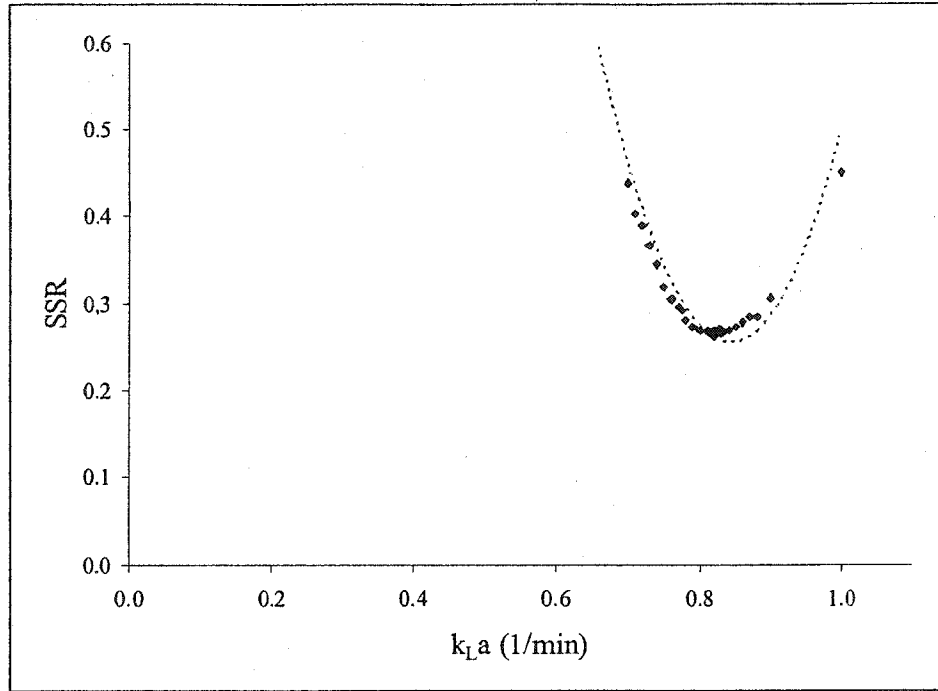


Figure 4-40: Sum of the squares of the residuals plot for trial #13

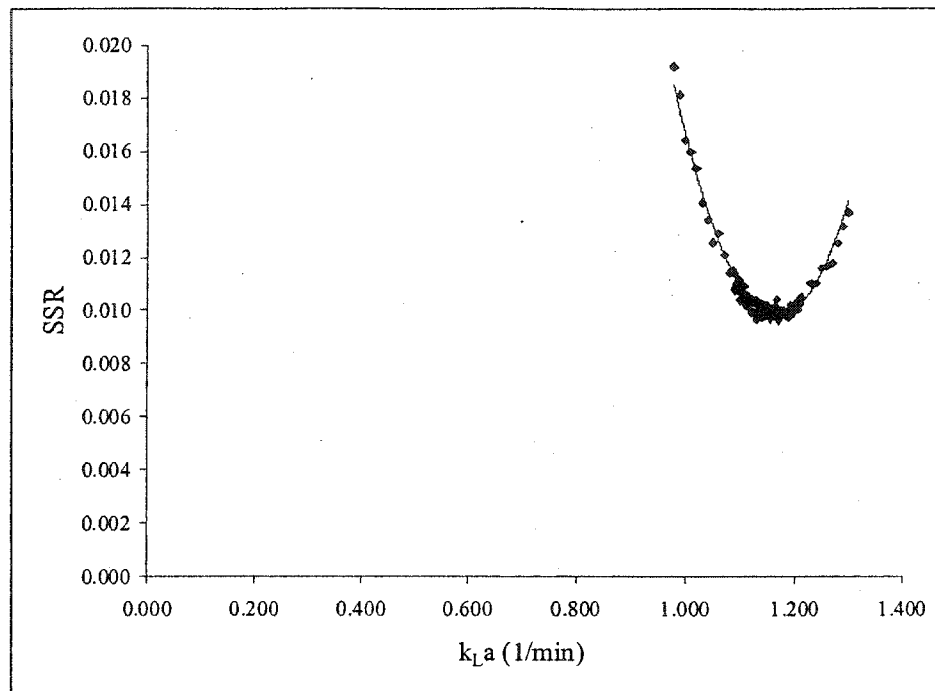


Figure 4-41: Sum of the squares of the residuals plot for trial #21

The volumetric mass transfer coefficients, corrected for the effects of temperature, for trials 6, 13, and 21 are 1.80, 0.80, and 1.11 min^{-1} respectively. The measured dissolved ozone concentrations were plotted against the predicted dissolved ozone concentrations at the appropriate mass transfer rates. Figure 4-42, Figure 4-43, and Figure 4-44 are plots of trials 6, 13, and 21 respectively.

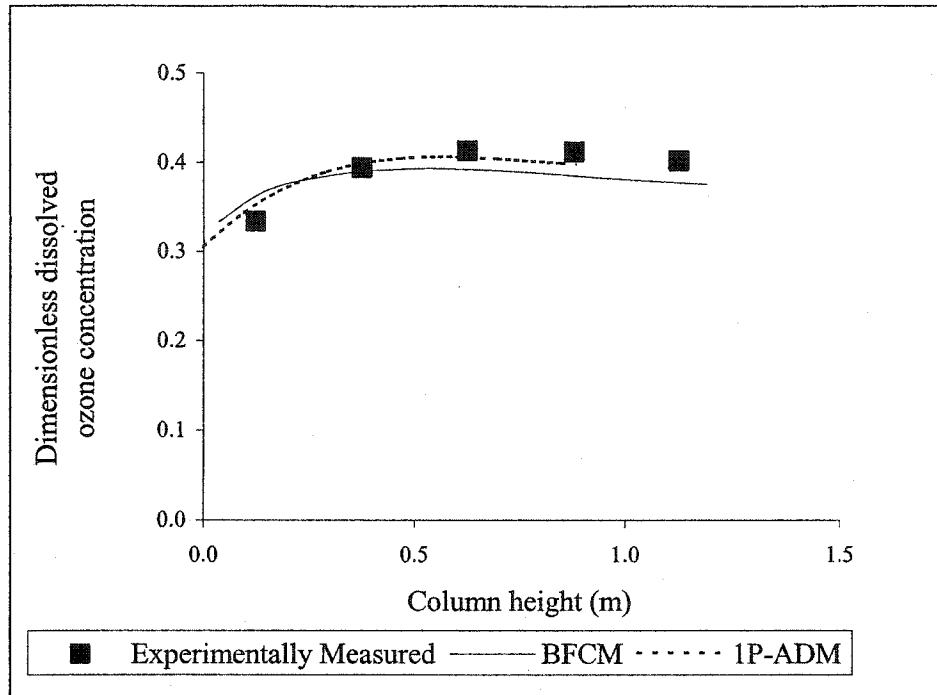


Figure 4-42: Dissolved ozone concentration profile for trial #6

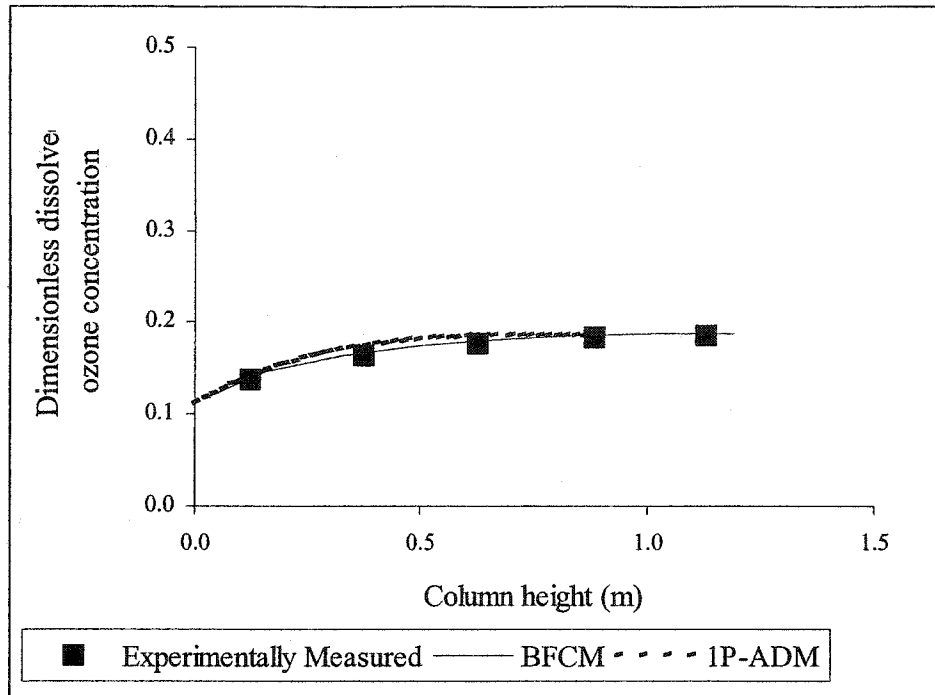


Figure 4-43: Dissolved ozone concentration profile for trial #13

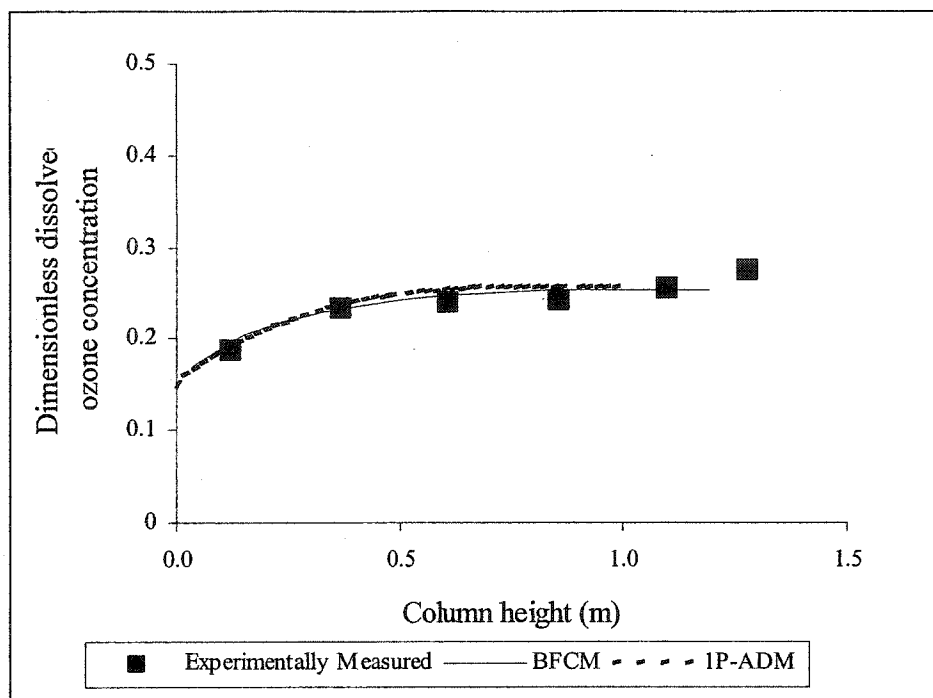


Figure 4-44: Dissolved ozone concentration profile for trial #21

It can be seen from these graphs that the predicted values are very similar to the measured dissolved ozone concentrations. All of the plots predict a more rapid increase in the dissolved ozone concentration in the entrance region of the bubble column. The increased rate of mass transfer is attributed to the increased shear rates generated from increased mixing (from turbulence), which promotes the transfer of ozone into the liquid phase. This mixing, and thus the rate of dissolution of ozone, decreases as the length away from the jets increases. Similar observations were made by Alvarez-Cuenca and Nerenberg (1981) when studying a bubble column employing four nozzles as gas injectors. These authors propose that this rapid increase can be attributed to the phase velocities of the system. A similar increase in the dissolved gas concentration near the distributor was also noted by Deckwer et al. (1974); the increase was attributed to the formation of bubbles in those columns employing a cross of nozzles or a porous plate distributor. Salazar et al.

(1993), whose bubble column included a conical inlet where the gas was introduced by a nozzle, attributed the increase in mass transfer near the distributors to more intense mixing occurring in the bubble column.

In all four figures, it can be seen that the model under-predicts, to varying degrees, the dissolved ozone concentration at the top of the bubble column. It is worth noting that, in some cases, samples were discarded from the uppermost sampling ports. In these cases, the samples drawn had a significant number of gas bubbles in them which would result in an inaccurate representation of the actual dissolved ozone concentration.

It was thought that, at increased gas flow rates, the model's ability to accurately predict dissolved ozone concentration decreased. However, preliminary investigations based on Table 4-8 indicate that this is not the case. It was also anticipated that the trials with the largest difference between predicted and measured $k_L a$ values (and thus, larger SSR values) would be those trials which displayed higher gas flow rates. This was not the case. In several instances, trials displaying large differences operated under low gas flow rates (i.e. trial 4, trial 11).

It is postulated, however, that there is a relationship between the superficial liquid velocity, superficial gas velocity, and volumetric mass transfer coefficient. The following figures, Figure 4-45 and Figure 4-46, illustrate this idea.

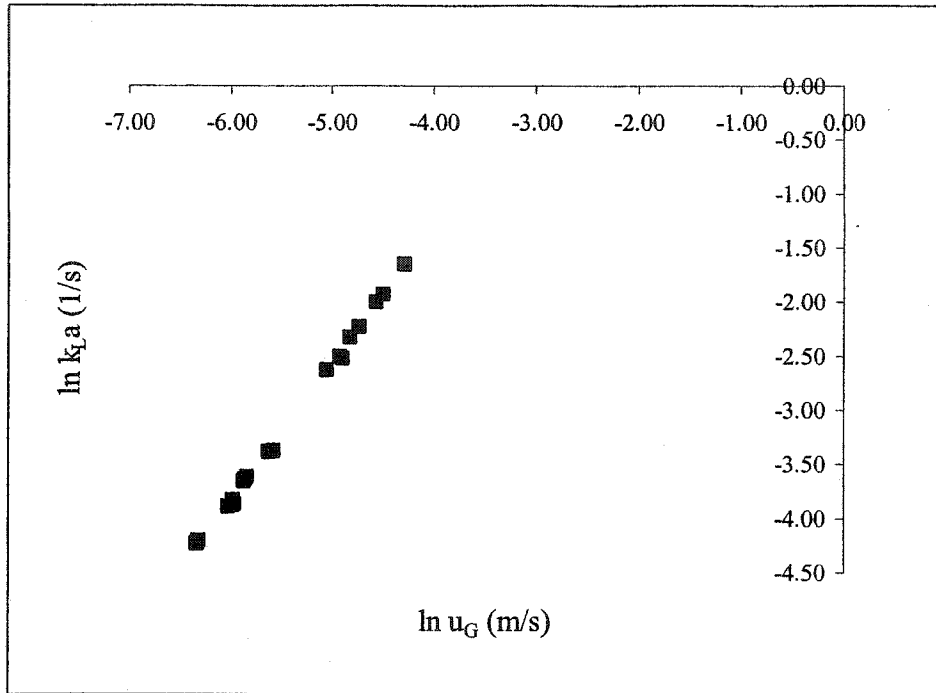


Figure 4-45: Relationship between the superficial gas velocity and the overall mass transfer coefficient

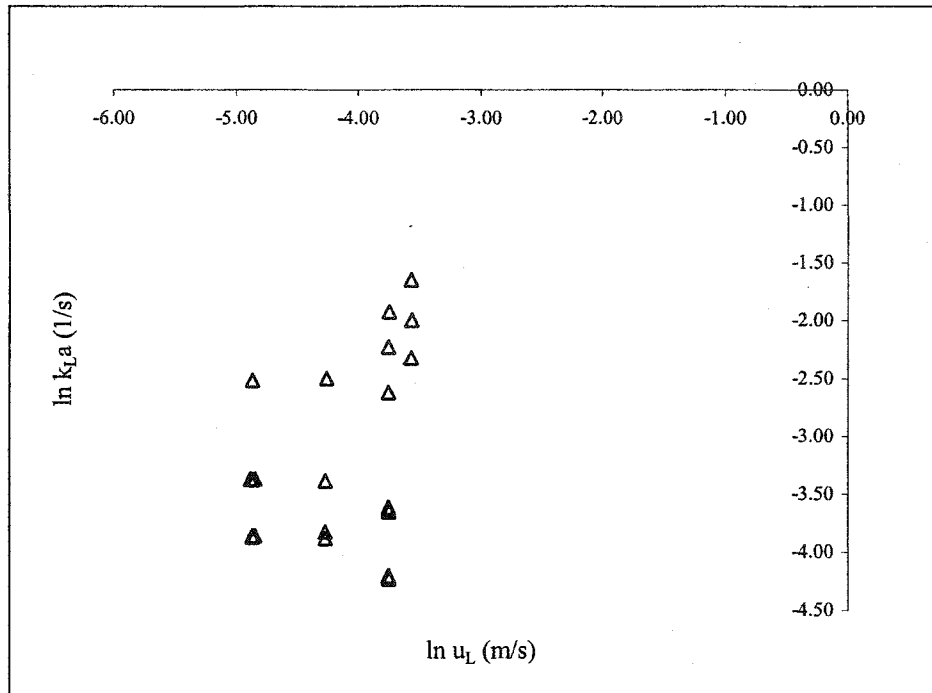


Figure 4-46: Relationship between the superficial liquid velocity and the volumetric mass transfer coefficient

From Figure 4-45 it is clear that there is a nearly linear dependence on superficial gas velocity and the volumetric mass transfer coefficient of the system. It can be said that, as the superficial gas velocity increases, the overall volumetric mass transfer coefficient increases as well. This dependency on the superficial gas velocity has been noted by many other researchers utilizing injectors as distributors in bubble column reactors (Briens et al. 1992, Deckwer et al. 1974, Havelka et al. 2000, Zahradník et al. 1985). Similarly, the use of various distributors resulted in the same relationship between superficial gas velocity and volumetric mass transfer rate as was demonstrated above (Alvarez-Cuenca (1980) used nozzle injectors, Biń et al. (2001) used a porous distributor, Chen et al. (2002) used a perforated plate, Jakubowski et al. (2003) studied a confined

plunging liquid jet contactor with a nozzle as an injector, Kulkarni et al. (1983) employed a ring type distributor, and Roustan et al. (1996) used a porous distributor).

However, when analyzing the relationship between the superficial liquid velocity and the volumetric mass transfer coefficient as shown in Figure 4-46, it is again difficult to notice a trend. To further determine the existence of a relationship between the superficial liquid velocity and the volumetric mass transfer coefficient, the following plot was created. Figure 4-47 illustrates the relationship between the superficial gas velocity and the volumetric mass transfer coefficient, at varying superficial liquid velocities. From Figure 4-47, it can be seen that the volumetric mass transfer rate is increased at higher superficial liquid velocities. In studying the mass transfer process in a downward venturi bubble column combination, Briens et al. (1992) also observed an increase in the rate of mass transfer as the superficial liquid velocity was increased.

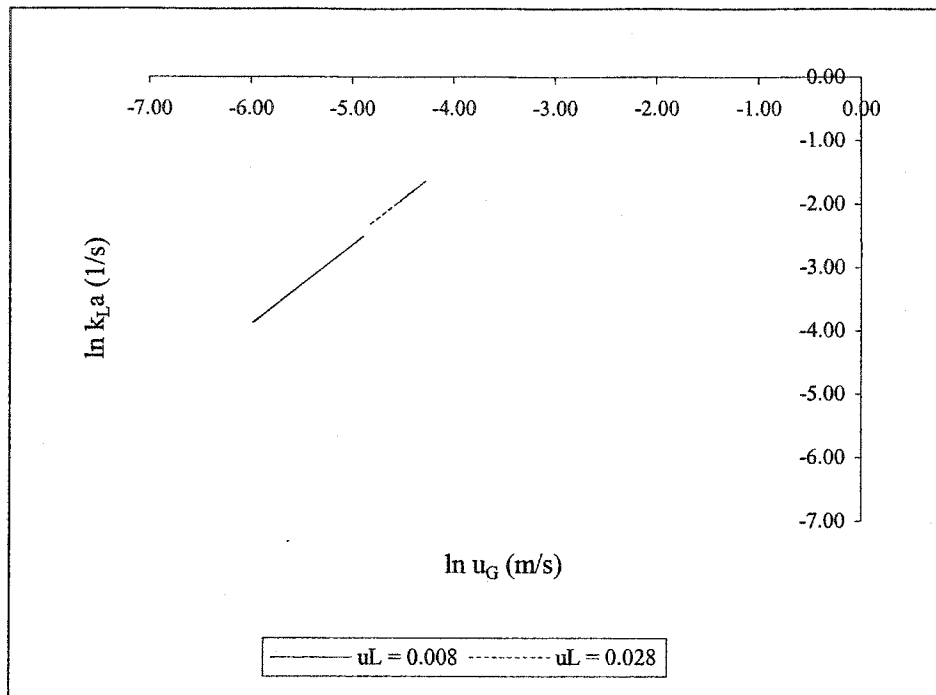


Figure 4-47: Relationship between the superficial gas velocity and the overall mass transfer coefficient at specific superficial liquid velocities

To determine the degree to which the above variables are related to the mass transfer coefficient, linear regression was performed. The resulting equation is as follows:

$$k_L a = 55.58 \cdot u_G^{1.256} \cdot u_L^{0.080} \quad [1/\text{sec}] \quad R^2 = 0.86 \quad \text{Equation 4-19}$$

Similar to what was noted earlier, there is a stronger relationship with the superficial gas velocity, as is indicated by the larger coefficient. The existence of a relationship with the superficial liquid velocity is confirmed, although it is small. The relationship proposed above is in the same form as many others previously discussed in the literature review (Table 2-4). In most instances, the volumetric mass transfer rate is dependent on the gas

flow rate, regardless of whether this relationship is described by the superficial gas velocity, the gas flow rate, the gas velocity, or the gas hold-up. It is evident that an increase in either of the phase velocities results in an increase in the rate of mass transfer, although the effects of the superficial liquid velocity are much less than those of the superficial gas velocity.

As there is a confirmed relationship between these two variables, it is suspected that there is a relationship between the gas hold-up of the system and the mass transfer coefficient. Figure 4-48 indicates that there exists a strong relationship between $k_L a$ and ϵ_G . As the gas hold-up of the bubble column increases, there is a resultant increase in the mass transfer of the bubble column reactor. This is to be expected; the more gas there is entrained in the liquid phase, the more gas there is available for transfer into the liquid phase. This observation is consistent with the observations of Akita and Yoshida (1973), Havelka et al. (2000), Huynh et al. (1991), Heyouni et al. (2002), and Zahradník et al. (1985).

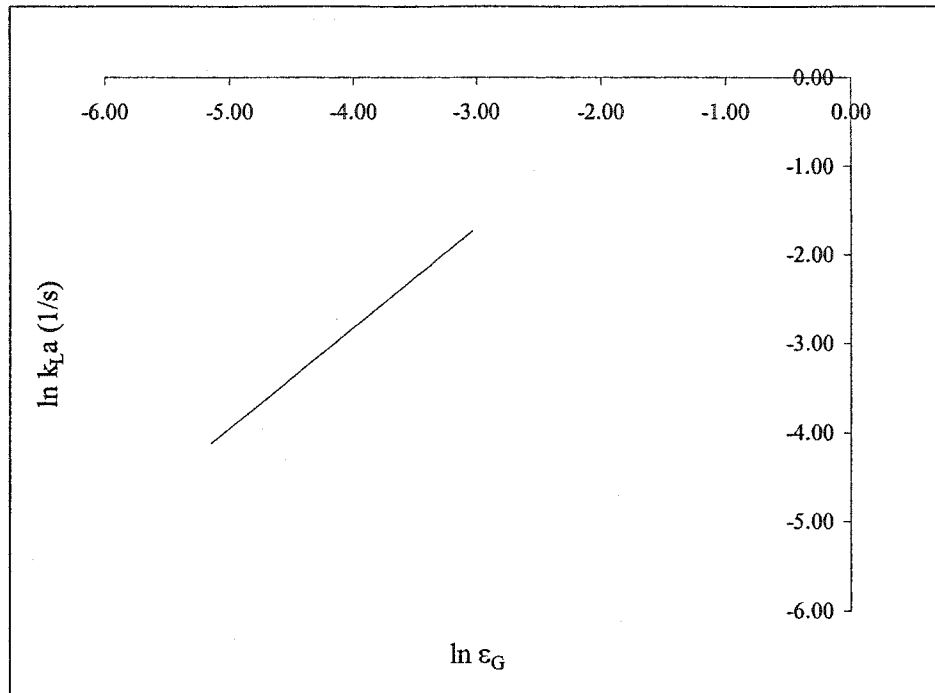


Figure 4-48: Relationship between the gas hold-up and the volumetric mass transfer coefficient at $u_L = 0.014$ m/s

Examining the volumetric mass transfer coefficient, $k_L a$, makes it clear that there exists a very strong relationship with the interfacial area. This relationship is illustrated in Figure 4-49, which shows a strong relationship between these two variables. Approach one refers to the interfacial area obtained using the first method of determining bubble diameter, while Approach two indicates use of the second method. The increasing relationship is explained by the idea that, as the amount of area available for the transfer of ozone gas into the liquid phase increases, there is a resultant increase in the transfer ability and thus, the rate of transfer.

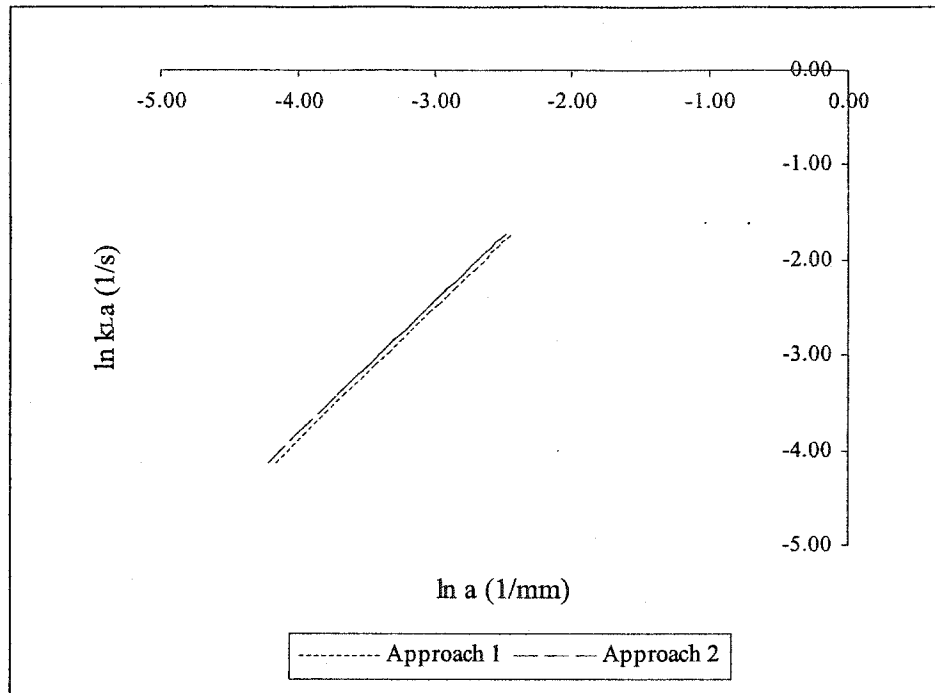


Figure 4-49: Relationship between the interfacial area and the volumetric mass transfer coefficient at $u_L = 0.014$ m/s

Since it is beneficial to determine the actual rate of mass transfer (k_L), the volumetric mass transfer rate was simply divided by the interfacial areas obtained using the two approaches. These results are displayed in Table 4-9.

Table 4-9: Volumetric mass transfer rate, based on two approaches of determining the interfacial area

			Approach 1	Approach 2
Trial #	u_L (m/s)	u_G (m/s)	k_L (1/s)	k_L (1/s)
1	0.008	0.003	1.050	1.103
10	0.008	0.003	1.053	1.106
12	0.008	0.003	1.055	1.109
13	0.024	0.002	1.056	1.111
16	0.023	0.002	1.060	1.115
20	0.023	0.002	1.063	1.119
4	0.014	0.002	1.108	1.165
2	0.014	0.003	1.126	1.184
5	0.008	0.004	1.206	1.267
3	0.008	0.004	1.207	1.269
11	0.008	0.004	1.212	1.274
14	0.024	0.003	1.241	1.306
17	0.023	0.003	1.247	1.312
21	0.023	0.003	1.255	1.320
6	0.014	0.004	1.275	1.341
7	0.008	0.007	1.538	1.617
8	0.014	0.007	1.638	1.723
18	0.023	0.006	1.660	1.747
23	0.028	0.008	1.838	1.936
22	0.023	0.009	1.856	1.954
19	0.028	0.010	2.018	2.125
9	0.024	0.011	2.022	2.129
15	0.028	0.014	2.223	2.341

The obvious trend displayed here is that, as the superficial gas velocity increases, the rate of mass transfer increases. Such a strong relationship is not evident from the superficial liquid velocity, however, a similar general trend is noted.

A comparison with other published literature clearly indicates the benefits of using an impinging-jet bubble column reactor. This reactor displays rates of mass transfer greater than any other previously modeled reactor. This idea is demonstrated in Figure 4-50. The compared reactors are summarized in Table 4-10.

Table 4-10: Relationships being compared in Figure 4-49

Author	Distributor Used	Proposed Correlation
Deckwer et al. (1974)	Cross of nozzles	$k_L a = 0.0086 \cdot u_G^{0.884}$
Cho and Wakao (1988)	Single nozzle sparger	$k_L a = 6.5 \times 10^3 \cdot D_L^{0.5} \cdot u_G^{0.81}$
Huynh et al. (1991)	Venturi/bubble column combination	$k_L a = 3.071 \cdot u_G^{0.5264} \cdot u_L^{0.958}$
Gamal El-Din and Smith (2003a)	Impinging-jet bubble column	$k_L a = 20.54 \cdot u_G^{1.13} \cdot u_L^{0.07}$

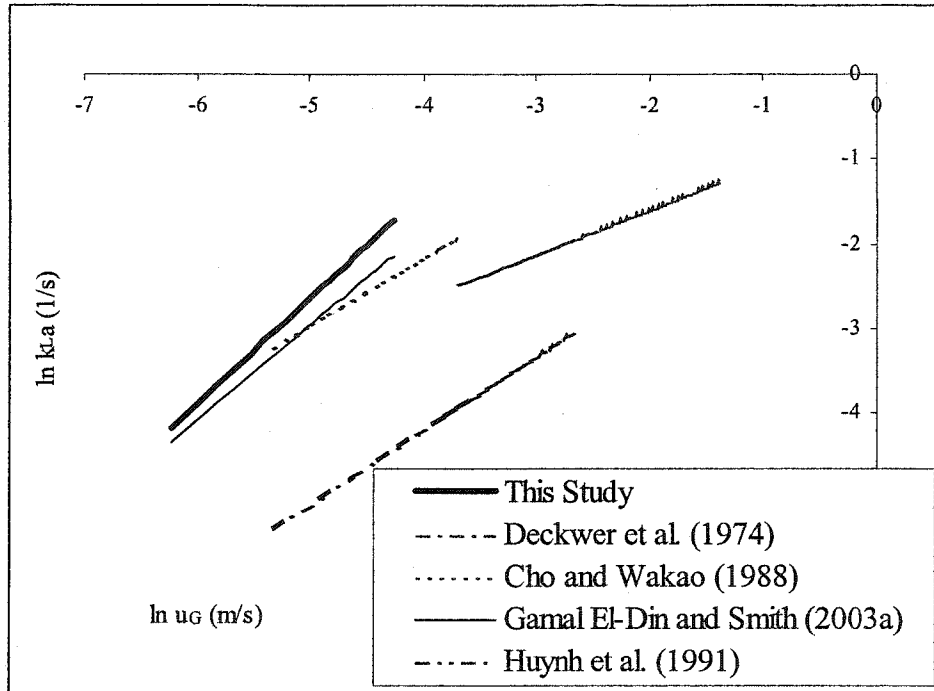


Figure 4-50: Comparison between correlations predicting the mass transfer coefficient, k_La

As a result of the smaller bubbles produced by the shearing action of the venturi injectors, a larger amount of interfacial area was created. This subsequently enhanced the rate of mass transfer. It is known that the use of gas injectors produces a significantly larger rate of mass transfer (higher shear rates lead to smaller bubble diameters), however, the impinging-jet bubble column proves to be even more advantageous within this elite category of bubble column configurations. Compared to bubble columns also operating with nozzle injectors (shown above), this configuration results in larger mass transfer capabilities when modeled with the steady-state BFCM. The model proposed by Gamal El-Din and Smith (2003a) also indicates large interfacial mass transfer capabilities when modeled with the ADM.

Chapter 5 Conclusions and Recommendations

From tracer experiments, the mixing characteristics of the impinging-jet bubble column were modeled using the transient backflow cell model (TBFCM). The residence time distribution (RTD) curves determined that the bubble column should be modeled based on the division of the bubble column into eight mixing cells. The backmixing of the bubble column was accurately modeled assuming the presence of only one zone of mixing along the height of the bubble column. The resulting power law type correlation is based on a relationship with the superficial gas and liquid velocities, and is as follows: $r = 0.13 \cdot u_G^{0.083} \cdot u_L^{-0.975}$. When compared with other bubble columns in the literature, it was shown that the mixing occurring in the impinging-jet bubble column has a much larger axial dispersion coefficient, and thus, a higher degree of mixing.

The gas hold-up of the impinging-jet bubble column was carried out based on collected data from pressure measurements taken in the bubble column under varied gas and liquid flow rates. A larger gas hold-up implies that there is more gas present in the bubble column, which increases the gas available for transfer into the liquid. Similarly, the average gas hold-up along the length of the impinging-jet bubble column was modeled based on a power law type relationship with the individual phase velocities of the system. This model is as follows: $\varepsilon_G = 4.67 \cdot u_G^{1.109} \cdot u_L^{-0.046}$. The gas hold-up produced in the impinging-jet bubble column is comparable to bubble columns previously presented in the literature; some literature produced larger hold-up values, while others produced smaller hold-up values.

Furthermore, the properties of the bubbles produced by the impinging-jet bubble column were investigated. Specifically, using photographic methods, the diameters of the bubbles were measured, and the specific interfacial areas were determined. Small bubbles are more desirable, as more numerous smaller bubbles have a larger interfacial area than less numerous bubbles with large diameters. This increase in interfacial area increases the area available for the transfer of ozone into the liquid phase. The prediction of bubble diameters is based on two approaches: 1) the assumption that the bubble is an oblate sphere; and 2) that the bubble is an ellipsoid. The resultant models of bubble diameters and interfacial areas, for each approach respectively, are as follows:

$$\text{Approach 1: } d_{B,1} = 6.93 \cdot u_G^{0.223} \cdot u_L^{-0.034} \text{ [mm]} \quad a_1 = 3.61 \cdot u_G^{0.902} \cdot u_L^{-0.038} \text{ [1/mm]}$$

$$\text{Approach 2: } d_{B,2} = 7.72 \cdot u_G^{0.224} \cdot u_L^{-0.020} \text{ [mm]} \quad a_2 = 3.40 \cdot u_G^{0.901} \cdot u_L^{-0.039} \text{ [1/mm]}$$

Approach one predicted smaller bubble diameters than Approach two, and consequently, larger interfacial areas.

With respect to the mass transfer abilities of the impinging-jet bubble column reactor, the rate of mass transfer was based on the mass balance equations used in the steady-state backflow cell model. Under varied gas and liquid flow rates, the overall mass transfer coefficient ranged from 0.753 to 10.555 [1/min]. Compared with the literature, the impinging-jet bubble column reactor, when modeled based on the steady state BFCM, resulted in an increased ability to transfer ozone into the liquid phase. The same reactor, modeled on the one phase axial dispersion model, produced a reduced rate of mass

transfer. The resulting power law type model is as follows: $k_L a = 55.58 \cdot u_G^{1.256} \cdot u_L^{0.080}$ [1/min].

In terms of future research regarding the impinging-jet bubble column reactor, the microbial reduction capabilities should be studied, as well as operation with variations in water temperature and water quality. This will provide more insight into the suitability of the impinging-jet bubble column reactor for water and wastewater treatment applications.

Chapter 6 References

Akita, K., and Yoshida, F. (1973). "Gas holdup and volumetric mass transfer coefficient in bubble columns." *Ind. Eng. Chem. Res.*, 12(1), 76-80.

Akita, K., and Yoshida, F. (1974). "Bubble size, interfacial area, and liquid-phase mass transfer coefficient in bubble columns." *Ind. Eng. Chem. Res.*, 13(1), 84-91.

Akosman, C., Orhan, R., and Dursun, G. (2004). "Effects of liquid property on gas holdup and mass transfer in cocurrent downflow contacting column." *Chemical Engineering and Processing*, 43, 503-509.

Alvarez-Cuenca, M., Baker, C. G. J., and Bergougnou, M. A. (1980). "Oxygen mass transfer in bubble columns." *Chemical Engineering Science*, 35, 1121-1127.

Alvarez-Cuenca, M., and Nerenberg, M. A. (1981). "Oxygen mass transfer in bubble columns working at large gas and liquid flow rates." *American Institute of Chemical Engineers*, 27(1), 66-73.

Anabtawi, M. Z. A., Abu-Eishah, S. I., Hilal, N., and Nabhan, M. B. W. (2003). "Hydrodynamic studies in both bi-dimensional and three-dimensional bubble columns with a single sparger." *Chemical Engineering and Processing*, 42, 403-408.

Association, A. P. H., Association, A. W. W., and Federation, W. E. (1995). *Standard methods for the examination of water and wastewater*, American Public Health Association, Washington, DC, U.S.A.

Bablon, G., Bellamy, W. D., Bourbigot, M.-M., Daniel, F. B., Dore, M., Franco, E., Gordon, G., Langlais, B., Laplanche, A., Legube, B., Martin, G., Masschelein, W. J., Pacey, G., Reckhow, D. A., and Ventresque, C. (1991). "Chapter 2 - Fundamental aspects." *Ozone in water treatment: application and engineering*, B. Langlais, D. A. Reckhow, and D. R. Brink, eds., AWWA Research Foundation and Lewis Publishers, Inc., U.S.A., 11 - 132.

Bando, Y., Kuraishi, M., Nishimura, M., Hattori, M., and Asada, T. (1988). "Cocurrent downflow bubble column with simultaneous gas-liquid injection nozzle." *Journal of Chemical Engineering of Japan*, 21(6), 607-612.

Bellamy, W. D. (1995). *Full -scale ozone contactor study*, A.W.W.A. Research Foundation and American Water Works Association, U.S.A.

Bellamy, W. D., Erb, F., Langlais, B., Montiel, A., Rakness, K. L., Reckhow, D. A., and Robson, C. M. (1991). "Chapter 4 - Engineering aspects." *Ozone in water treatment: Application and engineering*, B. Langlais, D. A. Reckhow, and D. R. Brink, eds., AWWA Research Foundation and Lewis Publishers, Inc., U.S.A., 317 - 469.

Beltrán, F. J., García-Araya, J. F., and Álvarez, P. M. (2001). "Domestic wastewater ozonation: A kinetic model approach." *Ozone: Science and Engineering*, 23, 219-228.

Beltrán, F. J., García-Araya, J. F., and Encinar, J. M. (1997). "Henry and mass transfer coefficients in the ozonation of wastewaters." *Ozone: Science and Engineering*, 19, 281-296.

Biń, A. K., Duczmal, B., and machniewski, P. (2001). "Hydrodynamics and ozone mass transfer in a tall bubble column." *Chemical Engineering Science*, 56, 6233-6240.

Bollyky, L. J. (1981). "The mass transfer of ozone into water: Energy requirements-State of the art." *Ozone: Science and Engineering*, 3, 181 - 210.

Borole, A., Joshi, B. G., and Wisecarver, K. (1993). "Phase distribution and mixing in a jet bubble column." *Chemical Engineering Communications*, 126, 189-203.

Briens, C. L., Huynh, L. X., Large, J. F., Catros, A., Bernard, J. R., and Bergougnou, M. A. (1992). "Hydrodynamics and gas-liquid mass transfer in a downward venturi-bubble column combination." *Chemical Engineering Science*, 47(13/14), 3549-3556.

Charpentier, J.-C. (1981). "Mass-transfer rates in gas-liquid absorbers and reactors." *Advances in Chemical Engineering*, T. B. Drew, G. R. Cokelet, J. John W. Hoopes, and T. Vermeulen, eds., Academic Press, Toronto.

Chen, Y. H., Chang, C. Y., Chiu, C. Y., Huang, W. H., Yu, Y. H., Chiang, P. C., Ku, Y., and Chen, J. N. (2002). "Dynamic model of ozone contacting process with oxygen mass transfer in a bubble column." *Journal of Environmental Engineering*, 128(11), 1036-1045.

Chen, Y. H., Chang, C. Y., Chiu, C. Y., Yu, Y. H., Chiang, P. C., Ku, Y., and Chen, J. N. (2003). "Dynamic behavior of ozonation with pollutant in a countercurrent bubble column with oxygen mass transfer." *Water Research*, 7, 2583-2594.

Cho, J. S., and Wakao, N. (1988). "Determination of liquid-side and gas-side volumetric mass transfer coefficients in a bubble column." *Journal of Chemical Engineering of Japan*, 21(6), 576-581.

Cockx, A., Do-Quang, Z., Liné, A., and Roustan, M. (1999). "Use of computational fluid dynamics for simulating hydrodynamics and mass transfer in industrial ozonation towers." *Chemical Engineering Science*, 54, 5085-5090.

Danckwerts, P. V. (1970). *Gas-liquid reactions*, McGraw-Hill, Inc., New York, U.S.A.

Deckwer, W.-D. (1985). *Bubble column reactors*, V. Cottrell, translator, John Wiley & Sons Ltd., Chichester, West Sussex, England.

Deckwer, W. D., Burckhart, R., and Zoll, G. (1974). "Mixing and mass transfer in tall bubble columns." *Chemical Engineering Science*, 29, 2177-2188.

Deckwer, W. D., Nguyen-Tien, K., Kelkar, B. G., and Shah, Y. T. (1983). "Applicability of axial dispersion model to analyze mass transfer measurements in bubble columns." *American Institute of Chemical Engineers*, 29(6), 915-922.

Deckwer, W. D., and Schumpe, A. (1993). "Improved tools for bubble column reactor design and scale-up." *Chemical Engineering Science*, 48(5), 889-911.

Farines, V., Baig, S., Albet, J., Molinier, J., and Legay, C. (2003). "Ozone transfer from gas to water in a co-current upflow packed bed reactor containing silica gel." *Chemical Engineering Journal*, 91, 67-73.

Finch, G. R., Haas, C. N., Oppenheimer, J. A., Gordon, G., and Trussell, R. R. (2001). "Design criteria for inactivation of *Cryptosporidium* by ozone in drinking water." *Ozone: Science and Engineering*, 23(4), 259-284.

Forret, A., Schweitzer, J.-M., Gauthier, T., Krishna, R., and Schweich, d. (2003). "Influence of scale on the hydrodynamics of bubble column reactors: Experimental study in columns of 0.1, 0.4, and 1 m diameters." *Chemical Engineering Science*, 58, 719-724.

Friedel, L., Herbrechtsmeier, P., and Steiner, R. (1980). "Mean gas hold-up in downflow bubble columns." *Ger. Chem. Eng.*, 3, 342-346.

Gamal El-Din, M., and Smith, D. W. (2001a). "Development of transient back flow cell model (BFCM) for bubble columns." *Ozone: Science and Engineering*, 23, 313-326.

Gamal El-Din, M., and Smith, D. W. (2001b). "Maximizing the enhanced ozone oxidation of Kraft pulp mill effluents in an impinging-jet bubble column." *Ozone: Science and Engineering*, 23, 479-493.

Gamal El-Din, M., and Smith, D. W. (2001c). "Ozone mass transfer in water treatment: Hydrodynamics and mass transfer modeling of ozone bubble columns." *Water Science and Technology: Water Supply*, 1(2), 123-130.

Gamal El-Din, M. (2001d). "Theoretical analysis and experimental investigation of the performance of ozone bubble columns: Ph.D. thesis." *University of Alberta*, Edmonton, AB, Canada

Gamal El-Din, M., and Smith, D. W. (2003a). "Mass transfer analysis in ozone bubble columns." *Journal of Environmental Engineering and Science*, 2, 63-76.

Gamal El-Din, M., and Smith, D. W. (2003b). "Measurements of the size, rise velocity, and specific interfacial area of bubbles in an impinging-jet bubble column." *Journal of Environmental Engineering and Science*, 2(2), 127-138.

Gavrilescu, M., and Tudose, R. Z. (1996). "Bubble column reactors of small dimensions I. Gas holdup in gas/liquid dispersions." *Hungarian Journal of Industrial Chemistry*, 24, 25-34.

Gurol, M. D., and Singer, P. C. (1982). "Kinetics of ozone decomposition: A dynamic approach." *Environmental Science and Technology*, 16(7), 377-383.

Havelka, P., Linek, V., Sinkule, J., Zahradník, J., and Fialová, M. (2000). "Hydrodynamic and mass transfer characteristics of ejector loop reactors." *Chemical Engineering Science*, 55, 535-549.

Heyouni, A., Roustan, M., and Do-Quang, Z. (2002). "Hydrodynamics and mass transfer in gas-liquid flow through static mixers." *Chemical Engineering Science*, 57, 3325-3333.

Hidaka, N., Mizuguchi, K.-I., and Matsumoto, T. (1998). "Axial mixing of liquid in counter-current bubble columns." *Journal of Chemical Engineering of Japan*, 31(6), 1016-1019.

Hikita, H., Asai, S., Tanigawa, K., Segawa, K., and Kitao, M. (1981). "The volumetric liquid-phase mass transfer coefficient in bubble columns." *The Chemical Engineering Journal*, 22, 61-69.

Holder, G. A., and Leow, J. M. (1994). "In-sewer oxygenation of wastewater using venturi side-stream dissolvers." *Water Science and Technology*, 30(1), 185-194.

Houzelot, J. L., Thiebaut, M. F., Charpentier, J. C., and Schiber, J. (1985). "Contribution to the hydrodynamic study of bubble columns." *International Chemical Engineering*, 25(4), 645-650.

Hsu, Y.-C., Chen, T.-Y., Chen, J.-H., and Lay, C.-W. (2002). "Ozone transfer into water in a gas-inducing reactor." *Industrial and Engineering Chemical Research*, 41, 120-127.

Huang, W. H., Chang, C. Y., Chiu, C. Y., Lee, S. J., Yu, Y. H., Liou, H. T., Ku, Y., and Chen, J. N. (1998). "A refined model for ozone mass transfer in a bubble column." *Journal of Environmental Science and Health*, A33 (3), 441-460.

Huynh, L. X., Briens, C. L., Large, J. F., Catros, A., Bernard, J. R., and Bergougnou, M. A. (1991). "Hydrodynamics and mass transfer in an upward venturi/bubble column combination." *The Canadian Journal of Chemical Engineering*, 69, 711-722.

Idogawa, K., Ikeda, K., Fukuda, T., and Morooka, S. (1987). "Effect of gas and liquid properties on the behavior of bubbles in a column under high pressure." *International Chemical Engineering*, 27(1), 93-99.

Jakubowski, C. A., Atkinson, B. W., Dennis, P., and Evans, G. M. (2003). "Ozone mass transfer in a confined plunging liquid jet contactor." *Ozone: Science and Engineering*, 25, 1-12.

Jamialahmadi, M., Müller-Steinhagen, H., Sarrafi, A., and Smith, J. M. (2000). "Studies of gas holdup in bubble column reactors." *Chemical Engineering and Technology*, 23(10), 919-921.

Kago, T., Sasaki, Y., Kondo, T., Morooka, S., and Kato, Y. (1989). "Gas holdup and axial dispersion of gas and liquid in bubble columns of homogeneous bubble flow regime." *Chemical Engineering Communications*, 75, 23-38.

Kantak, M. V., Shetty, S. A., and Kelkar, B. G. (1994). "Liquid phase backmixing in bubble column reactors - A new correlation." *Chemical Engineering Communications*, 127, 23-34.

Kastánek, F., Zahradník, J., Kratochvíl, J., and Čermák, J. (1993). *Chemical reactors for gas-liquid systems*, Ellis Horwood Limited, Chichester, West Sussex, England.

Kato, Y., and Nishiwaki, A. (1972). "Longitudinal dispersion coefficient of a liquid in a bubble column." *International Chemical Engineering*, 12(1), 182-187.

Kawagoe, M., Otake, T., and Robinson, C. W. (1989). "Gas-phase mixing in bubble columns." *Journal of Chemical Engineering of Japan*, 22(2), 136-142.

Kim, J.-H., Rennecker, J. L., Tomiak, R. B., Mariñas, B. J., Miltner, R. J., and Owens, J. H. (2002 b). "Inactivation of *Cryptosporidium* oocysts in a pilot-scale ozone bubble-diffuser contactor. I: Model validation and application." *Journal of Environmental Engineering*, 128(6), 522-532.

Kim, J.-H., Tomiak, R. B., and Mariñas, B. J. (2002 a). "Inactivation of *Cryptosporidium* oocysts in a pilot-scale ozone bubble-diffuser contactor. I: Model development." *Journal of Environmental Engineering*, 128(6), 514-521.

Krishna, R., and Ellenberger, J. (1996). "Gas holdup in bubble column reactors operating in the churn-turbulent flow regime." *American Institute of Chemical Engineers*, 42(9), 2627-2634.

Krishna, R., Wilkinson, P. M., and Van Dierendonck, L. L. (1991). "A model for gas holdup in bubble columns incorporating the influence of gas density on flow regime transitions." *Chemical Engineering Science*, 46(10), 2491-2496.

Kulkarni, A., Shah, Y., and Schumpe, A. (1983). "Hydrodynamics and mass transfer in downflow bubble column." *Chemical Engineering Communications*, 24, 307-337.

Kumar, A., Degaleensan, T. E., Laddha, G. S., and Heolscher, H. E. (1976). "Bubble swarm characteristics in bubble columns." *The Canadian Journal of Chemical Engineering*, 54, 503-508.

Kundu, G., Mukherjee, D., and Mitra, A. K. (1995). "Experimental studies on a co-current gas-liquid downflow bubble column." *International Journal of Multiphase Flow*, 21(5), 893-906.

Kuo, C. H. (1982). "Mass transfer in ozone absorption." *Environmental Progress*, 1(3), 189-195.

Kuo, C.-H., and Yocum, F. H. (1982). "Chapter 5 - Mass transfer of ozone into aqueous systems." Handbook of ozone technology and applications, R. G. Rice and A. Netzer, eds., Ann Arbor Science Publishers, Ann Arbor, Michigan, U.S.A., 105 - 141.

Laari, A., Kallas, J., and Palosaari, S. (1997). "Gas-liquid mass transfer in bubble columns with a T-junction nozzle for gas dispersion." *Chemical Engineering and Technology*, 20, 550-556.

Lage, P. L. C., and Espósito, R. O. (1999). "Experimental determination of bubble size distributions in bubble columns: Prediction of mean bubble diameter and gas hold up." *Powder Technology*, 101, 142-150.

Levenspiel, O. (1999). *Chemical reaction engineering*, John Wiley & Sons, Inc, New York.

Long, B. W., Hulsey, R. A., and Hoehn, R. C. (1999). "Complementary uses of chlorine dioxide and ozone for drinking water treatment." *Ozone Science and Engineering*, 21, 465-476.

Mandal, A., Kundu, G., and Mukherjee, D. (2003). "Gas holdup and entrainment characteristics in a modified downflow bubble column with Newtonian and non-Newtonian liquid." *Chemical Engineering and Processing*, 42, 777-787.

Mariñas, B. J., Liang, S., and Aieta, E. M. (1993). "Modeling hydrodynamics and ozone residual distribution in a pilot-scale ozone bubble-diffuser contactor." *Journal AWWA-Research and Technology*, 90-99.

Martin, N., Benezet-Toulze, M., Laplace, C., Faivre, M., and Langlais, B. (1992). "Design and efficiency of ozone contactors for disinfection." *Ozone: Science and Engineering*, 14, 391-405.

Masschelein, W. J. (2000). "Considerations on the Chick-Watson law applied to the ozonation of drinking water." *Ozone: Science and Engineering*, 22, 227-239.

Meikap, B. C., Kundu, G., and Biswas, M. N. (2001). "Prediction of the interfacial area of contact in a variable-area multistage bubble column." *Industrial and Engineering Chemical Research*, 40, 6194-6200.

Mersmann, A. (1978). "Design and scale-up of bubble and spray columns." *Ger. Chem. Eng.*, 1, 1-11.

Montgomery, Douglas C., Runger, G. C., and Hubele, N. F. (2001). *Engineering statistics*, John Wiley & Sons, Inc., U.S.A.

Moustiri, S., Hebrard, G., Thakre, S. S., and Roustan, M. (2001). "A unified correlation for predicting liquid axial dispersion coefficient in bubble columns." *Chemical Engineering Science*, 56, 1041-1047.

Nakao, K., Takeuchi, H., Kataoka, H., Kaji, H., Otake, T., and Miyauchi, T. (1983). "Mass transfer characteristics of bubble columns in recirculation flow regime." *Industrial and Engineering Chemical Research*, 22, 577-582.

Ohkawa, A., Shiokawa, Y., Sakai, N., and Imai, H. (1985). "Flow characteristics of downflow bubble columns with gas entrainment by a liquid jet." *Journal of Chemical Engineering of Japan*, 18(5), 466-469.

Oke, N. J., Smith, D. W., and Zhou, H. (1998). "An empirical analysis of ozone decay kinetics in natural waters." *Ozone: Science and Engineering*, 20, 361-379.

Otake, T., Tone, S., and Shinohar, K. (1981). "Gas holdup in the bubble column with cocurrent and countercurrent gas-liquid flow." *Journal of Chemical Engineering of Japan*, 14(4), 338-340.

Patil, V. K., Joshi, J. B., and Sharma, M. M. (1984). "Sectionalised bubble column: Gas hold-up and wall side solid-liquid mass transfer coefficient." *The Canadian Journal of Chemical Engineering*, 62(April), 228-232.

Petrucci, R. H., and Harwood, W. S. (1997). *General chemistry: Principles and modern applications*, Prentice-Hall, Inc., Upper Saddle River.

Radhakrishnan, V. R., and Mitra, A. K. (1984). "Pressure drop, holdup and interfacial area in vertical two-phase flow of multi-jet ejector induced dispersions." *The Canadian Journal of Chemical Engineering*, 62, 170-178.

Reckhow, D. A. (1999). "Chapter 9 - Control of disinfection by-product formation using ozone." *Formation and control of disinfection by-products in drinking water*, P. C. Singer, ed., American Water Works Association, Denver, CO, U.S.A., 179 - 204.

Reilly, I. G., Scott, D. S., De Bruijn, T. J. W., and MacIntyre, D. (1994). "The role of gas phase momentum in determining gas holdup and hydrodynamic flow regimes in bubble column operations." *The Canadian Journal of Chemical Engineering*, 72, 3-12.

Roustan, M., Wang, R. Y., and Wolbert, D. (1996). "Modeling hydrodynamics and mass transfer parameters in a continuous ozone bubble column." *Ozone: Science and Engineering*, 18, 99-115.

Sada, E., Kumazawa, H., Lee, C., and Iguchi, T. (1986). "Gas holdup and mass transfer characteristics in a three-phase bubble column." *Industrial and Engineering Chemical Research*, 25, 472-476.

Salazar, J. A., Wisecarver, K. D., Shah, Y. T., and Solari, B. (1993). "Gas-liquid mass transfer in jet bubble column." *Chemical Engineering Communications*, 124, 177-188.

Sarrafi, A., Jamialahmadi, M., Müller-Steinhagen, H., and Smith, J. M. (1999). "Gas holdup in homogeneous and heterogeneous gas-liquid bubble column reactors." *The Canadian Journal of Chemical Engineering*, 77, 11-21.

Sawyer, C. N., McCarty, P. L., and Parkin, G. F. (1994). *Chemistry for environmental engineering*, McGraw-Hill, Inc., New York.

Schulz, C. R., and Prendiville, P. W. (1993). "Designing high concentration ozone contactors for drinking water treatment plants." *Ozone: Science and Engineering*, 15, 245-266.

Schulz, C. R., Schafran, G. C., Garrett, L. B., and Hawkins, R. A. (1995). "Evaluating a high-efficiency ozone injection contactor." *Journal AWWA*, 85-99.

Shawaqfeh, A. T. (2003). "Gas holdup and liquid axial dispersion under slug flow conditions in gas-liquid bubble column." *Chemical Engineering and Processing*, 42, 767-775.

Shetty, S. A., Kantak, M. V., and Kelkar, B. G. (1992). "Gas-phase backmixing in bubble-column reactors." *American Institute of Chemical Engineers*, 38(7), 1013-1026.

Singer, P. C., and Reckhow, D. A. (1999). "Chapter 12: Chemical oxidation." *Water quality and treatment: A handbook of community water supplies*, R. D. Letterman, ed., McGraw-Hill, Inc., New York, 12.1-12.51.

Smith, D. W., and Gamal El-Din, M. (2002). "Theoretical analysis and experimental verification of ozone mass transfer in bubble columns." *Environmental Technology*, 23, 135-147.

Snoeyink, V. L., and Summers, R. S. (1999). "Chapter 13-Adsorption of organic compounds." *Water quality and treatment: A handbook of community water supplies*, R. d. Letterman, ed., McGraw-Hill, Inc, New York.

Sotelo, J. L., Beltrán, F. J., Benitez, F. J., and Beltrán-Heredia, J. (1989). "Henry's law constant for the ozone-water system." *Water Research*, 23(20), 1239-1246.

Thalasso, F., H.Naveau, and Nyns, E.-J. (1995). "Design and performance of a bioreactor equipped with a Venturi injector for high gas transfer rates." *The Chemical Engineering Journal*, 57, B1-B5.

Uchida, S., Tsuyutani, S., and Seno, T. (1989). "Flow regimes and mass transfer in counter-current bubble columns." *The Canadian Journal of Chemical Engineering*, 67, 866-869.

Wachi, S., Morikawa, H., and Ueyama, K. (1987). "Gas holdup and axial dispersion in gas-liquid concurrent bubble column." *Journal of Chemical Engineering of Japan*, 20(3), 309-316.

Winterton, R. H. S. (1994). "A simple method of predicting bubble size in bubble columns." *Chemical Engineering and Processing*, 33, 1-5.

Wright, P. C., Meeyoo, V., and Soh, W. K. (1997). "A study of ozone mass transfer in a cocurrent downflow jet pump contactor." *Ozone: Science and Engineering*, 20(1), 17-33.

Yamagiwa, K., Kusabiraki, D., and Ohkawa, A. (1990). "Gas holdup and gas entrainment rate in downflow bubble column with gas entrainment by a liquid jet operating at high liquid throughput." *Journal of Chemical Engineering of Japan*, 23(3), 343-348.

Yamashita, F. (1998). "Effect of clear liquid height and gas inlet height on gas holdup in a bubble column." *Journal of Chemical Engineering of Japan*, 31(2), 285-288.

Yamashita, F., Mori, Y., and Fujita, S. (1979). "Sizes and size distributions of bubble in a bubble column - Comparison between the two point electrode probe method and the photographic method." *Journal of Chemical Engineering of Japan*, 12(1), 5-9.

Yang, Y. B., Devanathan, N., and Dudukovic, M. P. (1992). "Liquid backmixing in bubble columns." *Chemical Engineering Science*, 47(9-11), 2859-2864.

Zahradník, J., and Fialová, M. (1996). "The effect of bubbling regime on gas and liquid phase mixing in bubble column reactors." *Chemical Engineering Science*, 51(10), 2491-2500.

Zahradník, J., Fialová, M., Růžička, M., Drahoš, J., Kaštánek, F., and Thomas, N. H. (1997). "Dispersion efficiency of ejector-type gas distributors in different operating modes." *Chemical Engineering Science*, 52(24), 4499-4510.

Zahradník, J., and Kaštánek, F. (1979). "Gas holdup in uniformly aerated bubble column reactors." *Chemical Engineering Communications*, 3, 413-429.

Zahradník, J., Kratochvíl, J., and Rylek, M. (1985). "Gas holdup and interfacial mass transfer in gas-liquid tower contactors with ejector-type gas distributors." *Collection Czechoslovak Chemical Communication*, 50, 2535-2544.

Zar, J. H. (1999). *Biostatistical analysis*, Pearson Education, Upper Saddle River, New Jersey.

Zhou, H., and Smith, D. W. "Modelling of mass transfer and ozone decomposition in a bubble column: Experimental verification." *12th World Congress of the International Ozone Association*, Lille, France, 240-252.

Zhou, H., and Smith, D. W. (2000). "Ozone mass transfer in water and wastewater treatment: Experimental observations using a 2D laser particle dynamics analyzer." *Water Research*, 34(3), 909-921.

Zhou, H., Smith, D. W., and Stanley, S. J. (1994). "Modeling of dissolved ozone concentration profiles in bubble columns." *Journal of Environmental Engineering*, 120(4), 821-840.

Chapter 7 Appendices

Raw Data: Mixing Study

Mode	Run #	Run ID	Q_L	Q_G	U_L (m/s)	U_G (m/s)	Q_G/Q_L	r_1	Pe_1
Ejection	1	19.1	8.820	0.400	0.019	0.001	0.045	5.785	0.076
	2	20.4	8.820	0.809	0.019	0.002	0.092	4.740	0.076
	3	21.1	11.050	0.726	0.023	0.002	0.066	3.372	0.076
	4	23.1	11.050	0.931	0.023	0.002	0.084	3.672	0.076
	5	26.4	11.050	1.507	0.023	0.003	0.136	4.324	0.076
	6	24.5	13.270	0.809	0.028	0.002	0.061	3.365	0.076
	8	29.7	13.270	2.939	0.028	0.006	0.221	2.855	0.076
Injection	5	1.1	3.630	0.463	0.008	0.001	0.128	12.374	0.076
	6	5.2	3.630	1.135	0.008	0.002	0.313	12.610	0.076
	7	7.9	3.630	1.751	0.008	0.004	0.482	12.514	0.077
	8	2.3	5.110	0.452	0.011	0.001	0.088	8.830	0.107
	9	3.3	5.110	0.894	0.011	0.002	0.175	8.940	0.106
	10	18.2	6.599	0.438	0.014	0.001	0.066	6.470	0.143
	11	4.3	6.600	0.866	0.014	0.002	0.131	6.500	0.143
	12	22.6	6.600	1.093	0.014	0.002	0.166	8.401	0.112
	13	15.1	8.830	6.886	0.019	0.015	0.780	4.852	0.187
	14	25.3	8.830	1.622	0.019	0.003	0.184	4.944	0.184
	15	12.1	8.850	5.673	0.019	0.012	0.641	4.816	0.188
	16	13.2	11.040	5.509	0.023	0.012	0.499	3.824	0.231
	17	16.1	11.050	6.703	0.023	0.014	0.607	3.705	0.238
	18	28.4	11.050	3.179	0.023	0.007	0.288	3.659	0.240
19	17.6	13.270	6.487	0.028	0.014	0.489	2.956	0.289	
20	14.8	13.270	5.278	0.028	0.011	0.398	2.916	0.293	

Mode	Run #	Run ID	r_2	Pe_2	$(r_1+r_2)/2$	$(r_1+r_2)/2 + 0.5$	r	$r + 0.5$
Ejection	1	19.1	0.545	6.700	3.165	3.665	2.407	2.907
	2	20.4	0.858	5.530	2.799	3.299	3.630	4.130
	3	21.1	0.785	5.446	2.079	2.579	2.425	2.925
	4	23.1	0.256	9.256	1.964	2.464	2.960	3.460
	5	26.4	0.732	5.683	2.528	3.028	2.794	3.294
	6	24.5	0.210	12.676	1.788	2.288	2.171	2.671
	8	29.7	1.478	3.538	2.167	2.667	2.337	2.837
	Injection	5	1.1	2.601	2.628	7.488	7.988	6.390
6		5.2	3.195	1.894	7.903	8.403	8.000	8.500
7		7.9	5.017	1.256	8.766	9.266	10.049	10.549
8		2.3	2.953	2.027	5.892	6.392	6.804	7.304
9		3.3	1.974	3.638	5.457	5.957	7.061	7.561
10		18.2	0.600	6.377	3.535	4.035	3.230	3.730
11		4.3	1.890		4.195	4.695	3.765	4.265
12		22.6	1.810		5.106	5.606	5.279	5.779
13		15.1	1.554	4.382	3.203	3.703	3.910	4.410
14		25.3	0.954	4.816	2.949	3.449	3.850	4.350
15		12.1	0.823	5.034	2.820	3.320	3.740	4.240
16		13.2	0.768	5.519	2.296	2.796	2.809	3.309
17	16.1	0.481	9.174	2.093	2.593	2.952	3.452	
18	28.4	0.834	5.831	2.247	2.747	2.979	3.479	
19	17.6	0.349	5.248	1.653	2.153	2.194	2.694	
20	14.8	0.245	9.398	1.581	2.081	2.186	2.686	

Mode	Run #	Run ID	$\log(u_L)$	$\log(u_G)$	$\log(r_1+0.5)$	$\log(r_2+0.5)$	$\log(r+0.5)$	$\log\left[\frac{(r_1+r_2)}{2} + 0.5\right]$
Ejection	1	19.1	-1.728	-3.071	0.798	0.019	0.463	0.564
	2	20.4	-1.728	-2.765	0.719	0.133	0.616	0.518
	3	21.1	-1.630	-2.812	0.588	0.109	0.466	0.411
	4	23.1	-1.630	-2.704	0.620	-0.121	0.539	0.392
	5	26.4	-1.630	-2.495	0.683	0.091	0.518	0.481
	6	24.5	-1.550	-2.765	0.587	-0.149	0.427	0.359
	8	29.7	-1.550	-2.205	0.526	0.296	0.453	0.426
	Injection	5	1.1	-2.113	-3.007	1.110	0.492	0.838
6		5.2	-2.113	-2.618	1.118	0.568	0.929	0.924
7		7.9	-2.113	-2.430	1.114	0.742	1.023	0.967
8		2.3	-1.965	-3.018	0.970	0.538	0.864	0.806
9		3.3	-1.965	-2.722	0.975	0.393	0.879	0.775
10		18.2	-1.854	-3.032	0.843	0.041	0.572	0.606
11		4.3	-1.853	-2.736	0.845	0.378	0.630	0.672
12		22.6	-1.853	-2.634	0.949	0.364	0.762	0.749
13		15.1	-1.727	-1.835	0.729	0.313	0.644	0.569
14		25.3	-1.727	-2.463	0.736	0.163	0.638	0.538
15		12.1	-1.726	-1.919	0.726	0.122	0.627	0.521
16		13.2	-1.630	-1.932	0.636	0.103	0.520	0.447
17	16.1	-1.630	-1.847	0.624	-0.008	0.538	0.414	
18	28.4	-1.630	-2.171	0.619	0.125	0.541	0.439	
19	17.6	-1.550	-1.861	0.539	-0.071	0.430	0.333	
20	14.8	-1.550	-1.951	0.534	-0.128	0.429	0.318	

Regression Analysis: Mixing Study - r_1

SUMMARY OUTPUT

<i>Regression Statistics</i>	
Multiple R	0.988
R Square	0.976
Adjusted R Square	0.973
Standard Error	0.031
Observations	23

ANOVA

	<i>df</i>	<i>SS</i>	<i>MS</i>	<i>F</i>	<i>Significance F</i>
Regression	2	0.796	0.398	402.304	0.000
Residual	20	0.020	0.001		
Total	22	0.815			

	<i>Coefficients</i>	<i>Standard Error</i>	<i>t Stat</i>	<i>P-value</i>	<i>Lower 95%</i>	<i>Upper 95%</i>
Intercept	-1.035	0.064	-16.110	0.000	-1.169	-0.901
u_L	-0.997	0.041	-24.381	0.000	-1.082	-0.912
u_G	-0.019	0.018	-1.040	0.311	-0.056	0.019

Regression Analysis: Mixing Study - r₂

SUMMARY OUTPUT

<i>Regression Statistics</i>	
Multiple R	0.876
R Square	0.767
Adjusted R Square	0.744
Standard Error	0.123
Observations	23

ANOVA

	<i>df</i>	<i>SS</i>	<i>MS</i>	<i>F</i>	<i>Significance F</i>
Regression	2	0.997	0.499	32.955	0.000
Residual	20	0.303	0.015		
Total	22	1.300			

	<i>Coefficients</i>	<i>Standard Error</i>	<i>t Stat</i>	<i>P-value</i>	<i>Lower 95%</i>	<i>Upper 95%</i>
Intercept	-1.693	0.251	-6.734	0.000	-2.217	-1.168
u _L	-1.248	0.160	-7.797	0.000	-1.581	-0.914
u _G	0.123	0.070	1.753	0.095	-0.023	0.270

Regression Analysis: Mixig Study - r

SUMMARY OUTPUT

<i>Regression Statistics</i>	
Multiple R	0.954
R Square	0.911
Adjusted R Square	0.902
Standard Error	0.055
Observations	23

ANOVA

	<i>df</i>	<i>SS</i>	<i>MS</i>	<i>F</i>	<i>Significance F</i>
Regression	2	0.621	0.310	102.422	0.000
Residual	20	0.061	0.003		
Total	22	0.681			

	<i>Coefficients</i>	<i>Standard Error</i>	<i>t Stat</i>	<i>P-value</i>	<i>Lower 95%</i>	<i>Upper 95%</i>
Intercept	-0.884	0.112	-7.858	0.000	-1.118	-0.649
u_L	-0.975	0.072	-13.614	0.000	-1.124	-0.825
u_G	0.083	0.031	2.649	0.015	0.018	0.149

Pressure sensor calibration data

Middle pressure sensor /sensor # (2)

Hydrostatic Pressure (m of water)	Hydrostatic Pressure (psi)	Hydrostatic Pressure (KPa)	Datalogger Reading (Volts)
Top			
0.223	0.317	2.187	0.366
0.019	0.027	0.186	0.085
0.000			
0.000	0.000	0.000	0.049
Middle			
0.690	0.980	6.767	0.997
0.486	0.691	4.766	0.716
0.236	0.335	2.314	0.379
0.086	0.122	0.843	0.176
0.000			
0.000	0.000	0.000	0.048
Bottom			
1.172	1.665	11.493	1.639
0.968	1.375	9.493	1.360
0.718	1.020	7.041	1.025
0.568	0.807	5.570	0.824
0.268	0.381	2.628	0.412
0.000	0.000	0.000	0.049

Raw Data: Pressure Calibration of Sensors

TIME HH:MM:SS	ANALOG 1		ANALOG 2		ANALOG 3	
	Bottom Pressure Sensor		Middle Pressure Sensor		Top Pressure Sensor	
	Volts	Hydrostatic Pressure (m)	Volts	Hydrostatic Pressure (m)	Volts	Hydrostatic Pressure (m)
13:53:36	1.607	1.171	0.962	0.688	0.362	0.225
13:53:37	1.609	1.173	0.963	0.689	0.362	0.225
13:53:38	1.609	1.172	0.961	0.688	0.362	0.226
13:53:39	1.605	1.170	0.962	0.688	0.361	0.225
13:53:40	1.606	1.171	0.962	0.688	0.361	0.225
13:53:41	1.606	1.170	0.962	0.688	0.361	0.225
13:53:42	1.606	1.170	0.960	0.687	0.360	0.224
13:53:43	1.605	1.170	0.960	0.687	0.359	0.224
13:53:44	1.608	1.172	0.961	0.687	0.361	0.225
13:53:45	1.606	1.170	0.962	0.688	0.361	0.225
13:53:46	1.607	1.171	0.961	0.687	0.360	0.225
13:53:47	1.605	1.170	0.962	0.688	0.361	0.225
13:53:48	1.607	1.171	0.960	0.687	0.360	0.224
13:53:49	1.606	1.171	0.963	0.689	0.362	0.225
↓	↓	↓	↓	↓	↓	↓
14:09:10	1.610	1.173	0.963	0.689	0.362	0.226
14:09:11	1.609	1.173	0.963	0.689	0.362	0.225
14:09:12	1.609	1.173	0.963	0.689	0.362	0.225
14:09:13	1.607	1.171	0.962	0.688	0.361	0.225
14:09:14	1.606	1.171	0.962	0.688	0.361	0.225
14:09:15	1.609	1.172	0.963	0.689	0.362	0.225
14:09:16	1.609	1.172	0.963	0.689	0.362	0.225
14:09:17	1.609	1.173	0.963	0.689	0.362	0.226
14:09:18	1.609	1.173	0.963	0.689	0.362	0.225
14:09:19	1.606	1.171	0.962	0.688	0.361	0.225
14:09:20	1.609	1.172	0.962	0.688	0.362	0.225
14:09:21	1.609	1.172	0.963	0.689	0.362	0.226
14:09:22	1.609	1.173	0.963	0.689	0.362	0.225
14:09:23	1.609	1.173	0.963	0.689	0.362	0.225
14:09:24	1.609	1.172	0.963	0.689	0.362	0.225
14:09:25	1.606	1.171	0.961	0.688	0.361	0.225
14:09:26	1.608	1.172	0.963	0.689	0.361	0.225
	1.607	1.172	0.962	0.688	0.361	0.225

TIME HH:MM:SS	Gas Holdup	
	Bottom - Middle	Middle - Top
13:53:36	-0.001	0.009
13:53:37	-0.003	0.007
13:53:38	-0.005	0.011
13:53:39	0.000	0.008
13:53:40	-0.001	0.008
13:53:41	-0.001	0.008
13:53:42	-0.003	0.009
13:53:43	-0.001	0.008
13:53:44	-0.005	0.010
13:53:45	-0.001	0.009
13:53:46	-0.003	0.009
13:53:47	0.001	0.008
13:53:48	-0.004	0.009
13:53:49	0.001	0.007
	↓	↓
14:09:10	-0.004	0.008
14:09:11	-0.004	0.008
14:09:12	-0.003	0.007
14:09:13	-0.002	0.008
14:09:14	-0.001	0.008
14:09:15	-0.003	0.008
14:09:16	-0.003	0.008
14:09:17	-0.004	0.009
14:09:18	-0.004	0.008
14:09:19	-0.001	0.008
14:09:20	-0.004	0.009
14:09:21	-0.002	0.008
14:09:22	-0.003	0.007
14:09:23	-0.003	0.007
14:09:24	-0.002	0.007
14:09:25	-0.002	0.009
14:09:26	-0.002	0.006
	-0.002	0.008

Raw Data: Gas Holdup Study

Run ID#	Date	Temperature	Area of Column (m ²)		0.00785
			Experimental	Experimental	Rotameter
			Barometric	Rotameter Exit	Reading
			Pressure	Gauge Pressure	Q _G (L/min)
1.1	12-May	22.000	704.600	1.700	0.500
1.2	12-May	22.000	704.600	1.700	0.500
1.3	12-May	22.000	704.600	1.700	0.500
1.4	12-May	22.000	704.600	1.700	0.500
1.5	12-May	22.000	704.600	1.700	0.500
1.6	31-May	22.000	710.950	1.650	0.500
1.7	31-May	22.000	710.950	1.650	0.500
2.1	12-May	22.000	704.600	0.950	0.500
2.2	12-May	22.000	704.600	0.950	0.500
2.3	12-May	22.000	704.600	0.950	0.500
2.4	12-May	22.000	704.600	0.950	0.500
2.5	12-May	22.000	704.600	0.950	0.500
2.6	31-May	22.000	710.950	0.950	0.500
2.7	31-May	22.000	710.950	0.950	0.500
3.1	15-May	22.000	700.280	1.450	0.900
3.2	15-May	22.000	700.280	1.500	0.900
3.3	15-May	22.000	700.280	1.500	0.900
3.4	15-May	22.000	700.280	1.500	0.900
3.5	15-May	22.000	700.280	1.500	0.900
3.6	1-Jun	22.000	709.170	1.375	0.900
3.7	1-Jun	22.000	709.170	1.325	0.900
4.1	15-May	22.000	700.280	0.550	0.900
4.2	15-May	22.000	700.280	0.550	0.900
4.3	15-May	22.000	700.280	0.550	0.900
4.4	15-May	22.000	700.280	0.550	0.900
4.5	15-May	22.000	700.280	0.550	0.900
4.6	1-Jun	22.000	709.170	0.450	0.900
4.7	1-Jun	22.000	709.170	0.500	0.900
5.1	16-May	22.000	704.340	2.050	1.100
5.2	16-May	22.000	704.340	2.050	1.100
5.3	16-May	22.000	704.340	2.050	1.100
5.4	16-May	22.000	704.340	2.050	1.100
5.5	16-May	22.000	704.340	2.050	1.100
5.6	17-May	22.000	702.310	2.050	1.100
5.7	17-May	22.000	702.310	2.050	1.100
5.8	17-May	22.000	702.310	2.050	1.100
5.9	17-May	22.000	702.310	2.050	1.100
5.10	17-May	22.000	702.310	2.050	1.100
5.11	17-May	22.000	702.310	2.050	1.100
5.12	1-Jun	22.000	709.170	1.875	1.100
5.13	1-Jun	22.000	709.170	1.875	1.100

6.1	17-May	22.000	702.310	1.650	1.100
6.2	17-May	22.000	702.310	1.650	1.100
6.3	17-May	22.000	702.310	1.650	1.100
6.4	17-May	22.000	702.310	1.650	1.100
6.5	17-May	22.000	702.310	1.650	1.100
6.6	17-May	22.000	702.310	1.650	1.100
6.7	1-Jun	22.000	709.170	1.500	1.100
6.8	1-Jun	22.000	709.170	1.500	1.100
7.1	19-May	22.000	702.310	2.250	2.000
7.2	19-May	22.000	702.310	2.250	2.000
7.3	19-May	22.000	702.310	2.250	2.000
7.4	19-May	22.000	702.310	2.250	2.000
7.5	19-May	22.000	702.310	2.250	2.000
7.6	19-May	22.000	702.310	2.250	2.000
7.7	19-May	22.000	702.310	2.250	2.000
7.8	24-May	22.000	701.550	2.300	2.000
7.9	24-May	22.000	701.550	2.300	2.000
7.10	24-May	22.000	701.550	2.300	2.000
7.11	24-May	22.000	701.550	2.300	2.000
7.12	24-May	22.000	701.550	2.300	2.000
7.13	24-May	22.000	701.550	2.300	2.000
7.14	24-May	22.000	701.550	2.300	2.000
7.15	2-Jun	22.000	707.140	2.175	2.000
7.16	2-Jun	22.000	707.140	2.175	2.000
8.1	19-May	22.000	702.310	2.050	2.000
8.2	19-May	22.000	702.310	2.050	2.000
8.3	19-May	22.000	702.310	2.050	2.000
8.4	19-May	22.000	702.310	2.050	2.000
8.5	19-May	22.000	702.310	2.050	2.000
8.6	19-May	22.000	702.310	2.050	2.000
8.7	19-May	22.000	702.310	2.050	2.000
8.8	24-May	22.000	701.550	2.050	2.000
8.9	24-May	22.000	701.550	2.050	2.000
8.10	24-May	22.000	701.550	2.050	2.000
8.11	24-May	22.000	701.550	2.050	2.000
8.12	24-May	22.000	701.550	2.050	2.000
8.13	24-May	22.000	701.550	2.050	2.000
8.14	2-Jun	22.000	707.140	1.975	2.000
8.15	2-Jun	22.000	707.140	1.925	2.000
9.1	25-May	22.000	699.260	2.700	3.500
9.2	25-May	22.000	699.260	2.700	3.500
9.3	25-May	22.000	699.260	2.700	3.500
9.4	25-May	22.000	699.260	2.700	3.500
9.5	25-May	22.000	699.260	2.700	3.500
9.6	25-May	22.000	699.260	2.700	3.500
9.7	3-Jun	22.000	708.410	2.550	3.500
9.8	3-Jun	22.000	708.410	2.550	3.500

10.1	26-May	22.000	698.250	2.500	3.500
10.2	26-May	22.000	698.250	2.500	3.500
10.3	26-May	22.000	698.250	2.500	3.500
10.4	26-May	22.000	698.250	2.500	3.500
10.5	26-May	22.000	698.250	2.500	3.500
10.6	26-May	22.000	698.250	2.500	3.500
10.7	3-Jun	22.000	708.410	2.400	3.500
10.8	3-Jun	22.000	708.410	2.400	3.500
11.1	26-May	22.000	698.250	1.300	3.500
11.2	26-May	22.000	698.250	1.300	3.500
11.3	26-May	22.000	698.250	1.300	3.500
11.4	26-May	22.000	698.250	1.300	3.500
11.5	26-May	22.000	698.250	1.300	3.500
11.6	26-May	22.000	698.250	1.300	3.500
11.7	3-Jun	22.000	708.410		3.500
11.8	3-Jun	22.000	708.410	1.135	3.500
12.1	13-May	22.000	707.640	2.100	5.500
12.2	13-May	22.000	707.640	2.100	5.500
12.3	13-May	22.000	707.640	2.100	5.500
12.4	13-May	22.000	707.640	2.100	5.500
12.5	13-May	22.000	707.640	2.200	5.500
12.6	2-Jun	22.000	707.140	2.050	5.500
12.7	2-Jun	22.000	707.140	2.050	5.500
13.1	13-May	22.000	707.640	1.200	5.500
13.2	13-May	22.000	707.640	1.200	5.500
13.3	13-May	22.000	707.640	1.200	5.500
13.4	13-May	22.000	707.640	1.200	5.500
13.5	2-Jun	22.000	707.140	1.075	5.500
14.1	14-May	22.000	706.370	0.000	5.500
14.2	14-May				
14.3	14-May	22.000	706.370	0.000	5.500
14.4	14-May	22.000	706.370	0.000	5.500
14.5	14-May	22.000	706.370	0.000	5.500
14.6	14-May				
14.7	14-May				
14.8	14-May	22.000	706.370	0.000	5.500
14.9	2-Jun	22.000	707.140	0.000	5.500
14.10	2-Jun	22.000	707.140	0.000	5.500
15.1	14-May	22.000	706.370	2.550	6.500
15.2	14-May	22.000	706.370	2.550	6.500
15.3	14-May	22.000	706.370	2.550	6.500
15.4	14-May	22.000	706.370	2.550	6.500
15.5	14-May	22.000	706.370	2.550	6.500
15.6	3-Jun	22.000	708.410	2.400	6.500
15.7	3-Jun	22.000	708.410	2.400	6.500

16.1	14-May	22.000	706.370	1.700	6.500
16.2	14-May	22.000	706.370	1.700	6.500
16.3	14-May	22.000	706.370	1.700	6.500
16.4	14-May	22.000	706.370	1.700	6.500
16.5	14-May	22.000	706.370	1.700	6.500
16.6	14-May	22.000	706.370	1.700	6.500
16.7	3-Jun	22.000	708.410	1.550	6.500
16.8	3-Jun	22.000	708.410	1.550	6.500
17.1	14-May	22.000	706.370	0.700	6.500
17.2	14-May	22.000	706.370	0.700	6.500
17.3	14-May	22.000	706.370	0.700	6.500
17.4	14-May	22.000	706.370	0.700	6.500
17.5	14-May	22.000	706.370	0.700	6.500
17.6	14-May	22.000	706.370	0.700	6.500
17.7	3-Jun	22.000	708.410	0.350	6.500
17.8	3-Jun	22.000	708.410	0.350	6.500
18.1	13-May	22.000	707.640	0.000	0.500
18.2	13-May	22.000	707.640	0.000	0.500
18.3	13-May	22.000	707.640	0.000	0.500
18.4	13-May	22.000	707.640	0.000	0.500
18.5	31-May	22.000	710.950	0.000	0.500
18.6	31-May	22.000	710.950	0.000	0.500
19.1	13-May	22.000	707.640	-15.500	0.500
19.2	13-May	22.000	707.640	-15.500	0.500
19.3	13-May	22.000	707.640	-15.500	0.500
19.4	13-May	22.000	707.640	-15.000	0.500
19.5	13-May	22.000	707.640	-15.000	0.500
19.6	31-May	22.000	710.950	-20.750	0.500
19.7	31-May	22.000	710.950	-20.750	0.500
20.1	15-May	22.000	700.280	-8.500	0.900
20.2	15-May	22.000	700.280	-8.500	0.900
20.3	15-May	22.000	700.280	-8.500	0.900
20.4	15-May	22.000	700.280	-8.500	0.900
20.5	15-May	22.000	700.280	-8.500	0.900
20.6	1-Jun	22.000	709.170	-9.500	0.900
20.7	1-Jun	22.000	709.170	-9.500	0.900
21.1	15-May	22.000	700.280	-25.000	0.900
21.2	15-May	22.000	700.280	-25.000	0.900
21.3	15-May	22.000	700.280	-25.000	0.900
21.4	15-May	22.000	700.280	-25.000	0.900
21.5	15-May	22.000	700.280	-25.000	0.900
21.6	1-Jun	22.000	709.170	-30.000	0.900
21.7	1-Jun	22.000	709.170	-30.000	0.900

22.1	17-May	22.000	702.310	0.950	1.100
22.2	17-May				
22.3	17-May				
22.4	17-May	22.000	702.310	0.950	1.100
22.5	17-May				
22.6	17-May	22.000	702.310	0.950	1.100
22.7	17-May				
22.8	1-Jun	22.000	709.170	0.750	1.100
22.9	1-Jun	22.000	709.170	0.750	1.100
23.1	17-May	22.000	702.310	-21.000	1.100
23.2	17-May				
23.3	17-May	22.000	702.310	-21.000	1.100
23.4	17-May	22.000	702.310	-21.000	1.100
23.5	17-May	22.000	702.310	-21.000	1.100
23.6	17-May	22.000	702.310	-21.000	1.100
23.7	1-Jun	22.000	709.170	-24.250	1.100
23.8	1-Jun	22.000	709.170	-24.250	1.100
24.1	18-May	22.000	703.580	-39.000	1.100
24.2	18-May	22.000	703.580	-39.000	1.100
24.3	18-May	22.000	703.580	-39.000	1.100
24.4	18-May	22.000	703.580	-39.000	1.100
24.5	18-May	22.000	703.580	-39.000	1.100
24.6	18-May	22.000	703.580	-39.000	1.100
24.7	1-Jun	22.000	709.170	-44.500	1.100
24.8	1-Jun	22.000	709.170	-44.500	1.100
25.1	18-May	22.000	703.580	0.000	2.000
25.2	18-May	22.000	703.580	0.000	2.000
25.3	18-May	22.000	703.580	0.000	2.000
25.4	18-May	22.000	703.580	0.000	2.000
25.5	18-May	22.000	703.580	0.000	2.000
25.6	18-May	22.000	703.580	0.000	2.000
25.7	18-May	22.000	703.580	0.000	2.000
25.8	2-Jun	22.000	707.140	0.000	2.000
25.9	2-Jun	22.000	707.140	0.000	2.000
26.1	18-May	22.000	703.580	-12.750	2.000
26.2	18-May	22.000	703.580	-12.750	2.000
26.3	18-May	22.000	703.580	-12.750	2.000
26.4	18-May	22.000	703.580	-12.750	2.000
26.5	18-May	22.000	703.580	-12.750	2.000
26.6	18-May	22.000	703.580	-12.750	2.000
26.7	2-Jun	22.000	707.140	-14.150	2.000
26.8	2-Jun	22.000	707.140	-14.150	2.000

27.1	18-May	22.000	703.580	-27.750	2.000
27.2	18-May	22.000	703.580	-27.750	2.000
27.3	18-May	22.000	703.580	-27.750	2.000
27.4	18-May	22.000	703.580	-27.750	2.000
27.5	18-May	22.000	703.580	-27.750	2.000
27.6	18-May	22.000	703.580	-27.750	2.000
27.7	2-Jun	22.000	707.140	-30.000	2.000
27.8	2-Jun	22.000	707.140	-30.000	2.000
28.1	24-May	22.000	701.550	0.000	3.500
28.2	24-May	22.000	701.550	0.000	3.500
28.3	24-May	22.000	701.550	0.000	3.500
28.4	24-May	22.000	701.550	0.000	3.500
28.5	24-May	22.000	701.550	0.000	3.500
28.6	24-May	22.000	701.550	0.000	3.500
28.7	3-Jun	22.000	708.410	0.000	3.500
28.8	3-Jun	22.000	708.410	0.000	3.500
29.1	24-May	22.000	701.550	-13.500	3.500
29.2	24-May	22.000	701.550	-13.500	3.500
29.3	24-May	22.000	701.550	-13.500	3.500
29.4	24-May	22.000	701.550	-13.500	3.500
29.5	24-May	22.000	701.550	-13.500	3.500
29.6	24-May	22.000	701.550	-13.500	3.500
29.7	3-Jun	22.000	708.410	-14.500	3.500
29.8	3-Jun	22.000	708.410	-14.500	3.500

Run ID#	Corrected Q_G (L/min)	Q_L (gal/min)	Q_L (total) (L/min)	u_L (m/s)	$\ln u_L$ (m/s)	u_G (m/s)	$\ln u_G$ (m/s)
1.1	0.463	0.600	3.630	0.008	-4.866	0.001	-6.925
1.2	0.463	0.600	3.630	0.008	-4.866	0.001	-6.925
1.3	0.463	0.600	3.630	0.008	-4.866	0.001	-6.925
1.4	0.463	0.600	3.630	0.008	-4.866	0.001	-6.925
1.5	0.463	0.600	3.630	0.008	-4.866	0.001	-6.925
1.6	0.464	0.600	3.630	0.008	-4.866	0.001	-6.923
1.7	0.464	0.600	3.630	0.008	-4.866	0.001	-6.923
2.1	0.452	0.800	5.115	0.011	-4.523	0.001	-6.949
2.2	0.452	0.800	5.115	0.011	-4.523	0.001	-6.949
2.3	0.452	0.800	5.115	0.011	-4.523	0.001	-6.949
2.4	0.452	0.800	5.115	0.011	-4.523	0.001	-6.949
2.5	0.452	0.800	5.115	0.011	-4.523	0.001	-6.949
2.6	0.454	0.800	5.115	0.011	-4.523	0.001	-6.945
2.7	0.454	0.800	5.115	0.011	-4.523	0.001	-6.945
3.1	0.893	0.800	5.115	0.011	-4.523	0.002	-6.269
3.2	0.894	0.800	5.115	0.011	-4.523	0.002	-6.267
3.3	0.894	0.800	5.115	0.011	-4.523	0.002	-6.267
3.4	0.894	0.800	5.115	0.011	-4.523	0.002	-6.267
3.5	0.894	0.800	5.115	0.011	-4.523	0.002	-6.267
3.6	0.896	0.800	5.115	0.011	-4.523	0.002	-6.265
3.7	0.894	0.800	5.115	0.011	-4.523	0.002	-6.267
4.1	0.866	1.000	6.599	0.014	-4.268	0.002	-6.299
4.2	0.866	1.000	6.599	0.014	-4.268	0.002	-6.299
4.3	0.866	1.000	6.599	0.014	-4.268	0.002	-6.299
4.4	0.866	1.000	6.599	0.014	-4.268	0.002	-6.299
4.5	0.866	1.000	6.599	0.014	-4.268	0.002	-6.299
4.6	0.868	1.000	6.599	0.014	-4.268	0.002	-6.297
4.7	0.869	1.000	6.599	0.014	-4.268	0.002	-6.296
5.1	1.135	0.600	3.630	0.008	-4.866	0.002	-6.029
5.2	1.135	0.600	3.630	0.008	-4.866	0.002	-6.029
5.3	1.135	0.600	3.630	0.008	-4.866	0.002	-6.029
5.4	1.135	0.600	3.630	0.008	-4.866	0.002	-6.029
5.5	1.135	0.600	3.630	0.008	-4.866	0.002	-6.029
5.6	1.134	0.600	3.630	0.008	-4.866	0.002	-6.030
5.7	1.134	0.600	3.630	0.008	-4.866	0.002	-6.030
5.8	1.134	0.600	3.630	0.008	-4.866	0.002	-6.030
5.9	1.134	0.600	3.630	0.008	-4.866	0.002	-6.030
5.10	1.134	0.600	3.630	0.008	-4.866	0.002	-6.030
5.11	1.134	0.600	3.630	0.008	-4.866	0.002	-6.030
5.12	1.132	0.600	3.630	0.008	-4.866	0.002	-6.031
5.13	1.132	0.600	3.630	0.008	-4.866	0.002	-6.031

6.1	1.119	0.800	5.115	0.011	-4.523	0.002	-6.043
6.2	1.119	0.800	5.115	0.011	-4.523	0.002	-6.043
6.3	1.119	0.800	5.115	0.011	-4.523	0.002	-6.043
6.4	1.119	0.800	5.115	0.011	-4.523	0.002	-6.043
6.5	1.119	0.800	5.115	0.011	-4.523	0.002	-6.043
6.6	1.119	0.800	5.115	0.011	-4.523	0.002	-6.043
6.7	1.118	0.800	5.115	0.011	-4.523	0.002	-6.044
6.8	1.118	0.800	5.115	0.011	-4.523	0.002	-6.044
7.1	1.749	0.600	3.630	0.008	-4.866	0.004	-5.596
7.2	1.749	0.600	3.630	0.008	-4.866	0.004	-5.596
7.3	1.749	0.600	3.630	0.008	-4.866	0.004	-5.596
7.4	1.749	0.600	3.630	0.008	-4.866	0.004	-5.596
7.5	1.749	0.600	3.630	0.008	-4.866	0.004	-5.596
7.6	1.749	0.600	3.630	0.008	-4.866	0.004	-5.596
7.7	1.749	0.600	3.630	0.008	-4.866	0.004	-5.596
7.8	1.749	0.600	3.630	0.008	-4.866	0.004	-5.596
7.9	1.751	0.600	3.630	0.008	-4.866	0.004	-5.595
7.10	1.751	0.600	3.630	0.008	-4.866	0.004	-5.595
7.11	1.751	0.600	3.630	0.008	-4.866	0.004	-5.595
7.12	1.751	0.600	3.630	0.008	-4.866	0.004	-5.595
7.13	1.751	0.600	3.630	0.008	-4.866	0.004	-5.595
7.14	1.751	0.600	3.630	0.008	-4.866	0.004	-5.595
7.15	1.750	0.600	3.630	0.008	-4.866	0.004	-5.596
7.16	1.750	0.600	3.630	0.008	-4.866	0.004	-5.596
8.1	1.738	0.800	5.115	0.011	-4.523	0.004	-5.603
8.2	1.738	0.800	5.115	0.011	-4.523	0.004	-5.603
8.3	1.738	0.800	5.115	0.011	-4.523	0.004	-5.603
8.4	1.738	0.800	5.115	0.011	-4.523	0.004	-5.603
8.5	1.738	0.800	5.115	0.011	-4.523	0.004	-5.603
8.6	1.738	0.800	5.115	0.011	-4.523	0.004	-5.603
8.7	1.738	0.800	5.115	0.011	-4.523	0.004	-5.603
8.8	1.737	0.800	5.115	0.011	-4.523	0.004	-5.603
8.9	1.737	0.800	5.115	0.011	-4.523	0.004	-5.603
8.10	1.737	0.800	5.115	0.011	-4.523	0.004	-5.603
8.11	1.737	0.800	5.115	0.011	-4.523	0.004	-5.603
8.12	1.737	0.800	5.115	0.011	-4.523	0.004	-5.603
8.13	1.737	0.800	5.115	0.011	-4.523	0.004	-5.603
8.14	1.739	0.800	5.115	0.011	-4.523	0.004	-5.602
8.15	1.737	0.800	5.115	0.011	-4.523	0.004	-5.603
9.1	3.477	0.600	3.630	0.008	-4.866	0.007	-4.909
9.2	3.477	0.600	3.630	0.008	-4.866	0.007	-4.909
9.3	3.477	0.600	3.630	0.008	-4.866	0.007	-4.909
9.4	3.477	0.600	3.630	0.008	-4.866	0.007	-4.909
9.5	3.477	0.600	3.630	0.008	-4.866	0.007	-4.909
9.6	3.477	0.600	3.630	0.008	-4.866	0.007	-4.909
9.7	3.479	0.600	3.630	0.008	-4.866	0.007	-4.909
9.8	3.479	0.600	3.630	0.008	-4.866	0.007	-4.909

10.1	3.453	0.800	5.115	0.011	-4.523	0.007	-4.916
10.2	3.453	0.800	5.115	0.011	-4.523	0.007	-4.916
10.3	3.453	0.800	5.115	0.011	-4.523	0.007	-4.916
10.4	3.453	0.800	5.115	0.011	-4.523	0.007	-4.916
10.5	3.453	0.800	5.115	0.011	-4.523	0.007	-4.916
10.6	3.453	0.800	5.115	0.011	-4.523	0.007	-4.916
10.7	3.463	0.800	5.115	0.011	-4.523	0.007	-4.913
10.8	3.463	0.800	5.115	0.011	-4.523	0.007	-4.913
11.1	3.321	1.300	8.826	0.019	-3.978	0.007	-4.955
11.2	3.321	1.300	8.826	0.019	-3.978	0.007	-4.955
11.3	3.321	1.300	8.826	0.019	-3.978	0.007	-4.955
11.4	3.321	1.300	8.826	0.019	-3.978	0.007	-4.955
11.5	3.321	1.300	8.826	0.019	-3.978	0.007	-4.955
11.6	3.321	1.300	8.826	0.019	-3.978	0.007	-4.955
11.7		1.300	8.826	0.019	-3.978		#NUM!
11.8	3.325	1.300	8.826	0.019	-3.978	0.007	-4.954
12.1	5.673	1.300	8.826	0.019	-3.978	0.012	-4.420
12.2	5.673	1.300	8.826	0.019	-3.978	0.012	-4.420
12.3	5.673	1.300	8.826	0.019	-3.978	0.012	-4.420
12.4	5.673	1.300	8.826	0.019	-3.978	0.012	-4.420
12.5	5.691	1.300	8.826	0.019	-3.978	0.012	-4.416
12.6	5.662	1.300	8.826	0.019	-3.978	0.012	-4.422
12.7	5.662	1.300	8.826	0.019	-3.978	0.012	-4.422
13.1	5.509	1.600	11.053	0.023	-3.753	0.012	-4.449
13.2	5.509	1.600	11.053	0.023	-3.753	0.012	-4.449
13.3	5.509	1.600	11.053	0.023	-3.753	0.012	-4.449
13.4	5.509	1.600	11.053	0.023	-3.753	0.012	-4.449
13.5	5.485	1.600	11.053	0.023	-3.753	0.012	-4.453
14.1	5.278	1.900	13.280	0.028	-3.569	0.011	-4.492
14.2				0.028	-3.569		
14.3	5.278	1.900	13.280	0.028	-3.569	0.011	-4.492
14.4	5.278	1.900	13.280	0.028	-3.569	0.011	-4.492
14.5	5.278	1.900	13.280	0.028	-3.569	0.011	-4.492
14.6				0.028	-3.569		
14.7				0.028	-3.569		
14.8	5.278	1.900	13.280	0.028	-3.569	0.011	-4.492
14.9	5.280	1.900	13.280	0.028	-3.569	0.011	-4.491
14.10	5.280	1.900	13.280	0.028	-3.569	0.011	-4.491
15.1	6.886	1.300	8.826	0.019	-3.978	0.015	-4.226
15.2	6.886	1.300	8.826	0.019	-3.978	0.015	-4.226
15.3	6.886	1.300	8.826	0.019	-3.978	0.015	-4.226
15.4	6.886	1.300	8.826	0.019	-3.978	0.015	-4.226
15.5	6.886	1.300	8.826	0.019	-3.978	0.015	-4.226
15.6	6.862	1.300	8.826	0.019	-3.978	0.015	-4.229
15.7	6.862	1.300	8.826	0.019	-3.978	0.015	-4.229

16.1	6.703	1.600	11.053	0.023	-3.753	0.014	-4.253
16.2	6.703	1.600	11.053	0.023	-3.753	0.014	-4.253
16.3	6.703	1.600	11.053	0.023	-3.753	0.014	-4.253
16.4	6.703	1.600	11.053	0.023	-3.753	0.014	-4.253
16.5	6.703	1.600	11.053	0.023	-3.753	0.014	-4.253
16.6	6.703	1.600	11.053	0.023	-3.753	0.014	-4.253
16.7	6.679	1.600	11.053	0.023	-3.753	0.014	-4.256
16.8	6.679	1.600	11.053	0.023	-3.753	0.014	-4.256
17.1	6.487	1.900	13.280	0.028	-3.569	0.014	-4.286
17.2	6.487	1.900	13.280	0.028	-3.569	0.014	-4.286
17.3	6.487	1.900	13.280	0.028	-3.569	0.014	-4.286
17.4	6.487	1.900	13.280	0.028	-3.569	0.014	-4.286
17.5	6.487	1.900	13.280	0.028	-3.569	0.014	-4.286
17.6	6.487	1.900	13.280	0.028	-3.569	0.014	-4.286
17.7	6.411	1.900	13.280	0.028	-3.569	0.014	-4.297
17.8	6.411	1.900	13.280	0.028	-3.569	0.014	-4.297
18.1	0.438	1.000	6.599	0.014	-4.268	0.001	-6.981
18.2	0.438	1.000	6.599	0.014	-4.268	0.001	-6.981
18.3	0.438	1.000	6.599	0.014	-4.268	0.001	-6.981
18.4	0.438	1.000	6.599	0.014	-4.268	0.001	-6.981
18.5	0.439	1.000	6.599	0.014	-4.268	0.001	-6.979
18.6	0.439	1.000	6.599	0.014	-4.268	0.001	-6.979
19.1	0.400	1.300	8.826	0.019	-3.978	0.001	-7.072
19.2	0.400	1.300	8.826	0.019	-3.978	0.001	-7.072
19.3	0.400	1.300	8.826	0.019	-3.978	0.001	-7.072
19.4	0.400	1.300	8.826	0.019	-3.978	0.001	-7.072
19.5	0.400	1.300	8.826	0.019	-3.978	0.001	-7.072
19.6	0.388	1.300	8.826	0.019	-3.978	0.001	-7.102
19.7	0.388	1.300	8.826	0.019	-3.978	0.001	-7.102
20.1	0.809	1.300	8.826	0.019	-3.978	0.002	-6.367
20.2	0.809	1.300	8.826	0.019	-3.978	0.002	-6.367
20.3	0.809	1.300	8.826	0.019	-3.978	0.002	-6.367
20.4	0.809	1.300	8.826	0.019	-3.978	0.002	-6.367
20.5	0.809	1.300	8.826	0.019	-3.978	0.002	-6.367
20.6	0.810	1.300	8.826	0.019	-3.978	0.002	-6.366
20.7	0.810	1.300	8.826	0.019	-3.978	0.002	-6.366
21.1	0.726	1.600	11.053	0.023	-3.753	0.002	-6.476
21.2	0.726	1.600	11.053	0.023	-3.753	0.002	-6.476
21.3	0.726	1.600	11.053	0.023	-3.753	0.002	-6.476
21.4	0.726	1.600	11.053	0.023	-3.753	0.002	-6.476
21.5	0.726	1.600	11.053	0.023	-3.753	0.002	-6.476
21.6	0.706	1.600	11.053	0.023	-3.753	0.001	-6.504
21.7	0.706	1.600	11.053	0.023	-3.753	0.001	-6.504

22.1	1.093	1.000	6.599	0.014	-4.268	0.002	-6.066
22.2				0.014	-4.268		
22.3				0.014	-4.268		
22.4	1.093	1.000	6.599	0.014	-4.268	0.002	-6.066
22.5				0.014	-4.268		
22.6	1.093	1.000	6.599	0.014	-4.268	0.002	-6.066
22.7				0.014	-4.268		
22.8	1.091	1.000	6.599	0.014	-4.268	0.002	-6.068
22.9	1.091	1.000	6.599	0.014	-4.268	0.002	-6.068
23.1	0.931	1.600	11.053	0.023	-3.753	0.002	-6.227
23.2				0.023	-3.753		
23.3	0.931	1.600	11.053	0.023	-3.753	0.002	-6.227
23.4	0.931	1.600	11.053	0.023	-3.753	0.002	-6.227
23.5	0.931	1.600	11.053	0.023	-3.753	0.002	-6.227
23.6	0.931	1.600	11.053	0.023	-3.753	0.002	-6.227
23.7	0.916	1.600	11.053	0.023	-3.753	0.002	-6.243
23.8	0.916	1.600	11.053	0.023	-3.753	0.002	-6.243
24.1	0.809	1.900	13.280	0.028	-3.569	0.002	-6.367
24.2	0.809	1.900	13.280	0.028	-3.569	0.002	-6.367
24.3	0.809	1.900	13.280	0.028	-3.569	0.002	-6.367
24.4	0.809	1.900	13.280	0.028	-3.569	0.002	-6.367
24.5	0.809	1.900	13.280	0.028	-3.569	0.002	-6.367
24.6	0.809	1.900	13.280	0.028	-3.569	0.002	-6.367
24.7	0.773	1.900	13.280	0.028	-3.569	0.002	-6.413
24.8	0.773	1.900	13.280	0.028	-3.569	0.002	-6.413
25.1	1.622	1.300	8.826	0.019	-3.978	0.003	-5.672
25.2	1.622	1.300	8.826	0.019	-3.978	0.003	-5.672
25.3	1.622	1.300	8.826	0.019	-3.978	0.003	-5.672
25.4	1.622	1.300	8.826	0.019	-3.978	0.003	-5.672
25.5	1.622	1.300	8.826	0.019	-3.978	0.003	-5.672
25.6	1.622	1.300	8.826	0.019	-3.978	0.003	-5.672
25.7	1.622	1.300	8.826	0.019	-3.978	0.003	-5.672
25.8	1.626	1.300	8.826	0.019	-3.978	0.003	-5.669
25.9	1.626	1.300	8.826	0.019	-3.978	0.003	-5.669
26.1	1.507	1.600	11.053	0.023	-3.753	0.003	-5.745
26.2	1.507	1.600	11.053	0.023	-3.753	0.003	-5.745
26.3	1.507	1.600	11.053	0.023	-3.753	0.003	-5.745
26.4	1.507	1.600	11.053	0.023	-3.753	0.003	-5.745
26.5	1.507	1.600	11.053	0.023	-3.753	0.003	-5.745
26.6	1.507	1.600	11.053	0.023	-3.753	0.003	-5.745
26.7	1.499	1.600	11.053	0.023	-3.753	0.003	-5.751
26.8	1.499	1.600	11.053	0.023	-3.753	0.003	-5.751

27.1	1.361	1.900	13.280	0.028	-3.569	0.003	-5.847
27.2	1.361	1.900	13.280	0.028	-3.569	0.003	-5.847
27.3	1.361	1.900	13.280	0.028	-3.569	0.003	-5.847
27.4	1.361	1.900	13.280	0.028	-3.569	0.003	-5.847
27.5	1.361	1.900	13.280	0.028	-3.569	0.003	-5.847
27.6	1.361	1.900	13.280	0.028	-3.569	0.003	-5.847
27.7	1.342	1.900	13.280	0.028	-3.569	0.003	-5.861
27.8	1.342	1.900	13.280	0.028	-3.569	0.003	-5.861
28.1	3.179	1.600	11.053	0.023	-3.753	0.007	-4.999
28.2	3.179	1.600	11.053	0.023	-3.753	0.007	-4.999
28.3	3.179	1.600	11.053	0.023	-3.753	0.007	-4.999
28.4	3.179	1.600	11.053	0.023	-3.753	0.007	-4.999
28.5	3.179	1.600	11.053	0.023	-3.753	0.007	-4.999
28.6	3.179	1.600	11.053	0.023	-3.753	0.007	-4.999
28.7	3.195	1.600	11.053	0.023	-3.753	0.007	-4.994
28.8	3.195	1.600	11.053	0.023	-3.753	0.007	-4.994
29.1	2.941	1.900	13.280	0.028	-3.569	0.006	-5.077
29.2	2.941	1.900	13.280	0.028	-3.569	0.006	-5.077
29.3	2.941	1.900	13.280	0.028	-3.569	0.006	-5.077
29.4	2.941	1.900	13.280	0.028	-3.569	0.006	-5.077
29.5	2.941	1.900	13.280	0.028	-3.569	0.006	-5.077
29.6	2.941	1.900	13.280	0.028	-3.569	0.006	-5.077
29.7	2.939	1.900	13.280	0.028	-3.569	0.006	-5.077
29.8	2.939	1.900	13.280	0.028	-3.569	0.006	-5.077

Run ID#	$e_G(\text{Bot } 1/2)$	$\ln e_G(\text{Bot } 1/2)$	$e_G(\text{Top } 1/2)$	$\ln e_G(\text{Top } 1/2)$
1.1	0.001	-7.076	-0.004	
1.2	0.002	-6.492	-0.005	
1.3	0.002	-6.327	-0.006	
1.4	0.000	-7.626	-0.002	
1.5	0.002	-6.133	-0.005	
1.6	-0.002		0.008	-4.819
1.7	-0.002		0.008	-4.802
2.1	0.003	-5.871	-0.005	
2.2	0.003	-5.851	-0.005	
2.3	0.004	-5.632	-0.006	
2.4	0.003	-5.732	-0.005	
2.5	0.004	-5.540	-0.005	
2.6	-0.002		0.007	-4.908
2.7	-0.003		0.009	-4.750
3.1	0.005	-5.233	0.008	-4.850
3.2	0.005	-5.315	0.008	-4.775
3.3	0.005	-5.352	0.009	-4.741
3.4	0.004	-5.407	0.009	-4.724
3.5	0.005	-5.345	0.009	-4.728
3.6	-0.001		0.005	-5.269
3.7	-0.001		0.006	-5.157
4.1	0.005	-5.391	0.009	-4.674
4.2	0.005	-5.276	0.009	-4.746
4.3	0.005	-5.316	0.009	-4.698
4.4	0.006	-5.181	0.008	-4.773
4.5	0.006	-5.115	0.008	-4.793
4.6	0.001	-7.571	0.003	-5.888
4.7	0.000	-7.690	0.003	-5.855
5.1	0.008	-4.832	0.009	-4.721
5.2	0.008	-4.827	0.009	-4.692
5.3	0.008	-4.889	0.009	-4.691
5.4	0.007	-4.969	0.010	-4.651
5.5	0.007	-4.951	0.010	-4.652
5.6	0.006	-5.190	0.014	-4.262
5.7	0.005	-5.253	0.015	-4.208
5.8	0.004	-5.500	0.016	-4.140
5.9	0.003	-5.742	0.016	-4.131
5.10	0.004	-5.497	0.016	-4.160
5.11	0.004	-5.587	0.016	-4.132
5.12	0.005	-5.270	0.005	-5.367
5.13	0.006	-5.081	0.003	-5.739

6.1	0.003	-5.811	0.016	-4.121
6.2	0.004	-5.566	0.016	-4.166
6.3	0.005	-5.363	0.015	-4.214
6.4	0.004	-5.472	0.016	-4.146
6.5	0.005	-5.368	0.015	-4.201
6.6	0.002	-6.042	0.016	-4.138
6.7	0.004	-5.423	0.003	-5.742
6.8	0.004	-5.457	0.003	-5.685
7.1	0.007	-4.958	0.019	-3.987
7.2	0.007	-4.985	0.018	-3.991
7.3	0.002	-6.006	0.023	-3.787
7.4	0.002	-6.126	0.023	-3.785
7.5	0.006	-5.112	0.017	-4.053
7.6	0.006	-5.191	0.018	-4.044
7.7	0.006	-5.178	0.019	-3.950
7.8	0.007	-5.024	0.016	-4.147
7.9	0.008	-4.843	0.017	-4.049
7.10	0.007	-5.026	0.017	-4.059
7.11	0.007	-4.928	0.019	-3.990
7.12	0.007	-4.930	0.019	-3.976
7.13	0.008	-4.874	0.018	-4.022
7.14	0.007	-5.015	0.019	-3.956
7.15	0.013	-4.363	0.014	-4.239
7.16	0.014	-4.293	0.017	-4.080
8.1	0.007	-5.007	0.019	-3.963
8.2	0.007	-4.914	0.018	-3.998
8.3	0.007	-5.000	0.019	-3.943
8.4	0.007	-5.028	0.019	-3.938
8.5	0.007	-4.920	0.019	-3.960
8.6	0.008	-4.892	0.019	-3.981
8.7	0.007	-4.950	0.019	-3.982
8.8	0.009	-4.734	0.018	-4.028
8.9	0.009	-4.721	0.018	-4.044
8.10	0.009	-4.713	0.018	-4.033
8.11	0.009	-4.724	0.018	-4.035
8.12	0.010	-4.645	0.017	-4.079
8.13	0.009	-4.740	0.018	-4.013
8.14	0.013	-4.316	0.016	-4.124
8.15	0.013	-4.315	0.016	-4.127
9.1	0.028	-3.577	0.025	-3.686
9.2	0.027	-3.594	0.025	-3.678
9.3	0.028	-3.589	0.025	-3.694
9.4	0.028	-3.584	0.025	-3.708
9.5	0.028	-3.562	0.024	-3.711
9.6	0.028	-3.570	0.025	-3.706
9.7	0.037	-3.298	0.026	-3.646
9.8	0.044	-3.117	0.015	-4.169

10.1	0.031	-3.489	0.023	-3.752
10.2	0.030	-3.522	0.024	-3.719
10.3	0.030	-3.506	0.023	-3.770
10.4	0.030	-3.521	0.023	-3.773
10.5	0.029	-3.546	0.024	-3.714
10.6	0.028	-3.581	0.025	-3.682
10.7	0.054	-2.919	0.003	-5.949
10.8	0.053	-2.935	0.003	-5.719
11.1	0.024	-3.723	0.023	-3.756
11.2	0.024	-3.721	0.023	-3.765
11.3	0.024	-3.717	0.023	-3.758
11.4	0.024	-3.730	0.024	-3.748
11.5	0.024	-3.723	0.024	-3.750
11.6	0.024	-3.728	0.024	-3.746
11.7	0.046	-3.081	0.004	-5.477
11.8	0.046	-3.083	0.004	-5.449
12.1	0.036	-3.336	0.049	-3.025
12.2	0.036	-3.322	0.048	-3.030
12.3	0.036	-3.334	0.049	-3.026
12.4	0.036	-3.314	0.048	-3.045
12.5	0.038	-3.258	0.046	-3.080
12.6	0.044	-3.116	0.055	-2.902
12.7	0.046	-3.082	0.055	-2.901
13.1	0.034	-3.369	0.045	-3.101
13.2	0.035	-3.351	0.044	-3.121
13.3	0.036	-3.337	0.044	-3.126
13.4	0.035	-3.341	0.044	-3.133
13.5	0.041	-3.196	0.053	-2.944
14.1	0.037	-3.294	0.046	-3.071
14.2				
14.3	0.036	-3.319	0.046	-3.081
14.4	0.036	-3.336	0.046	-3.084
14.5	0.036	-3.338	0.047	-3.059
14.6				
14.7				
14.8	0.035	-3.360	0.048	-3.028
14.9	0.037	-3.303	0.049	-3.007
14.10	0.037	-3.304	0.049	-3.007
15.1	0.052	-2.956	0.062	-2.777
15.2	0.052	-2.954	0.060	-2.811
15.3	0.052	-2.955	0.061	-2.796
15.4	0.051	-2.966	0.061	-2.796
15.5	0.053	-2.942	0.061	-2.789
15.6	0.074	-2.605	0.048	-3.027
15.7	0.070	-2.657	0.049	-3.024

16.1	0.048	-3.045	0.056	-2.887
16.2	0.047	-3.048	0.055	-2.893
16.3	0.048	-3.039	0.055	-2.906
16.4	0.048	-3.034	0.054	-2.917
16.5	0.049	-3.014	0.055	-2.909
16.6	0.048	-3.038	0.054	-2.911
16.7	0.062	-2.781	0.046	-3.072
16.8	0.066	-2.718	0.045	-3.101
17.1	0.045	-3.098	0.050	-2.997
17.2	0.045	-3.095	0.050	-2.991
17.3	0.045	-3.100	0.050	-2.991
17.4	0.045	-3.092	0.050	-2.992
17.5	0.046	-3.080	0.050	-2.999
17.6	0.046	-3.077	0.049	-3.011
17.7	0.060	-2.820	0.047	-3.068
17.8	0.060	-2.811	0.047	-3.066
18.1	-0.006		0.006	-5.170
18.2	-0.006		0.006	-5.084
18.3	-0.007		0.007	-5.002
18.4	-0.007		0.006	-5.202
18.5	-0.003		0.008	-4.855
18.6	-0.003		0.008	-4.781
19.1	-0.005		0.006	-5.114
19.2	-0.006		0.006	-5.161
19.3	-0.005		0.005	-5.312
19.4	-0.006		0.005	-5.299
19.5	-0.006		0.005	-5.303
19.6	-0.003		0.006	-5.154
19.7	-0.003		0.006	-5.130
20.1	0.007	-5.017	0.008	-4.785
20.2	0.007	-5.007	0.008	-4.814
20.3	0.007	-5.021	0.008	-4.815
20.4	0.005	-5.272	0.009	-4.758
20.5	0.006	-5.192	0.008	-4.848
20.6	0.000	-8.372	0.001	-6.646
20.7	0.000	-8.392	0.001	-6.692
21.1	0.006	-5.191	0.007	-4.927
21.2	0.005	-5.318	0.007	-4.903
21.3	0.004	-5.448	0.007	-4.959
21.4	0.004	-5.648	0.008	-4.859
21.5	0.003	-5.676	0.008	-4.848
21.6	-0.001		-0.001	
21.7	0.000		0.000	

22.1	0.002	-6.338	0.016	-4.118
22.2				
22.3				
22.4	0.003	-5.914	0.015	-4.215
22.5				
22.6	0.002	-6.221	0.015	-4.221
22.7				
22.8	0.004	-5.516	0.003	-5.885
22.9	0.004	-5.584	0.003	-5.733
23.1	0.001	-7.387	0.016	-4.151
23.2				
23.3	-0.001		0.016	-4.151
23.4	-0.001		0.015	-4.169
23.5	-0.001		0.015	-4.186
23.6	0.000		0.015	-4.197
23.7	0.000	-8.323	0.001	-6.715
23.8	0.000		0.001	-6.507
24.1	0.002	-6.090	0.006	-5.055
24.2	0.001	-6.886	0.006	-5.161
24.3	0.000		0.007	-4.919
24.4	0.001	-7.459	0.006	-5.050
24.5	-0.001		0.007	-5.011
24.6	-0.001		0.007	-5.014
24.7	-0.001		0.000	
24.8	-0.002		0.000	-8.662
25.1	0.008	-4.777	0.013	-4.327
25.2	0.009	-4.705	0.013	-4.372
25.3	0.009	-4.723	0.013	-4.356
25.4	0.009	-4.750	0.013	-4.349
25.5	0.009	-4.715	0.013	-4.379
25.6	0.009	-4.704	0.012	-4.388
25.7	0.009	-4.715	0.013	-4.362
25.8	0.009	-4.725	0.021	-3.865
25.9	0.009	-4.673	0.020	-3.901
26.1	0.006	-5.106	0.013	-4.360
26.2	0.006	-5.150	0.012	-4.398
26.3	0.005	-5.226	0.013	-4.324
26.4	0.005	-5.232	-0.451	
26.5	0.006	-5.098	0.012	-4.387
26.6	0.006	-5.056	0.013	-4.375
26.7	0.007	-4.979	0.018	-4.039
26.8	0.006	-5.070	0.018	-4.028

27.1	0.002	-6.312	0.009	-4.674
27.2	0.003	-5.796	0.011	-4.514
27.3	0.003	-5.875	0.011	-4.495
27.4	0.002	-6.055	0.011	-4.480
27.5	0.002	-6.112	0.012	-4.450
27.6	0.003	-5.873	0.012	-4.430
27.7	0.004	-5.542	0.017	-4.076
27.8	0.004	-5.452	0.017	-4.095
28.1	0.015	-4.168	0.028	-3.580
28.2	0.015	-4.187	0.093	-2.378
28.3	0.015	-4.197	0.028	-3.566
28.4	0.015	-4.185	0.028	-3.567
28.5	0.015	-4.167	0.028	-3.573
28.6	0.016	-4.131	0.027	-3.599
28.7	0.040	-3.214	0.004	-5.620
28.8	0.040	-3.215	0.004	-5.406
29.1	0.012	-4.401	0.026	-3.653
29.2	0.012	-4.395	0.026	-3.653
29.3	0.012	-4.426	0.026	-3.648
29.4	0.012	-4.391	0.026	-3.664
29.5	0.012	-4.399	0.026	-3.668
29.6	0.012	-4.388	0.026	-3.658
29.7	0.034	-3.386	0.006	-5.063
29.8	0.031	-3.478	0.007	-4.965

Regression Analysis: Gas Holdup

SUMMARY OUTPUT

<i>Regression Statistics</i>	
Multiple R	0.958
R Square	0.918
Adjusted R Square	0.917
Standard Error	0.234
Observations	178

ANOVA

	<i>df</i>	<i>SS</i>	<i>MS</i>	<i>F</i>	<i>Significance F</i>
Regression	2	106.984	53.492	980.531	0.000
Residual	175	9.547	0.055		
Total	177	116.531			

	<i>Standard</i>					
	<i>Coefficients</i>	<i>Error</i>	<i>t Stat</i>	<i>P-value</i>	<i>Lower 95%</i>	<i>Upper 95%</i>
Intercept	1.542	0.175	8.830	0.000	1.197	1.887
ln u_L	-0.046	0.041	-1.133	0.259	-0.127	0.034
ln u_G	1.109	0.027	40.969	0.000	1.055	1.162

Bubble Properties: Raw Data

Trial	Mode of Operation	Flowmeters' Readings			
		Q _G (L/min)	Q _L (gal/min)	Q _G (m ³ /s)	Q _L (m ³ /s)
1	injection	0.500	0.800	0.000	0.000
2	ejection	0.500	1.000	0.000	0.000
3	ejection	0.500	1.000	0.000	0.000
4	ejection	0.500	1.320	0.000	0.000
5	ejection	0.500	1.320	0.000	0.000
6	injection	1.100	0.600	0.000	0.000
7	injection	1.100	0.600	0.000	0.000
8	injection	1.100	0.800	0.000	0.000
9	injection	1.100	0.800	0.000	0.000
10	injection	1.100	1.010	0.000	0.000
11	injection	1.100	1.010	0.000	0.000
12	ejection	1.100	1.610	0.000	0.000
13	ejection	1.100	1.610	0.000	0.000
14	ejection	1.100	1.900	0.000	0.000
15	ejection	1.100	1.900	0.000	0.000
16	injection	2.000	0.590	0.000	0.000
17	injection	2.000	0.590	0.000	0.000
18	injection	2.000	0.810	0.000	0.000
19	injection	2.000	0.810	0.000	0.000
20	ejection	2.000	1.310	0.000	0.000
21	ejection	2.000	1.310	0.000	0.000
22	ejection	2.000	1.600	0.000	0.000
23	ejection	2.000	1.890	0.000	0.000
24	injection	3.500	0.600	0.000	0.000
25	injection	3.500	0.810	0.000	0.000
26	injection	3.500	1.313	0.000	0.000
27	injection	3.500	1.610	0.000	0.000
28	ejection	3.500	1.890	0.000	0.000
29	injection	4.500	1.300	0.000	0.000
30	ejection	4.500	1.900	0.000	0.000
31	injection	5.500	1.290	0.000	0.000
32	injection	5.500	1.620	0.000	0.000
33	ejection	5.500	1.900	0.000	0.000

Trial	u_G (m/s)	u_L (m/s)	Approach 1		Approach 2	
			d_B (mm)	d_S (mm)	d_B (mm)	d_S (mm)
1	0.001	0.011	1.797	1.999	1.847	2.085
2	0.001	0.014	1.930	2.147	2.022	2.255
3	0.001	0.014	1.959	2.166	2.061	2.279
4	0.001	0.019	1.601	1.886	1.682	1.983
5	0.001	0.019	1.532	1.769	1.607	1.857
6	0.002	0.008	2.159	2.072	2.002	2.174
7	0.002	0.008	2.072	2.297	2.178	2.418
8	0.002	0.011	1.978	2.235	2.036	2.354
9	0.002	0.011	2.133	2.352	2.236	2.463
10	0.002	0.014	2.305	2.497	2.419	2.627
11	0.002	0.014	2.222	2.385	2.338	2.515
12	0.002	0.024	1.875	2.154	1.967	2.266
13	0.002	0.024	1.993	2.102	2.093	2.205
14	0.002	0.028	1.822	2.046	1.879	2.144
15	0.002	0.028	1.885	2.110	1.973	2.216
16	0.004	0.008	2.338	2.597	2.413	2.720
17	0.004	0.008	2.216	2.423	2.317	2.538
18	0.004	0.011	2.301	2.468	2.416	2.595
19	0.004	0.011	2.226	2.443	2.337	2.560
20	0.003	0.019	2.092	2.348	2.191	2.462
21	0.003	0.019	2.167	2.646	2.261	2.743
22	0.003	0.023	2.176	2.458	2.292	2.596
23	0.003	0.028	1.956	2.232	2.050	2.345
24	0.007	0.008	2.777	2.993	2.918	3.148
25	0.007	0.011	2.744	3.021	2.881	3.171
26	0.007	0.019	2.575	2.832	2.698	2.976
27	0.007	0.024	2.582	2.784	2.708	2.914
28	0.006	0.028	2.593	2.812	2.725	2.958
29	0.010	0.019	2.951	3.221	3.103	3.383
30	0.009	0.028	2.388	2.602	2.508	2.737
31	0.012	0.019	2.953	3.282	3.094	3.448
32	0.012	0.024	3.095	3.405	3.244	3.585
33	0.011	0.028	3.072	3.351	3.232	3.529
		MAX	3.095	3.405	3.244	3.585
		MIN	1.532	1.769	1.607	1.857

Regression Analysis: Arithmetic Mean Bubble Diameter - Approach 1

SUMMARY OUTPUT

<i>Regression Statistics</i>	
Multiple R	0.947
R Square	0.897
Adjusted R Square	0.890
Standard Error	0.064
Observations	35

ANOVA					
	<i>df</i>	<i>SS</i>	<i>MS</i>	<i>F</i>	<i>Significance F</i>
Regression	2	1.140	0.570	138.626	0.000
Residual	32	0.132	0.004		
Total	34	1.272			

	<i>Standard</i>					
	<i>Coefficients</i>	<i>Error</i>	<i>t Stat</i>	<i>P-value</i>	<i>Lower 95%</i>	<i>Upper 95%</i>
Intercept	1.936	0.111	17.412	0.000	1.710	2.162
ln u_G	0.223	0.014	16.399	0.000	0.195	0.251
ln u_L	-0.034	0.024	-1.400	0.171	-0.084	0.016

Regression Analysis: Arithmetic Mean Bubble Diameter - Approach 2

SUMMARY OUTPUT

<i>Regression Statistics</i>	
Multiple R	0.942
R Square	0.888
Adjusted R Square	0.881
Standard Error	0.068
Observations	35

ANOVA

	<i>df</i>	<i>SS</i>	<i>MS</i>	<i>F</i>	<i>Significance F</i>
Regression	2	1.168	0.584	127.138	0.000
Residual	32	0.147	0.005		
Total	34	1.315			

	<i>Coefficients</i>	<i>Standard Error</i>	<i>t Stat</i>	<i>P-value</i>	<i>Lower 95%</i>	<i>Upper 95%</i>
Intercept	2.044	0.118	17.390	0.000	1.804	2.283
ln u_G	0.224	0.014	15.597	0.000	0.195	0.253
ln u_L	-0.020	0.026	-0.777	0.443	-0.072	0.032

Regression Analysis: Sauter Mean Bubble Diameter - Approach 1

SUMMARY OUTPUT

<i>Regression Statistics</i>	
Multiple R	0.944
R Square	0.890
Adjusted R Square	0.884
Standard Error	0.062
Observations	35

ANOVA

	<i>df</i>	<i>SS</i>	<i>MS</i>	<i>F</i>	<i>Significance F</i>
Regression	2	1.008	0.504	130.099	0.000
Residual	32	0.124	0.004		
Total	34	1.132			

	<i>Coefficients</i>	<i>Standard Error</i>	<i>t Stat</i>	<i>P-value</i>	<i>Lower 95%</i>	<i>Upper 95%</i>
Intercept	2.051	0.108	19.010	0.000	1.832	2.271
ln u_G	0.207	0.013	15.681	0.000	0.180	0.234
ln u_L	-0.008	0.024	-0.352	0.727	-0.056	0.040

Regression Analysis: Sauter Mean Bubble Diameter - Approach 2

SUMMARY OUTPUT

<i>Regression Statistics</i>	
Multiple R	0.944
R Square	0.891
Adjusted R Square	0.884
Standard Error	0.062
Observations	35

ANOVA

	<i>df</i>	<i>SS</i>	<i>MS</i>	<i>F</i>	<i>Significance F</i>
Regression	2	1.014	0.507	130.500	0.000
Residual	32	0.124	0.004		
Total	34	1.139			

	<i>Coefficients</i>	<i>Standard Error</i>	<i>t Stat</i>	<i>P-value</i>	<i>Lower 95%</i>	<i>Upper 95%</i>
Intercept	2.107	0.108	19.495	0.000	1.887	2.327
ln u_G	0.207	0.013	15.696	0.000	0.181	0.234
ln u_L	-0.007	0.024	-0.313	0.756	-0.056	0.041

Regression Analysis: Interfacial Area - Approach 1

SUMMARY OUTPUT

<i>Regression Statistics</i>	
Multiple R	1.000
R Square	1.000
Adjusted R Square	1.000
Standard Error	0.000
Observations	34

ANOVA					
	<i>df</i>	<i>SS</i>	<i>MS</i>	<i>F</i>	<i>Significance F</i>
Regression	2	17.242	8.621	3.784E+28	0.000
Residual	31	0.000	0.000		
Total	33	17.242			

	<i>Coefficients</i>	<i>Standard Error</i>	<i>t Stat</i>	<i>P-value</i>	<i>Lower 95%</i>	<i>Upper 95%</i>
Intercept	1.282	0.000	4.517E+13	0.000	1.282	1.282
X Variable 1	0.902	0.000	2.721E+14	0.000	0.902	0.902
X Variable 2	-0.038	0.000	-6.395E+12	0.000	-0.038	-0.038

Regression Analysis: Interfacial Area - Approach 2

SUMMARY OUTPUT

<i>Regression Statistics</i>	
Multiple R	1.000
R Square	1.000
Adjusted R Square	1.000
Standard Error	0.000
Observations	34

ANOVA

	<i>df</i>	<i>SS</i>	<i>MS</i>	<i>F</i>	<i>Significance F</i>
Regression	2	17.220	8.610	1.445E+28	0.000
Residual	31	0.000	0.000		
Total	33	17.220			

	<i>Coefficients</i>	<i>Standard Error</i>	<i>t Stat</i>	<i>P-value</i>	<i>Lower 95%</i>	<i>Upper 95%</i>
Intercept	1.227	0.000	2.672E+13	0.000	1.227	1.227
X Variable 1	0.901	0.000	1.682E+14	0.000	0.901	0.901
X Variable 2	-0.039	0.000	-4.049E+12	0.000	-0.039	-0.039

Mass Transfer Study: Raw Data

Trial #	N	k_w (min ⁻¹)	Pe_L	u_L (m/s)	u_G (m/s)	r	ϵ_G	ϵ_L	ρ_w (kg/m ³)	g (m/s ²)
1	8	0.022	0.910	0.008	0.003	9.114	0.008	0.992	997.440	9.810
2	8	0.019	1.567	0.014	0.003	5.090	0.008	0.992	997.765	9.810
3	8	0.021	0.885	0.008	0.004	9.418	0.012	0.988	997.533	9.810
4	8	0.018	1.573	0.014	0.002	5.070	0.007	0.993	997.974	9.810
5	8	0.025	0.868	0.008	0.004	9.613	0.012	0.988	997.184	9.810
6	8	0.021	1.528	0.014	0.004	5.240	0.011	0.989	997.533	9.810
7	8	0.024	0.842	0.008	0.007	9.971	0.026	0.974	997.254	9.810
8	8	0.022	1.467	0.014	0.007	5.497	0.024	0.976	997.509	9.810
9	8	0.021	2.264	0.024	0.011	3.460	0.038	0.962	997.602	9.810
10	8	0.021	0.910	0.008	0.003	9.120	0.008	0.992	997.602	9.810
11	8	0.024	0.901	0.008	0.004	9.238	0.012	0.988	997.300	9.810
12	8	0.018	0.927	0.008	0.003	8.941	0.008	0.992	997.974	9.810
13	8	0.018	2.586	0.024	0.002	2.970	0.005	0.995	997.928	9.810
14	8	0.018	2.502	0.024	0.003	3.085	0.008	0.992	997.928	9.810
15	8	0.017	2.619	0.028	0.014	2.964	0.048	0.952	997.998	9.810
16	8	0.015	2.568	0.023	0.002	2.992	0.005	0.995	998.230	9.810
17	8	0.021	2.484	0.023	0.003	3.109	0.008	0.992	997.626	9.810
18	8	0.020	2.343	0.023	0.006	3.325	0.021	0.979	997.719	9.810
19	8	0.020	2.686	0.028	0.010	2.881	0.035	0.965	997.672	9.810
20	8	0.019	2.566	0.023	0.002	2.994	0.005	0.995	997.765	9.810
21	8	0.020	2.481	0.023	0.003	3.113	0.009	0.991	997.672	9.810
22	8	0.016	2.290	0.023	0.009	3.414	0.029	0.971	998.253	9.810
23	8	0.016	2.723	0.028	0.008	2.834	0.026	0.974	998.253	9.810

Trial #	L (m)	T _{air} (°K)	RT/H	P _T (atm)	P _T (kgf/m ²)	P ₀ (kgf/m ²)	α	kLa (min ⁻¹)
1	1.260	295.450	0.2326	0.930	9609.676	21843.043	-0.070	0.806
2	1.260	296.150	0.2332	0.930	9609.676	21849.645	-0.070	1.070
3	1.265	295.150	0.2324	0.932	9626.942	21857.334	-0.070	1.660
4	1.265	294.950	0.2322	0.932	9626.942	21922.813	-0.070	1.283
5	1.265	295.150	0.2324	0.930	9609.676	21834.999	-0.070	1.361
6	1.265	295.150	0.2324	0.930	9609.676	21851.071	-0.070	1.364
7	1.295	295.250	0.2324	0.931	9623.543	21967.506	-0.070	3.036
8	1.295	295.250	0.2324	0.931	9623.543	21988.171	-0.070	3.221
9	1.295	295.650	0.2328	0.911	9412.816	21604.443	-0.071	6.334
10	1.265	295.450	0.2326	0.932	9626.942	21909.967	-0.070	1.347
11	1.265	295.650	0.2328	0.941	9723.604	21950.449	-0.070	1.309
12	1.265	295.150	0.2324	0.932	9626.942	21914.727	-0.070	1.559
13	1.260	295.950	0.2330	0.930	9609.676	21883.401	-0.070	0.776
14	1.265	295.450	0.2326	0.932	9626.942	21908.831	-0.070	1.074
15	1.305	295.650	0.2328	0.933	9640.809	21809.784	-0.070	7.326
16	1.265	295.250	0.2324	0.932	9626.942	21952.189	-0.070	0.811
17	1.265	295.350	0.2325	0.930	9609.676	21886.102	-0.070	1.061
18	1.295	294.850	0.2321	0.931	9623.543	22038.192	-0.070	3.102
19	1.295	295.550	0.2327	0.911	9412.816	21643.512	-0.071	5.802
20	1.265	294.950	0.2322	0.932	9626.942	21945.877	-0.070	0.678
21	1.300	295.050	0.2323	0.941	9723.604	22338.255	-0.071	0.979
22	1.285	295.150	0.2324	0.933	9640.809	21857.954	-0.070	5.639
23	1.285	295.850	0.2329	0.933	9640.809	21894.851	-0.070	4.539

Trial #	kLa (s^{-1})	St_L (value)	St_L (formula)	St_G (value)	St_G (formula)	D_a	y_0	$C_{L,0}$ (mg/L)
1	0.013	0.274	0.274	0.194	0.194	0.008	0.041	19.690
2	0.018	0.200	0.200	0.258	0.258	0.004	0.040	19.546
3	0.028	0.568	0.568	0.270	0.270	0.007	0.040	19.362
4	0.021	0.241	0.241	0.324	0.324	0.003	0.020	9.930
5	0.023	0.475	0.475	0.221	0.221	0.009	0.020	9.772
6	0.023	0.257	0.257	0.232	0.232	0.004	0.021	9.947
7	0.051	1.063	1.063	0.255	0.255	0.008	0.020	9.876
8	0.054	0.613	0.613	0.277	0.277	0.004	0.020	9.866
9	0.106	0.723	0.723	0.357	0.357	0.002	0.020	9.666
10	0.022	0.461	0.461	0.323	0.323	0.007	0.006	3.045
11	0.022	0.439	0.439	0.212	0.212	0.008	0.006	2.972
12	0.026	0.522	0.522	0.373	0.373	0.006	0.020	9.851
13	0.013	0.086	0.086	0.267	0.267	0.002	0.041	19.632
14	0.018	0.120	0.120	0.234	0.234	0.002	0.041	19.843
15	0.122	0.706	0.706	0.337	0.337	0.002	0.012	5.963
16	0.014	0.091	0.091	0.276	0.276	0.002	0.021	10.000
17	0.018	0.119	0.119	0.228	0.228	0.002	0.020	9.927
18	0.052	0.357	0.357	0.304	0.304	0.002	0.020	9.963
19	0.097	0.552	0.552	0.349	0.349	0.002	0.021	10.052
20	0.011	0.076	0.076	0.228	0.228	0.002	0.008	3.799
21	0.016	0.113	0.113	0.212	0.212	0.002	0.006	3.132
22	0.094	0.643	0.643	0.400	0.400	0.002	0.012	5.831
23	0.076	0.431	0.431	0.352	0.352	0.001	0.012	5.884

Correction Factors: Mass Transfer Study

Cell #	Correction Factor (pressure)	Correction Factor (liquid)	Correction Factor (straight column cross-sectional area)
1	0.470	0.836	1.051
2	0.672	1.023	1.051
3	0.834	1.023	1.051
4	0.903	1.023	1.051
5	0.941	1.023	1.051
6	0.966	1.023	1.051
7	0.983	1.023	1.051
8	0.995	1.023	1.051

Input Cells to TK Solver® Software

Cell #	Variable	Formula	Trail #	1.000	2.000	3.000	4.000	5.000
				0.806	1.070	1.660	1.283	1.361
1	A1	$1+r_1+f_1f_A Da+f_1f_A St_L$		10.361	6.269	10.923	6.285	11.038
1	B1	r_1		9.114	5.090	9.418	5.070	9.613
1	C1	$f_1f_A St_L(1+\alpha f_z 0.5)$		0.237	0.173	0.490	0.208	0.410
2	D2	$1+r_{j-1}$		10.114	6.090	10.418	6.070	10.613
3	D3	↓		10.114	6.090	10.418	6.070	10.613
4	D4	↓		10.114	6.090	10.418	6.070	10.613
5	D5	↓		10.114	6.090	10.418	6.070	10.613
6	D6	↓		10.114	6.090	10.418	6.070	10.613
7	D7	↓		10.114	6.090	10.418	6.070	10.613
2	E2	$1+2r_j+f_2f_A Da+f_2f_A St_L$		19.531	11.399	20.454	11.403	20.746
3	E3	↓		19.531	11.399	20.454	11.403	20.746
4	E4	↓		19.531	11.399	20.454	11.403	20.746
5	E5	↓		19.531	11.399	20.454	11.403	20.746
6	E6	↓		19.531	11.399	20.454	11.403	20.746
7	E7	↓		19.531	11.399	20.454	11.403	20.746
2	F2	f_{j+1}		9.114	5.090	9.418	5.070	9.613
3	F3	↓		9.114	5.090	9.418	5.070	9.613
4	F4	↓		9.114	5.090	9.418	5.070	9.613
5	F5	↓		9.114	5.090	9.418	5.070	9.613
6	F6	↓		9.114	5.090	9.418	5.070	9.613
7	F7	↓		9.114	5.090	9.418	5.070	9.613
2	G2	$f_2f_A St_L(1+\alpha f_z(j-0.5))$		0.274	0.200	0.567	0.241	0.475
3	G3	↓		0.252	0.184	0.521	0.222	0.436
4	G4	↓		0.230	0.168	0.475	0.202	0.398
5	G5	↓		0.208	0.152	0.429	0.182	0.359
6	G6	↓		0.185	0.135	0.384	0.163	0.321
7	G7	↓		0.163	0.119	0.338	0.143	0.283
8	H8	$1+r_7$		10.114	6.090	10.418	6.070	10.613
8	I8	$1+r_8+f_2f_A Da+f_2f_A St_L$		10.417	6.309	11.036	6.333	11.133
8	J8	$f_2f_A St_L(1+\alpha f_z(7.5))$		0.141	0.103	0.292	0.124	0.244
1	K1	$1+\alpha f_z(j-1.5)$		1.016	1.016	1.016	1.016	1.016
2	K2	↓		0.976	0.976	0.976	0.976	0.976
3	K3	↓		0.912	0.912	0.913	0.912	0.912
4	K4	↓		0.842	0.842	0.842	0.842	0.842
5	K5	↓		0.769	0.769	0.770	0.769	0.769
6	K6	↓		0.696	0.696	0.696	0.695	0.696
7	K7	↓		0.622	0.622	0.622	0.621	0.622
8	K8	↓		0.547	0.547	0.548	0.547	0.547

1	L1	$1+\alpha f_2(j-0.5)$	0.984	0.984	0.984	0.984	0.984
2	L2		0.929	0.929	0.929	0.929	0.929
3	L3		0.854	0.854	0.854	0.854	0.854
4	L4		0.779	0.779	0.779	0.778	0.779
5	L5		0.704	0.703	0.704	0.703	0.704
6	L6		0.628	0.628	0.629	0.628	0.628
7	L7		0.553	0.553	0.553	0.552	0.553
8	L8		0.478	0.477	0.478	0.477	0.478
1	M1	$f_1 f_A St_G (1+\alpha f_2(j-0.5))$	0.168	0.223	0.233	0.280	0.191
2	M2	$f_2 f_A St_G (1+\alpha f_2(j-0.5))$	0.194	0.258	0.270	0.324	0.220
3	M3		0.178	0.237	0.248	0.298	0.203
4	M4		0.162	0.216	0.226	0.272	0.185
5	M5		0.147	0.195	0.204	0.245	0.167
6	M6		0.131	0.174	0.182	0.219	0.149
7	M7		0.115	0.153	0.161	0.193	0.131
8	M8		0.100	0.133	0.139	0.166	0.113
1	N1	$f_1 f_A St_G$	0.170	0.227	0.237	0.285	0.194
2	N2	$f_2 f_A St_G$	0.209	0.278	0.290	0.349	0.237
3	N3		0.209	0.278	0.290	0.349	0.237
4	N4		0.209	0.278	0.290	0.349	0.237
5	N5		0.209	0.278	0.290	0.349	0.237
6	N6		0.209	0.278	0.290	0.349	0.237
7	N7		0.209	0.278	0.290	0.349	0.237
8	N8		0.209	0.278	0.290	0.349	0.237
1	O1	$f_1 f_A St_{Gy_0} (1+\alpha f_2(j-0.5))$	0.007	0.009	0.009	0.006	0.004
2	O2	$f_2 f_A St_{Gy_0} (1+\alpha f_2(j-0.5))$	0.008	0.010	0.011	0.007	0.004
3	O3		0.007	0.010	0.010	0.006	0.004
4	O4		0.007	0.009	0.009	0.006	0.004
5	O5		0.006	0.008	0.008	0.005	0.003
6	O6		0.005	0.007	0.007	0.004	0.003
7	O7		0.005	0.006	0.006	0.004	0.003
8	O8		0.004	0.005	0.006	0.003	0.002
1	P1	$f_1 f_A St_{Gy_0}$	0.007	0.009	0.009	0.006	0.004
2	P2	$f_2 f_A St_{Gy_0}$	0.008	0.011	0.012	0.007	0.005
3	P3		0.008	0.011	0.012	0.007	0.005
4	P4		0.008	0.011	0.012	0.007	0.005
5	P5		0.008	0.011	0.012	0.007	0.005
6	P6		0.008	0.011	0.012	0.007	0.005
7	P7		0.008	0.011	0.012	0.007	0.005
8	P8		0.008	0.011	0.012	0.007	0.005

Mass Transfer Study, Trial #1

	Column Cell #	Column Height	Trial	1.000	Predicted X	Predicted C		
			$k_L a$	0.911				
			$C_{L,0}$	19.690				
			Measured X	Measured C	0.359	7.074	SR	
	1.000	0.035	↓	↓	0.385	7.571	↓	
	2.000	0.157			0.398	7.845		
	3.000	0.329			0.405	7.967		
	4.000	0.501			0.406	7.989		
	5.000	0.673			0.404	7.952		
	6.000	0.846			0.401	7.894		
	7.000	1.018			0.399	7.847		
	8.000	1.190	↓	↓			↓	
Z	0.098	1.000	0.125	0.368	7.240	0.380	7.475	0.055
	0.296	2.000	0.378	0.385	7.580	0.401	7.890	0.096
	0.493	3.000	0.629	0.411	8.100	0.406	7.993	0.011
	0.693	4.000	0.884	0.419	8.260	0.403	7.937	0.104
	0.886	5.000	1.130	0.432	8.509	0.400	7.870	0.409
	1.000	6.000	1.276		N/A			
							SSR	0.676

Overall Mass Transfer Coefficient: Regression Analysis

SUMMARY OUTPUT

<i>Regression Statistics</i>	
Multiple R	0.926
R Square	0.857
Adjusted R Square	0.843
Standard Error	0.347
Observations	23

<i>ANOVA</i>					
	<i>df</i>	<i>SS</i>	<i>MS</i>	<i>F</i>	<i>Significance F</i>
Regression	2	14.470	7.235	60.153	0.000
Residual	20	2.406	0.120		
Total	22	16.876			

	<i>Coefficients</i>	<i>Standard Error</i>	<i>t Stat</i>	<i>P-value</i>	<i>Lower 95%</i>	<i>Upper 95%</i>
Intercept	8.11221922	0.775	10.466	0.000	6.495	9.729
$\ln u_L$	0.079636981	0.146	0.546	0.591	-0.225	0.384
$\ln u_G$	1.255760593	0.120	10.426	0.000	1.005	1.507